

# Plasticity of neural networks

Diagnostic and therapeutic transcranial magnetic stimulation of healthy and infarcted brains



Jord JT Vink

# Plasticity of neural networks

Copyright © 2023 Jord JT Vink

ISBN: 978-90-393-7565-5

DOI: <https://doi.org/10.33540/1847>

Printing: Ridderprint

The cover shows the author sculpting the primary motor cortex of his own brain. The brain is a 3D print of the gray matter segmentation of the author's T1-weighted anatomical scan. The image refers to the concept of neuroplasticity. Neuroplasticity is the process of 'sculpting' your own neural circuitry through training. This process can be enhanced by neurostimulation, as described in this thesis.

The research in this thesis was conducted at the University Medical Center Utrecht and Utrecht University in Utrecht, The Netherlands and Massachusetts General Hospital and Beth Israel Deaconess Medical Center in Boston, Massachusetts, United States of America.

The research in this thesis was supported by the Netherlands Organization for Scientific Research (VICI 016.130.662) and Brain Science Tools B.V.

Financial support by the Dutch Heart Foundation for the publication of this thesis is gratefully acknowledged. Additionally financial contribution for publication of this thesis by Brain Science Tools B.V. and MagVenture is greatly appreciated.

Copyright © Jord Vink 2023. All rights reserved. No parts of this thesis may be reproduced, stored in a retrieval system of any nature, or transmitted in any form or by any means, without prior consent of the author. The copyright of the articles that have been published has been transferred to the respective journals.

# **Plasticity of neural networks**

Diagnostic and therapeutic transcranial magnetic stimulation  
of healthy and infarcted brains

## **Plasticiteit van neurale netwerken**

(met een samenvatting in het Nederlands)

### **Proefschrift**

ter verkrijging van de graad van doctor aan de  
Universiteit Utrecht  
op gezag van de  
rector magnificus, prof.dr. H.R.B.M. Kummeling,  
ingevolge het besluit van het college voor promoties  
in het openbaar te verdedigen op

woensdag 27 september 2023  
des middags te 2.15 uur

door

**Jord Jan-Teunis Vink**  
geboren op 19 januari 1992  
te Valkenswaard

**Promotoren:**

Prof. dr. R.M. Dijkhuizen

Prof. dr. J.M.A. Visser-Meily

Prof. dr. H.B. van der Worp

**Copromotor:**

Dr. S.F.W. Neggers

**Beoordelingscommissie:**

Prof. dr. L.J. Kapelle (voorzitter)

Prof. dr. G.M. Ribbers

Prof. dr. B.K. Velthuis

Prof. dr. N.F. Ramsey

Dr. F.S.S. Leijten

# Contents

<b>Chapter 1</b>	<b>7</b>
General introduction and outline of this thesis	
<b>Chapter 2</b>	<b>19</b>
A novel concurrent TMS-fMRI method to reveal propagation patterns of prefrontal magnetic brain stimulation	
<b>Chapter 3</b>	<b>43</b>
EEG functional connectivity is a weak predictor of causal brain interactions	
<b>Chapter 4</b>	<b>67</b>
Spatial topography of TMS-based motor mapping depends on TMS current direction	
<b>Chapter 5</b>	<b>85</b>
Continuous theta-burst stimulation of the contralesional primary motor cortex for promotion of upper limb recovery after stroke: a randomized controlled trial	
<b>Chapter 6</b>	<b>103</b>
Treatment efficacy of contralesional rTMS for post-stroke upper limb recovery is associated with residual motor function and corticospinal tract integrity	
<b>Chapter 7</b>	<b>119</b>
Continuous theta-burst stimulation of the contralesional primary motor cortex leads to expansion of the ipsilesional motor-eloquent area in recovering stroke patients	
<b>Chapter 8</b>	<b>137</b>
General discussion	
<b>Chapter 9</b>	<b>149</b>
Supplemental materials	
Nederlandse samenvatting	
Acknowledgements	
List of publications	
Curriculum Vitae	



Chapter 1

## **General introduction and outline of this thesis**

## Organization of the brain network

The healthy human brain consists of billions of interconnected neurons, which are organized in a single network. This network is responsible for almost everything we do in life, from something fundamental as breathing to complex behavior like reading this thesis. The brain network can be subdivided into macro-scale functional networks that consist of interacting brain regions. Activity in these networks can be associated with certain brain states or functionality.<sup>2</sup> For example, the sensorimotor network is a network of functionally connected brain regions that control movement and process sensory information.<sup>2</sup> The brain regions that make up these networks are functionally connected, as these regions show synchronous metabolic activity, which can be determined based on functional MRI (fMRI) of resting-state brain activity.<sup>1</sup>

The motor network consists of several interconnected cortical and subcortical regions that control movement via a neuroanatomical connection with the peripheral nervous system, the corticospinal tract (CST).<sup>3</sup> These brain regions have been subdivided anatomically based on a large number of histological and neurophysiological studies in animals.<sup>4</sup> Initially, the regions of the motor network were believed to play a specific and specialized role in the processing of movement. For example, activity in the supplementary motor area (SMA) has been associated with coordinating movement sequences.<sup>5</sup> However, recent evidence suggests that neural activity that lies at the origin of movement depends on modulation of the interactions between the different regions of the motor network.<sup>3</sup>

## Understanding motor networks through brain stimulation

Conventionally, the human motor network has been studied primarily through the measurement of voluntarily-induced neurophysiological activity using neuroimaging modalities such as positron emission tomography (PET), fMRI, diffusion-weighted imaging (DWI), and electroencephalography (EEG). These approaches have greatly advanced our understanding of brain networks, but they depend on task performance, which can vary between individuals.<sup>6</sup>

Today, the human motor network can be studied by stimulating the network with non-invasive brain stimulation (NIBS) methods. Transcranial magnetic stimulation (TMS) is a NIBS method that allows activation of cortical neurons through electromagnetic induction (**Figure 1**).<sup>7</sup> When applied concurrently with fMRI, the propagation of TMS-induced effects throughout the network can be measured. Such measurements have shown that activity evoked by a single TMS pulse is not restricted to the stimulated area, but can propagate to distant brain regions.<sup>8</sup>

When TMS is used to stimulate the motor cortex, the evoked activity is not restricted to the brain, but can travel down the CST, spinal cord, nerve roots, and nerve to the targeted muscle. Within the targeted muscle, it can generate a motor-evoked potential (MEP) that can be recorded using electromyography (EMG). Combined with EMG, TMS allows the assessment of motor cortex excitability, which is a measure of the motor cortex's sensitivity to artificial stimulation. When combined with MRI-guided neuronavigation, TMS-EMG can also be used to stimulate a grid of cortical targets while simultaneously recording the motor-evoked responses to spatially delineate the motor-eloquent area (**Figure 2**). These TMS measurements provide a deeper understanding of how the healthy motor network operates and can also be used to investigate damaged motor networks. **Part one** of this thesis focuses on how these methods can be used to increase our understanding of the healthy motor network.



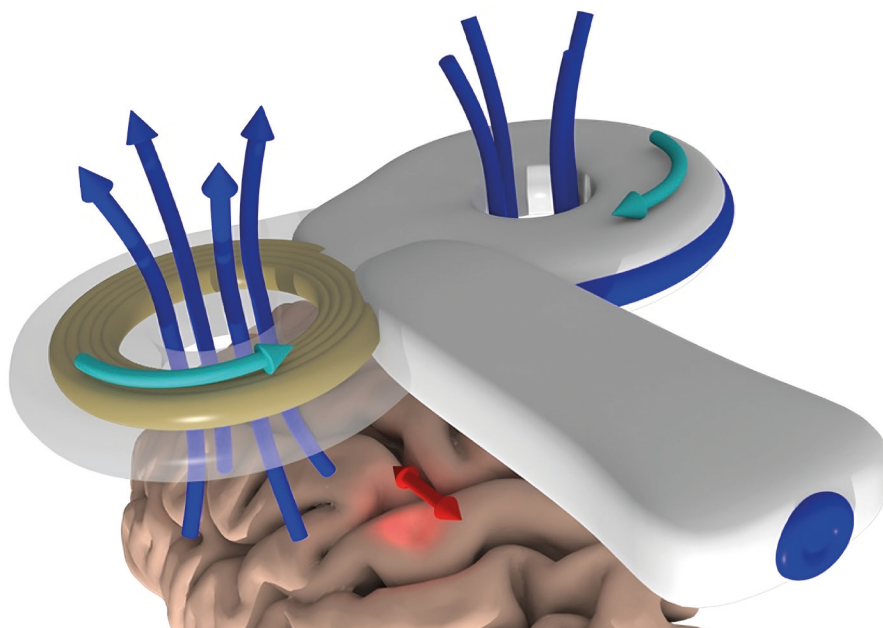


**Figure 1.** Simplified schematic representation of a TMS coil positioned over a brain. Arrows indicate the electrical current (light blue) that flows through the windings of the TMS coil, the induced magnetic field (dark blue) and the direction of the TMS-evoked electrical field (red).

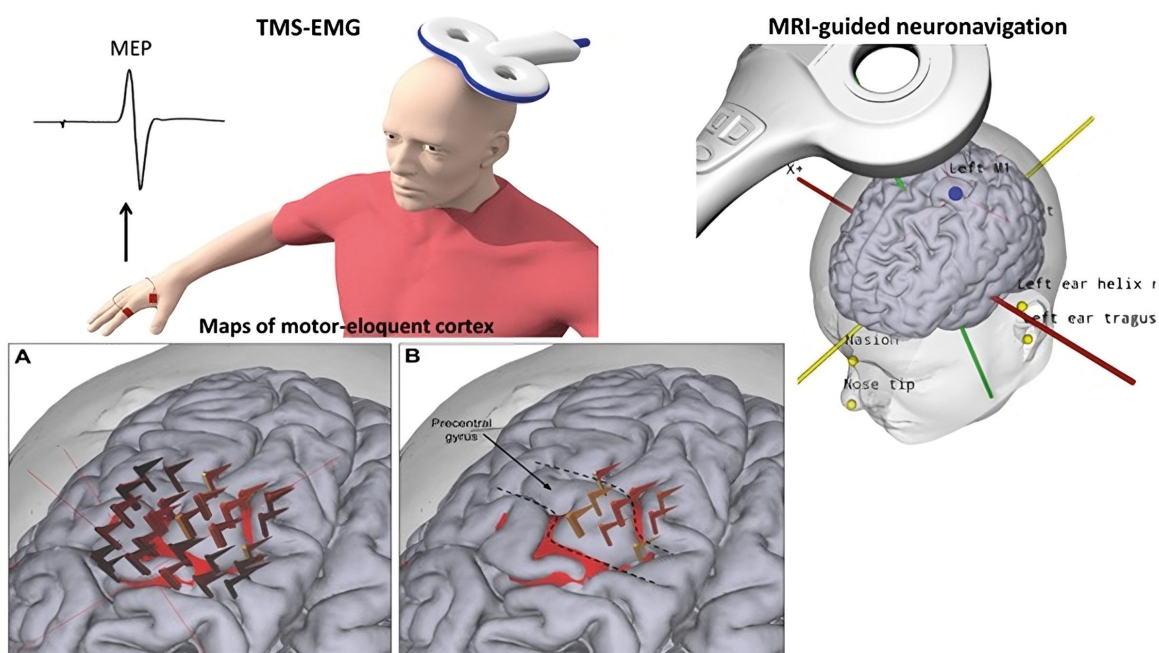


**Figure 2.** Schematic overview of delineation of motor-eloquent cortex with navigated TMS-EMG. The upper left panel shows an overview of the TMS-EMG procedure, in which TMS is used to evoke motor-evoked potentials (MEPs), which are recorded using electromyography (EMG). The upper right panel shows MRI-guided neuronavigation, where electromagnetic tracking is used to record the TMS coil position when a TMS pulse is delivered. The panel in the bottom left shows the results of a TMS-EMG session, in which each flag represents a stimulated cortical target. The color of the flag corresponds to the amplitude of the MEP, with more bright colors indicating higher amplitudes. Filtering of stimulated targets shows that motor-eloquent cortex is located in and around the precentral gyrus. Panel A shows all stimulated targets and panel B shows all stimulated targets with an MEP amplitude of over 1mV.

### A damaged motor network

A stroke can damage the motor network, which happens in over 80% of stroke patients, causing long-term motor impairment.<sup>10,11</sup> Consequently, stroke is a leading cause of adult disability worldwide.<sup>9</sup> There are two types of stroke: ischemic and hemorrhagic stroke. Ischemic stroke is caused by the occlusion of an artery or arteriole, causing a sudden loss of oxygenation of brain tissue.<sup>12</sup> The infarcted area and directly neighboring tissue are subjected to neuronal cell death and scar formation, resulting in permanent damage and limited potential for recovery.<sup>12,13</sup> Intracerebral hemorrhage is caused by rupture of an artery or arteriole, leading to neuronal cell death, aggravated by secondary processes.<sup>14</sup>

Stroke often results in impairment of the structural integrity of the motor network, which frequently involves damage to the CST.<sup>15</sup> Ischemia or hemorrhage can directly damage descending white matter bundles of the CST, for example in the case of subcortical stroke (**Figure 3**),<sup>16</sup> or it can indirectly affect structural CST integrity through Wallerian degeneration.<sup>17</sup> The level of residual motor function in the early subacute post-stroke phase is associated with the structural integrity of the remaining CST.<sup>16</sup>

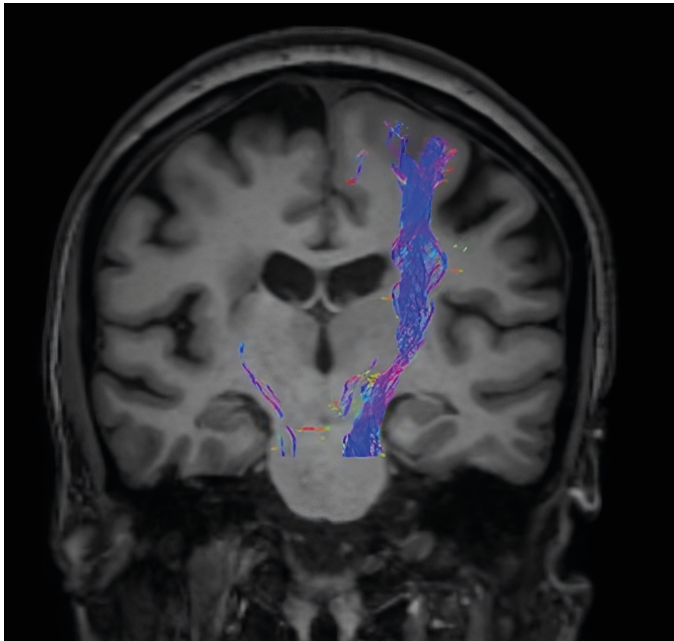


**Figure 3.** Coronal slice of a T1-weighted anatomical MRI scan of a patient with a subcortical stroke in the right hemisphere (left side of the image). A reconstruction of the corticospinal tracts based on tractography of diffusion-weighted imaging data is overlaid on the anatomical image. The lesion included the right corticospinal tract, complicating tract reconstruction.

The impact of stroke is not limited to direct or indirect structural damage to parts of the motor network, e.g. the corticospinal tract, but also impacts the functional integrity of the entire motor network. Excitability of the motor cortex may reflect the functional integrity of the motor network. After stroke, the ipsilesional motor cortex can be less excitable or completely unresponsive to external stimulation due to functional or structural damage.<sup>18</sup>

The impact of stroke is not limited to the infarcted area but extends throughout the connected network, known as diaschisis.<sup>19</sup> Post-stroke reorganization of the entire motor network can become apparent from fMRI and PET imaging during the performance of a motor task with the stroke-affected upper limb. For example, stroke patients may exhibit increased activity in the contralesional primary motor cortex (M1) and dorsolateral premotor cortex (PMC) and reduced activity in bilateral cerebellar and parietal regions compared to healthy

individuals.<sup>20</sup> These post-stroke changes in motor network activity are characterized by a reduction in lateralization, i.e. a shift toward activity in the contralesional M1.<sup>21</sup>

Earlier neurophysiological studies suggested that an observed interhemispheric imbalance was exacerbated by increased interhemispheric inhibitory drive from an overactive contralesional M1 (**Figure 4**).<sup>22,23</sup> However, the role of (altered) interhemispheric inhibitory drive in the pathophysiology of motor impairment remains controversial. Firstly, recent studies have failed to find evidence supporting the presence of an increased inhibitory drive towards the ipsilesional hemisphere.<sup>24</sup> Secondly, measures of interhemispheric inhibition may not adequately reflect the complex physiology of motor behavior.<sup>25</sup> Thirdly, increased contralesional inhibitory drive might be a compensatory mechanism in response to poor motor recovery.<sup>26</sup>

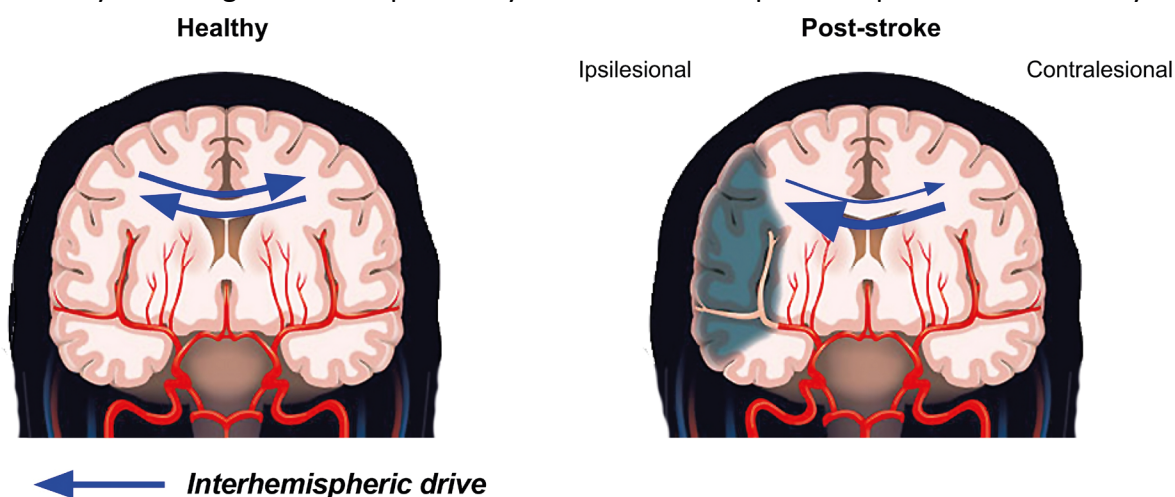


**Figure 4.** Schematic overview of the hypothesis that increased interhemispheric inhibitory drive from the contralesional hemisphere forms the basis of interhemispheric imbalance after stroke.

### Recovery of the motor network

Motor recovery after stroke may be related to changes in the peri-infarct area, as processes of tissue repair and recovery through axonal sprouting, angiogenesis, and neurogenesis remodel the area.<sup>27</sup> These neurobiological processes develop within the first weeks after stroke and this state of enhanced neural plasticity may underlie increased responsiveness to training.<sup>28</sup> Accordingly, recovery of upper limb function predominantly occurs within these first weeks post-stroke.<sup>29</sup> Neurophysiological evidence of such a period of enhanced plasticity is limited in humans, but recent TMS studies provide corroborating data.<sup>30,31</sup>

Enhanced neural plasticity may facilitate recovery of motor function through functional reorganization of peri-infarct areas. This is supported by a study that identified the motor-eloquent area in nonhuman primates using intracranial stimulation of cortical targets while monitoring the presence of motor responses in the targeted muscles before and after stroke induction and rehabilitative training.<sup>32</sup> Recovery of the upper limb in response to rehabilitative training was associated with functional reorganization of motor-eloquent areas in the peri-infarct area, while the infarcted area itself had become motor-ineloquent.<sup>32</sup> Navigated TMS-EMG (nTMS-EMG) provides a non-invasive alternative to measure functional reorganization of the motor-eloquent area in humans. Navigated TMS measurements have revealed an association between an increase in motor-eloquent area size and favorable upper limb recovery in stroke patients.<sup>33</sup> Such an increase in motor area size could indicate the recruitment of latent motor representations in the peri-infarct area.<sup>34</sup>

## Stimulating motor network recovery with neuromodulation

The process of motor recovery has been related to restoration of pre-stroke neurophysiology.<sup>20,35</sup> For example, normalization of ipsilesional motor cortex excitability and lateralization of ipsilesional M1 activity in response to affected hand movement are associated with favorable recovery.<sup>20,35</sup> Therefore, research has focused on the development of treatments that can restore pre-stroke neurophysiology.<sup>36</sup>

One of these treatment options is repetitive TMS (rTMS), which can be used to modulate motor cortex activity. Similar to single-pulse TMS, the effect of rTMS is not restricted to the stimulated area, as rTMS can modulate activity in connected brain regions.<sup>37</sup> Moreover, rTMS can be used to up- or downregulate activity in the stimulated area, depending on the stimulation paradigm.<sup>38</sup> Repetitive TMS has been investigated for the promotion of upper limb recovery after stroke, through modulation of the aforementioned interhemispheric imbalance. The interhemispheric balance may potentially be restored through upregulation of ipsilesional M1 activity with excitatory rTMS or through downregulation of contralesional M1 activity with inhibitory rTMS. Recently, contralesional inhibitory rTMS applied within the first month post-stroke in combination with upper limb physical therapy has been shown to be the most promising rTMS variant in promoting upper limb recovery (**Figure 5**).<sup>39,40</sup>

Although rTMS provides a promising treatment option for the promotion of upper limb recovery in stroke patients, the amount of currently available evidence is insufficient for its application in a clinical rehabilitation setting. Therefore, further research is required to increase the amount of evidence supporting its clinical efficacy. Additionally, it remains unclear which patients may benefit from contralesional inhibitory rTMS.<sup>41,42</sup> Selecting patients based on factors that inform on their structural brain reserve, i.e. structural integrity of the CST,<sup>41</sup> residual motor function<sup>42</sup> or stroke location<sup>43</sup>, might further increase the clinical efficacy of rTMS treatment through personalized protocols. Finally, the working mechanism of contralesional inhibitory rTMS remains poorly understood. It is unclear whether it would promote upper limb recovery through restoration of normal neurophysiology, facilitation of the recruitment of latent motor representations, or other mechanisms. These topics will be the focus of **part two** of this thesis.

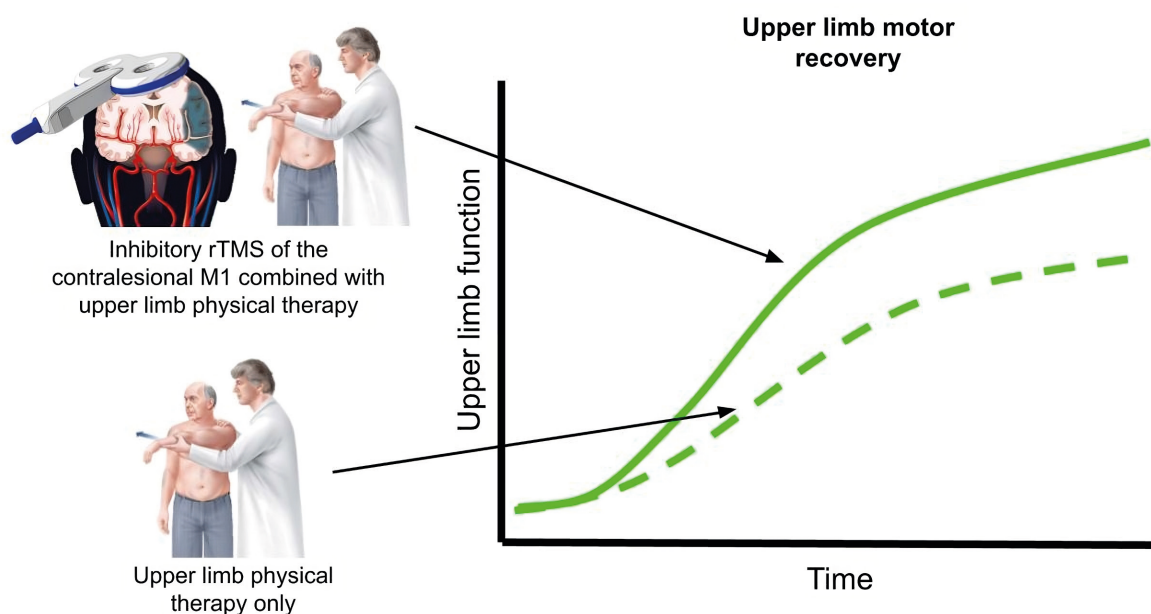


**Figure 5.** Schematic overview of the hypothesized effect of contralesional inhibitory rTMS treatment combined with regular care upper limb physical therapy on recovery of upper limb motor function.

## Outline of this thesis

**Part 1**, consisting of the first three chapters, focuses on understanding healthy brain networks and how we can interact with them using non-invasive brain stimulation methods, like TMS.

Little is known about the direct whole brain metabolic response to single pulses of TMS delivered to different cortical areas. In **chapter 2**, we investigate whether TMS-induced network activity in response to single-pulse TMS can be measured using a novel method, in which TMS is applied concurrently with functional MRI.

In chapter 2, we show that the effect of TMS spreads beyond the stimulated area to other brain regions. However, it remains unclear whether the effects of TMS preferentially spread through functionally connected brain regions, i.e. brain regions with synchronous neural activity. In **chapter 3**, we investigate whether EEG functional connectivity was informative on the spread of TMS-induced brain activity.

The initial response of cortical motor neurons to a single TMS pulse lies at the root of TMS-induced brain activity. However, activation of cortical motor neurons is likely to depend on the direction of the TMS-induced electrical field, due to anisotropic cortical conductance. In **chapter 4**, we investigate the effect of two different TMS-induced current directions on the spatial representation of the motor-eloquent cortex.

**Part 2**, consisting of chapters 5 to 7, applies the knowledge obtained in part 1, to understand how rTMS modulates the stroke-affected brain network to promote upper limb recovery.

Despite improvements in acute stroke therapies and rehabilitation strategies, many stroke patients are left with long-term upper limb motor impairment. In **chapter 5**, we investigate whether inhibitory rTMS treatment of the contralesional motor cortex within the first three weeks post-stroke can promote upper limb recovery after stroke.

It is unclear whether specific patients benefit from contralesional inhibitory rTMS. Selecting patients based on their structural reserve, i.e. structural integrity of the CST, residual motor function or stroke location might further increase the clinical efficacy of rTMS treatment. In **chapter 6**, we investigate whether selecting patients based on these stroke characteristics can increase the efficacy of the aforementioned rTMS treatment.

Finally, the mechanism of inhibitory rTMS treatment in the promotion of upper limb recovery is poorly understood. It is unclear whether the proposed rTMS treatment promotes upper limb recovery through restoration of normal neurophysiology, facilitation of the recruitment of latent motor representations or other mechanisms. In **chapter 7**, we use navigated TMS-EMG to measure cortical reorganization of the motor network after inhibitory rTMS treatment to elucidate the working mechanism of the treatment.

Finally, **chapter 8** summarizes and discusses the implications of the work presented in this thesis.

## REFERENCES

1. van den Heuvel MP, Hulshoff Pol HE. Exploring the brain network: A review on resting-state fMRI functional connectivity. *European Neuropsychopharmacology*. 2010;20(8):519-534. doi:10.1016/j.euroneuro.2010.03.008
2. Fox MD, Corbetta M, Snyder AZ, Vincent JL, Raichle ME. Spontaneous neuronal activity distinguishes human dorsal and ventral attention systems. *Proceedings of the National Academy of Sciences*. 2006;103(26):10046-10051.
3. Swinnen SP, Wenderoth N. Two hands, one brain: Cognitive neuroscience of bimanual skill. *Trends Cogn Sci*. 2004;8(1):18-25. doi:10.1016/j.tics.2003.10.017
4. Tanji J, Okano K, Sato KC. Relation of neurons in the nonprimary motor cortex to bilateral hand movement. *Nature*. 1987;327(6123):618-620.
5. Gaymard B, Pierrot-Deseilligny C, Rivaud S. Impairment of sequences of memory-guided saccades after supplementary motor area lesions. *Annals of Neurology: Official Journal of the American Neurological Association and the Child Neurology Society*. 1990;28(5):622-626.
6. McGonigle DJ, Howseman AM, Athwal BS, Friston KJ, Frackowiak RSJ, Holmes AP. Variability in fMRI: An examination of intersession differences. *Neuroimage*. 2000;11(6 1):708-734. doi:10.1006/nimg.2000.0562
7. Barker AT, Jalinous R, Freeston IL. Non-invasive magnetic stimulation of human motor cortex. *The Lancet*. 1985;325(8437):1106-1107.
8. Ruff CC, Blankenburg F, Bjoertomt O, et al. Concurrent TMS-fMRI and psychophysics reveal frontal influences on human retinotopic visual cortex. *Current Biology*. 2006;16(15):1479-1488.
9. Virani SS, Alonso A, Aparicio HJ, et al. Heart Disease and Stroke Statistics-2021 Update: A Report From the American Heart Association. *Circulation*. 2021;143(8):e254-e743. doi:10.1161/CIR.0000000000000950
10. Langhorne P, Bernhardt J, Kwakkel G. Stroke rehabilitation. *The Lancet*. 2011;377(9778):1693-1702. doi:10.1016/S0140-6736(11)60325-5
11. Langhorne P, Coupar F, Pollock A. Motor recovery after stroke: a systematic review. *Lancet Neurol*. 2009;8(8):741-754.
12. Sharp FR, Lu A, Tang Y, Millhorn DE. Multiple molecular penumbras after focal cerebral ischemia. *Journal of Cerebral Blood Flow & Metabolism*. 2000;20(7):1011-1032.
13. Fernández-Klett F, Potas JR, Hilpert D, et al. Early loss of pericytes and perivascular stromal cell-induced scar formation after stroke. *Journal of Cerebral Blood Flow & Metabolism*. 2013;33(3):428-439.
14. Bai Q, Liu J, Wang G. Ferroptosis, a regulated neuronal cell death type after intracerebral hemorrhage. *Front Cell Neurosci*. 2020;14:591874.
15. Gonzalez-Aquines A, Moreno-Andrade T, Gongora-Rivera F, et al. The Role of Tractography in Ischemic Stroke: A Review of the Literature. *Revista Medicina Universitaria*. 2019;20(4):161-165. doi:10.24875/rmu.18000021
16. Radlinska B, Ghinani S, Leppert IR, Minuk J, Pike GB, Thiel A. Diffusion tensor

- imaging, permanent pyramidal tract damage, and outcome in subcortical stroke. *Neurology*. 2010;75(12):1048-1054.
17. Thomalla G, Glauche V, Weiller C, Röther J. Time course of wallerian degeneration after ischaemic stroke revealed by diffusion tensor imaging. *J Neurol Neurosurg Psychiatry*. 2005;76(2):266-268.
  18. McDonnell MN, Stinear CM. TMS measures of motor cortex function after stroke: A meta-analysis. *Brain Stimul*. 2017;10(4):721-734. doi:10.1016/j.brs.2017.03.008
  19. Carrera E, Tononi G. Diaschisis: past, present, future. *Brain*. 2014;137(9):2408-2422.
  20. Favre I, Zeffiro TA, Detante O, Krainik A, Hommel M, Jaillard A. Upper limb recovery after stroke is associated with ipsilesional primary motor cortical activity: A meta-analysis. *Stroke*. 2014;45(4):1077-1083. doi:10.1161/STROKEAHA.113.003168
  21. Calautti C, Jones PS, Naccarato M, et al. The relationship between motor deficit and primary motor cortex hemispheric activation balance after stroke: Longitudinal fMRI study. *J Neurol Neurosurg Psychiatry*. 2010;81(7):788-792. doi:10.1136/jnnp.2009.190512
  22. Duque J, Hummel F, Celnik P, Murase N, Mazzocchio R, Cohen LG. Transcallosal inhibition in chronic subcortical stroke. *Neuroimage*. 2005;28(4):940-946. doi:10.1016/j.neuroimage.2005.06.033
  23. Murase N, Duque J, Mazzocchio R, Cohen LG. Influence of Interhemispheric Interactions on Motor Function in Chronic Stroke. *Ann Neurol*. 2004;55(3):400-409. doi:10.1002/ana.10848
  24. Gerges ANH, Hons B, Hordacre B, Pietro F Di, Moseley GL, Berryman C. Do Adults with Stroke have Altered Interhemispheric Inhibition? A Systematic Review with Meta-Analysis. *Journal of Stroke and Cerebrovascular Diseases*. 2022;31(7):106494. doi:10.1016/j.jstrokecerebrovasdis.2022.106494
  25. Carson RG. Inter-hemispheric inhibition sculpts the output of neural circuits by co-opting the two cerebral hemispheres. *J Physiol*. 2020;598(21):4781-4802. doi:10.1113/jp279793
  26. Xu J, Branscheidt M, Schambra H, et al. Rethinking interhemispheric imbalance as a target for stroke neurorehabilitation. *Ann Neurol*. 2019;85(4):502-513. doi:10.1002/ana.25452
  27. Thomas Carmichael S, Wei L, Rovainen CM, et al. New patterns of intracortical projections after focal cortical stroke. *Neurobiol Dis*. 2001;8(5):910-922. doi:10.1006/nbdi.2001.0425
  28. Ng KL, Gibson EM, Hubbard R, et al. Fluoxetine maintains a state of heightened responsiveness to motor training early after stroke in a mouse model. *Stroke*. 2015;46(10):2951-2960.
  29. van der Vliet R, Selles RW, Andrinopoulou ER, et al. Predicting Upper Limb Motor Impairment Recovery after Stroke: A Mixture Model. *Ann Neurol*. 2020;87(3):383-393. doi:10.1002/ana.25679
  30. Hordacre B, Austin D, Brown KE, et al. Evidence for a Window of Enhanced Plasticity in the Human Motor Cortex Following Ischemic Stroke. *Neurorehabil Neural Repair*. 2021;35(4):307-320. doi:10.1177/1545968321992330
  31. Dromerick AW, Geed S, Barth J, et al. Critical Period After Stroke Study (CPASS): A phase II clinical trial testing an optimal time for motor recovery after stroke in humans. *Proceedings of the National Academy of Sciences*. 2021;118(39):e2026676118.

32. Nudo RJ, Milliken GW. Reorganization of movement representations in primary motor cortex following focal ischemic infarcts in adult squirrel monkeys. *J Neurophysiol.* 1996;75(5):2144-2149. doi:10.1152/jn.1996.75.5.2144
33. Lüdemann-Podubecká J, Nowak DA. Mapping cortical hand motor representation using TMS: A method to assess brain plasticity and a surrogate marker for recovery of function after stroke? *Neurosci Biobehav Rev.* 2016;69:239-251. doi:10.1016/j.neubiorev.2016.07.006
34. Chen R, Cohen LG, Hallett M. Nervous system reorganization following injury. *Neuroscience.* 2002;111(4):761-773. doi:10.1016/S0306-4522(02)00025-8
35. Stinear CM, Petoe MA, Byblow WD. Primary motor cortex excitability during recovery after stroke: Implications for neuromodulation. *Brain Stimul.* 2015;8(6):1183-1190. doi:10.1016/j.brs.2015.06.015
36. Boddington LJ, Reynolds JNJ. Targeting interhemispheric inhibition with neuromodulation to enhance stroke rehabilitation. *Brain Stimul.* 2017;10(2):214-222. doi:10.1016/j.brs.2017.01.006
37. Smoski MJ, Felder J, Bizzell J, et al. fMRI of alterations in reward selection, anticipation, and feedback in major depressive disorder. *J Affect Disord.* Published online 2009. doi:10.1016/j.jad.2009.01.034
38. Rossi S, Antal A, Bestmann S, et al. Safety and recommendations for TMS use in healthy subjects and patient populations, with updates on training, ethical and regulatory issues: Expert Guidelines. *Clinical Neurophysiology.* 2021;132(1):269-306. doi:10.1016/j.clinph.2020.10.003
39. van Lieshout ECC, van der Worp HB, Visser-Meily JMA, Dijkhuizen RM. Timing of Repetitive Transcranial Magnetic Stimulation Onset for Upper Limb Function After Stroke: A Systematic Review and Meta-Analysis. *Front Neurol.* 2019;10(1269):1-16. doi:10.3389/fneur.2019.01269
40. Lefaucheur JP, Aleman A, Baeken C, et al. Evidence-based guidelines on the therapeutic use of repetitive transcranial magnetic stimulation (rTMS): An update (2014–2018). *Clinical Neurophysiology.* 2020;131(2):474-528. doi:10.1016/j.clinph.2019.11.002
41. Di Pino G, Pellegrino G, Assenza G, et al. Modulation of brain plasticity in stroke: A novel model for neurorehabilitation. *Nat Rev Neurol.* 2014;10(10):597-608. doi:10.1038/nrneurol.2014.162
42. Bertolucci F, Chisari C, Fregni F. The potential dual role of transcallosal inhibition in post-stroke motor recovery. *Restor Neurol Neurosci.* 2018;36(1):83-97. doi:10.3233/RNN-170778
43. Kim WS, Kwon BS, Seo HG, Park J, Paik NJ. Low-Frequency Repetitive Transcranial Magnetic Stimulation Over Contralesional Motor Cortex for Motor Recovery in Subacute Ischemic Stroke: A Randomized Sham-Controlled Trial. *Neurorehabil Neural Repair.* 2020;34(9):856-867. doi:10.1177/1545968320948610







## Chapter 2

# **A novel concurrent TMS-fMRI method to reveal propagation patterns of prefrontal magnetic brain stimulation**

Jord JT Vink

Stefano Mandija

Petar I Petrov

Nico CAT van den Berg

Iris E Sommer

Sebastiaan FW Neggers

*Vink, Jord JT, et al. "A novel concurrent TMS-fMRI method to reveal propagation patterns of prefrontal magnetic brain stimulation." Human brain mapping 39.11 (2018): 4580-4592.*

## **ABSTRACT**

### **Introduction**

Major depressive disorder (MDD) is a severe mental disorder associated with high morbidity and mortality rates, which remains difficult to treat, as both resistance and recurrence rates are high. Repetitive transcranial magnetic stimulation (TMS) of the left dorsolateral prefrontal cortex (DLPFC) provides a safe and effective treatment for selected patients with treatment-resistant MDD. Little is known about the mechanisms of action of TMS provided to the left DLPFC in MDD and we can currently not predict who will respond to this type of treatment, precluding effective patient selection.

### **Methods**

We applied single pulse TMS to the left DLPFC in 10 healthy participants using a unique TMS-fMRI set-up, in which we could record the direct effects of TMS.

### **Results**

Stimulation of the DLPFC triggered activity in a number of connected brain regions, including the subgenual anterior cingulate cortex (sgACC) in 4 out of 9 participants. The sgACC is of particular interest, because normalization of activity in this region has been associated with relief of depressive symptoms in MDD patients.

### **Conclusion**

This is the first direct evidence that TMS pulses delivered to the DLPFC can propagate to the sgACC. The propagation of TMS-induced activity from the DLPFC to sgACC may be an accurate biomarker of efficacy for rTMS. Further research is required to determine whether this method can contribute to selection of patients with treatment resistant MDD who will respond to rTMS treatment.

## INTRODUCTION

Major depressive disorder (MDD) is a complex disorder characterized by a depressed mood and/or loss of interest or pleasure in (almost) all activities<sup>1</sup>. It affects 4.7% of the global population and is the second leading cause of disability worldwide<sup>2,3</sup>. MDD is currently treated by means of antidepressant medication, psychotherapy (often behavioral therapy) or a combination of these two. Treatment resistant patients are treated with electroconvulsive therapy or, in rare cases, with deep brain stimulation. Both psychotherapy and pharmacotherapy have small effect sizes of around 0.3, leaving a substantial amount of patients without adequate therapy due to intolerance or unresponsiveness<sup>4-6</sup>. Up to two thirds of the patients with MDD do not respond to the first medication prescribed and approximately 15 to 33% of patients suffer from treatment resistance, which is defined as unresponsiveness or intolerance to at least 2 different classes of antidepressants<sup>7</sup>. This stresses the need for more treatment options for patients with treatment-resistant major depressive disorder (TR-MDD). Repetitive transcranial magnetic stimulation (rTMS) and electroconvulsive therapy (ECT) provide treatment alternatives for patients with TR-MDD. Unfortunately, ECT has major disadvantages, including the need for anesthesia and severe side effects like amnesia<sup>8</sup>.

Unlike ECT, rTMS is a targeted non-invasive brain stimulation method with only mild side effects and has proven to be effective in the treatment of TR-MDD<sup>9</sup>. TMS is a means of using electromagnetic induction in order to stimulate a brain region. Repetitive delivery of TMS pulses (rTMS) to a brain region modulates the excitability of the stimulated area, inducing changes in neural plasticity<sup>10</sup>. These neuroplastic changes outlast the duration of stimulation and are believed to be induced through long-term potentiation/depression mechanisms<sup>11,12</sup>. High (> 5 Hz) or low (< 5 Hz) frequency stimulation results in a lasting increase or decrease in excitability, respectively<sup>12,13</sup>. Stimulation is applied to a focal region in the brain, but the effects of TMS are not limited to the stimulated brain region, but spread to other cortical areas<sup>14-16</sup>. Repetitive stimulation has been shown to induce a clinically relevant effect in MDD and has recently obtained FDA approval for its application in MDD<sup>9,17</sup>. Patients with MDD are treated through high frequency stimulation of the dorsolateral prefrontal cortex (DLPFC), which causes an antidepressant effect in around 25% of patients with TR-MDD<sup>17</sup>.

Although already applied clinically, little is known about the mechanism of action of high frequency stimulation of the DLPFC. Over the last decades, neuroimaging studies have investigated changes in the brain related to MDD intensively and several neuroanatomical regions have been found to exhibit abnormal activity in patients with MDD, with the subgenual anterior cingulate cortex (sgACC) attracting most attention. Neuroimaging studies have shown that baseline metabolic activity in the sgACC is increased in patients with MDD and that normalization of the sgACC activity correlates with relief of depressive symptoms<sup>18-21</sup>. It is hypothesized that rTMS of the DLPFC induces an antidepressant effect through direct or indirect neuromodulation of the abnormal activity in the sgACC<sup>22</sup>. MRI functional connectivity studies show that treatment outcome positively correlates with functional connectivity strength between the sgACC and the DLPFC, providing some evidence for this hypothesis<sup>23</sup>. However, the evidence is limited as only a small number of patients received TMS treatment. Furthermore, Fox and others assume that a functional connection based on resting state fMRI data provides the pathway for TMS effects evoked in the DLPFC, while there is no evidence that shows that TMS-induced activity can actually propagate from the DLPFC to the sgACC.

The antidepressant effect of rTMS is restricted to a quarter of the patients with TR-MDD and is known to vary substantially between patients<sup>17</sup>. This stresses the need for a better understanding of the effects of rTMS treatment of the DLPFC in order to select only patients predicted to respond to rTMS for this treatment. Identification of the individual propagation

pattern of TMS-evoked activity in response to stimulation of the left DLPFC can reveal the mechanisms of action of rTMS treatment and provide clues for further improvement of such treatment using individualized treatment methods. This can be done by using a patient's individual neural response to TMS to optimize the effects after subsequent treatment with repetitive stimulation. More specifically, identification of the propagation patterns can reveal whether TMS-induced activity evoked at the DLPFC has the ability to propagate to the sgACC, and potentially modulate the activity in the sgACC<sup>22</sup>.

Therefore, we investigated the propagation pattern of TMS-induced activity after stimulation of the left DLPFC using single pulse TMS. Because TMS effects are strongly affected by TMS coil placement (with respect to individual brain morphology), we also investigated the effect of TMS coil placement on propagation patterns of TMS-induced activity<sup>24,25</sup>. In order to achieve these goals, we applied single pulses of TMS to the left DLPFC during a functional MRI recording in 10 healthy participants, using a novel concurrent TMS-fMRI technique<sup>14</sup>.

## METHODS

### Study design

The experimental procedure was approved by the medical ethical committee of the University Medical Center Utrecht (UMCU), Utrecht, The Netherlands. All participants provided written informed consent and were screened for MRI and TMS exclusion criteria. MRI data were acquired in 10 right-handed participants (**Table 1**). One participant had to be excluded due to unavailability during the follow-up session. During the experimental procedure, we strictly adhered to the guidelines and recommendations for TMS endorsed by the International Federation for Clinical Neurophysiology<sup>26</sup>.

**Table 1.** Participant details.

Participant number	Sex	Age	RMT	Comment	COG of TMS area			Max displacement from the COG (mm)	TMS-MRI of M1
					X	Y	Z		
1	F	21	66		-43	23	45	4.4	Yes
2	M	34	73		-25	18	62	3.3	No
3	F	25	76	Excluded	-	-	-	-	-
4	M	18	58		-29	41	37	6.1	No
5	F	19	83		-33	25	47	5.2	Yes
6	F	24	83		-30	33	41	5.0	Yes
7	M	23	80		-29	28	52	2.1	Yes
8	F	20	78		-35	25	47	3.6	Yes
9	F	19	83		-33	22	57	2.9	Yes
10	F	20	82		-30	14	51	2.5	No

*The MNI coordinates of the normalized center of gravity (COG) of the TMS area are shown for each participant. The TMS area is based on initial TMS coil placement and corrected for subsequent head motion during image acquisition. The maximum displacement of the TMS target from the center of gravity reflects the effect of head movement on the displacement of the TMS coil isocenter. RMT: Resting motor threshold*

## Procedures

Our concurrent TMS-fMRI setup has previously been used to successfully detect TMS-induced activity in the motor network in response to TMS pulses delivered to the primary motor cortex (M1) of healthy participants<sup>14</sup>. We used this setup to stimulate M1 again, but primarily investigated TMS-induced activity in response to stimulation of the left DLPFC of healthy participants. Both experiments were done using a biphasic Magstim Rapid<sup>2</sup> magnetic stimulator, an MR-compatible TMS coil and a custom designed TMS filter box (all manufactured by Magstim Inc., UK, [www.magstim.com](http://www.magstim.com))<sup>14,27</sup>. All MR sequences (MRI-only and concurrent TMS-MRI) were performed in a 3T MR scanner (Achieva, Philips Healthcare, Best, The Netherlands).

The experiment was divided into two parts: an intake session (MRI-only) and a TMS session (concurrent TMS-MRI) (**Figure 1**). These sessions are described below.

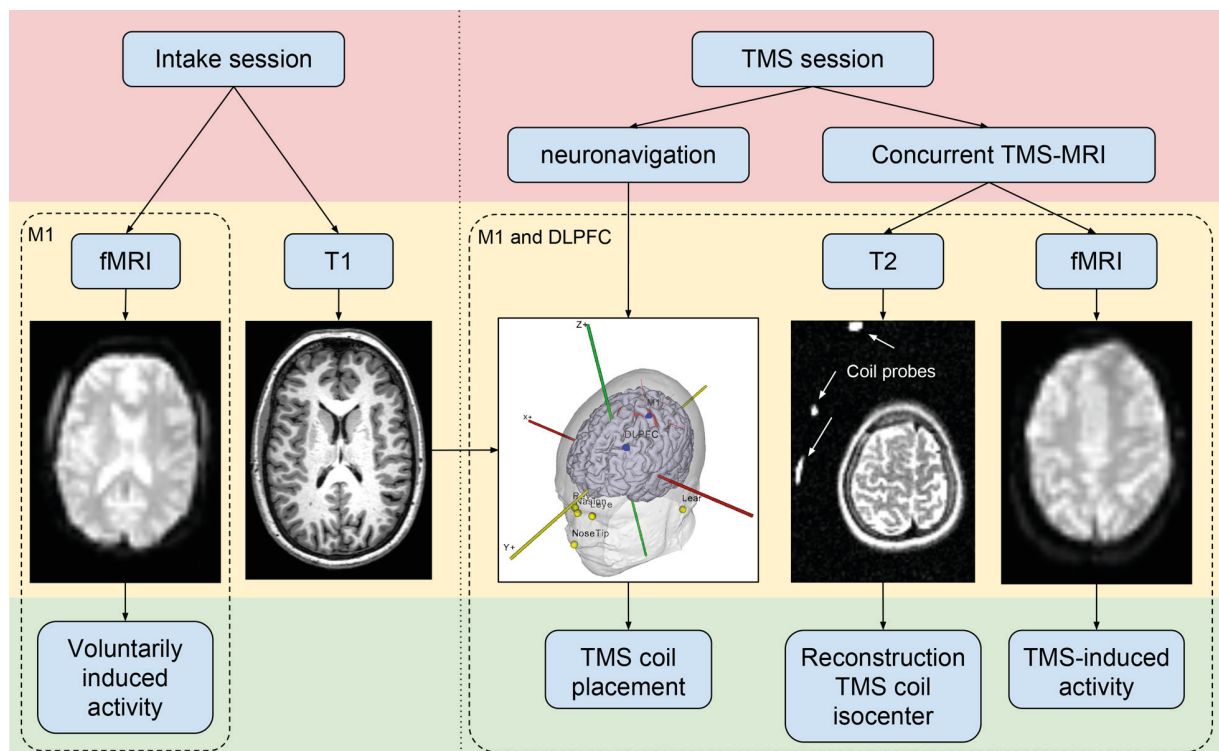


**Figure 1.** A flowchart of the experimental procedure. The fMRI scan during the intake was used in order to compare voluntarily induced motor network activity with TMS-induced activity. The concurrent TMS-fMRI session consisted of two subsections: An M1 and a DLPFC subsection.

### Intake session

First, a 3D T1 weighted anatomical scan was acquired with a TR/TE of 10.0/4.6 ms, a flip angle of 8°, voxel size of 0.75x0.75x0.8 mm<sup>3</sup>, scan duration of 11.3 min, 225 slices with a slice gap of 0 mm. This scan was used for neuronavigation during the TMS session and other visualization purposes.

Next, a single-shot echo-planar imaging (EPI) scan was acquired with 250 dynamics, a TR/TE of 2,000.0/23.0 ms, flip angle of 70°, voxel size of 4x4x4 mm<sup>3</sup>, a scan duration of 8.5 min and 30 slices with a slice thickness of 3.6 mm and a slice gap of 0.4 mm. During this scan, participants were instructed to move the thumb of the right hand upon presentation of an auditory cue. This scan was used to validate our concurrent TMS-fMRI setup by comparing voluntarily induced motor network activity with TMS-induced network activity in response to TMS of the primary motor cortex. Preprocessing and statistical analysis are described in the data analysis section.

### *TMS session*

For each participant, the T1 weighted image acquired during the intake session was segmented with SPM12 to obtain skin, skull, cerebrospinal fluid (CSF), white matter and grey matter (GM) masks<sup>28</sup>. The segmentations were used to visualize the 3D brain and skin surface in the Neural Navigator (Brain Science Tools, The Netherlands, [www.neuralnavigator.com](http://www.neuralnavigator.com)). The location of M1 was obtained from the statistical map acquired during the intake session and marked on the 3D brain surface. The TMS coil was oriented with the TMS coil handle perpendicular to the orientation of the precentral gyrus (at an angle of 30 to 45 degrees to the midline depending on individual morphology) and pointing in posterior direction. The DLPFC target was placed 3 gyri (i.e. 3cm) anterior to the premotor gyrus within the middle frontal gyrus, corresponding to the border between Brodmann areas 46 and 9.<sup>29</sup> For the DLPFC, the TMS coil handle was oriented perpendicular to the orientation of the middle frontal gyrus with the handle at 90 degrees with the midline. Eight facial markers were used to align world space with the MRI coordinates: the upper and lower left and right ear, the left and right inner eye lid, the tip of the nose and the nasion (**Figure 2A**). Neuronavigation was then used to determine the TMS coil position for stimulation of M1. Markings were made on the bathing cap in order to be able to replicate the TMS coil position inside the scanner, since neuronavigation could not be performed inside the MRI scanner room. These markings were also made for the DLPFC.

Next, the TMS coil was placed over the left M1 guided by neuronavigation to determine the resting motor threshold (RMT). This was done by applying single pulses of TMS (with an inter-stimulus interval of 7s) to the primary motor cortex while increasing the TMS stimulator output until a response in the APB muscle was visible in 5 out of 10 TMS pulses<sup>30</sup>.

The concurrent TMS-MRI session was divided in two parts: In the first part, TMS was applied to M1 and in the other part TMS was applied to the DLPFC. For the concurrent TMS-MRI experiments, a custom made setup was used. The head was positioned in a custom designed setup between 2 MR receive coils (**Figure 2C**). The TMS coil was attached to a custom made mount which was positioned over the participant's cranium, eliminating potential TMS coil movement. Additionally, to minimize Lorentz forces on the TMS coil wings, the angle between the TMS coil plane and the MRI static magnetic field was limited to 25 degrees. The head was tilted backwards and rotated slightly to match the coil position with the markings on the bathing cap. The head and neck of the participant were supported to increase comfort and to minimize head movement during the scan.

After TMS coil positioning, two sequences were acquired. First, a T2-weighted scan with a TR/TE of 13,609.0/80.0 ms, flip angle of 90°, voxel size of 2x2x2 mm<sup>3</sup>, scan duration of 3.6 min. The purpose of this scan was to visualize the coil location and orientation with respect to the head. This was done by attaching 6 custom made markers (small capsules filled with water) to the back of the TMS coil (**Figure 2B**), which appear hyperintense on the T2-weighted scan (**Figure 1**). Second, a single-shot EPI sequence was acquired with 500 dynamics, a TR/TE of 2,000.0/23.0 ms, flip angle of 70°, FOV of 256x119.6x208 mm<sup>3</sup>, matrix of 64x63, voxel size of 4x4x4 mm<sup>3</sup>, scan duration of 17 min, 30 slices with a slice thickness of 3.6 mm and a slice gap of 0.4 mm. We acquired 500 dynamics to make sure that we had sufficient power to detect the effects of single pulses of TMS. During the EPI sequence, single pulses of TMS with an intensity of 115% RMT were interleaved with pulses with an intensity of 60% RMT. TMS pulses were delivered with a random interval of 5 to 8 dynamics (10 to 16s) to avoid habituation.



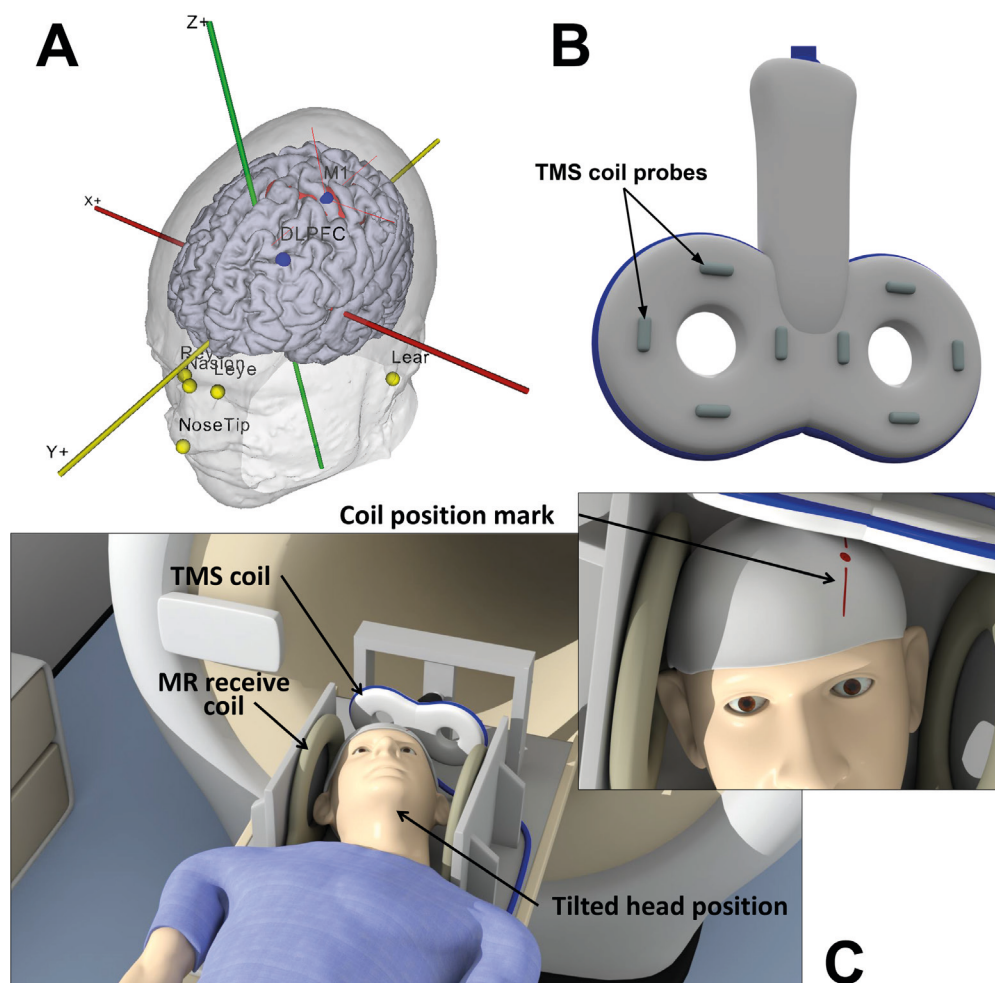


**Figure 2.** **Panel A.** Location of facial markers and TMS targets in the Neural Navigator. The statistical map of voluntarily induced motor activity is thresholded and shown in red. Facial markers: tip of the nose; nasion, left and right inner eyelid; left and right upper and lower ear. TMS targets: primary motor cortex (M1); dorsolateral prefrontal cortex (DLPFC). **Panel B.** TMS coil probes. The probes are visualized in a T2-weighted scan to determine their location with respect to the head. **Panel C.** Participant is lying on the MR bed with the head positioned in between two MR receive coils and the TMS coil located over the cranium.

### Data analysis

The data obtained for stimulation of M1 and the DLPFC were analyzed in the same way. Analysis of the structural and fMRI data was performed with custom scripts and SPM12<sup>28</sup> in the Matlab R2014a environment (Mathworks Inc., USA).

The T1-weighted image was segmented with SPM through unified segmentation with 6 tissue type priors to obtain a grey matter, white matter and CSF mask<sup>31</sup>.

All EPI volumes were inspected to determine image quality and to identify the presence of potential artifacts. This revealed small random deflections from the baseline signal level in a single slice of a few functional volumes per time series acquired during the TMS session. A small number of artifacts were present in most of the time series data. These deflections are short (one sample) and can only be observed in the vicinity of the TMS coil. All slices of the realigned EPI scans were automatically scanned for the presence of a sharp peak in the average grey matter signal with a custom algorithm to detect distortions. The distorted slices were then interpolated based on the BOLD signal in the previous and next slice with custom

Matlab code. 15 to 70 slices were interpolated out of 30 slices and 500 volumes depending on the participant. These artifacts are discussed in more detail in section 4.2.

All EPI volumes were realigned and normalized using the non-linear normalization parameters obtained from segmentation of the T1-weighted scan. The EPI volumes were subsequently resliced at a resolution of  $4 \times 4 \times 4 \text{ mm}^3$  and smoothed with a FWHM of 8mm.

The location of the TMS coil isocenter was reconstructed with respect to the brain based on the location of the fluid markers on the TMS coil. In order to reconstruct the TMS coil isocenter with respect to the brain, the T2-weighted scan was first co-registered to the anatomical T1-weighted scan using SPM12. Then, based on the location of the TMS coil markers in the T2-weighted scan, we were able to reconstruct the TMS coil position and isocenter, as described in De Weijer et al.<sup>14</sup>. Thereafter, the EPI volumes were realigned using SPM12. Next, the mean EPI scan was co-registered to the T1-weighted scan. The inverse of the EPI to T1 affine transformation and the inverse of the EPI realignment affine transformations were used to create a head movement-corrected reconstruction of the location of the TMS coil isocenter. Thereafter, the center of gravity (COG) of the TMS coil isocenter was calculated by calculating the average of the 3D coordinates of the TMS coil isocenter over all volumes.

For the functional data obtained during the intake session, the thumb movements were modeled with the canonical hemodynamic response function (HRF) and its first-order derivative in a standard event-related GLM analysis with 2 nuisance regressors: the average BOLD signal in the white matter and the CSF. Statistical images were constructed based on an F-statistic with the F-threshold at  $P < 0.05$ , family wise error (FWE) corrected<sup>28</sup>.

We performed subject-level event-related GLM analyses in SPM12. A group-level analysis was not performed due to the limited sample size<sup>32,33</sup>. The generalized linear model (GLM) included two events: single pulses of 115% RMT and 60% RMT. The BOLD response was modeled with the canonical hemodynamic response function (HRF) and its first-order derivative. The mechanism through which TMS induces brain activity is different from conventional MRI tasks which investigate voluntary brain activity. Inclusion of the first-order derivative allows more variability in the hemodynamic response, which allows more accurate modeling of the BOLD response during TMS pulse delivery. Two nuisance regressors were included in the analysis: the average BOLD signal in the white matter and the CSF. BOLD signals were filtered with a high pass filter of 80Hz before construction of the GLM. Statistical images were constructed based on the contrast between TMS pulses of 115% RMT and TMS pulses of 60% RMT. An F-statistic was used to test for variance explained by either the canonical hemodynamic response function or the first order derivative as the sum of both weighted regressors in a first order Taylor expansion, using a threshold at  $P < 0.05$ , family wise error (FWE) corrected<sup>28</sup>. TMS pulses of 115% RMT were contrasted with TMS pulses of 60% RMT to minimize the neural response to the sensation or sound that is accompanied by TMS pulse delivery.

## RESULTS

### Voluntary versus TMS-induced motor activity (M1 session)

We compared motor network activity in response to voluntary hand movements with TMS-induced activity after stimulation of M1.

Observations are described in detail for participant 1, who shows strong similarities between voluntarily induced brain activity and TMS-induced activity. In this participant, voluntary movement of the right thumb results in observable activity in, among other regions, the left primary motor cortex (M1) and supplementary motor area (SMA), the right hemisphere

of the cerebellum and the bilateral putamen and thalamus ( $P < 0.05$ , FWE corrected; **Figure 3B**). Because the participants were instructed to move their thumb based on auditory cues, activity can also be observed in the primary auditory cortex (A1). The full findings on TMS-induced activity are summarized in **Table 3** and all individual activation maps can be found in the supplementary materials.

During the concurrent TMS-fMRI session, the TMS coil isocenter was located slightly medio-anterior to the maximum BOLD response in the precentral gyrus, with limited displacement of the TMS coil isocenter due to head movement during the session (**Figure 3A**). TMS-induced activity was defined as the contrast between TMS pulses of 115% RMT and 60% RMT. The participant reported thumb movement in response to high intensity TMS pulses throughout the majority of the session and reported no thumb movements for low intensity TMS pulses. TMS-induced activity can be observed in the bilateral M1 and thalamus, the left SMA and putamen and the right hemisphere of the cerebellum ( $P < 0.05$ , FWE corrected; **Figure 3C**). Because TMS pulse delivery is accompanied by an auditory 'click', activity can also be observed in A1. Additionally, TMS-induced activity can be observed in the bilateral primary visual cortices.

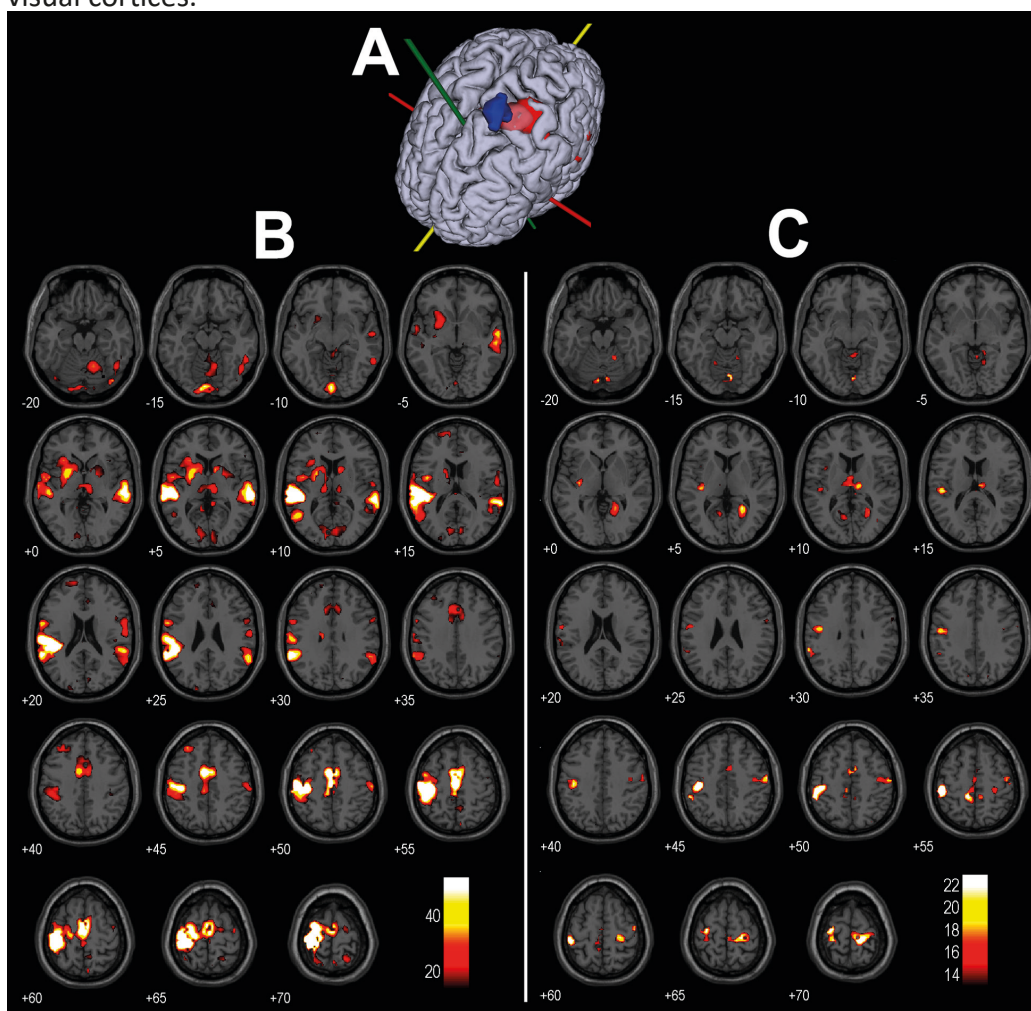


**Figure 3.** **Panel A.** Activity in the primary motor cortex in response to voluntary thumb movements (in red) and the location of the TMS coil isocenter during the TMS-fMRI session is shown (in blue). **Panel B.** Activity in response to voluntary thumb movements contrasted with baseline activity ( $P < 0.05$ , FWE corrected). Axial slices of an MNI brain are shown (left = left). **Panel C.** TMS-induced activity in response to TMS pulses of 115% RMT contrasted with baseline activity ( $P < 0.05$ , FWE corrected). The same slices are shown as in panel B.

### TMS target (DLPFC session)

The locations of the COG of the TMS coil isocenters were located well within the anatomical landmarks of the DLPFC in all participants (**Figure 4A**). The TMS coil isocenter remained within the DLPFC for the majority of the session in all participants, despite small head movements. Head movement resulted in a maximum displacement of the TMS coil isocenter from the COG of 2.1 mm to 6.1 mm (mean: 4 mm) depending on the participant (Table I), which shows that TMS coil placement was accurate and head movement was limited. In the majority of the participants, the TMS coil isocenter was located in the posterior part of the DLPFC, while the TMS coil isocenter was located in the anterior part of the DLPFC for participants 4 and 6. The normalized COGs of the TMS coil isocenter cluster in the left DLPFC (Figure 4B), with the COGs of participants 2 and 4 located on the edges of the middle frontal gyrus.

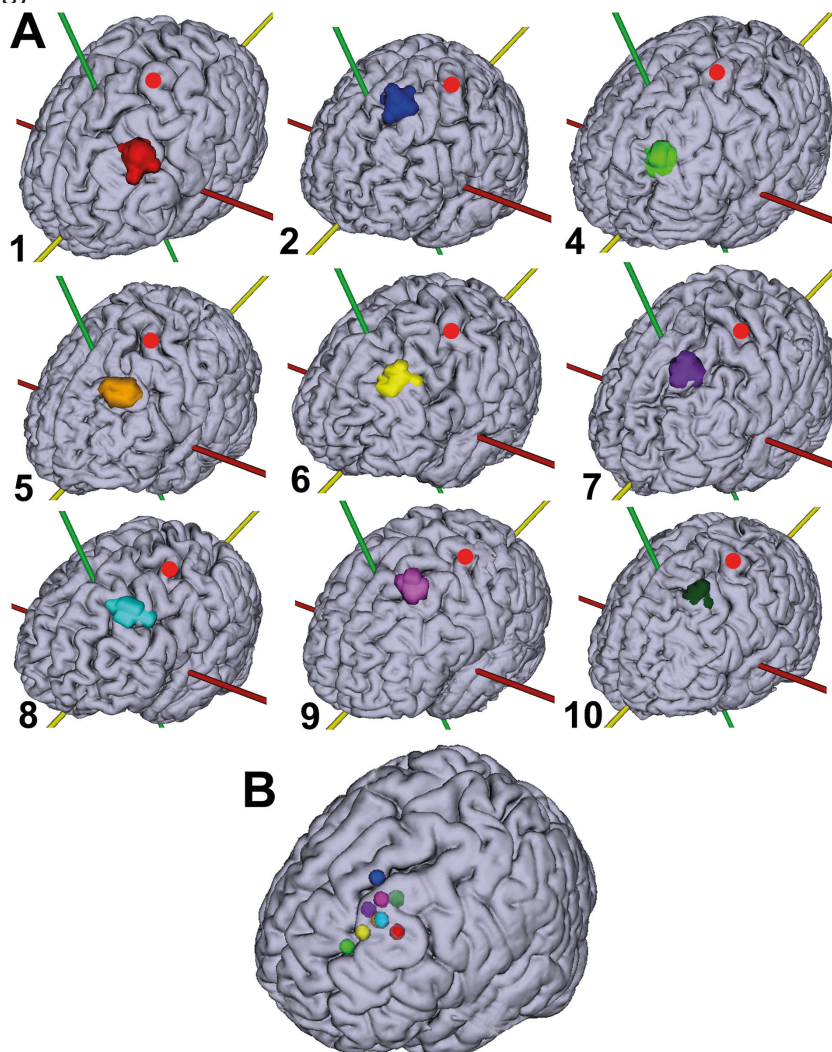


**Figure 4. Panel A.** TMS targets projected onto individual brain surfaces. The numbers refer to the participant numbers in table 1. The red dot indicates the location of the hand area in the primary motor cortex (M1) as determined through fMRI. **Panel B.** The normalized centre of gravity of each individual TMS target projected onto an MNI brain. The TMS targets are based on initial TMS coil placement (as determined through a T2-weighted scan) and corrected for subsequent head movement during image acquisition (as determined through realignment of the EPI volumes). Corresponding colors are used in panel A and B and table 1.

### TMS-induced activity (DLPFC + M1 session)

An overview of neuroanatomical regions that show TMS-induced activity in response to TMS pulses delivered to the left DLPFC (**Table 2**) and the left M1 (**Table 3**) are shown for all participants.

An overview of TMS-induced activity in response to left DLPFC stimulation is shown on four slices of an MNI brain for each participant (**Figure 5**). These slices show activity in response to TMS pulses of 115% RMT contrasted with TMS pulses of 60% RMT ( $P < 0.05$ , FWE corrected). The observed propagation patterns of TMS-induced activity showed substantial variation between participants. However, all participants showed TMS-induced activity in one or more subdivisions of the left prefrontal cortex. Interestingly, TMS-induced activity was generally absent in right hemisphere (contralateral to the stimulation site). Although TMS-induced activity was predominantly present in the left prefrontal area, it did also propagate to distant areas: including parietal and temporal areas.

**Figure 6** shows TMS-induced activity evoked by stimulation of the left M1 and DLPFC of participant 9. Stimulation of the left M1 revealed TMS-induced activity in the bilateral M1 and premotor cortex, which was more abundant in the lateral parts (representation of the face). Activity could also be observed in left SMA. Application of TMS to the left DLPFC revealed activity in a large part of the left prefrontal cortex and a small cluster in the left M1 and S1.

**Figure 7** shows TMS-induced activity in the limbic region in response to DLPFC stimulation, specifically focusing on activity in the sgACC. The delivery of TMS pulses to the DLPFC caused activity in the sgACC in 4 out of 9 participants, all of whom showed activity in the left (ipsilateral to stimulation) sgACC (**Table 2**). However, participant 7 showed TMS-induced activity on the boundary between the subgenual ACC and the neighbouring ACC. Activation of the sgACC was observed exclusively for stimulation of the DLPFC.

**Table 2.** Summary of TMS-induced activity observed in individual participants.

#	DLPFC	VLPFC	APFC	MPFC	PM	OFC	S1	sgACC	SPL	Temp
1	Left									
2	Left	Left	Left		Left					Right
3	-	-	-	-	-	-	-	-	-	-
4		Left			Left					
5	Left	Left	Left	Left	Left	Bi		Left		Right
6	Left	Left					Left			
7	Left	Left	Left	Left				Left		
8		Left					Left	Left		
9	Left	Left	Left	Left	Left		Left	Left		
10	Left								Left	Bi

*DLPFC: Dorsolateral prefrontal cortex; VLPFC: Ventrolateral prefrontal cortex; APFC: Anterior prefrontal cortex; MPFC: medial prefrontal cortex; PM: Premotor cortex; OFC: Orbitofrontal cortex; S1: Primary somatosensory cortex; sgACC: subgenual anterior cingulate cortex; SPL: superior parietal lobule; Temp: Temporal lobe.*

**Table 3.** Summary of TMS-induced activity after stimulation of M1 with 115% RMT contrasted with 60% RMT of individual participants.

#	M1	PM	S1	SMA	Put	Thal	A1	Cer	Temp
1	Bi	Left	Left		Left				
2	-	-	-	-	-	-	-	-	-
3	-	-	-	-	-	-	-	-	-
4	-	-	-	-	-	-	-	-	-
5	Bi	Bi					Left		Left
6	Bi	Bi	Bi	Bi				Left	Bi
7	Bi	Bi	Right	Left	Left		Left	Left	Bi
8	Left	Right	Left					Left	
9	Bi	Bi	Bi	Bi	Bi			Left	Left
10	-	-	-	-	-	-	-	-	-

*M1: Primary motor cortex; PM: Premotor cortex; S1: Somatosensory cortex; SMA: supplementary motor area; Put: Putamen; Thal: Thalamus; A1: primary auditory cortex; Cer: cerebellum; Temp: Temporal lobe.*

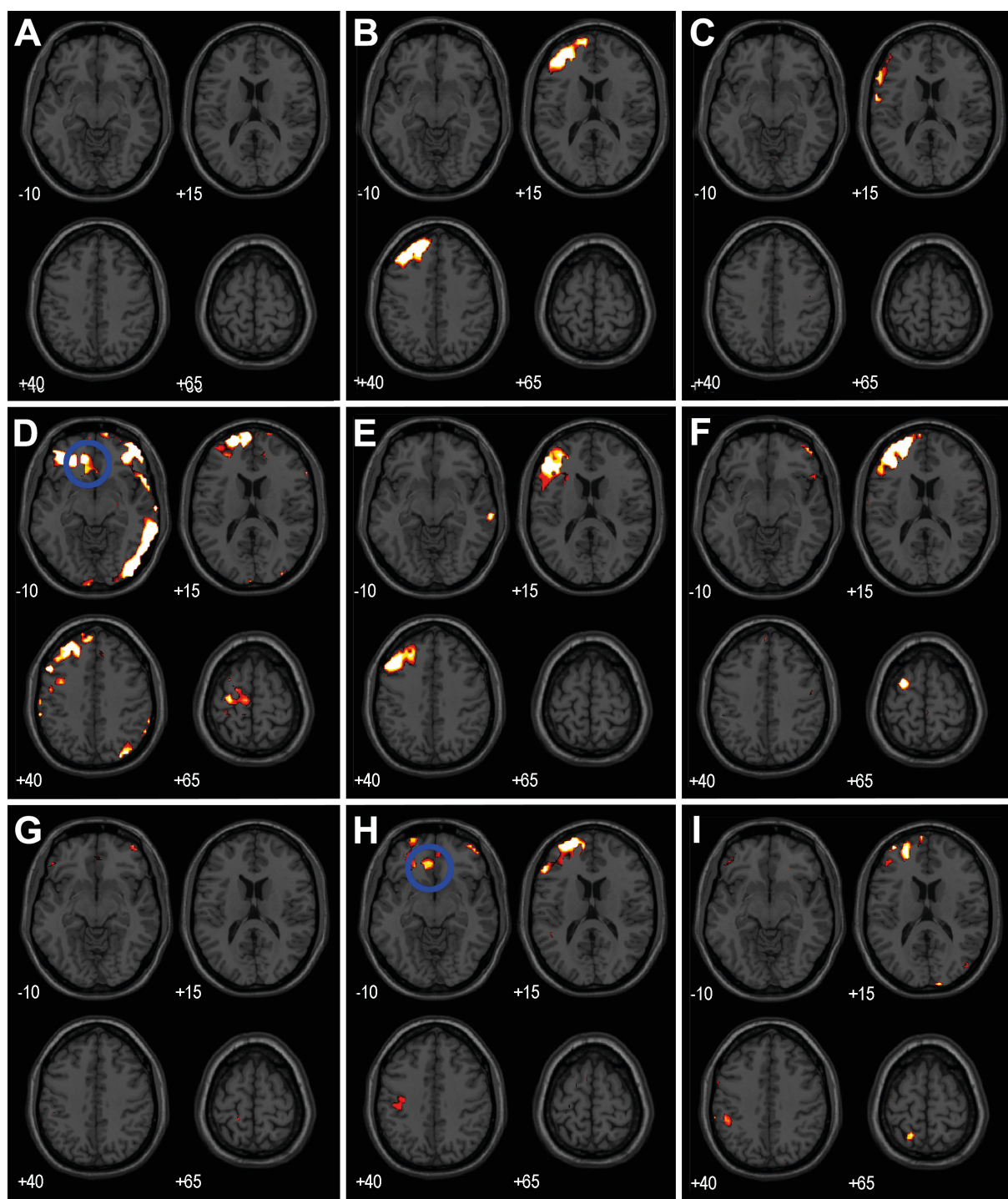


**Figure 5.** TMS-induced activity in response to TMS pulses of 115% RMT contrasted with TMS pulses of 60% RMT delivered to the left DLPFC ( $P < 0.05$ , FWE corrected). Axial slices of an MNI brain are shown (left = left). TMS-induced activity in the subgenual anterior cingulate cortex is encircled. Panels A to I show TMS-induced activity of participants 1, 2 and 4 to 10. A more detailed overview of these data can be found in the supplemental materials.

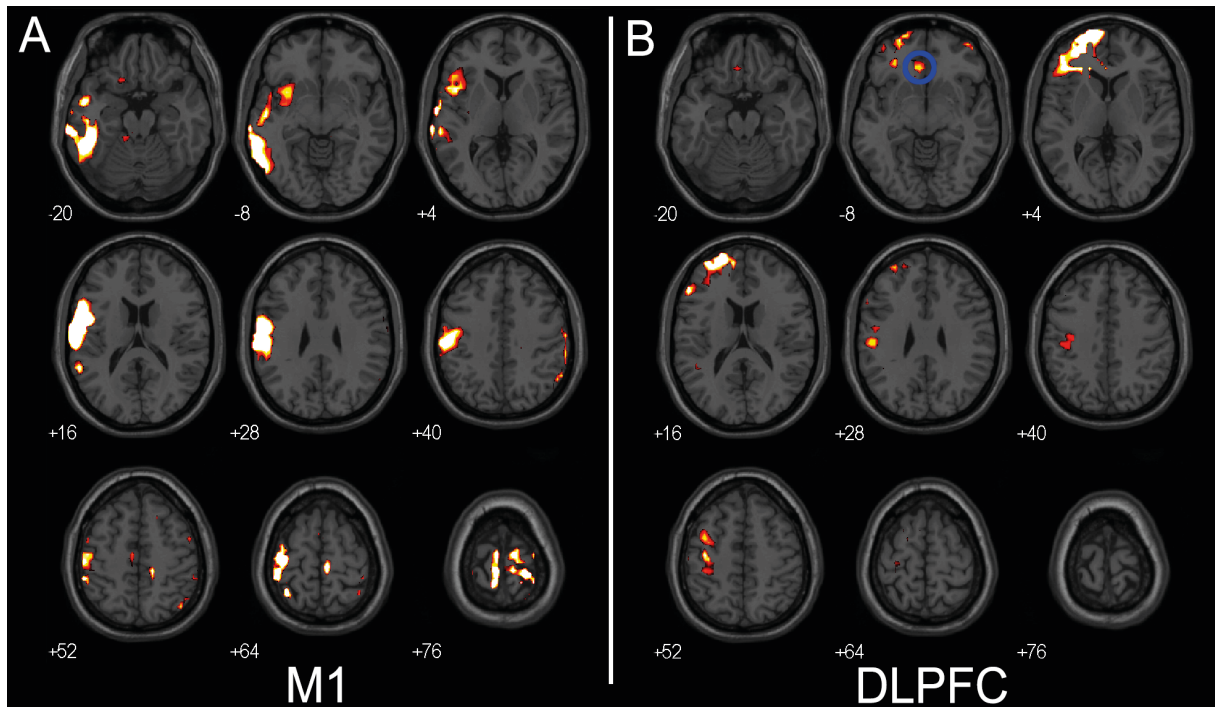


**Figure 6.** TMS-induced activity in response to TMS pulses of 115% RMT contrasted with TMS pulses of 60% RMT in participant 9 for two different TMS targets: M1 and DLPFC ( $P < 0.05$ , FWE corrected). Axial slices of an MNI brain are shown (left = left). **Panel A.** TMS-induced activity for stimulation of the left M1. **Panel B.** TMS-induced activity for stimulation of the left DLPFC. TMS-induced activity in the subgenual anterior cingulate cortex is encircled.



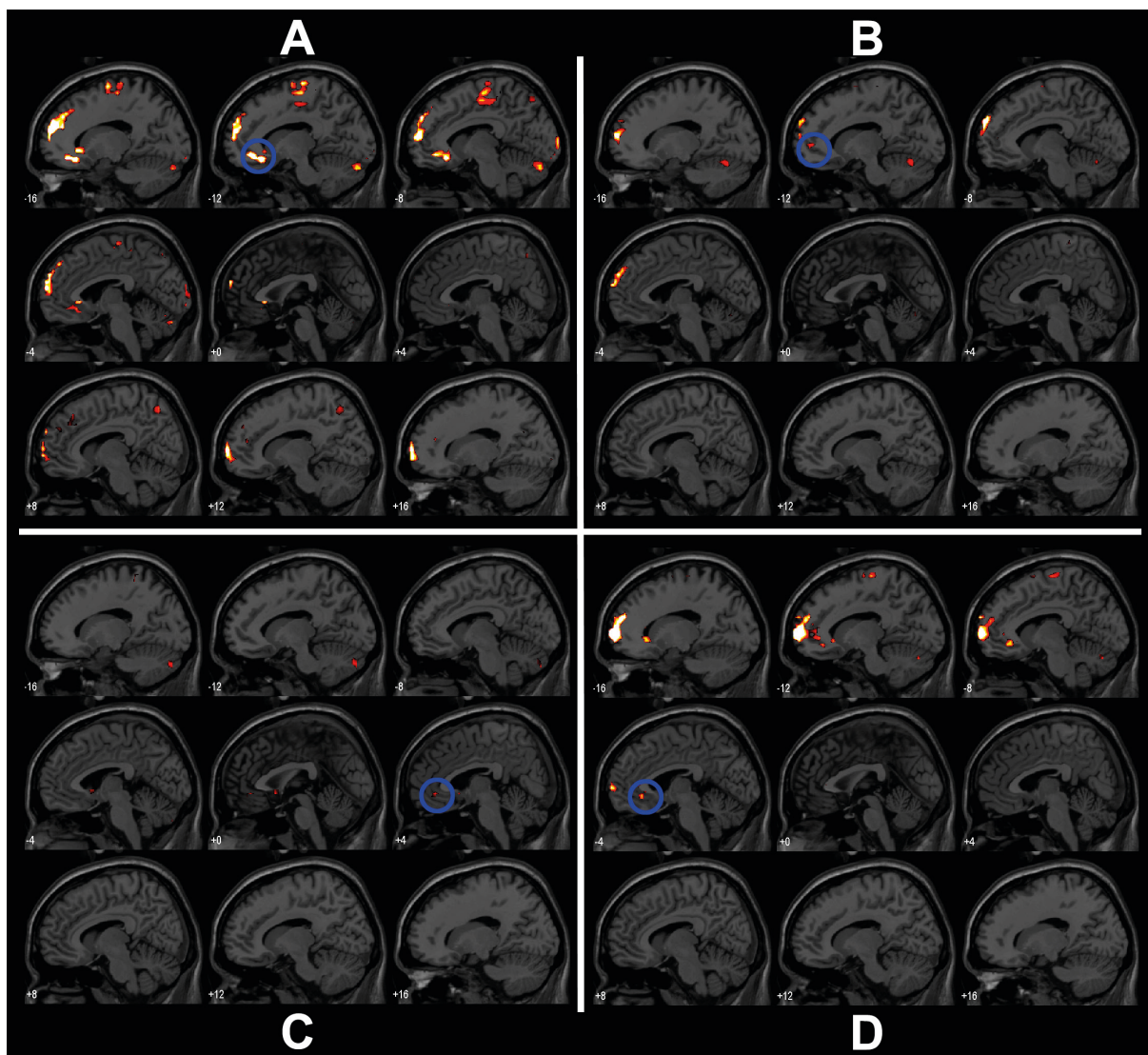


**Figure 7.** TMS-induced activity in response to TMS pulses of 115% RMT contrasted with TMS pulses of 60% RMT ( $P < 0.05$ , FWE corrected). Sagittal slices of an MNI brain are shown (first slice = left side; last slice = right side). TMS-induced activity in the subgenual anterior cingulate cortex is encircled. **Panel A.** TMS-induced activity of participant 5. **Panel B.** TMS-induced activity of participant 7. **Panel C.** TMS-induced activity of participant 8. **Panel D.** TMS-induced activity of participant 9.

## DISCUSSION

Using a novel concurrent TMS-MRI setup, we investigated the propagation patterns of TMS-induced activity after stimulation of the left DLPFC and left M1. We found that TMS delivered to the DLPFC results in activity in the sgACC in 4 out of 9 participants, while TMS delivered to the left M1 does not result in sgACC activity. This indicates that TMS-induced activity evoked by TMS of the left DLPFC has the ability to, directly or indirectly, propagate from the DLPFC to the sgACC. The existence of such a pathway was already suggested by others who investigated the mechanisms of action of rTMS of the left DLPFC in MDD by exploring resting state functional connectivity<sup>22</sup>. That work showed that the strength of the functional connection between the DLPFC and the sgACC correlated positively with treatment outcome after rTMS, implying that rTMS utilizes this functional connection<sup>23</sup>. However, evidence for a direct structural connection between these regions is lacking. Our observations provide the

first direct evidence that TMS-induced activity can propagate to the sgACC (at least in some individuals). Combining our observations with prior literature, it becomes apparent that the modulatory effect of rTMS of the DLPFC can potentially, directly or indirectly, propagate to the sgACC, depending on individual structural connectivity. The sgACC is an important area for psychiatric treatment as deep brain stimulation (DBS) of this area has shown to have both antidepressant and anti-compulsive effects.<sup>34–38</sup>

As stated previously, the treatment response is related to the strength of the functional connection between the DLPFC and the sgACC, which indicates that rTMS treatment of the DLPFC induces an antidepressant effect through modulation of the activity in the sgACC.<sup>23</sup> If this is indeed the therapeutic effect of DLPFC rTMS, the variability in propagation patterns of TMS-induced activity provides a potential explanation for the limited response rate of <30% of rTMS in the treatment of MDD.<sup>17</sup> The propagation of TMS-induced activity from the DLPFC to the sgACC in individual patients with MDD could be a predictor of a response to rTMS treatment. Further research is required to better understand propagation patterns of TMS-induced activity and the relationship with treatment outcome.

It is important to note that we validated our concurrent TMS-MRI setup by stimulating M1 and comparing TMS-induced network activity to voluntarily induced motor network activity (**Figure 3**). This was done by stimulating M1 because of the extensive literature on motor networks and the ability to directly determine adequate stimulation through observation of induced thumb movements. For M1 stimulation, we observed TMS-induced activity in neuroanatomical regions which are strongly associated with motor activity, like M1, SMA, putamen, thalamus and cerebellar subregions, and most of those regions were also observed in other concurrent TMS-fMRI studies.<sup>14,39</sup> TMS-induced activity in the sgACC has only been observed for DLPFC stimulation and not for stimulation of M1. The activation of known motor regions for stimulation of M1, and differences in propagation patterns between two different stimulation sites provides adequate evidence that concurrent single pulse TMS-fMRI can be used to investigate individual propagation patterns.

### **Variability in propagation patterns**

Although TMS coil placement was well-controlled and head movement was limited, we observe that TMS-induced brain activity is variable between participants (**Figure 5**). More specifically, we observe that stimulation of the same neuroanatomical region results in substantially different propagation patterns of TMS-evoked activity. A potential explanation of the variability in the observed propagation patterns are differences in (functional) neuroanatomy<sup>40–42</sup>. Stimulation of the same neuroanatomical region does not necessarily mean stimulation of the same functional region and stimulation of different functional regions can lead to differences in propagation pathways, depending on functional connectivity. Another explanation could be variability in structural brain connectivity, and thus propagation pathways, between participants<sup>43,44</sup>. Finally, functional brain connectivity shows substantial variability between participants, with strong variability observed in the prefrontal cortex<sup>45</sup>. Moreover, resting state functional connectivity studies show that brain functional connectivity shows substantial temporal variability, especially in the sgACC (among other regions)<sup>45–47</sup>. To summarize, the structural and functional organization of the brain together with the dynamic nature of functional connectivity could explain the variability in propagation patterns of TMS-induced activity.

Finally, the complex interaction of the TMS E-field with the neuronal populations in the cortex has been shown to be brain-state dependent and therefore not consistent over time<sup>48,49</sup>. EEG recordings have revealed that the pre-existing neuronal oscillatory activity in

the TMS target region affects properties of TMS-evoked activity. For example, the amplitude of TMS-induced motor-evoked potentials depends on pre-existing oscillatory activity of the primary motor cortex while phosphene thresholds depend on pre-existing activity in the visual cortex<sup>48,49</sup>. Since local neuronal oscillatory activity shows temporal and spatial variability, the TMS effects will also show temporal and spatial variability, which is likely to contribute to the observed variability of propagation patterns of TMS-induced activity<sup>46,50,51</sup>.

Our findings are in agreement with prior literature, which indicates that propagation of evoked activity is a complex process that, similar to functional connectivity, varies significantly between individuals<sup>45,47,48,50</sup>. Consequently, the ability of rTMS to modulate specific brain regions, and thus inducing an antidepressant effect, is likely to depend on the state of the individual brain network. Concurrent TMS-fMRI allows identification of the present individual structural and functional brain organization and connectivity, related to stimulation of a specific area of interest, such as the DLPFC. This concept can potentially be used to predict treatment outcome or to increase treatment efficacy of repetitive stimulation of the DLPFC in MDD. For example, by targeting treatment at the functional region near the DLPFC that leads to individual sgACC activation, assuming the pathway from prefrontal cortex to sgACC is the mechanism of action of the antidepressant effect of rTMS, as has been suggested<sup>22,23</sup>. In this way, future studies can investigate whether propagation of TMS-induced activity to sgACC is an accurate predictor of a clinical response to rTMS treatment of the DLPFC in a clinical population of patients with MDD.

We discussed possible (functional) neuroanatomical and state dependent explanations for the variability in TMS-induced activity between participants. However, the observed variability might originate from other sources. Variability can arise from the physiological interaction between the MRI static magnetic field and the electrophysiology of the individual brain or from the physical interaction between the TMS coil position with respect to the MRI static magnetic field. These complex interactions are subject of extensive research by others and were not directly investigated in this study<sup>52</sup>. Future research is required for correct characterization of these interactions and to understand whether they could be responsible for the observed inter-participant variability.

Finally, TMS-evoked activity consists of the activity of interest and confounding activity, such as auditory and somatosensory activity induced by the 'clicking' sound of the TMS coil and the superficial stimulation of the skin respectively<sup>53</sup>. We attempted to minimize confounding brain activity by contrasting TMS pulses of 115% RMT with TMS pulses of 60% RMT. However, a contrast with low intensity TMS does not completely eliminate confounding activity. Consequently, somatosensory and auditory activity should be interpreted with caution.

### **TMS-induced activity in the TMS target area**

TMS-induced activity can generally be observed in the TMS target area. However, 2 participants did not show activity in the vicinity of the TMS coil for stimulation of the left DLPFC. The absence of TMS-induced activity in the TMS target area has been reported previously<sup>14,15,54</sup>. A possible explanation is that in some cases the TMS-induced currents depolarize the descending white matter tracts, rather than the cell bodies, bypassing synaptic transmission in the TMS target area. As synaptic transmission makes up the majority of the hemodynamic signal measured using fMRI, concurrent TMS-fMRI is predominantly sensitive to synaptic transmission evoked by TMS<sup>55</sup>.

### **Image artifact**

The application of concurrent TMS-fMRI is challenged by numerous technical difficulties,

a few of which have already been addressed in other works<sup>39,56</sup>. A technical issue which was not previously described is that we observed short deflections (one sample) in baseline activity in a single slice in the vicinity of the TMS coil in EPI volumes during inspection of the BOLD signal (section 2.2). These artifacts were only observed during sessions in which TMS intensity was changed during the experiment and were absent when the machine output was kept constant. This suggests that currents leaked in the TMS coil, creating a local magnetic field around the TMS coil. This local magnetic field perturbed the MRI static magnetic field during image acquisition, resulting in image distortions. Unfortunately, the cause of the artifact could not be identified with complete certainty.

Fortunately, the effect on the results is negligible, as only a few slices were affected per participant (in less than 0.5% of all acquired slices per participant) and the artifact in these slices could effectively be removed through interpolation. However, TMS-induced activity in the vicinity of the TMS coil should be interpreted with caution.

## **CONCLUSION**

TMS pulses delivered to the left DLPFC induce activity in a number of connected brain regions, including the sgACC in some participants (4 out of 9). This indicates that the effects of stimulation of the left DLPFC stimulation have the ability to propagate to the sgACC, depending on individual structural connectivity, providing a potential mechanism for the antidepressant effect of rTMS delivered to the left DLPFC. This individual propensity could potentially be used as a predictor of the response to rTMS treatment in patients with MDD. Additionally, the propagation patterns of TMS-evoked activity show substantial variability between participants while TMS coil placement was well-controlled during image acquisition. Combining our observations with prior literature, this implies that the propagation pattern of TMS-induced activity, and thus the ability of rTMS to modulate specific brain areas, could depend on the current state of the individual brain network.

## REFERENCES

1. American Psychiatric Association. *Diagnostic and Statistical Manual of Mental Disorders (DSM-5®)*. American Psychiatric Pub; 2013.
2. Ferrari AJ, Somerville A, Baxter A, et al. Global variation in the prevalence and incidence of major depressive disorder: a systematic review of the epidemiological literature. *Psychological medicine*. 2013;43(3):471-481. doi:10.1017/S0033291712001511
3. Ferrari AJ, Charlson FJ, Norman RE, et al. Burden of depressive disorders by country, sex, age, and year: findings from the global burden of disease study 2010. *PLoS Medicine*. 2013;10(11):e1001547. doi:10.1371/journal.pmed.1001547
4. Cuijpers P, Cristea IA, Karyotaki E, Reijnders M, Hollon SD. Component studies of psychological treatments of adult depression: A systematic review and meta-analysis. *Psychotherapy Research*. 2017;0(0):1-15. doi:10.1080/10503307.2017.1395922
5. Little A. Treatment-resistant depression. *American Family Physician*. 2009;80(2):167-172. doi:10.1136/thx.2008.108217
6. Locher C, Koechlin H, Zion SR, et al. Efficacy and safety of selective serotonin reuptake inhibitors, serotonin-norepinephrine reuptake inhibitors, and placebo for common psychiatric disorders among children and adolescents: A systematic review and meta-analysis. *JAMA Psychiatry*. 2017;74(10):1011-1020. doi:10.1001/jamapsychiatry.2017.2432
7. Cain RA. Navigating the Sequenced Treatment Alternatives to Relieve Depression (STAR D) Study: Practical Outcomes and Implications for Depression Treatment in Primary Care. *Primary Care: Clinics in Office Practice*. 2007;34(3):505-519.
8. Ingram A, Saling MM, Schweitzer I. Cognitive side effects of brief pulse electroconvulsive therapy: a review. *The journal of ECT*. 2008;24(1):3-9.
9. George MS, Lisanby SH, Avery D, McDonald WM, Durkalski V. Daily Left Prefrontal Transcranial Magnetic Stimulation Therapy for Major Depressive Disorder. 2014;67(5):507-516.
10. Allen EA, Pasley BN, Duong T, Freeman RD. Transcranial magnetic stimulation elicits coupled neural and hemodynamic consequences. *Science*. 2007;317(5846):1918-1921.
11. Ishikawa S, Matsunaga K, Nakanishi R, et al. Effect of theta burst stimulation over the human sensorimotor cortex on motor and somatosensory evoked potentials. *Clinical Neurophysiology*. 2007;118(5):1033-1043.
12. Esser SK, Huber R, Massimini M, Peterson MJ, Ferrarelli F, Tononi G. A direct demonstration of cortical LTP in humans: A combined TMS/EEG study. *Brain Research Bulletin*. 2006;69(1):86-94. doi:10.1016/j.brainresbull.2005.11.003
13. Valero-Cabré A, Payne BR, Pascual-Leone A. Opposite impact on 14C-2-deoxyglucose brain metabolism following patterns of high and low frequency repetitive transcranial magnetic stimulation in the posterior parietal cortex. *Experimental Brain Research*. 2007;176(4):603-615. doi:10.1007/s00221-006-0639-8
14. de Weijer AD, Sommer IEC, Bakker EJ, et al. A setup for administering TMS to medial and lateral cortical areas during whole-brain fMRI recording. *Journal of clinical neurophysiology*. 2014;31(5):474-487. doi:10.1097/WNP.0000000000000075
15. Bestmann S, Baudewig J, Siebner HR, Rothwell JC, Frahm J. BOLD MRI responses

to repetitive TMS over human dorsal premotor cortex. *Neuroimage*. 2005;28(1):22-29. doi:10.1016/j.neuroimage.2005.05.027

16. Rahman A, Reato D, Arlotti M, et al. Cellular effects of acute direct current stimulation: somatic and synaptic terminal effects. *The Journal of physiology*. 2013;591(Pt 10):2563-2578. doi:10.1113/jphysiol.2012.247171

17. O'Reardon JP, Solvason HB, Janicak PG, et al. Efficacy and Safety of Transcranial Magnetic Stimulation in the Acute Treatment of Major Depression: A Multisite Randomized Controlled Trial. *Biological Psychiatry*. 2007;62(11):1208-1216. doi:10.1016/j.biopsych.2007.01.018

18. Videbech P. PET measurements of brain glucose metabolism and blood flow in major depressive disorder: a critical review. *Acta Psychiatrica Scandinavica*. 2000;101(1):11-20. doi:10.1034/j.1600-0447.2000.101001011.x

19. Mayberg HS, Brannan SK, Tekell JL, et al. Regional metabolic effects of fluoxetine in major depression: serial changes and relationship to clinical response. *Biological psychiatry*. 2000;48(8):830-843.

20. Mayberg HS, Lozano AM, Voon V, et al. Deep brain stimulation for treatment-resistant depression. *Neuron*. 2005;45(5):651-660. doi:10.1016/j.neuron.2005.02.014

21. Kennedy SH, Evans KR, Krüger S, et al. Changes in Regional Brain Glucose Metabolism Measured With Positron Emission Tomography After Paroxetine Treatment of Major Depression. *American Journal of Psychiatry*. 2001;158(6):899-905. doi:10.1176/appi.ajp.158.6.899

22. Fox MD, Buckner RL, White MP, Greicius MD, Pascual-Leone A. Efficacy of transcranial magnetic stimulation targets for depression is related to intrinsic functional connectivity with the subgenual cingulate. *Biological Psychiatry*. 2012;72(7):595-603. doi:10.1016/j.biopsych.2012.04.028

23. Baeken C, Marinazzo D, Wu GR, et al. Accelerated HF-rTMS in treatment-resistant unipolar depression: Insights from subgenual anterior cingulate functional connectivity. *The world journal of biological psychiatry : the official journal of the World Federation of Societies of Biological Psychiatry*. 2014;32(0):1-12. doi:10.3109/15622975.2013.872295

24. Fitzgerald PB, Hoy K, Mcqueen S, et al. A Randomized Trial of rTMS Targeted with MRI Based Neuro-Navigation in Treatment-Resistant Depression. *Neuropsychopharmacology*. 2009;34. doi:10.1038/npp.2008.233

25. Sack AT, Cohen Kadosh R, Schuhmann T, Moerel M, Walsh V, Goebel R. Optimizing Functional Accuracy of TMS in Cognitive Studies: A Comparison of Methods. *Journal of Cognitive Neuroscience*. 2009;21(2):207-221. doi:10.1162/jocn.2009.21126

26. Rossi S, Hallett M, Rossini PM, et al. Safety, ethical considerations, and application guidelines for the use of transcranial magnetic stimulation in clinical practice and research. *Clinical Neurophysiology*. 2009;120(12):2008-2039. doi:10.1016/j.clinph.2009.08.016

27. Mandija S, Petrov PI, Neggers SFW, Luijten PR, Berg CAT. MR-based measurements and simulations of the magnetic field created by a realistic transcranial magnetic stimulation (TMS) coil and stimulator. *NMR in Biomedicine*. 2016;29(11):1590-1600.

28. Penny WD, Friston KJ, Ashburner JT, Kiebel SJ, Nichols TE. *Statistical Parametric Mapping: The Analysis of Functional Brain Images*. Academic press; 2011.

29. Ahdab R, Ayache SS, Brugières P, Goujon C, Lefaucheur JP. Comparison of "standard"

- and “navigated” procedures of TMS coil positioning over motor, premotor and prefrontal targets in patients with chronic pain and depression. *Neurophysiologie Clinique/Clinical Neurophysiology*. 2010;40(1):27-36. doi:10.1016/j.neucli.2010.01.001
30. Schutter DJLG, van Honk J. A standardized motor threshold estimation procedure for transcranial magnetic stimulation research. *The journal of ECT*. 2006;22(3):176-178. doi:10.1097/01.yct.0000235924.60364.27
  31. Ashburner J, Friston KJ. Unified segmentation. *Neuroimage*. 2005;26(3):839-851.
  32. Desmond JE, Glover GH. Estimating sample size in functional MRI (fMRI) neuroimaging studies: statistical power analyses. *Journal of neuroscience methods*. 2002;118(2):115-128.
  33. Thirion B, Pinel P, Mériaux S, Roche A, Dehaene S, Poline JB. Analysis of a large fMRI cohort: Statistical and methodological issues for group analyses. *Neuroimage*. 2007;35(1):105-120.
  34. Conen S, Matthews JC, Patel NK, Anton-Rodriguez J, Talbot PS. Acute and chronic changes in brain activity with deep brain stimulation for refractory depression. *Journal of psychopharmacology (Oxford, England)*. Published online 2017:269881117742668. doi:10.1177/0269881117742668
  35. Tsolaki E, Espinoza R, Pouratian N. Using probabilistic tractography to target the subcallosal cingulate cortex in patients with treatment resistant depression. *Psychiatry Research - Neuroimaging*. 2017;261(January):72-74. doi:10.1016/j.pscychresns.2017.01.006
  36. Kibleur A, Polosan M, Favre P, et al. Stimulation of subgenual cingulate area decreases limbic top-down effect on ventral visual stream: A DBS-EEG pilot study. *NeuroImage*. 2017;146(April 2016):544-553. doi:10.1016/j.neuroimage.2016.10.018
  37. Dougherty D, Chou T, Corse andrew K, et al. Acute deep brain stimulation changes in regional cerebral blood flow in obsessive-compulsive disorder. *J neurosurg*. 2016;125(November):1087-1093. doi:10.3171/2015.9.JNS151387
  38. De Ridder D, Leong SL, Manning P, Vanneste S, Glue P. Anterior Cingulate Implant for Obsessive-Compulsive Disorder. *World Neurosurgery*. 2017;97:754.e7-754.e16. doi:10.1016/j.wneu.2016.10.046
  39. Bestmann S, Baudewig J, Siebner HR, Rothwell JC, Frahm J. Functional MRI of the immediate impact of transcranial magnetic stimulation on cortical and subcortical motor circuits. *European Journal of Neuroscience*. 2004;19(7):1950-1962. doi:10.1111/j.1460-9568.2004.03277.x
  40. Amunts K, Schleicher A, Bürgel U, Mohlberg H, Uylings H, Zilles K. Broca’s region revisited: cytoarchitecture and intersubject variability. *Journal of Comparative Neurology*. 1999;412(2):319-341.
  41. Watson J, Myers R, Frackowiak RS, et al. Area V5 of the human brain: evidence from a combined study using positron emission tomography and magnetic resonance imaging. *Cerebral Cortex*. 1993;3(2):79-94. doi:10.1093/cercor/3.2.79
  42. der Malsburg C, Phillips WA, Singer W. *Dynamic Coordination in the Brain: From Neurons to Mind*. MIT Press; 2010.
  43. Thiebaut de Schotten M, ffytche DH, Bizzi A, et al. Atlasing location, asymmetry and inter-subject variability of white matter tracts in the human brain with MR diffusion tractography.

*NeuroImage*. 2011;54(1):49-59. doi:10.1016/j.neuroimage.2010.07.055

44. Bürgel U, Amunts K, Hoemke L, Mohlberg H, Gilsbach JM, Zilles K. White matter fiber tracts of the human brain: three-dimensional mapping at microscopic resolution, topography and intersubject variability. *Neuroimage*. 2006;29(4):1092-1105.

45. Mueller S, Wang D, Fox MD, et al. Individual variability in functional connectivity architecture of the human brain. *Neuron*. 2013;77(3):586-595.

46. Allen EA, Damaraju E, Plis SM, Erhardt EB, Eichele T, Calhoun VD. Tracking whole-brain connectivity dynamics in the resting state. *Cerebral Cortex*. 2014;24(3):663-676. doi:10.1093/cercor/bhs352

47. Handwerker DA, Roopchansingh V, Gonzalez-Castillo J, Bandettini PA. Periodic changes in fMRI connectivity. *Neuroimage*. 2012;63(3):1712-1719.

48. Sauseng P, Klimesch W, Gerloff C, Hummel FC. Spontaneous locally restricted EEG alpha activity determines cortical excitability in the motor cortex. *Neuropsychologia*. 2009;47(1):284-288. doi:10.1016/j.neuropsychologia.2008.07.021

49. Romei V, Brodbeck V, Michel C, Amedi A, Pascual-Leone A, Thut G. Spontaneous fluctuations in posterior alpha-band EEG activity reflect variability in excitability of human visual areas. *Cerebral cortex*. 2008;18(9):2010-2018.

50. Fox MD, Corbetta M, Snyder AZ, Vincent JL, Raichle ME. Spontaneous neuronal activity distinguishes human dorsal and ventral attention systems. *Proceedings of the National Academy of Sciences*. 2006;103(26):10046-10051.

51. Arieli A, Sterkin A, Grinvald A, Aertsen AD. Dynamics of ongoing activity: explanation of the large variability in evoked cortical responses. *Science*. 1996;273(5283):1868.

52. Yau JM, Jalinous R, Cantarero GL, Desmond JE. Static field influences on transcranial magnetic stimulation: Considerations for TMS in the scanner environment. *Brain Stimulation*. 2014;7(3):388-393. doi:10.1016/j.brs.2014.02.007

53. Lisanby SH, Gutman D, Luber B, Schroeder C, Sackeim HA. Sham TMS: Intracerebral measurement of the induced electrical field and the induction of motor-evoked potentials. *Biological Psychiatry*. 2001;49(5):460-463. doi:10.1016/S0006-3223(00)01110-0

54. Baudewig J, Siebner HR, Bestmann S, et al. Functional MRI of cortical activations induced by transcranial magnetic stimulation (TMS). *Neuroreport*. 2001;12(16):3543-3548.

55. Tagamets MA, Horwitz B. Interpreting PET and fMRI measures of functional neural activity: The effects of synaptic inhibition on cortical activation in human imaging studies. *Brain Research Bulletin*. 2001;54(3):267-273. doi:10.1016/S0361-9230(00)00435-4

56. Ruff CC, Bestmann S, Blankenburg F, et al. Distinct causal influences of parietal versus frontal areas on human visual cortex: Evidence from concurrent TMS-fMRI. *Cerebral Cortex*. 2008;18(4):817-827. doi:10.1093/cercor/bhm128







## Chapter 3

# EEG functional connectivity is a weak predictor of causal brain interactions

Jord JT Vink

Deborah CW Klooster

Recep A. Ozdemir

M Brandon Westover

Alvaro Pascual-Leone

Mouhsin M Shafi

*Vink, Jord JT, et al. "EEG functional connectivity is a weak predictor of causal brain interactions." Brain topography 33.2 (2020): 221-237.*

## **ABSTRACT**

### **Introduction**

In recent years, there has been an explosion of research evaluating resting-state brain functional connectivity (FC) using different modalities. However, the relationship between such measures of FC and the underlying causal brain interactions has not been well characterized.

### **Methods**

To further characterize this relationship, we assessed the relationship between EEG resting state FC and propagation of transcranial magnetic stimulation (TMS) evoked potentials (TEPs) at the sensor and source level in healthy participants. TMS was applied to 6 different cortical regions in 10 healthy individuals (9 male; 1 female), and effects on brain activity were measured using simultaneous EEG. Pre-stimulus FC was assessed using 5 different FC measures (Pearson's correlation, mutual information, weighted phase lag index, coherence and phase locking value). Propagation of the TEPs was quantified as the root mean square (RMS) of the TEP voltage and current source density (CSD) at the sensor and source level, respectively. The relationship between pre-stimulus FC and the spatial distribution of TEP activity was determined using a generalized linear model (GLM) analysis.

### **Results**

On the group level, all FC measures correlated significantly with TEP activity over the early (15-75ms) and full range (15 – 400ms) of the TEP at the sensor and source level. However, the predictive value of all FC measures was quite limited, accounting for less than 10% of the variance of TEP activity, and varied substantially across participants and stimulation sites.

### **Conclusion**

These results suggest that EEG functional connectivity studies in sensor and source space should be interpreted with caution.

## INTRODUCTION

In recent years, it has become apparent that normal brain function results from activity across distributed networks of brain regions that engage in complex, dynamic interactions. Consequently, brain connectomics has emerged as a major area of investigation<sup>1,2</sup>. Brain connectivity is generally studied in the task-free resting state using modalities such as electroencephalography (EEG), magnetoencephalography (MEG), and functional Magnetic Resonance Imaging (fMRI). The evaluation of functional connectivity (FC) is used to understand brain function in healthy individuals and in patients with a wide range of neuropsychiatric diseases ranging from stroke to schizophrenia<sup>3-5</sup>. In FC studies, two regions are said to be functionally connected if their activity is statistically correlated, and this FC is often interpreted to indicate causal interactions between those brain regions. However, the fundamental assumption that resting-state FC reflects causal brain interactions has not been adequately verified. Specifically, there is limited evidence that FC between two regions is related to direct electrophysiological interactions between them.

A problem in the study of EEG and MEG connectivity is the appropriate level of analysis. Specifically, EEG signals are recorded from the scalp, and reflect the superposition of the signals originating from the entire cortical surface. Consequently, some studies suggest that sensor-space analyses are sub-optimal for the assessment of causal interactions between brain regions<sup>6</sup>. However, the localization of the underlying brain signals is fundamentally ambiguous because the inverse problem of identifying the cortical sources that generate the scalp EEG signals is “ill-posed”, with an infinite number of possible solutions. Consequently, a wide variety of different methods exist for estimating source solutions, often with varying results for the same scalp recording<sup>6,7</sup>. Thus, despite the intensive interest in FC, the relationship between these different measures of FC and the underlying neurophysiological interactions remains poorly understood<sup>8</sup>, at the sensor and source level. An additional problem in the interpretation of FC is the variety of FC measures that are used in the literature. These measures capture different aspects of the underlying brain signal, and thus produce different connectivity patterns<sup>9,10</sup>.

Previous efforts have tried to shed light on the relationship between functional connectivity and the spatial distribution of evoked activity by combining fMRI and invasive stimulation/recording techniques in macaques<sup>11</sup> and human patients with epilepsy<sup>12</sup>, intracranial EEG recording and stimulation in epilepsy patients<sup>13</sup>, or optogenetic stimulation and intracranial EEG recording in macaques<sup>14</sup>. However, these studies only investigated a small sample, often focused primarily on connectivity within the primary somatomotor network (which is known to exhibit relatively stable connectivity), and are necessarily limited in their scope insofar as these techniques cannot be applied in human populations without implanted intracranial EEG electrodes (which are currently limited to patients with refractory epilepsy).

Transcranial Magnetic Stimulation (TMS) uses electromagnetic induction to directly stimulate a targeted cortical region. Although stimulation is applied focally, the effects of TMS do not remain local (in the targeted cortical region), but spread to other brain regions<sup>15-17</sup>, with the propagation pattern presumably determined by connectivity between the stimulated region and other brain areas<sup>18</sup>. When combined with EEG, TMS can be used to assess local and distant brain responses to controlled perturbations. Consequently, TMS in combination with EEG can be used to test the hypothesis that resting-state FC reflects electrophysiological interactions between brain regions. Recent work has already indicated that such a relationship exists for hemodynamic data, by comparing resting state fMRI FC of the DLPFC with the spatial distribution of activity evoked at the DLPFC<sup>19</sup>. To the best of our knowledge, this relationship has not yet been investigated using electro-cortical oscillations as measured with concurrent TMS-EEG.

To test whether the relationship between resting-state FC and causal brain interactions also exists for electro-cortical oscillations, we acquired concurrent TMS-EEG data of ten healthy volunteers. Because of the above mentioned limitations, we performed a broad study, using EEG in sensor- and source-space and quantifying FC with multiple measures. Specifically, we hypothesized that sensor- and source-level measures of EEG resting-state FC predict the spatial distribution of TMS-evoked potentials (TEPs).

## METHODS

### Data acquisition

TMS-EEG data was recorded from 11 healthy right-handed participants. Written informed consent was provided by all and the experimental procedure was approved by the Committee for Clinical Investigations of Beth Israel Deaconess Medical Center. One participant was excluded from the study because of TMS intolerance (excessive discomfort with TMS-induced scalp muscle contractions), leaving 10 participants (mean age: 38 (20-63 years); 9 males, 1 female; all right-handed) for data analysis.

EEG was recorded with a 60-channel TMS-compatible eXimia EEG system (Nexstim, Helsinki, Finland). The reference and ground electrodes were placed on the forehead. EEG signals were recorded at 1450 Hz with 16-bit resolution, and were band-pass filtered between 0.1 and 500 Hz. Two additional sensors were used to record the electro-oculogram (EOG). Electrode impedance was kept below 5kOhms.

Single biphasic pulses of TMS were administered via a Nexstim eXimia stimulator using a figure-of-eight coil (mean diameter 59 mm, outer diameter 70 mm). Stimulation was applied using MRI-guided neuronavigation to six different anatomically defined target sites in each individual (Figure 1A): the left and right dorsolateral prefrontal cortex (DLPFC), primary motor cortex (M1) and parietal cortex (PAR). The DLPFC target was anatomically defined as a point on the superior aspect of the middle frontal gyrus, 1-2 cm anterior to the premotor gyrus. The M1 target was the motor hotspot, defined as the point that produced the largest EMG response in the first dorsal interosseous (FDI) muscle. The parietal target was the posterior half of the angular gyrus, 1-2 cm below the intraparietal sulcus. These sites were selected because: (1) The targets in the middle frontal gyrus and angular gyrus are part of the prefrontal and parietal association cortices respectively, with relatively complex connectivity across participants (Mueller et al, 2013, Neuron), whereas M1 is part of the somatomotor network with more stereotyped connectivity; (2) These sites are generally part of distinct functional networks (middle frontal gyrus - frontoparietal control network; Angular – DMN; M1 – somatomotor network) and thus should have distinct functional connectivity. The TMS coil was oriented so that the direction of the TMS electrical field was oriented perpendicular to the orientation of the target gyrus, with the coil handle oriented posterolaterally to the site of stimulation. For example, for left M1, the coil handle was oriented posteriorly at approximately 45° to the mid-sagittal line. Stimulation was applied at 120% resting motor threshold (RMT), defined as the lowest intensity at which TMS to M1 induced a motor evoked potential (MEP) in the contralateral FDI muscle of more than 50  $\mu$ V in 5 out of 10 trials. In addition, all participants received sham stimulation, in which the TMS coil was positioned over the left M1 while rotated 90 degrees (with the plane of the coil perpendicular rather than parallel to the scalp), so that the TMS coil rested on the participant's scalp on edge. This was done in order to obtain the sham-evoked potential, which was used to control for auditory and some of the somatosensory sensations associated with the TMS pulse<sup>20</sup>. Participants received between 80 and 110 single pulses to each site, with a random inter stimulus interval of 4 to 6s to avoid

conditioning. Participants were seated comfortably in a reclining chair with their eyes open and were asked to look straight ahead at a fixation point, while TMS was delivered according to the guidelines and recommendations for TMS endorsed by the International Federation for Clinical Neurophysiology<sup>21</sup>.

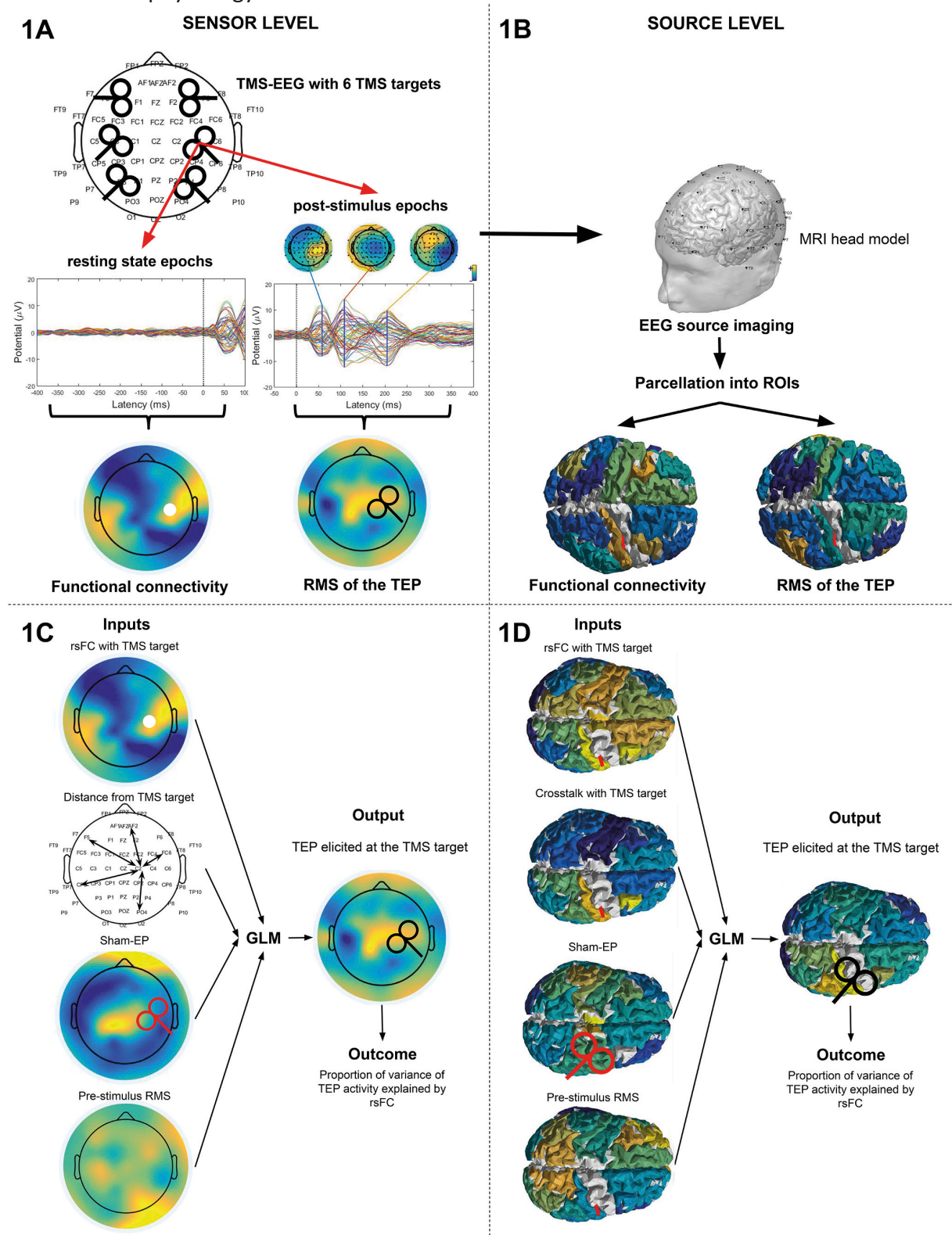


**Figure 1.** Schematic overview of the analysis. **A.** TMS targets during the TMS-EEG acquisition. The DLPFC, M1 and parietal cortices of both hemispheres were stimulated. Pre-stimulus and post-stimulus epochs were obtained from the data for resting state functional connectivity

analyses and TEP analysis, respectively. **B.** EEG source imaging was used for analysis in source space. **C.** Inputs and output of the GLM analysis: FC map with the TMS target as the seed region; the distance between the TMS target and the other channels; the sham-EP and the pre-stimulus RMS; An evoked activity map. The white circle illustrates the TMS target (RM1), the red TMS coil indicates sham stimulation while the black coil indicates active stimulation. **D.** Similar inputs were used at the source level. The distance between the electrodes was replaced with crosstalk. The white circle illustrates the TMS target (RM1), the red TMS coil indicates sham stimulation while the black coil indicates active stimulation.

## Preprocessing

Data analysis was performed with custom scripts, EEGLAB 14.1.2b<sup>22</sup>, Brainstorm<sup>23</sup> and Fieldtrip<sup>24</sup> in the Matlab R2015a environment (MathWorks Inc., USA). An ICA-based cleaning procedure was used to remove artifacts from the pre- and post-stimulus segments<sup>25</sup>. The data were divided into pre- and post-stimulus segments of -2900 to -400ms and -500 to 1000ms, respectively, with TMS pulse delivery at 0ms (**Figure 1A**). An average of 3.4 (range: 1-6) and 3.3 bad channels (range: 0-6) were removed and interpolated from the pre- and post-stimulus data, respectively. Pre- and post-stimulus segments were baseline corrected on -3300 to -2500ms and -900 to -100ms, respectively. All data were baseline-corrected to minimize the difference between the two preprocessing pipelines. The TMS artifact in the post-stimulus segment was zero-padded from 0 to 14ms. A semi-automated procedure was used to detect and remove noisy epochs in all data<sup>25</sup>, resulting in the removal of an average of 18 pre-stimulus epochs (range: 3-50) and 14 post-stimulus epochs (range: 5-41), leaving an average of 80 pre-stimulus epochs (range: 50-112) and 83 post-stimulus epochs (range: 65-116). The TMS-evoked exponential decay artifact was removed from the post-stimulus segment in a first round of ICA. Thereafter, Gaussian interpolation was used to fill in the missing data from 0 to 14ms. Both the pre- and post-stimulus segments were filtered with a bandpass filter of 1 to 100Hz and a bandstop filter of 55 to 65Hz using a fourth-order Butterworth filter with forward and backward filtering. Both segments were referenced to the average reference and then subjected to another round of ICA in which blink artefacts, muscle artefacts and other noise related artefacts were removed. After the cleaning procedure, an average of 20 ICA components (range: 12 - 26) were removed from the pre-stimulus data, and 16 ICA components (range: 8 - 24) were removed from the post-stimulus data.

Individual electrode data, topoplots from -50 to 300ms around stimulation with intervals of 10ms, and the global mean field potential (GMFP), were visually inspected by an experienced investigator (MMS) for the presence of non-physiological activity. The preprocessing procedure was repeated in case of non-physiological activity.

Volume conduction has been shown to affect functional connectivity in scalp level EEG data<sup>6</sup>. To minimize any potential confounding effects of volume conduction, we also evaluated the relationship between functional connectivity and evoked activity data using the surface laplacian reference<sup>26</sup>. For this analysis, the data was rereferenced to the surface laplacian reference after completing the aforementioned preprocessing procedure.

## Source Analysis

The relationship between functional connectivity and evoked activity was also assessed at the source level. EEG source imaging (ESI) was performed (**Figure 1B**) using BrainStorm<sup>23</sup>. Individual three-layer head models were generated based on individual anatomical MRI data using OpenMEEG<sup>27</sup>. The cortical surface was sampled at 15,000 vertices, to minimize



computational load while maintaining accuracy of individual brain morphology. A current dipole was assigned to each of the vertices of the cortical surface. The dipoles are oriented perpendicular to the cortical surface, so that they align with the cortical pyramidal neurons which are presumed to generate most of the EEG activity. The coordinates of the EEG electrodes (as captured using the neuronavigation system) were used to position them within the individual head model. OpenMEEG, which is based on a symmetric boundary element method, was used to compute the leadfield matrix with the default parameter settings. The noise covariance matrix was computed from -2900 to -2400ms and from -500 to 0ms of the pre- and post-stimulus segments, respectively. Subsequently, the linear L2-minimum norm estimates (wMNI) algorithm was used to solve the ill-posed inverse problem<sup>28</sup>. We selected 42 parcels from the Desikan-Killiany atlas<sup>29</sup> for analysis (a table of included parcels is shown in supplemental materials), disregarding the deeper parcels. We disregarded deeper parcels because the accuracy of source estimation is controversial for deeper structures<sup>30</sup>, although advances in the detection of activity in deeper sources has been made<sup>31</sup>. As the dipoles are oriented perpendicular to the cortical surface, the average signal of a parcel which contains opposing gyral surfaces cancels out. Therefore, the dominant dipole orientation of each parcel was determined by means of singular value decomposition of the orientations of all dipoles within the parcel. The time-series of the dipoles that were not aligned with the dominant orientation of the parcel were flipped. Subsequently, the source-space time-series were averaged to obtain a single time-series for each parcel.

### Data analysis

We set out to identify whether resting state FC measured prior to the delivery of a TMS-pulse predicts the spatial distribution of the TEP, by introducing these variables in a generalized linear model (GLM). The pre- and post-stimulus scalp and source segments data were filtered with second-order Butterworth filters to organize the data into 5 frequency bands: broadband (1 – 80Hz), theta (4 – 8Hz), alpha (8 – 12Hz), beta (12 – 30Hz) and gamma (30-80Hz) band. The analyses were based on broadband data unless specified otherwise. In addition to pre-stimulus FC and post-stimulus TEP activity, we used a volume conduction control, sham-EP and pre-stimulus RMS as nuisance regressors in the GLM analysis. The inputs and output are shown schematically in Figure 1C and 1D, for sensor and source space respectively. Calculation of the GLM inputs is described in more detail in sections 2.4.1 to 2.4.4. GLMs were constructed for each participant and stimulation site separately. The GLMs were fitted using a gamma distribution (with reciprocal link function), due to the non-negative nature of the outcome variable (the RMS of the TEP). Calculation of the input and response variables is described in more detail below. The input variables were calculated for the sensor- and source-level data, unless explicitly mentioned otherwise in the sections below.

#### *Resting state functional connectivity maps*

The MRI-guided navigation system registers the position of the TMS coil isocenter with respect to the positions of the EEG electrodes; the TMS target electrode was defined as the EEG electrode or the parcel closest to the TMS coil isocenter. The FC strength between the TMS target electrode (seed) and all the other channels (and the stimulated parcel and all other parcels in the source analysis) was calculated for each pre-stimulus epoch, individually. The FC values for the individual epochs were averaged together to obtain a single FC map per participant and stimulation site. We included five different FC measures in our analysis, producing five FC maps per stimulation site and participant (**Figure 3**). We selected weighted phase lag index (wPLI;<sup>32</sup>), phase-locking value (PLV;<sup>33</sup>), magnitude squared interchannel

coherence (ICC;<sup>34</sup>), Pearson's correlation (R) and mutual information (MI;<sup>35</sup>) for our FC analysis. Because concerns have been raised on the reliability of directed connectivity measures<sup>36</sup>, we restricted our analysis to non-directional measures of connectivity. We included a diverse group of FC measures, as MI and C are time-based FC measures, wPLI and PLV are phase-based FC measures and the ICC is a power-based FC measure.

All FC measures were calculated using Fieldtrip<sup>24</sup>. FC measures were calculated for the interval of -2900 to -400ms, with TMS pulse delivery at 0ms, to minimize the effect of edge artefacts. MI was calculated with 13 bins and equipopulated binning. Both the wPLI and the ICC were determined from cross power spectral density data, which was calculated with a single taper with 0.5Hz smoothing. The formulae for the connectivity and evoked activity measures are provided in **Table 1**.

Pearson's correlation and wPLI potentially exhibit negative FC, while the other measures are positive by default. To maintain consistency we decided to calculate the absolute value of all FC values. However, negative FC potentially indicates inhibitory connectivity, which might not result in evoked activity. Therefore, we also investigated whether the predictive value of Pearson's correlation and wPLI increased when negative FC values were excluded from analysis.

**Table 1.** Details on connectivity and evoked activity measures.

Measure	Formula	Details
Pearson's correlation	$\rho(X, Y) = \frac{cov(X, Y)}{\sigma(X)\sigma(Y)}$	With covariance <i>cov</i> and standard deviation $\sigma$ .
Mutual information	$MI(X, Y) = H(X) + H(Y) - H(X, Y)$	With entropy <i>H</i> .
Weighted phase lag index	$wPLI = \frac{ imag(S_{xy}) sgn(imag(S_{xy}))}{ imag(S_{xy}) }$	With cross power spectral density $S_{xy}$ .
Coherence	$C_{xy}(\omega) = \frac{ S_{xy}(\omega) ^2}{S_{xx}(\omega)S_{yy}(\omega)}$	With the spectral densities $S_{xx}$ , $S_{yy}$ and $S_{xy}$ .
Phase locking value	$PLV(t) =  E[e^{j\Delta\varphi(t)}] $	With the expected value <i>E</i> and the relative phase $\varphi$ .
Root mean square	$RMS = \sqrt{\frac{1}{n} \sum_i^n X_i^2}$	With the time data series <i>X</i> .

### Evoked activity maps

For all channels, the post-stimulus epochs of active and sham TMS data were averaged to obtain the average TEP and sham-EP, respectively. TEP and sham-EP activity maps were obtained by calculating the root mean square (RMS) voltage and the current source density (CSD) of the EP in sensor and source space, respectively. The RMS voltage and CSD were calculated for the early interval (15 to 75ms; **Fig 4**) and the full interval (15 to 400ms) of the TEP. As it is possible that TEP activity beyond 75ms is not directly related to activation of the stimulated site, but rather related to activation of remote regions, we specifically evaluated the early time window (from 15 – 75ms) to identify whether functional connectivity only captures TEP propagation directly from the stimulated target. Additionally, the activity beyond the first 75ms of the TEP may include peripherally evoked potentials (PEPs)<sup>37</sup>, contaminating

our analysis.

### *Nuisance variables*

We included three nuisance variables in the analysis: a volume conduction control, the spatial distribution of the sham-EP and the pre-stimulus RMS voltage or CSD.

In the sensor space analysis, a volume conduction control was determined by calculating the absolute Euclidean distance between the TMS target electrode and all the other electrodes, based on the coordinates provided by the navigation system. For the source space analysis, cross-talk functions (CTFs) were used to estimate volume conduction effects between sources<sup>38</sup>. The volume conduction control was included as a nuisance regressor to correct for a spurious relationship between FC and TEP activity due to shared volume conduction effects. As an additional control to ensure that volume conduction was not responsible for our results, we also repeated our analysis using EEG data with a surface laplacian reference (in sensor space only).

The spatial distribution of the sham-EP was included in the GLM analysis as a nuisance regressor in order to control for confounding evoked activity which is not directly related to activation of the stimulation target (e.g. the PEPs).

Pre-stimulus RMS was included to correct for baseline differences in signal strength across electrodes. Pre-stimulus RMS was determined between -250 and -50ms with respect to TMS pulse delivery at 0ms.

### **Statistical analysis**

The proportion of variance of TEP activity ( $R^2_{\text{total}}$ ) explained by all input variables was calculated for each participant at each stimulation site. This was corrected for the variance explained by the nuisance regressors ( $R^2_{\text{nuisance}}$ ), leaving the proportion of variance of the TEP explained by FC only ( $R^2_{\text{FC}}$ ).

$$R^2_{\text{total}} = R^2_{\text{FC}} + R^2_{\text{nuisance}}$$

Random permutation statistics was used to determine significance on the individual level. This was done by calculating 2,000 random permutations of the rank order of the FC map for each analysis. We randomly permuted the rank order to maintain a biologically feasible range of FC values. The randomly permuted FC map was used in the previously described GLM analysis to calculate a random distribution of  $R^2_{\text{FC}}$  values. On the individual level, a p-value was calculated for each participant and stimulation site, separately, using the following formula:

$$p = \frac{(\text{amount of permutations} > R^2_{\text{FC}}) + 1}{\text{total amount of permutations} + 1}$$

To determine significance on the group-level, the  $R^2_{\text{FC}}$  values of all participants and stimulation sites were averaged together for each permutation to obtain a group-level distribution of  $R^2_{\text{FC}}$  values. Next, a group-level p-value was calculated by calculating the amount of permutations that exceed the mean  $R^2_{\text{FC}}$  using the previously described formula. The family wise error (FWE) rate was used to correct the alpha level of different analyses for multiple comparisons.

A Kruskal Wallis test was performed to test whether the investigated FC measures are equally informative on TEP activity. In case of significance, multiple Mann Whitney U tests were performed to determine whether the measure which explained most variance was significantly more informative than the other measures. Finally, a paired t-test was used to determine whether combining the FC measures in a single analysis improved the predictive value with respect to the single best-performing FC measure (FC measure with the highest

mean  $R^2_{FC}$ ). As the inclusion of more variables to the GLM increases the proportion of variance explained, random permutations of the single FC measure were added to the GLM analysis of the individual FC measure to match the number of variables in the GLM analysis of the combination of FC measures.

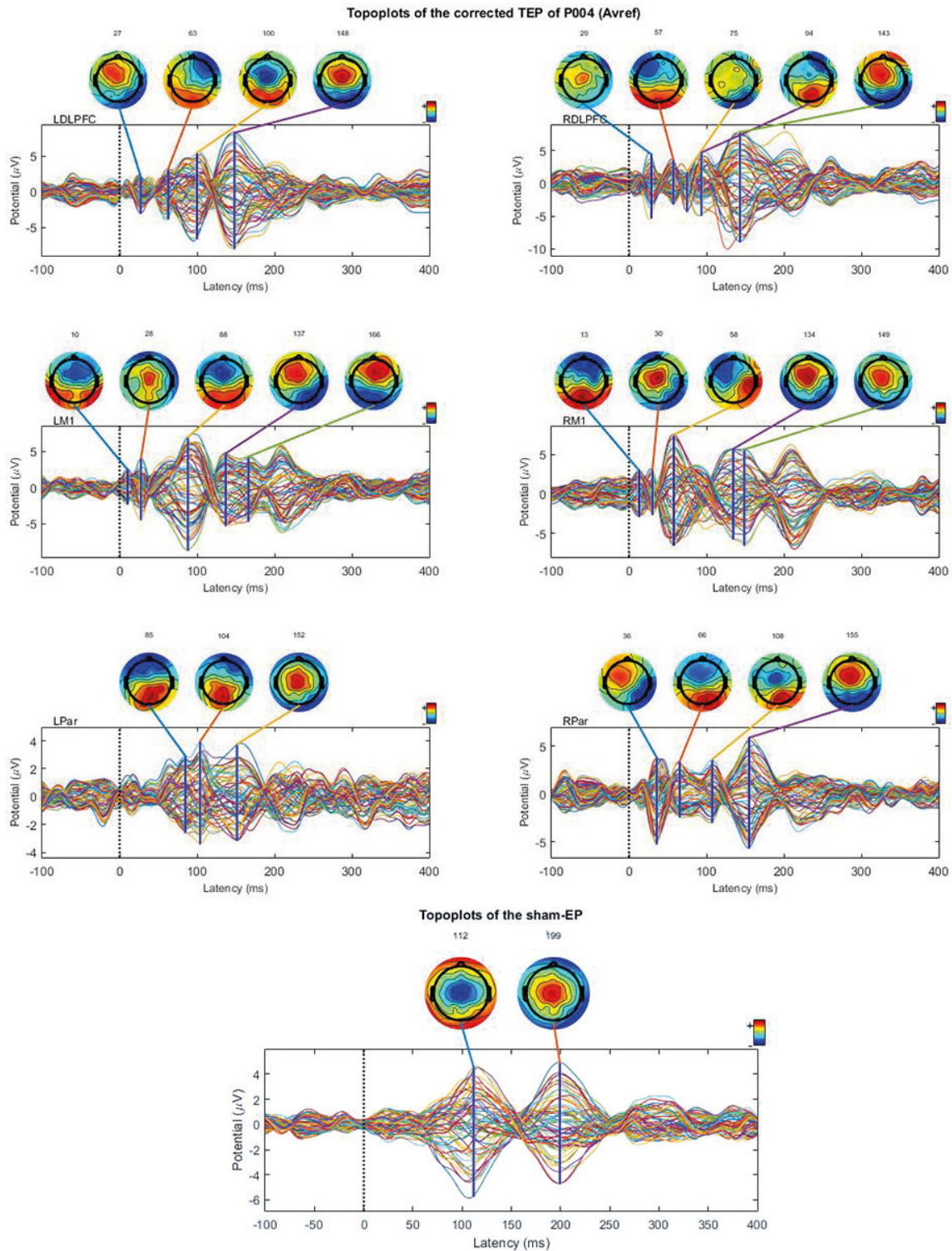
Further statistical testing was restricted to Pearson's correlation based FC (R-FC). One-sided paired t-tests were also used to determine whether the predictive value of R-FC improved when the analysis was restricted to the early interval of the TEP at the sensor and source level, as might be expected given the recent literature suggesting that later TEP activity may be contaminated by peripheral-evoked potentials<sup>37,39</sup>. A one sided paired t-test was used to investigate whether moving from sensor space to source space increased the predictive value of R-FC, as recent literature indicates a greater reliability of source-space connectivity<sup>6</sup>. Kruskal-Wallis tests were used to identify whether the informative value of R-FC varied between stimulation locations and frequency bands. In case of significance, multiple Mann Whitney U tests were performed to determine whether a single stimulation location or frequency band outperformed the others.

## RESULTS

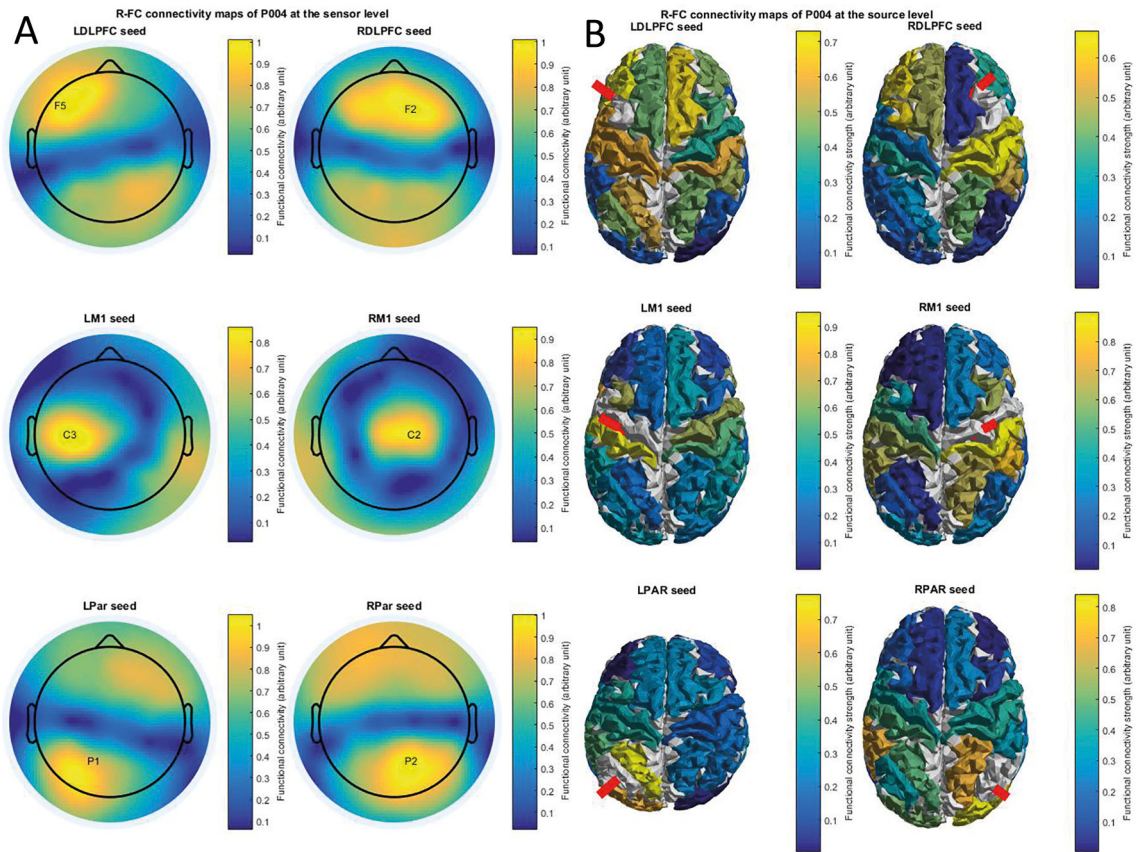
Time series of the sham-corrected TEPs elicited at the 6 different stimulation sites and the sham EP are shown for a representative participant (**Figure 2**; time series and topoplots of the uncorrected, sham-EPs and sham-corrected TEPs are presented in the supplemental materials). The sham-corrected TEP was calculated by subtracting the sham-EP time series from the TEP time series. Topoplots were constructed from the time series data at different time points, which were based on peaks in the GMFP of the EP. The topoplots show a dipole originating at the stimulation site which spreads to other regions. For example, the data obtained during stimulation of the LM1 shows a dipole near Cz at 28ms, which shifts posteriorly at 88ms. The TEP data clearly shows a distinct spatial distribution of activity compared to the sham-EP data.

Figure 3 shows Pearson's correlation based FC maps at the sensor (**Figure 3A**) and the source (**Figure 3B**) level of a representative participant. The sensor level maps show the stimulated electrode which was used as a seed for the connectivity analysis. In the source level maps the stimulated parcel which was used as a seed for the connectivity analysis is indicated by a red beam. The sensor level connectivity maps show strong local connectivity near the stimulation site, as well as connected foci more distally (e.g. the RDLPFC shows functional connectivity with the contralateral DLPFC and the bilateral parieto-occipital regions). The source level connectivity maps show more focal and complex connectivity patterns with high site specificity.

Figure 4 shows evoked activity for stimulation of 6 different TMS targets and for sham stimulation at the sensor (**Figure 4A**) and the source (**Figure 4B**) level of the same participant. In the source level maps the stimulated parcel is indicated by a red beam. Both sensor and source level maps show evoked activity at the stimulated site and distant regions, with variability across stimulation sites. The site-specificity of the evoked response is more prominent at the source level.



**Figure 2.** Sham-corrected time series of the TEPs elicited at the 6 different stimulation sites and the sham EP are shown for a representative participant. The sham-corrected time series have been obtained by subtracting the sham-EP from the raw TEP time series. Topoplots are constructed from the time series data at different time points, which are based on peaks in the GMFP of the EP.



**Figure 3.** Heatmaps of mean functional connectivity with different seed regions. Mean functional connectivity was averaged over multiple trials ranging from 2900 to 400ms before TMS pulse delivery. Color scales from minimum to maximum FC strength.

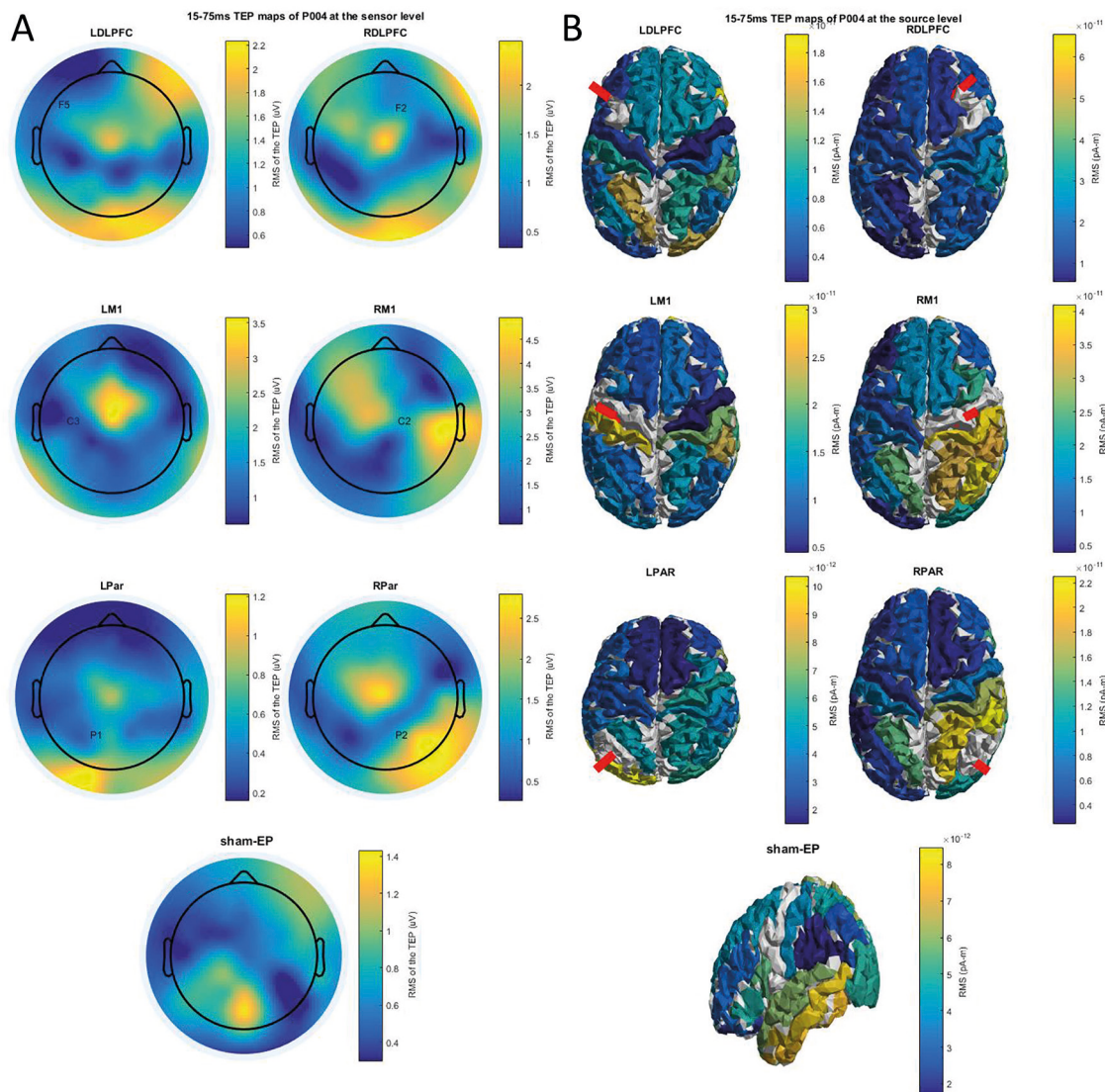


**Figure 4.** Heatmaps of the spatial distribution of the TEP as determined by the RMS of the TEP over a period 15 to 75ms after TMS pulse delivery, elicited at different cortical targets. Color scales between minimum and maximum RMS.

### Predictability

Our goal was to test the hypothesis that FC measures predict the spatial distribution of a TEP at the source and sensor level. We found that all of the resting state FC measures deliver a significant contribution to the explained variance of early (15 to 75ms) and full (15 to 400ms) TEP activity at both the sensor and source level, when corrected for nuisance regressors ( $p < 0.05$ , FWE corrected; **Figure 5**).

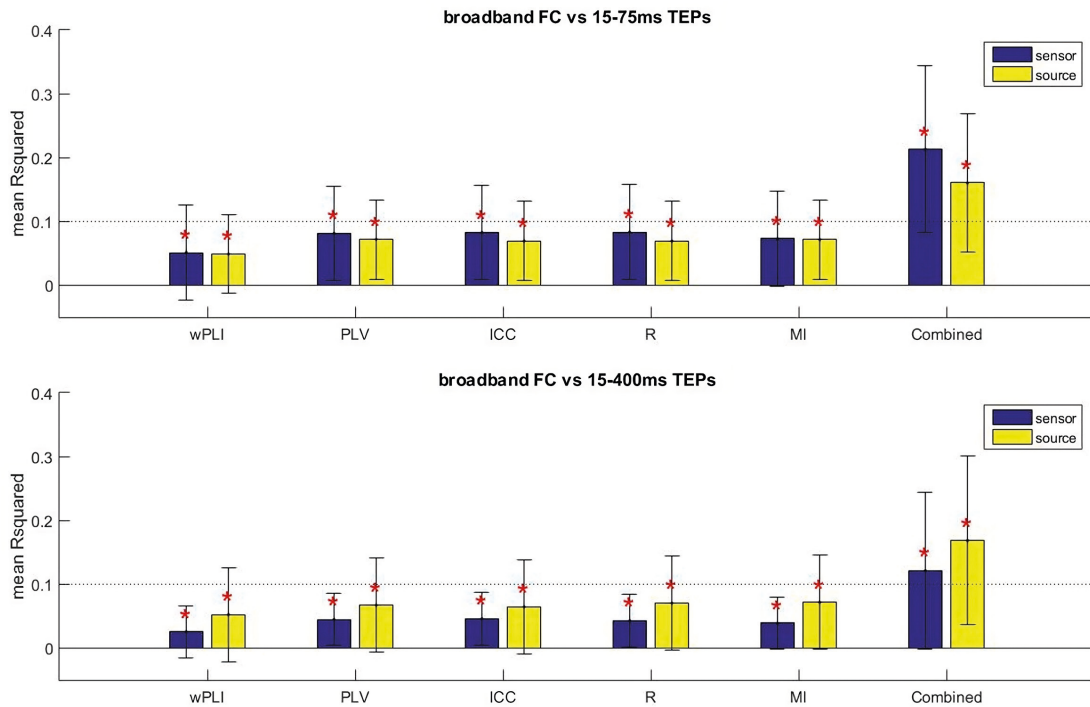


**Figure 5.** Mean proportion of variance of the spatial distribution of early (15-75ms) and full (15-400ms) TEP activity explained by functional connectivity (FC) at the sensor and source level. Different FC measures are shown. The error bar indicates the standard deviation. \*Significant contribution of FC ( $p < 0.05$ , FWE corrected).

The different FC measures performed equally well in the prediction of early (15-75ms) TEP activity at the sensor (Chi square = 2.36,  $p = 0.67$ ,  $df = 4$ , 295) and the source level (Chi square = 0.54,  $p = 0.97$ ,  $df = 4$ , 295). Adding all FC measures together into the model significantly improved the predictive value with respect to the single best FC measure (highest mean) at the sensor level (t-stat = 7.61,  $p < 0.05$ ,  $df = 59$ ), while this was not the case at the source level (t-stat = 1.15,  $p = 0.25$ ,  $df = 59$ ).

The different FC measures were also equally predictive of full TEP activity at the sensor (Chi square = 1.73,  $p = 0.79$ ,  $df = 4$ , 295) and source level (Chi square = 2.99,  $p = 0.56$ ,  $df = 4$ , 295). Combining all FC also significantly improved the predictive value at the sensor (t-stat = 2.79,  $p < 0.05$ ,  $df = 59$ ) and the source level (t-stat = 3.29,  $p < 0.05$ ,  $df = 59$ ). The results for the surface laplacian data were not substantially different from the average reference and are therefore restricted to supplemental materials.

We also investigated whether the predictive value of Pearson's correlation and wPLI increased when negative FC values were removed from the analysis. We found that removing negative FC values from the analysis did not consistently improve the predictive value of these measures at either the sensor and source level (see supplemental materials).

As all measures performed equally well, we restricted subsequent detailed description to R-FC. We found that R-FC is significantly more predictive of early (15-75ms) TEP activity compared to full (15-400ms) TEP activity at the sensor level (t-stat = 2.69,  $p < 0.05$ ,  $df = 59$ ). Interestingly, this was not the case at the source level (t-stat = -0.12,  $p = 0.55$ ,  $df = 59$ ).

We hypothesized that the relationship between R-FC and TEP activity was strengthened by going from sensor to source space, as source-space connectivity has been shown to be more reliable<sup>6</sup>. However, the relationship between FC and the TEP was not significantly different



between sensor and source space for the early TEP (t-stat = -0.68,  $p = 0.75$ ,  $df = 59$ ) or the full TEP (t-stat = 1.45,  $p = 0.08$ ,  $df = 59$ ).

As R-FC was more predictive of early TEP activity at the sensor level, and the predictive value did not increase when moving the analysis to source space, we restricted subsequent description to the relationship between R-FC and early TEP activity. The relationship between R-FC and early TEP activity was analyzed in more detail by investigating the different stimulation sites separately (**Figure 6**). The relationship between R-FC and early TEP activity did not vary between stimulation sites at the sensor (Chi square = 8.07,  $p = 0.15$ ,  $df = 5$ , 54) or source level (Chi square = 7.44,  $p = 0.19$ ,  $df = 5$ , 54). We also investigated the relationship between frequency band specific FC and the spatial distribution of the broadband TEP (**Figure 7**; supplemental materials). R-FC was equally informative on the spatial distribution of the broadband early TEP for all frequency bands in sensor (Chi square = 0.29,  $p = 0.99$ ,  $df = 4$ , 295) and source (Chi square = 0.75,  $p = 0.94$ ,  $df = 4$ , 295) space.

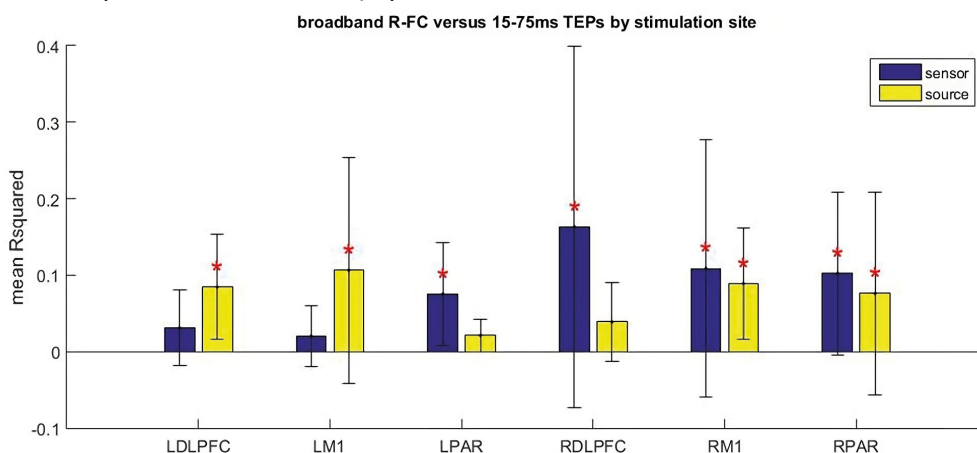


**Figure 6.** Mean proportion of variance of the spatial distribution of early TEP activity explained by Pearson's correlation based FC (R-FC) at the sensor and source level for different stimulation sites. The error bar indicates the standard deviation. \*Significant contribution of R-FC ( $p < 0.05$ , FWE corrected).

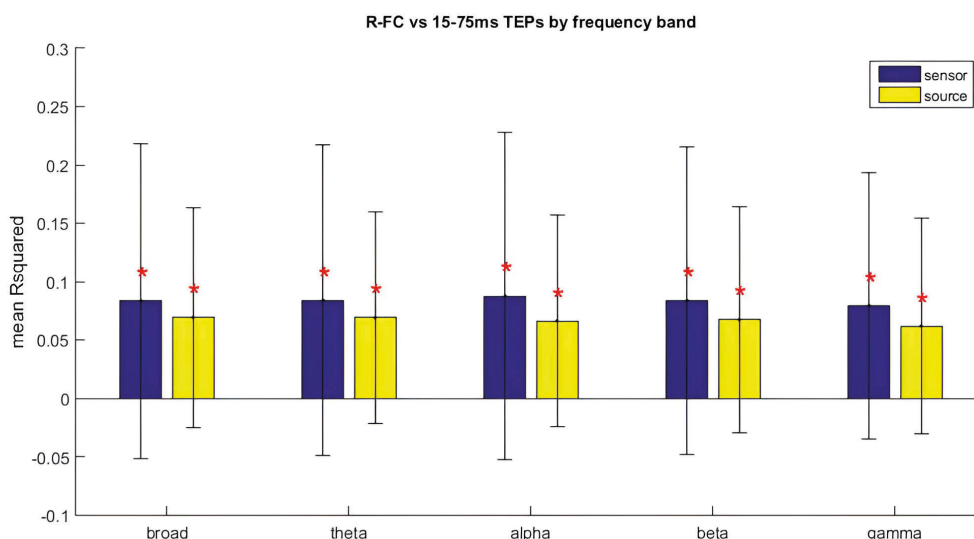


**Figure 7.** Mean proportion of variance of the spatial distribution of early TEP activity explained by Pearson's correlation based FC (R-FC) at the sensor and source level for different frequency bands. The error bar indicates the standard deviation. \*Significant contribution of R-FC ( $p < 0.05$ , FWE corrected).

## Variability

The relationship between FC and TEP activity was highly variable between participants and stimulation sites. On an individual level, R-FC correlated significantly with early TEP activity in less than half (24 out of 60) of cases at the sensor level and a fourth (15 out of 60 cases) of cases at the source level ( $P < 0.05$ , uncorrected). The variability can be observed clearly in Figure 8 (supplemental materials). For example, at the sensor level, R-FC predicted early TEP activity in participants 1, 2, 4, 5 and 8 with stimulation of right M1, but did not predict early TEP activity in any of these participants with stimulation of left M1 (significant prediction only with participant 7).

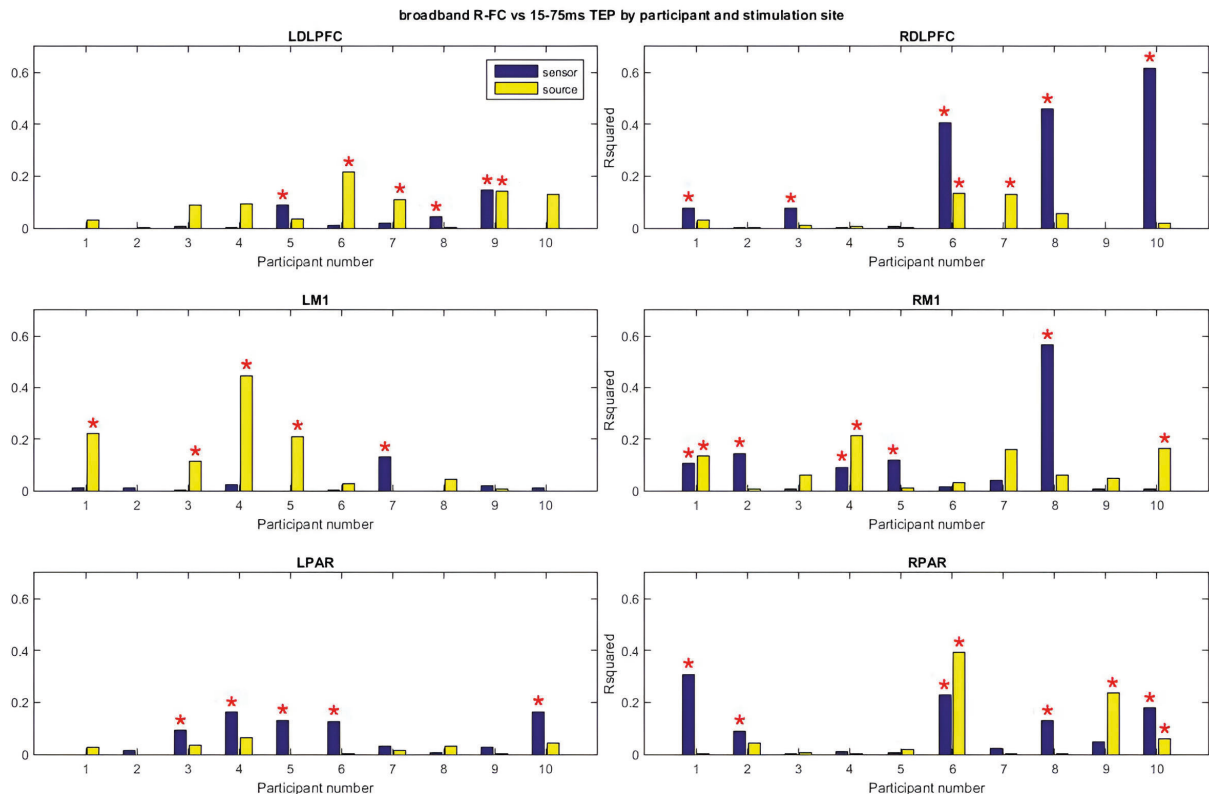


**Figure 8.** Proportion of the variance of the spatial distribution of early TEP activity explained by Pearson's correlation based FC (R-FC) at the sensor and source level for individual participants. The error bar indicates the standard deviation. \*Significant contribution of ICC ( $p < 0.05$ , uncorrected).

## DISCUSSION

Recent work has emphasized the importance of evaluating brain connectivity to understand normal brain function and neuropsychiatric diseases<sup>3-5</sup>, but the relationship between FC and the underlying causal interactions between brain regions is poorly understood. TMS allows for a controlled perturbation of activity in a given cortical target, and its local and distributed impact can be assessed by concurrent EEG recording. Consequently, the spread of the TEP may reflect causal interactions between the targeted brain region and the rest of the cortex. Therefore, we used TMS in combination with EEG to probe brain connectivity in human participants *in vivo*, and compared the resulting evoked activity with measures of EEG connectivity at the sensor and source level. We found that EEG FC patterns prior to delivery of a TMS pulse are weakly informative on the spatial distribution of evoked activity in response to the TMS pulse. This is in line with previous literature<sup>40,41</sup>, suggesting that coordination of

brain oscillatory activity plays a fundamental role in the organization of neuronal activity (and thereby information) across macroscopic brain regions. Specifically, the spatial distribution and magnitude of TMS-evoked activity can be partially predicted by resting-state FC measured prior to stimulation at the sensor and source level. Although the relationship between resting state FC prior to stimulation and the spatial distribution evoked activity was significant, we observed that the predictive value of all FC measures is poor (the proportion of the explained variance is less than 10%). The limited predictive value is likely related to the substantial variability across participants and stimulation sites.

In our study, we found that the relationship between individual EEG FC measures and evoked activity is weak and highly variable across individuals in both sensor and source space. Recent studies have already raised concerns about the utility of EEG connectivity measures in sensor space<sup>6,7,36</sup> and source space<sup>7,42</sup>. Our findings confirm these concerns, and should raise caution in the interpretation of studies involving EEG FC.

These findings also highlight the limitations of current functional connectivity analyses, and raise concern that current methods of characterizing EEG functional connectivity (at least the methods explored in this paper) do not adequately characterize the nature and dynamics of interactions between different brain regions. However, we also found that when combining multiple measures, the predictive value increased significantly (with the exception of the prediction of early TEP activity in source space), suggesting that there may be some measure or a combination of measures that do capture the nature of neuronal interactions.

Because recent studies have raised concern that the TEP, particularly later components, may be contaminated by auditory and somatosensory evoked potentials<sup>37,39,43</sup> and early TEP activity has been shown to be more consistent between participants<sup>44</sup>, we specifically looked at the relationship between R-FC and the early interval (15 – 75ms) of evoked activity. At the sensor level, we found that R-FC is more predictive of the first 75ms of evoked activity compared to the full range (400 ms) of the TEP. Putting together these observations, we believe that our findings are consistent with the idea that early evoked activity is more specific to the stimulation site compared to late intervals (> 75ms) of the TEP, and therefore more likely to be caused directly by the TMS-induced electrical field. However, we also found that functional connectivity is equally predictive of early and full TEP activity at the source level. A possible explanation for this is our measure of the relationship between functional connectivity and TEP activity might be more strongly affected by the presence of PEPs at the sensor level compared to the source level. Specifically, although PEPs would clearly cause spurious activity in both sensor and source space, at the source level PEPs may occur primarily in the auditory and somatosensory cortices, two relatively well-defined and localized cortical parcels; however, due to volume conduction, activity in these brain regions might affect multiple electrodes (and thus our measure of the relationship between functional connectivity and TEP activity) at the scalp level.

We did not observe significant systematic differences in the strength of the relationship between R-FC and TEP activity between stimulation sites or frequency bands, suggesting that the predictive value of FC is consistent across brain regions and frequency bands. However, we did observe substantial variability in the relationship between resting state FC and TEP activity in individual participants. Specifically, for the same stimulation site, the relationship between R-FC and TEP activity was significant in some individuals but absent in others. This can be explained by variability in TEP activity patterns, which have been shown to become more variable at later intervals with respect to the stimulus delivery<sup>44</sup>. Furthermore, this variability suggests that the degree to which measures of static resting-state FC capture causal brain interactions may not be consistent across individuals. This has also been reported by

Hawco et al.<sup>19</sup>, who identified a relationship between resting state fMRI FC and the spatial distribution of TMS-evoked activity on the group level but also observed substantial variability between individuals. The cause for this inter-individual variability remains unclear but could potentially be explained by the fact that the chosen functional connectivity measures capture the fundamental nature of the interregional dynamics only in some participants, because of differences in intrinsic physiology, input-output relations, and network dynamics across participants. Other factors which are likely to contribute to the variability are differences in structural connectivity, metabolism, brain state and neurochemistry between participants. Further studies are warranted to explore this important finding.

## Limitations

Our study has a number of limitations. Although we observed significant correlations between the investigated FC measures and the spatial distribution of evoked activity, the magnitude of the correlations was limited (mean values typically in the 0.03 - 0.09 range). There are a number of possible explanations for this.

First, we assessed the correlation between FC and the spatial distribution of a TEP in sensor space as a substantial amount of recent studies continue to analyze functional connectivity in sensor space<sup>45-47</sup>. Therefore, we wanted to determine whether EEG FC analyses in sensor space are physiologically meaningful by comparing FC with TMS-evoked activity. However, concerns have been raised about the reliability of FC in sensor space<sup>6,48</sup>, as FC results have been shown to depend on the electrical reference<sup>49</sup>. In our study, we found that sensor-space connectivity does significantly predict the propagation of TMS-evoked potentials, but the correlation is weak and not entirely reliable across individuals; these findings are thus consistent with the aforementioned studies on the limited reliability of sensor-space FC. Another potential concern for sensor-space studies is spurious correlations induced by volume conduction. We made several attempts to minimize these effects, by analyzing the data using the surface laplacian reference and by including the distance between the electrodes as a nuisance regressor in our model (for the average reference data). It is possible that this did not entirely eliminate the problem. Because of the aforementioned concerns regarding sensor space FC, interest has shifted to source space.

However, source space analysis of FC introduces a second limitation, as source space analysis is complicated by the fact that the inverse problem (the identification of brain signals that generate sensor level EEG activity) is 'ill-posed', with an infinite number of possible solutions. Several methods exist to solve the inverse problem (one of which we investigated in this study), but the accuracy of these methods is not clearly defined, particularly in cases where multiple different cortical regions may be simultaneously activated (as might be expected to occur after TMS)<sup>7</sup>, but also particularly with regard to resting-state functional connectivity analysis<sup>42</sup>. We found that the relationship between FC and evoked activity did not improve when moving to source space, demonstrating the complexity of the ill-posed inverse problem.

Third, we calculated the correlation between connectivity and the spatial distribution of TEPs by averaging the values obtained over multiple epochs, in part because this is how connectivity and TEPs are typically measured, and also because assessing the spatial distribution of TEPs on a single-trial level is not trivial. Therefore, our analysis assumed that the connectivity distribution and the spatial distribution of evoked activity, and the relationship between the two, are constant through the experiment. However, resting state FC has been shown to vary within sessions<sup>48,50-52</sup>, and this may therefore limit the absolute correlation between connectivity and the spatial distribution of the TEP. This is especially relevant for regions which exhibit strong connectivity dynamics, such as the bilateral DLPFC and parietal cortices<sup>53</sup>, which could potentially explain why these regions show a weaker relationship between FC

and the spatial distribution of evoked activity in source space. A related possibility is that the TMS-evoked potential also varies substantially over time, perhaps due to state differences in the stimulated cortex affecting the TMS-evoked activity, as has been shown for the phase of ongoing rhythms affecting MEP amplitude with stimulation of M1<sup>54</sup>.

Fourth, TMS also causes a somatosensory, auditory and motor response, which affects the observed spatial distribution of the TMS-evoked response<sup>43,55</sup>. We attempted to control for this effect by including the sham-EP as a nuisance regressor in our model, but this might not be a perfect control. However, the cortical activity evoked by these nonspecific responses to TMS should be independent of the functional connectivity of the stimulated regions, and thus may also contribute to the relatively low explained variance.

Fifth, directed measures of connectivity are limited by the biological structure of neurons, which are restricted by directional distribution of activity. However, concerns have been raised regarding the reliability of EEG measures of directed connectivity, particularly at the sensor level<sup>36</sup>. We therefore decided to limit our analyses to non-directional measures of connectivity. In future work, directed measures should also be investigated.

Finally, TMS target regions for stimulation of the DLPFC and parietal targets were defined based on anatomical landmarks, rather than functional regions. However, the underlying functional regions vary in localization relative to macroscopic anatomical landmarks, especially for prefrontal and parietal regions<sup>56,57</sup>. It is possible that some variability exists in the functional regions that were targeted with TMS, providing a potential explanation for the observed variability in the relationship between FC and TEP activity between participants.

## CONCLUSION

In summary, our results indicate that FC measures weakly predict the spatial distribution of subsequent TEPs at both the sensor and source level, and thus may contain some relevant causal information regarding brain networks and cortico-cortical interactions. However, the overall predictive power is limited, partly due to substantial variability across participants and stimulation sites. This variability raises concerns about whether studies characterizing EEG FC in cognitive function and disease states are physiologically meaningful. Further work is needed to better characterize the relationship between connectivity measures and the underlying cerebral dynamics.

## REFERENCES

1. Sakkalis V. Review of advanced techniques for the estimation of brain connectivity measured with EEG/MEG. *Comput Biol Med.* 2011;41(12):1110-1117. doi:10.1016/j.combiomed.2011.06.020
2. van den Heuvel MP, Hulshoff Pol HE. Exploring the brain network: A review on resting-state fMRI functional connectivity. *European Neuropsychopharmacology.* 2010;20(8):519-534. doi:10.1016/j.euroneuro.2010.03.008
3. Micheloyannis S, Pachou E, Stam CJ, et al. Small-world networks and disturbed functional connectivity in schizophrenia. *Schizophr Res.* 2006;87(1-3):60-66. doi:10.1016/j.schres.2006.06.028
4. Greicius M. Resting-state functional connectivity in neuropsychiatric disorders. *Curr Opin Neurol.* 2008;21(4):424-430. doi:10.1097/WCO.0b013e328306f2c5
5. Grefkes C, Fink GR. Reorganization of cerebral networks after stroke: New insights from neuroimaging with connectivity approaches. *Brain.* 2011;134(5):1264-1276. doi:10.1093/brain/awr033
6. Mahjoory K, Nikulin V V., Botrel L, Linkenkaer-Hansen K, Fato MM, Haufe S. Consistency of EEG source localization and connectivity estimates. *Neuroimage.* 2017;152(August 2016):590-601. doi:10.1016/j.neuroimage.2017.02.076
7. Becker H, Albera L, Comon P, et al. Brain source imaging : from sparse to tensor models  
To cite this version : HAL Id : hal-01190559 Brain source imaging : from sparse to tensor models.  
Published online 2015.
8. Chen A, Oathes D, Chang C, et al. Causal interactions between fronto-parietal central executive and default-mode networks in humans. *Proceedings of the National Academy of Sciences.* 2013;110(49):19944-19949.
9. David O, Cosmelli D, Friston KJ. Evaluation of different measures of functional connectivity using a neural mass model. *Neuroimage.* 2004;21(2):659-673. doi:10.1016/j.neuroimage.2003.10.006
10. Wendling F, Ansari-Asl K, Bartolomei F, Senhadji L. From EEG signals to brain connectivity: A model-based evaluation of interdependence measures. *J Neurosci Methods.* 2009;183(1):9-18. doi:10.1016/j.jneumeth.2009.04.021
11. Matsui T, Tamura K, Koyano KW, et al. Direct comparison of spontaneous functional connectivity and effective connectivity measured by intracortical microstimulation: An fMRI study in macaque monkeys. *Cerebral Cortex.* 2011;21(10):2348-2356. doi:10.1093/cercor/bhr019
12. Keller CJ, Bickel S, Entz L, et al. Erratum: Intrinsic functional architecture predicts electrically evoked responses in the human brain (Proceedings of the National Academy of Sciences of the United States of America (2011) 108, 25, (10308-10313) DOI: 10.1073/pnas.1019750108). *Proc Natl Acad Sci U S A.* 2011;108(41):17234. doi:10.1073/pnas.1114425108
13. Hebbink J, van Blooijis D, Huiskamp G, Leijten FSS, van Gils SA, Meijer HGE. A Comparison of Evoked and Non-evoked Functional Networks. *Brain Topogr.* 2019;32(3):405-417. doi:10.1007/s10548-018-0692-1
14. Yazdan-Shahmorad A, Silversmith DB, Kharazia V, Sabes PN. Targeted cortical reorganization using optogenetics in non-human primates. *Elife.* 2018;7:1-21. doi:10.7554/

15. Bestmann S, Baudewig J, Siebner HR, Rothwell JC, Frahm J. BOLD MRI responses to repetitive TMS over human dorsal premotor cortex. *Neuroimage*. 2005;28(1):22-29. doi:10.1016/j.neuroimage.2005.05.027
16. Shafi MM, Westover MB, Oberman L, Cash SS, Pascual-Leone A. Modulation of EEG functional connectivity networks in subjects undergoing repetitive transcranial magnetic stimulation. *Brain Topogr*. 2014;27(1):172-191.
17. Vink JJTT, Mandija S, Petrov PIPI, van den Berg CATCAT, Sommer IECIEC, Neggers SFWSFW. A novel concurrent TMS-fMRI method to reveal propagation patterns of prefrontal magnetic brain stimulation. *Hum Brain Mapp*. 2018;39(11). doi:10.1002/hbm.24307
18. Rahman A, Reato D, Arlotti M, et al. Cellular effects of acute direct current stimulation: somatic and synaptic terminal effects. *J Physiol*. 2013;591(Pt 10):2563-2578. doi:10.1113/jphysiol.2012.247171
19. Hawco C, Voineskos AN, Steeves JKE, et al. Spread of activity following TMS is related to intrinsic resting connectivity to the salience network: A concurrent TMS-fMRI study. *Cortex*. 2018;108:160-172. doi:10.1016/j.cortex.2018.07.010
20. Lisanby SH, Gutman D, Luber B, Schroeder C, Sackeim HA. Sham TMS: Intracerebral measurement of the induced electrical field and the induction of motor-evoked potentials. *Biol Psychiatry*. 2001;49(5):460-463. doi:10.1016/S0006-3223(00)01110-0
21. Rossi S, Hallett M, Rossini PM, et al. Safety, ethical considerations, and application guidelines for the use of transcranial magnetic stimulation in clinical practice and research. *Clinical Neurophysiology*. 2009;120(12):2008-2039. doi:10.1016/j.clinph.2009.08.016
22. Delorme A, Makeig S. EEGLAB: an open source toolbox for analysis of single-trial EEG dynamics including independent component analysis. *J Neurosci Methods*. 2004;134(1):9-21.
23. Tadel F, Baillet S, Mosher JC, Pantazis D, Leahy RM. Brainstorm: a user-friendly application for MEG/EEG analysis. *Comput Intell Neurosci*. 2011;2011:8.
24. Oostenveld R, Fries P, Maris E, Schoffelen JMM. FieldTrip: Open source software for advanced analysis of MEG, EEG, and invasive electrophysiological data. *Comput Intell Neurosci*. 2011;2011. doi:10.1155/2011/156869
25. Rogasch NC, Thomson RH, Farzan F, et al. Removing artefacts from TMS-EEG recordings using independent component analysis: Importance for assessing prefrontal and motor cortex network properties. *Neuroimage*. 2014;101:425-439. doi:10.1016/j.neuroimage.2014.07.037
26. Perrin F, Pernier J, Bertrand O, Echallier JF. Spherical splines for scalp potential and current density mapping. *Electroencephalogr Clin Neurophysiol*. 1989;72(2):184-187. doi:10.1016/0013-4694(89)90180-6
27. Gramfort A, Papadopoulo T, Olivi E, Clerc M. OpenMEEG: opensource software for quasistatic bioelectromagnetics. *Biomed Eng Online*. 2010;9(1):45.
28. Baillet S, Mosher JC, Leahy RM. Electromagnetic brain mapping. *IEEE Signal Process Mag*. 2001;18(6):14-30. doi:10.1109/79.962275
29. Desikan RS, Ségonne F, Fischl B, et al. An automated labeling system for subdividing the human cerebral cortex on MRI scans into gyral based regions of interest. *Neuroimage*.

2006;31(3):968-980.

30. Whittingstall K, Stroink G, Gates L, Connolly JF, Finley A. Effects of dipole position, orientation and noise on the accuracy of EEG source localization. *Biomed Eng Online*. 2003;2:1-5. doi:10.1186/1475-925X-2-14
31. Seeber M, Cantonas LM, Hoevels M, Sesia T, Visser-Vandewalle V, Michel CM. Subcortical electrophysiological activity is detectable with high-density EEG source imaging. *Nat Commun*. 2019;10(1):1-7. doi:10.1038/s41467-019-08725-w
32. Vinck M, Oostenveld R, Van Wingerden M, Battaglia F, Pennartz CMA. An improved index of phase-synchronization for electrophysiological data in the presence of volume-conduction, noise and sample-size bias. *Neuroimage*. 2011;55(4):1548-1565. doi:10.1016/j.neuroimage.2011.01.055
33. Lachaux JP, Rodriguez E, Martinerie J, Varela FJ, others. Measuring phase synchrony in brain signals. *Hum Brain Mapp*. 1999;8(4):194-208.
34. Rosenberg JR, Amjad AM, Breeze P, Brillinger DR, Halliday DM. The Fourier approach to the identification of functional coupling between neuronal spike trains. *Prog Biophys Mol Biol*. 1989;53(1):1-31.
35. Magri C, Whittingstall K, Singh V, Logothetis NK, Panzeri S. A toolbox for the fast information analysis of multiple-site LFP, EEG and spike train recordings. *BMC Neurosci*. 2009;10. doi:10.1186/1471-2202-10-81
36. de Steen F, Faes L, Karahan E, Songsiri J, Valdes-Sosa PA, Marinazzo D. Critical comments on EEG sensor space dynamical connectivity analysis. *Brain Topogr*. Published online 2016:1-12.
37. Freedberg M, Reeves JA, Hussain SJ, Zaghoul KA, Wassermann EM. Identifying site- and stimulation-specific TMS-evoked EEG potentials using a quantitative cosine similarity metric. *bioRxiv*. Published online 2019:612499. doi:10.1101/612499
38. Hauk O, Stenroos M. A framework for the design of flexible cross-talk functions for spatial filtering of EEG/MEG data: DeFleCT. *Hum Brain Mapp*. 2014;35(4):1642-1653. doi:10.1002/hbm.22279
39. Biabani M, Fornito A, Mutanen T, Morrow J, Rogasch N. Sensory contamination in TMS-EEG recordings: Can we isolate TMS-evoked neural activity? *Brain Stimul*. 2019;12(2):473. doi:10.1016/j.brs.2018.12.543
40. Draguhn A, Buzsaki G. Neuronal Oscillations in Cortical Networks. *Science (1979)*. 2004;304(5679):1926-1929. doi:10.1126/science.1099745
41. Engel AK, Fries P, Singer W. Dynamic predictions: oscillations and synchrony in top-down processing. *Nat Rev Neurosci*. 2001;2(10):704-716.
42. Colclough GL, Woolrich MW, Tewarie PK, Brookes MJ, Quinn AJ, Smith SM. How reliable are MEG resting-state connectivity metrics? *Neuroimage*. 2016;138:284-293. doi:10.1016/j.neuroimage.2016.05.070
43. Conde V, Tomasevic L, Akopian I, et al. The non-transcranial TMS-evoked potential is an inherent source of ambiguity in TMS-EEG studies. *Neuroimage*. 2019;185:300-312.
44. Salo KST, Vaalto SMI, Mutanen TP, Stenroos M, Ilmoniemi RJ. Individual Activation



- Patterns after the Stimulation of Different Motor Areas: A Transcranial Magnetic Stimulation-Electroencephalography Study. *Brain Connect.* 2018;8(7):420-428. doi:10.1089/brain.2018.0593
45. Hordacre B, Moezzi B, Ridding MC. Neuroplasticity and network connectivity of the motor cortex following stroke: A transcranial direct current stimulation study. *Hum Brain Mapp.* 2018;39(8):3326-3339. doi:10.1002/hbm.24079
46. Nasserroleslami B, Dukic S, Broderick M, et al. Characteristic Increases in EEG Connectivity Correlate With Changes of Structural MRI in Amyotrophic Lateral Sclerosis. *Cerebral Cortex.* 2017;(January):1-15. doi:10.1093/cercor/bhx301
47. Tóth B, Urbán G, Háden GP, et al. Large-scale network organization of EEG functional connectivity in newborn infants. *Hum Brain Mapp.* 2017;38(8):4019-4033. doi:10.1002/hbm.23645
48. O'Neill GC, Tewarie P, Vidaurre D, Liuzzi L, Woolrich MW, Brookes MJ. Dynamics of large-scale electrophysiological networks: A technical review. *Neuroimage.* 2017;(October):1-18. doi:10.1016/j.neuroimage.2017.10.003
49. Nolte G, Ziehe A, Nikulin V V, et al. Robustly estimating the flow direction of information in complex physical systems. *Phys Rev Lett.* 2008;100(23):234101.
50. Honey CJ, Honey CJ, Sporns O, et al. Predicting human resting-state functional connectivity from structural connectivity. *Proc Natl Acad Sci U S A.* 2009;106(6):2035-2040. doi:10.1073/pnas.0811168106
51. Handwerker DA, Roopchansingh V, Gonzalez-Castillo J, Bandettini PA. Periodic changes in fMRI connectivity. *Neuroimage.* 2012;63(3):1712-1719.
52. Chang C, Glover GH. Time--frequency dynamics of resting-state brain connectivity measured with fMRI. *Neuroimage.* 2010;50(1):81-98.
53. Chen B, Xu T, Zhou C, et al. Individual variability and test-retest reliability revealed by ten repeated resting-state brain scans over one month. *PLoS One.* 2015;10(12):1-21. doi:10.1371/journal.pone.0144963
54. Schaworonkow N, Triesch J, Ziemann U, Zrenner C. EEG-triggered TMS reveals stronger brain state-dependent modulation of motor evoked potentials at weaker stimulation intensities. *Brain Stimul.* 2019;12(1):110-118. doi:10.1016/j.brs.2018.09.009
55. Rogasch N, Zipser C, Darmani G, et al. TMS-evoked EEG potentials from prefrontal and parietal cortex: reliability, site specificity, and effects of NMDA receptor blockade. *bioRxiv.* Published online 2019:480111. doi:10.1101/480111
56. Yeo BTT, Krienen FM, Sepulcre J, et al. The organization of the human cerebral cortex estimated by intrinsic functional connectivity. *J Neurophysiol.* 2011;106:1125-1165. doi:10.1152/jn.00338.2011.
57. Goldman-Rakic PS. Circuitry of primate prefrontal cortex and regulation of behavior by representational memory. *Handbook of physiology: the nervous system.* Published online 1987:373-417. doi:10.1002/cphy.cp010509



## Chapter 4

# **Spatial topography of TMS-based motor mapping depends on TMS current direction**

Jord JT Vink

Petar I Petrov

Stefano Mandija

Rick M Dijkhuizen

Sebastiaan FW Neggers

*Vink, Jord JT, et al. "Outcome of TMS-based motor mapping depends on TMS current direction." bioRxiv (2018): 371997.*

## **ABSTRACT**

### **Introduction**

Navigated transcranial magnetic stimulation (nTMS) combined with electromyography (EMG) is increasingly used for the identification of motor eloquent cortical areas in the preparation of neurosurgical interventions. However, TMS effects have been shown to depend on the TMS-induced current direction and the effect of the induced current on the spatial representation of TMS-based motor maps remains largely unknown. Consequently, it remains unclear what TMS-induced current direction is optimal for the identification of the motor eloquent cortex.

### **Methods**

To answer this question, we acquired TMS-based motor maps with posterior-to-anterior (PA)- and lateral-to-medial (LM)-induced currents by stimulating targets in a grid of locations over the left primary motor cortex of 8 healthy participants (4 male; 4 female), while simultaneously recording EMG responses in muscles of the right lower arm. Additionally, we acquired fMRI data during an opposing thumb movement task and compared the TMS-based motor maps with fMRI-based localization of the motor area.

### **Results**

The investigated TMS current directions resulted in different localizations of the motor area, with PA-induced currents identifying a motor area that was located significantly more anterior (8.7 – 10.4 mm, depending on the muscle) compared to the motor area identified using LM-induced currents for the same muscle. However, both TMS-induced current directions performed similarly when compared to fMRI-based localization.

### **Conclusion**

We hypothesized that different TMS-induced current directions identify different representations of the same motor area due to anisotropic cortical conductance. However, a post-hoc analysis with personalized head models to model the TMS-induced electrical field demonstrated that anisotropic cortical conductance did not explain this observation.

## INTRODUCTION

Transcranial magnetic stimulation (TMS) combined with MRI-guided neuronavigation is an increasingly popular non-invasive tool for the identification of motor eloquent brain regions in preparation of neurosurgical interventions<sup>1,2,3,4,5</sup>. Navigated TMS (nTMS) utilizes electromyography (EMG) to identify the cortical target in which TMS elicits motor-evoked potentials (MEPs) in the EMG recordings of the investigated muscles<sup>6,7</sup>. Using a standardized grid of stimulation targets, the motor eloquent area can be delineated systematically, based on the amplitudes of the MEPs as a function of stimulation location. In this way, TMS has been shown to be able to identify significantly separated motor area centers for different muscles in the upper extremity<sup>8</sup>. Besides its application in neurosurgical planning, nTMS can be used to monitor changes in the primary motor cortex during the course of rehabilitation (of motor function) after brain injury, e.g. stroke<sup>9</sup>.

However, TMS effects have been shown to depend on the orientation of the TMS coil, and thus the direction of the induced current, with respect to the local morphology of the stimulated area, complicating the interpretability of TMS-based motor maps. For example, the direction of the TMS-induced current with respect to the curvature of the precentral gyrus has been shown to affect the amplitude of the MEPs<sup>10-12</sup>, with a posterior-to-anterior (PA)-induced current eliciting larger MEPs in weakly and strongly curved hand knobs<sup>13</sup>. Consequently, the optimal TMS-induced current direction for motor mapping has been shown to vary between participants<sup>14</sup>. Others have found that the spatial representation of the motor eloquent area also varies as a function of the TMS-induced current direction. For example, a PA-induced current reveals a more anteriorly located motor area compared to an anterior-to-posterior (AP) induced current<sup>15</sup>. These effects are potentially mediated by the anisotropy of the white matter and grey matter, which have been shown to play an important role in the distribution of the TMS-evoked fields<sup>12</sup>. TMS induces a primary current, which is generated by the electrical field (E-field) resulting from the magnetic flux of the TMS coil. In addition to the primary current, secondary currents arise from charge accumulations at tissue boundaries due to differences in tissue conductivity (i.e. grey matter, white matter, skin)<sup>16</sup>. Differences in cortical morphology, the presence of varying tissue types and different neuronal fiber orientations introduce anisotropy in the distribution of the TMS-induced current<sup>17,12</sup>. Consequently, the spatial representation of the TMS-based motor map with respect to neuroanatomy is likely affected by the distribution of the TMS-induced current.

In order to verify the accuracy of the spatial representation of TMS-based motor maps, the motor maps have been compared to the representation of motor eloquent cortex based on fMRI<sup>18,19,20</sup>. TMS applied with a PA-induced current has been shown to identify a motor eloquent area that is consistently located anterior to the anatomical and functional MRI representation, with a discrepancy of up to 10mm<sup>18</sup>. This raises the question whether the use of a different TMS-induced current direction provides a motor map that more closely resembles the fMRI-based motor area, as the spatial representation of the TMS-based motor area has been shown to depend on the TMS-induced current direction. However, this remains unclear, as TMS-based motor maps obtained with other TMS-induced current directions have not been systematically compared with the fMRI-based motor area.

In this work, we therefore systematically investigated the spatial representation of TMS-based motor maps obtained with a lateral-to-medial (LM)-induced current and a PA-induced current and compared those with the functional motor area based on fMRI. We stimulated targets in a grid over the left primary motor cortex of 8 healthy participants, using a novel nTMS-EMG technique, and compared the TMS-based motor maps obtained with different induced current directions with an fMRI-based motor map obtained in the same participants. We also

investigated the sensitivity of navigated TMS-EMG in the identification of separate TMS-based motor maps for the FDI, ADM and ECR muscles. We performed a post hoc analysis to further investigate whether the difference in the representation of the functional motor areas obtained using different TMS-induced current directions can be explained by inhomogeneous electrical conductivities of the stimulated tissues. For this, we modeled the TMS-induced electrical field (E-field) using personalized 3D head models of different tissue conductivities and investigated two different models of how the TMS-induced E-field generates motor activity.

## **METHODS**

### **Study design**

The experimental procedure was approved by the medical ethical committee of the University Medical Center Utrecht (UMCU), Utrecht, The Netherlands. MRI data were acquired in 8 healthy right-handed participants (4 male; 4 female; mean age: 26.4). All participants provided written informed consent and were screened for MRI and TMS exclusion criteria. During the experimental procedure, we strictly adhered to the guidelines and recommendations for TMS endorsed by the International Federation for Clinical Neurophysiology<sup>21</sup>.

### **Materials**

All MR experiments were performed on a 3T MR scanner (Philips Achieva, Best, The Netherlands, [www.philips.nl](http://www.philips.nl)). Navigated TMS was performed using the Neural Navigator 3.1 'navigated MEP' (Brain Science Tools BV, De Bilt, The Netherlands, [www.brainsciencetools.com](http://www.brainsciencetools.com)). A monophasic magnetic stimulator Neuro-MS (Neurosoft, Ivanovo, Russia, [www.neurosoft.com](http://www.neurosoft.com)) with a figure-of-8 TMS coil 100mm FEC-02-100 (Neurosoft, Ivanovo, Russia) and a 4 channel EMG amplifier Neuro-EMG (Neurosoft, Ivanovo, Russia) were used to evoke and record MEPs simultaneously. The EMG signals were recorded, amplified and digitized with a sampling frequency of 20 kHz.

### **Procedures**

The experiment was divided into two parts: an MRI session and a TMS-EMG session (**Figure 1**).

#### *MRI session*

During the MRI session, a 3D T1-weighted anatomical scan was obtained, which was used for neuronavigation during the TMS-EMG session. This scan was acquired with a TR/TE of 10.0/4.6ms, a flip angle of 8°, voxel size of 0.75x0.75x0.8mm<sup>3</sup>, scan duration of 677s, and 225 slices with no slice gap.

Thereafter, a functional MRI time series was obtained to identify the maximum blood-oxygenation-level-dependent (BOLD) response in response to voluntary right thumb movements. A single-shot EPI sequence was acquired with 250 dynamics, a TR/TE of 2,000/23ms, flip angle of 70°, voxel size of 4x4x4mm<sup>3</sup>, scan duration of 510s, and 30 slices with a slice thickness of 3.6mm and a slice gap of 0.4mm. During the EPI sequence, the participant was instructed to perform opposing thumb movements upon presentation of an auditory cue (which was presented every 10 to 16 s to avoid habituation). The movements of the right abductor pollicis brevis (APB) muscle were recorded using a wireless MR-compatible electrocardiography device (Invivo, Best, The Netherlands). EMG was recorded at a frequency of 496Hz, in order to detect voluntarily-induced muscle activity, allowing us to verify the timing of the voluntary thumb movements.

### *TMS-EMG session*

For each participant, 3D surface renderings of the skin and cortex from the anatomical MRI scans were visualized in the Neural Navigator software. The location of the left hand knob (based on the statistical activation map computed from the BOLD data of the fMRI scan) was marked in the Neural Navigator. In the Neural Navigator software, a 5 by 5 grid of stimulation targets with 7 mm distance between the targets and a total area of 2.8 by 2.8 cm was centered on the hand area in the left M1. This grid was placed to aid the real time targeting of the TMS pulse on preplanned locations on the motor cortex.

The participant was seated comfortably on a chair with the arms resting on a table. Surface electrodes were placed over the right first dorsal interosseous (FDI), abductor digiti minimi (ADM) and extensor carpi radialis (ECR) muscles in a belly-tendon montage and the ground electrode was attached to the left wrist. The navigation procedure was performed using at least 6 facial landmarks to assure accurate alignment between tracker space and MRI space. Head movement compensation was performed by the neural navigator in real time, using continuous readings of two position tracking sensors attached to the head, which allowed for correction of small head movements in real time<sup>19</sup>.

The resting motor threshold (RMT) determination and single pulse stimulation of the grid targets was performed for the two TMS-induced current directions (PA and LM current directions), separately. A PA current was induced using a PA TMS coil orientation with the coil handle oriented perpendicular to the orientation of the individual participant's precentral gyrus (at a 20° to 40° angle with the mid-sagittal plane depending on individual cortical morphology)(**Figure 1**). An LM current was induced using a LM TMS coil orientation with the coil handle oriented parallel to the orientation of the precentral gyrus (at a 90° to 110° angle with the mid-sagittal plane depending on individual cortical morphology)(**Figure 1**). The RMT was determined at the location where the maximum MEP was observed by probing different target in the vicinity of the precentral gyrus for the PA- and LM-induced current directions, separately. This method was chosen to avoid getting insufficient MEP responses for the LM session as from previous literature it is known that a higher RMT is needed for LM orientation<sup>1011</sup>. The RMT was obtained by increasing the stimulator output until MEPs with a peak-to-peak amplitude of over 50  $\mu$ V were observed in the EMG recording of the contralateral FDI muscle in 5 out of 10 trials with an inter-stimulus interval of 7s<sup>6,21</sup>. For each session, the machine output was then set at 120% of the previously determined RMT. Targets in the grid were stimulated with 5 consecutive TMS pulses with an inter-stimulus interval of 3s. A total of 125 TMS pulses was delivered per TMS current direction (total of 250 pulses). The targets were stimulated in a random order to make sure that the stimulation order would not affect statistical analysis. The target grids were obtained for both TMS-induced current directions (PA and LM), separately.

The EMG trace and TMS coil position, orientation and angulation (with respect to the head) were captured during TMS pulse delivery. The data were exported to an XML format text file for further analysis in Matlab.

### **Data analysis**

All data were analyzed using custom scripts and SPM12<sup>22</sup> in a Matlab 2014a environment (Mathworks Inc., USA). For each participant, the T1 weighted image was segmented using unified segmentation in SPM12 to obtain a grey matter, white matter and CSF mask<sup>23</sup>. The location of the maximum response to thumb movements was obtained from the statistical activation map from the BOLD data of the fMRI scan (fMRI-based hand area). The statistical map was constructed based on a subject-level event-related generalized linear model (GLM) analysis, in which the thumb movements were modeled with the canonical hemodynamic

response function (HRF). The timing of the thumb movements was obtained from the EMG recordings which were acquired during MRI acquisition using custom Matlab code. The GLM included two nuisance regressors: the average BOLD signal in the white matter and the CSF. Statistical images were constructed based on a T-statistic with the T-threshold at  $P < 0.05$ , family wise error (FWE) whole-brain corrected<sup>22</sup>.

The EMG traces of all muscles were filtered with a low-pass filter with a cutoff frequency of 500Hz, in order to eliminate the noise caused by the electromagnetic tracking device from the EMG signals. A custom peak detection algorithm (minima and maxima were determined between 15 and 40ms post-stimulus) was used to determine the peak-to-peak amplitude of the MEP. The 5 MEP amplitudes per target grid point were averaged. Next, the center of gravity (COG) of the MEP motor map was calculated. This was done by weighing all the target coordinates by the amplitude of the corresponding MEP. MEPs with amplitude less than 50 $\mu$ V or MEPs with noise levels exceeding the maximum MEP amplitude were excluded from analysis. Separations between COGs of MEP motor maps obtained with different coil orientations or muscles were determined by calculating the absolute distance between the X and Y coordinates (anterior-posterior and lateral-medial direction, respectively) of the COG, since separation in the Z direction is predominantly dependent on brain morphology and sulcal depth, as all grids were only slightly tilted with respect to the axial plane.

The latencies of all the MEPs within the MEP motor maps obtained using PA- and LM-induced current directions were also compared.

### Modeling analysis

We calculated TMS-induced electrical fields (E-fields) for all stimulated targets using individual volumetric head models in SClrun 4.7. Individual head models consisted of 4 different tissue types, which were derived from the previously obtained segmentations of the MRI scan: gray matter, white matter, CSF, and skull. The conductivities of the different tissue types were assumed to be isotropic and derived from previous literature (gray matter: 0.27; white matter 0.12; CSF: 1.67; skull: 0.002)<sup>24</sup>. The TMS coil was modeled as a single layer of 10 windings in the form of circular rings with an inner diameter of 15mm and an outer diameter of 55mm, as obtained from the technical specifications of the TMS coil provided by the manufacturer. The location and orientation of the TMS coil for the stimulated targets were obtained from the neuronavigation system, and converted to the SClrun coordinate system using custom Matlab code. The Neuro-MS monophasic stimulator is capable of delivering currents up to 12.52 kA, with a pulse duration of 0.2ms and a 0.05 ramp time at 100% machine output. The stimulation intensities, reported as %RMT, were converted to the delivered current, which were used in the model. Finite element modeling (FEM) was used to calculate the E-field strength for each element of the head model and for each stimulation target. Activation of the hand motor area was defined as the total E-field summed over all elements within the hand motor area within the precentral gyrus, called the CE metric<sup>25</sup>.

Previous studies have shown that activity evoked by TMS is affected by the direction of the induced current with respect to the orientation of the gyrus, with a current perpendicular to the precentral gyrus resulting in MEPs with higher amplitude compared to a current oriented parallel to the precentral gyrus<sup>12,11</sup>. Therefore, it is assumed that activation of neuronal axons which are oriented perpendicular to the cortical sheet is making up the majority of the effect of TMS (the radial component of the E-field in **Figure 2**). This orientation dependence has been described using the C3 metric, which describes activation as the inner product between the surface normal of the cortical element and the total E-field through that element<sup>26</sup>. Therefore, we also evaluated the C3 metric, in addition to the CE metric<sup>25</sup>.



The CE and C3 metric were calculated for each TMS coil position and for both TMS coil orientations. Similar to the analysis of the measured data, a COG was calculated for the simulated data, resulting in a COG for both TMS coil orientations and both metrics.

### **Statistical analysis**

The difference between the RMTs for PA- and LM-induced current directions was assessed through a one-sided Student's paired t-test, because the literature clearly states that the RMT is higher for an LM-induced current (parallel to the precentral gyrus)<sup>27</sup>. The separation in anterior-posterior direction between the COG for a PA TMS-induced current and the location (voxel) with the maximum BOLD response to voluntary thumb movements was also determined through a one-sided paired Student's t-test, guided by existing evidence that the COG lies anterior of the maximum BOLD response<sup>18</sup>. The same tests were used to evaluate the difference between the location of COG between the two TMS coil orientations for the simulated data. All the other separations were evaluated with two-sided paired Student's t-tests, as we had no a-priori hypotheses for these comparisons. Statistical tests evaluating separations in the X and Y direction were corrected for multiple comparisons by using a Bonferroni-corrected alpha of 0.025 (2 comparisons). Statistical tests of differences between the cortical representations of different muscles were also corrected for multiple comparisons, resulting in a Bonferroni-corrected alpha of 0.0125 (4 comparisons). Finally, differences in latency were evaluated with a one-sided paired Student's t-test because prior literature suggests increased latencies for a PA-induced current with respect to LM-induced current<sup>28,29</sup>.

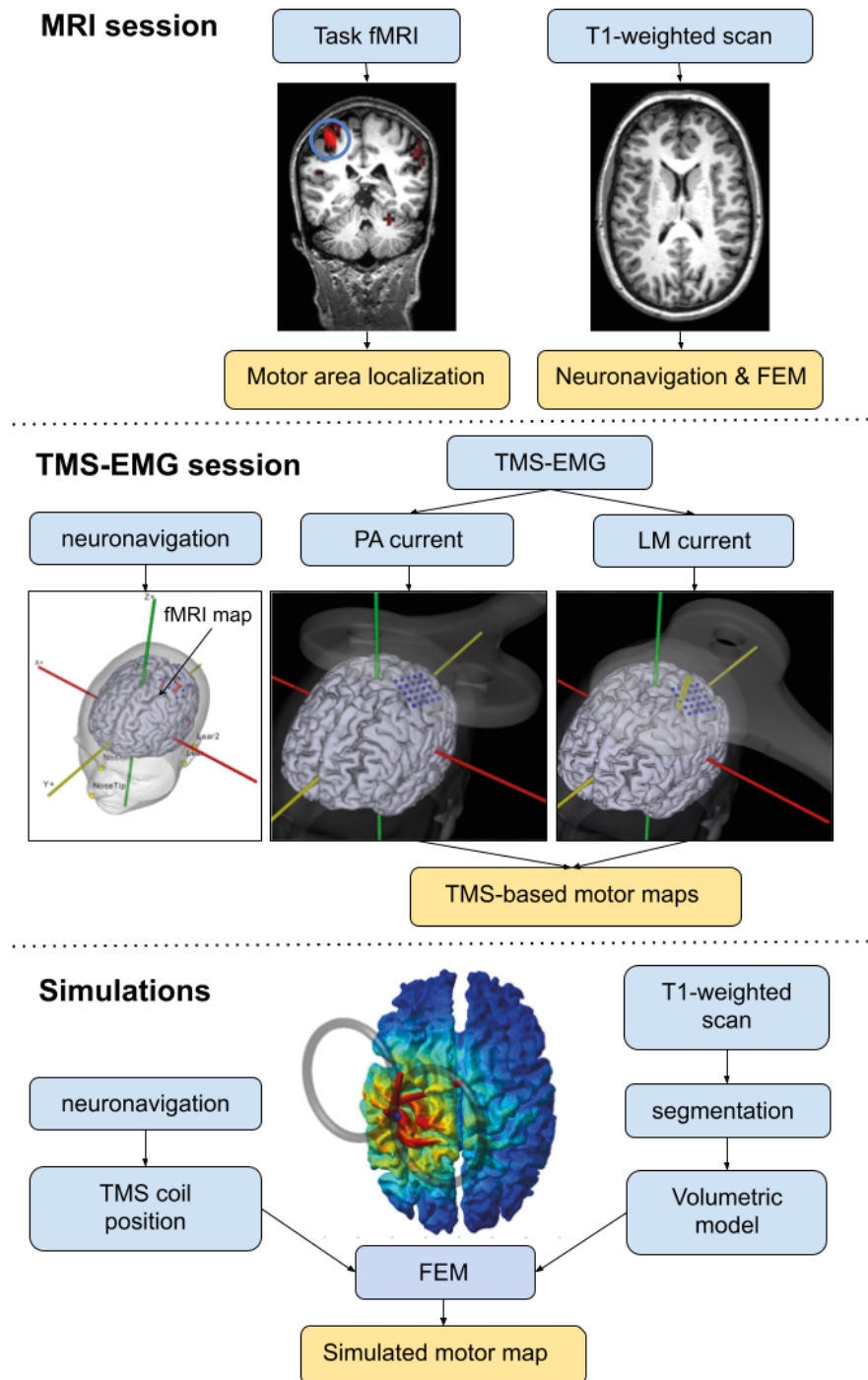


**Figure 1.** Schematic overview of the experimental procedure. A T1-weighted scan and a task fMRI scan were acquired during the MRI session. TMS-based motor maps were acquired using two different TMS-induced current directions during the TMS-EMG session. Afterward, finite element modeling (FEM) was used to simulate activation of the hand motor area. The simulated motor maps were compared to the measured motor maps. The yellow boxes below the figures denote the most important derived measures from each procedure. PA-current: posterior-to-anterior current. LM current: lateral-to-medial current.

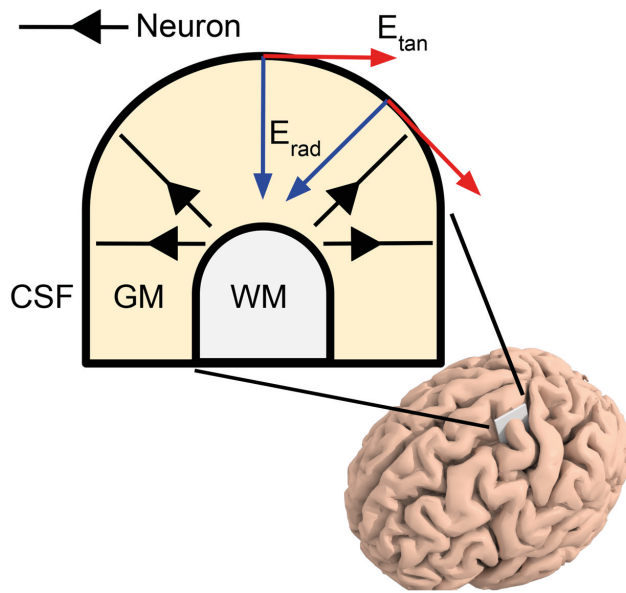


**Figure 2.** Schematic overview of the E-field evaluated by the CE and C3 method. TMS evokes an electrical field ( $E_{tot}$ ) which consists of a tangential ( $E_{tan}$ ) and a radial component ( $E_{rad}$ ) with respect to the cortical surface. The CE method describes the total E-field through the ‘hand knob’, irrespective of the direction. The C3 method only describes the radial component of the E-field.

## RESULTS

### MEP motor mapping and fMRI

The RMT was determined separately for sessions with PA- and LM-induced currents. The average RMT was 36.9 (range: 27 - 41) for a PA-induced current and 42.5 (range: 33 – 50) for a LM-induced current. The RMT increased significantly (mean increase: 5.3%) for coil orientations with an LM-induced current with respect to a PA-induced current ( $p$ : 0.0005,  $T$ : 5.4,  $df$ : 7).

The COGs of the measured MEP motor maps of the FDI, ADM and ECR muscles obtained using a PA-induced current were located significantly more anterior with respect to the COGs obtained with an LM-induced current, with average separations of 9.3 (SD: 5.4;  $T$ : 4.6;  $p$ : 0.003), 10.4 (SD: 5.0;  $T$ : 5.5;  $p$ : < 0.0001) and 8.7 (SD: 5.5;  $T$ : 4.2;  $p$ : 0.004) mm respectively. No significant separation was observed in medio-lateral direction. Figure 3 shows the relative distances between the COGs of the MEP motor maps obtained using PA-induced currents with respect to the COGs using LM-induced currents for all participants.

We did not find a significant difference between the distance between the COGs of the TMS-based motor maps and the fMRI-based hand area. We did observe that the COGs of the MEP motor maps obtained with PA-induced currents were located slightly anterior to the fMRI-based hand area, while medial-lateral separation was negligible. The anterior separation was only significant for the ADM muscle with a mean separation of 6.0 mm (SD: 8.2;  $T$ : 1.9;  $p$ : 0.047), but showed a trend for the other muscles. The COGs of the MEP motor maps of the FDI, ADM and ECR muscles obtained with a LM-induced current were not significantly separated from the fMRI-based hand area.

The COGs of MEP motor maps of some of the individual muscles were significantly separated. The COG of the MEP motor map of the FDI muscle was significantly separated in the lateral direction with respect to the COG of the ADM muscle for both TMS current directions.

Details on the separations between the COGs of MEP motor maps for different muscles can be found in the supplementary materials.

Finally, the latencies of all the MEPs in the MEP motor area obtained with a PA- and LM-induced current were similar: 23.5 and 23.6ms respectively. Details can be found in the supplementary materials.

### FEM simulations

**Figure 4** shows simulated activity within the ‘hand knob’ of a single representative participant. Each column shows a different TMS coil position. Two different TMS coil orientations and two different metrics of activity are shown. The activity within the ‘hand knob’ was averaged to obtain a single measure of motor activity for each stimulation site. Next, a COG was calculated in the same way as for the measured data. **Figure 5** shows the relative distances between the COGs of the MEP motor maps obtained using PA-induced currents with respect to the COGs using LM-induced currents for the simulated data. The COGs of the simulated MEP motor maps of the FDI did not show a significant difference between the PA-induced current and the LM-induced current, with an average separation of 1.9mm.

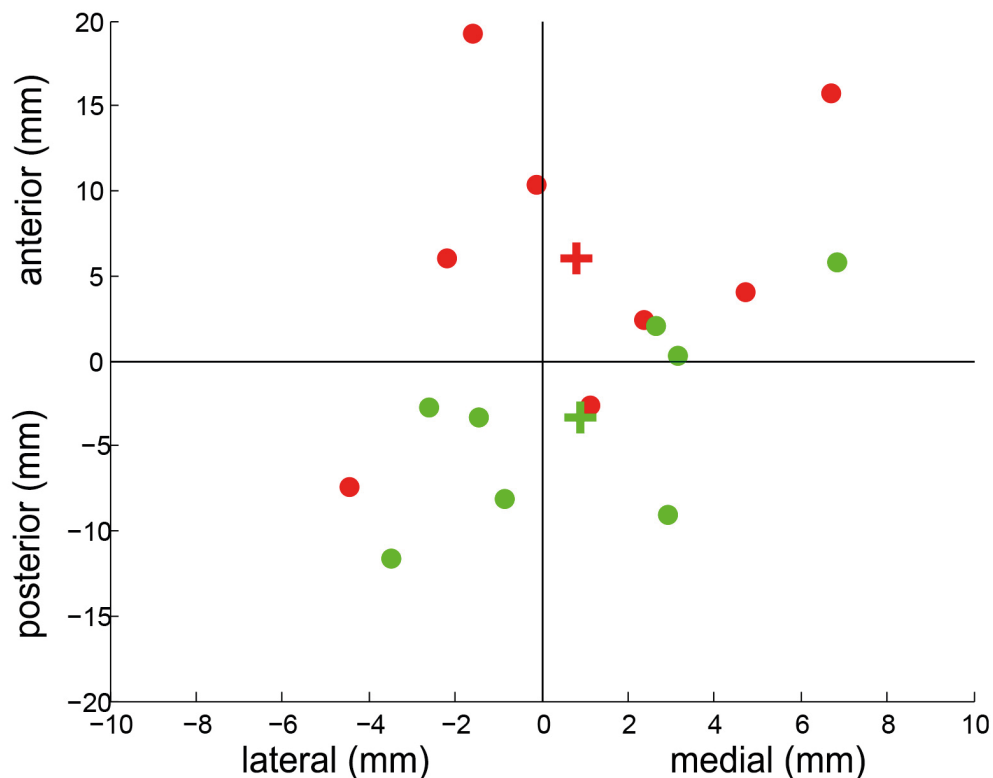


**Figure 3.** The relative locations of the COGs (FDI muscle) with respect to the location of the maximum BOLD response to voluntary thumb movements. Each dot represents an individual participant. The COGs obtained using PA- and LM-induced currents are shown as red and green dots, respectively. The mean COGs are indicated by a plus (+). It can be observed that PA-induced currents evoke anteriorly located COGs.

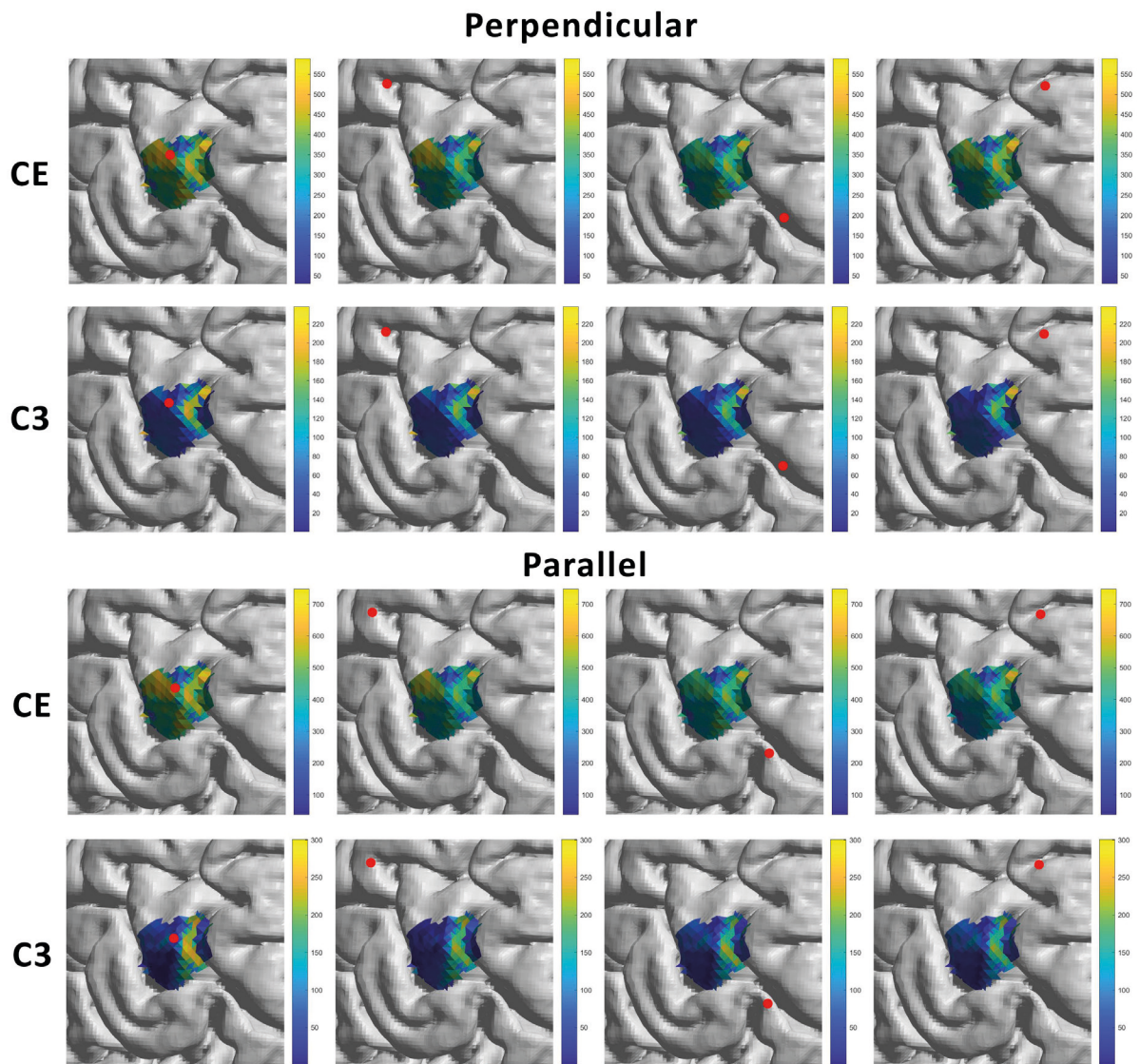


**Figure 4.** FEM-modeling results of activation within the hand knob based on two different metrics (CE and C3). Four different TMS coil positions are shown, with the position of the TMS coil isocenter indicated by a red dot. The CE and C3 metric are unitless.

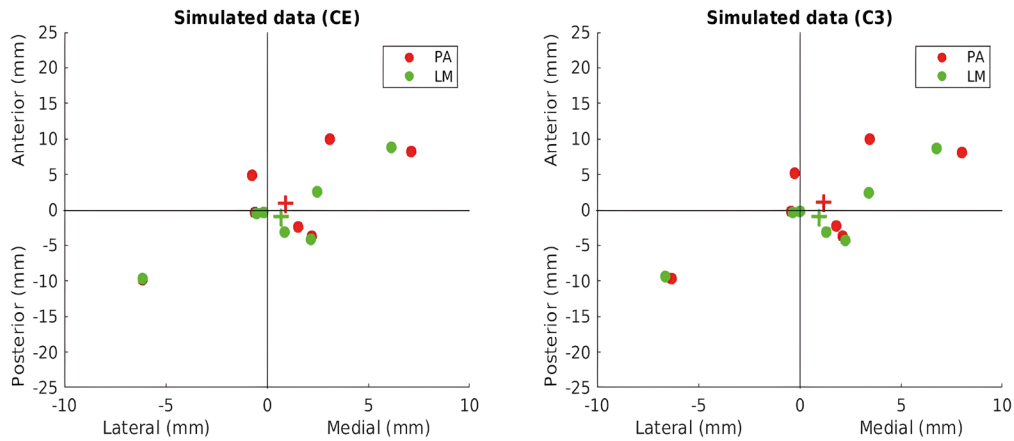


**Figure 5.** The relative locations of the COGs (FDI muscle) with respect to the location of the maximum BOLD response to voluntary thumb movements based on the FEM simulations. Two different metrics for activation of the hand knob were used (CE and C3 metric). Each dot represents an individual participant. The COGs obtained using PA- and LM-induced currents are shown as red and green dots, respectively. The mean simulated COGs are indicated by a plus (+).

## DISCUSSION

In this work, we identified the motor-eloquent cortex using two TMS-induced current directions and investigated how these representations relate to one another and to the spatial representation of the motor area as measured with fMRI.

Our main finding is that a PA-induced current identifies a motor representation which is located more anterior compared to an LM-induced current, for all the investigated muscles (FDI, ADM and ECR). These findings indicate that the interaction between the TMS-induced current and the cortical morphology of the stimulated cortex affects the spatial representation of the motor area identified with TMS. We hypothesized that our observations could be explained by the effect of anisotropic cortical conductance mediated by complex gyral folding patterns on the distribution of the TMS-induced E-field. We investigated this by constructing individual geometric volume conduction models based on individual MRI scans and subsequently evaluating the total E-field (CE) exerted on the hand motor area as a proxy for motor activity. We found that the difference in spatial representation of the TMS-based motor area as identified using two different TMS-induced current directions (PA and LM) cannot be explained by individual geometric volume conduction models alone. Consequently, the magnitude of the TMS-induced E-field within the hand motor area does not fully explain motor activity.

Previous work has highlighted the role of the orientation of the TMS-induced current with respect to the precentral gyrus<sup>10,11</sup>, the composition and conductivities of different tissues in the cortical layer<sup>12</sup>, and the gyral curvature<sup>13</sup>. We hypothesized that those aspects, which are relatively consistent between participants, affect the distribution of TMS-induced currents in such a way that PA-induced currents reveal an MEP motor area that is located anterior with respect to the motor area identified using LM-induced currents. We investigated the previously described orientation dependence through the C3 metric, which takes into account the orientation of the E-field with respect to the cortical surface. However, the C3 metric also did not explain the spatial separation between the TMS-based motor areas as identified using PA- and LM-induced currents. Therefore, activation of pyramidal motor neurons cannot be fully explained by taking into account the proportion of the TMS-induced electrical field perpendicular to the cortical surface.

The investigated models failed to capture the effect of the TMS coil orientation on the spatial representation of the TMS-based motor area. A potential explanation is that the investigated models do not fully capture the complexity of the interaction between the TMS-induced E-field and activation of pyramidal neurons within the hand motor area. However, the investigated models do not include multi-compartmental neuronal models, which provide a more detailed account of activation of different populations of pyramidal neurons<sup>30,31</sup>.

Another potential explanation comes from activation of different elements of the cortico-spinal neurons (CSNs), as different TMS-induced current directions have been shown to preferentially activate different elements of CSNs. More specifically, LM-induced currents have been shown to primarily elicit D-waves, which originate from axonal activation of CSNs<sup>28</sup>, while PA-induced currents have been shown to preferentially evoke I-waves, which originate from synaptic inputs of the CSNs<sup>32</sup>. Consequently, PA-induced currents evoke MEPs with longer latencies compared to LM-induced currents during stimulation of a single cortical target where the maximum MEP is evoked<sup>29,33</sup>. However, our findings show that if all the MEPs in the MEP motor map are considered, the average latency of MEPs obtained with a PA-induced current is not significantly different from that of MEPs obtained with an LM-induced current. This suggests that different TMS-induced current directions do not consistently recruit different elements of CSNs for different targets in the grid<sup>29</sup>. Therefore, it is unlikely that activation of different elements of the CSNs is the cause of the spatial shift between MEP motor maps obtained with PA- and LM-induced currents.

Finally, it is possible that the TMS-induced field also activates CSNs in the premotor area rather than just in M1, which means that the TMS-based motor area is truly dislocated with respect to the anatomical location. Two studies that applied DCS and navigated TMS have shown that stimulation of the premotor cortex can indeed induce motor activity<sup>34,35</sup>. Unfortunately, both studies only used a PA-induced current direction during TMS motor mapping, which precluded a comparison with LM-induced current.

Further research is required to determine the mechanism(s) behind the spatial distribution of MEP-eliciting cortical targets in response to different TMS-induced current directions. This can be done using concurrent TMS-fMRI in order to directly measure TMS-induced brain activity, and/or geometric volume conduction models and multi-compartmental neuronal models.

### **Navigated TMS-EMG can depict different muscle representations**

A secondary aim of this study was to confirm the sensitivity of navigated TMS-EMG in the identification of separate MEP motor areas for different muscles: the FDI, ADM and ECR muscles. Previous work has reported that the maps of different muscles of the upper extremities showed a consistent organization within the precentral gyrus, as described by Penfield, based on TMS-EMG results<sup>36,37</sup>. However, the separation between muscle motor maps was not quantified in this work.

We found that, at the group level, the COG of the MEP spatial distribution of the FDI muscle is significantly more lateral compared to the COG of the ADM muscle for both induced current directions, which is in line with layout of the motor homunculus as observed by Penfield<sup>38</sup>. Similar to our observations, Wilson et al. reported a significant separation between the centers of the FDI and ADM motor areas<sup>8</sup>. Although we found significantly separated COGs for the FDI and ADM muscles, the spatial distributions of the MEPs showed substantial overlap as well.

## **Comparison with fMRI**

The two motor maps identified using different TMS-induced current directions were not significantly separated from the fMRI-based motor area, except for the ADM. However, this separation can be explained by the fact that the fMRI task did not involve contraction of the ADM. The COGs obtained with a PA-induced current were located anterior to the location of the fMRI-based motor area for the APB and FDI. Although not statistically significant, this separation is in agreement with prior literature<sup>18-20,39</sup>. The average separation between the TMS-based COG and the fMRI-based hand area was slightly smaller for an LM-induced current compared to a PA-induced current, which might suggest that an MEP motor map obtained with an LM-induced current corresponds better with the fMRI-based hand area.

The current golden standard for mapping of the motor area is pre- or intraoperative direct current stimulation (DCS), which has been compared to both fMRI and TMS localization techniques. Krieg et al. (2012) compared TMS-based motor mapping using a PA-induced current with fMRI-based motor mapping and DCS, and found that motor maps obtained with TMS corresponded better with DCS compared to fMRI (average separations of 4.4 mm versus 9.8 mm). Nevertheless, they did not establish statistical significance and they did not observe a unidirectional systematic deviation between these modalities. Forster et al. (2011) and Coburger et al. (2013) observed a similar trend<sup>40,41</sup>. However, these findings should be interpreted with caution as the findings are based on measurements in patients with brain tumors, and brain tumors have different tissue conductivities, potentially resulting in different TMS-induced current distributions. Future studies should evaluate differences in overlap with DCS-obtained motor maps for different TMS-induced current directions.

## **CONCLUSION**

In conclusion, we found that the spatial representation of the motor eloquent cortex identified with TMS depends significantly on the direction of the induced current. We showed that this cannot be explained by the effect of complex gyral folding patterns on the TMS-induced E-field and/or taking into account the orientation dependence of neurons within the hand motor area. Our findings are relevant for the interpretation and use of nTMS-EMG motor maps for presurgical planning. Further research is required to identify the mechanism(s) through which differences in the TMS-induced current direction affect the spatial distribution of MEPs on the brain surface, as the electrophysiological principles that underlie these differences remain poorly understood.



## REFERENCES

1. Krieg SM, Sollmann N, Obermueller T, et al. Changing the clinical course of glioma patients by preoperative motor mapping with navigated transcranial magnetic brain stimulation. *BMC Cancer*. 2015;15(1):1-11. doi:10.1186/s12885-015-1258-1
2. Frey D, Schilt S, Strack V, et al. Navigated transcranial magnetic stimulation improves the treatment outcome in patients with brain tumors in motor eloquent locations. *Neuro-Oncology*. 2014;16(10):1365-1372. doi:10.1093/neuonc/nou110
3. Krieg SM, Sabih J, Bulubasova L, et al. Preoperative motor mapping by navigated transcranial magnetic brain stimulation improves outcome for motor eloquent lesions. *Neuro-Oncology*. 2014;16(9):1274-1282. doi:10.1093/neuonc/nou007
4. Krieg SM, Picht T, Sollmann N, et al. Resection of Motor Eloquent Metastases Aided by Preoperative nTMS-Based Motor Maps—Comparison of Two Observational Cohorts. *Frontiers in Oncology*. 2016;6(December):1-10. doi:10.3389/fonc.2016.00261
5. Tarapore PE, Picht T, Bulubas L, et al. Safety and tolerability of navigated TMS for preoperative mapping in neurosurgical patients. *Clinical Neurophysiology*. 2016;127(3). doi:10.1016/j.clinph.2015.11.042
6. Rossini PM, Burke D, Chen R, et al. Non-invasive electrical and magnetic stimulation of the brain, spinal cord, roots and peripheral nerves: Basic principles and procedures for routine clinical and research application: An updated report from an I.F.C.N. Committee. *Clinical Neurophysiology*. 2015;126(6):1071-1107. doi:10.1016/j.clinph.2015.02.001
7. Lüdemann-Podubecká J, Nowak DA. Mapping cortical hand motor representation using TMS: A method to assess brain plasticity and a surrogate marker for recovery of function after stroke? *Neurosci Biobehav Rev*. 2016;69:239-251. doi:10.1016/j.neubiorev.2016.07.006
8. Wilson S a., Thickbroom GW, Mastaglia FL. Transcranial magnetic stimulation mapping of the motor cortex in normal subjects. *Journal of the Neurological Sciences*. 1993;118(2):134-144. doi:10.1016/0022-510X(93)90102-5
9. Freundlieb N, Philipp S, Drabik A, Gerloff C, Forkert ND, Hummel FC. Ipsilesional motor area size correlates with functional recovery after stroke: A 6-month follow-up longitudinal TMS motor mapping study. *Restorative Neurology and Neuroscience*. 2015;33(2):221-231. doi:10.3233/RNN-140454
10. Mills KR, Boniface SJ, Schubert M. Magnetic brain stimulation with a double coil: the importance of coil orientation. *Electroencephalography and Clinical Neurophysiology/Evoked Potentials Section*. 1992;85(1):17-21.
11. Richter L, Neumann G, Oung S, Schweikard A, Trillenber P. Optimal Coil Orientation for Transcranial Magnetic Stimulation. *PLoS ONE*. 2013;8(4):1-10. doi:10.1371/journal.pone.0060358
12. Opitz A, Windhoff M, Heidemann RM, Turner R, Thielscher A. How the brain tissue shapes the electric field induced by transcranial magnetic stimulation. *Neuroimage*. 2011;58(3):849-859.
13. Opitz A, Legon W, Rowlands A, Bickel WK, Paulus W, Tyler WJ. Physiological observations validate finite element models for estimating subject-specific electric field distributions induced by transcranial magnetic stimulation of the human motor cortex. *NeuroImage*. 2013;81:253-364. doi:10.1016/j.neuroimage.2013.04.067

14. Bashir S, Perez JM, Horvath JC, Pascual-Leone A. Differentiation of motor cortical representation of hand muscles by navigated mapping of optimal TMS current directions in healthy subjects. *Journal of Clinical Neurophysiology*. 2013;30(4):390-395. doi:10.1097/WNP.0b013e31829dda6b
15. Stephani C, Paulus W, Sommer M. The effect of current flow direction on motor hot spot allocation by transcranial magnetic stimulation. *Physiological reports*. 2016;4(1):1-12. doi:10.14814/phy2.12666
16. Neggers SFW, Petrov PI, Mandija S, Sommer IEC, van den Berg NAT. *Understanding the Biophysical Effects of Transcranial Magnetic Stimulation on Brain Tissue: The Bridge between Brain Stimulation and Cognition*. Vol 222. 1st ed. Elsevier B.V.; 2015. doi:10.1016/bs.pbr.2015.06.015
17. Salinas FS, Lancaster JL, Fox PT. 3D modeling of the total electric field induced by transcranial magnetic stimulation using the boundary element method. *Physics in Medicine & Biology*. 2009;54(12):3631.
18. Sparing R, Buelte D, Meister IG, Pauš T, Fink GR. Transcranial magnetic stimulation and the challenge of coil placement: A comparison of conventional and stereotaxic neuronavigational strategies. *Human Brain Mapping*. 2008;29(1):82-96. doi:10.1002/hbm.20360
19. Neggers SFW, Langerak TR, Schutter D, et al. A stereotactic method for image-guided transcranial magnetic stimulation validated with fMRI and motor-evoked potentials. *Neuroimage*. 2004;21(4):1805-1817.
20. Herwig U, Kölbl K, Wunderlich AP, et al. Spatial congruence of neuronavigated transcranial magnetic stimulation and functional neuroimaging. *Clinical Neurophysiology*. 2002;113(4):462-468. doi:10.1016/S1388-2457(02)00026-3
21. Rossi S, Hallett M, Rossini PM, et al. Safety, ethical considerations, and application guidelines for the use of transcranial magnetic stimulation in clinical practice and research. *Clinical Neurophysiology*. 2009;120(12):2008-2039. doi:10.1016/j.clinph.2009.08.016
22. Penny WD, Friston KJ, Ashburner JT, Kiebel SJ, Nichols TE. *Statistical Parametric Mapping: The Analysis of Functional Brain Images*. Academic press; 2011.
23. Ashburner J, Friston KJ. Unified segmentation. *Neuroimage*. 2005;26(3):839-851.
24. Wagner TA, Zahn M, Grodzinsky AJ, Pascual-Leone A. Three-dimensional head model simulation of transcranial magnetic stimulation. *IEEE Transactions on Biomedical Engineering*. 2004;51(9):1586-1598.
25. Petrov PI, Mandija S, Sommer IEC, Van Den Berg CAT, Neggers SFW. How much detail is needed in modeling a transcranial magnetic stimulation figure-8 coil: Measurements and brain simulations. *PLoS ONE*. 2017;12(6):1-20. doi:10.1371/journal.pone.0178952
26. Fox PT, Narayana S, Tandon N, et al. Column-Based Model of Electric Field Excitation of Cerebral Cortex. *Human Brain Mapping*. 2004;22(1):1-14. doi:10.1002/hbm.20006
27. Laakso I, Hirata A, Ugawa Y. Effects of coil orientation on the electric field induced by TMS over the hand motor area. *Physics in Medicine and Biology*. 2014;59(1):203-218. doi:10.1088/0031-9155/59/1/203
28. Volz LJ, Hamada M, Rothwell JC, Grefkes C. What Makes the Muscle Twitch: Motor System Connectivity and TMS-Induced Activity. *Cerebral Cortex*. 2015;25(9):2346-2353.

doi:10.1093/cercor/bhu032

29. Hamada M, Murase N, Hasan A, Balaratnam M, Rothwell JC. The role of interneuron networks in driving human motor cortical plasticity. *Cerebral Cortex*. 2013;23(7):1593-1605. doi:10.1093/cercor/bhs147
30. Seo H, Schaworonkow N, Jun SC, Triesch J. A multi-scale computational model of the effects of TMS on motor cortex [version 1; referees: 2 approved with reservations]. *F1000Research*. 2016;5:1-24. doi:10.12688/F1000RESEARCH.9277.1
31. Rusu C V., Murakami M, Ziemann U, Triesch J. A model of TMS-induced I-waves in motor cortex. *Brain Stimulation*. 2014;7(3):401-414. doi:10.1016/j.brs.2014.02.009
32. Di Lazzaro V, Profice P, Ranieri F, et al. I-wave origin and modulation. *Brain Stimulation*. 2012;5(4):512-525. doi:10.1016/j.brs.2011.07.008
33. Di Lazzaro V, Pilato F, Dileone M, et al. Modulating cortical excitability in acute stroke: a repetitive TMS study. *Clinical Neurophysiology*. 2008;119(3):715-723.
34. Moser T, Bulubas L, Sabih J, et al. Resection of Navigated Transcranial Magnetic Stimulation-Positive Prerolandic Motor Areas Causes Permanent Impairment of Motor Function. 2018;81(1):99-110. doi:10.1093/neuros/nyw169
35. Bulubas L, Sabih J, Wohlschlaeger A, et al. Motor areas of the frontal cortex in patients with motor eloquent brain lesions. *Journal of neurosurgery*. 2016;125(6):1431-1442.
36. Wassermann EM, McShane LM, Hallett M, Cohen LG. Noninvasive mapping of muscle representations in human motor cortex. *Electroencephalography and Clinical Neurophysiology/ Evoked Potentials*. 1992;85(1):1-8. doi:10.1016/0168-5597(92)90094-R
37. Malcolm MP, Triggs WJ, Light KE, Shechtman O, Khandekar G, Rothi LJG. Reliability of motor cortex transcranial magnetic stimulation in four muscle representations. *Clinical neurophysiology*. 2006;117(5):1037-1046.
38. Penfield W, Rasmussen T. The cerebral cortex of man; a clinical study of localization of function. Published online 1950.
39. Lotze M, Kaethner RJ, Erb M, Cohen LG, Grodd W, Topka H. Comparison of representational maps using functional magnetic resonance imaging and transcranial magnetic stimulation. *Clinical Neurophysiology*. 2003;114(2):306-312.
40. Forster MT, Hattingen E, Senft C, Gasser T, Seifert V, Szelényi A. Navigated transcranial magnetic stimulation and functional magnetic resonance imaging: Advanced adjuncts in preoperative planning for central region tumors. *Neurosurgery*. 2011;68(5):1317-1324. doi:10.1227/NEU.0b013e31820b528c
41. Coburger J, Musahl C, Henkes H, et al. Comparison of navigated transcranial magnetic stimulation and functional magnetic resonance imaging for preoperative mapping in rolandic tumor surgery. *Neurosurgical Review*. 2013;36(1):65-75. doi:10.1007/s10143-012-0413-2



## Chapter 5

# **Continuous theta-burst stimulation of the contralesional primary motor cortex for promotion of upper limb recovery after stroke: a randomized controlled trial**

Jord JT Vink

Eline CC van Lieshout

Willem M Otte

Ruben PA van Eijk

Mirjam Kouwenhoven

Sebastiaan FW Neggers

H Bart van der Worp

Johanna MA Visser-Meily

Rick M Dijkhuizen

*Vink, Jord J T et al. "Continuous Theta-Burst Stimulation of the Contralesional Primary Motor Cortex for Promotion of Upper Limb Recovery After Stroke: A Randomized Controlled Trial." Stroke, 10.1161/STROKEAHA.123.042924. 22 Jun. 2023*

## **ABSTRACT**

### **Background**

Despite improvements in acute stroke therapies and rehabilitation strategies, many stroke patients are left with long-term upper limb motor impairment. We assessed whether an inhibitory repetitive transcranial magnetic stimulation (rTMS) treatment paradigm started within three weeks after stroke onset promotes upper limb motor recovery.

### **Methods**

We performed a single-center randomized, sham-controlled clinical trial. Patients with ischemic stroke or intracerebral hemorrhage and unilateral upper limb motor impairment were randomized to ten daily sessions of active or sham continuous theta burst stimulation (cTBS) of the contralesional primary motor cortex (M1) combined with standard upper limb therapy, started within three weeks after stroke onset. The primary outcome was the change in the Action Research Arm Test (ARAT) score from baseline (pre-treatment) at three months after stroke. Secondary outcomes included the score on the modified Rankin Scale (mRS) at three months and the length of stay (LOS) at the rehabilitation center. Statistical analyses were performed using mixed models for repeated measures.

### **Results**

We enrolled 60 patients between April, 2017 and February, 2021, of whom 29 were randomized to active cTBS and 31 to sham cTBS. One patient randomized to active cTBS withdrew consent before the intervention and was excluded from the analyses. The mean difference in the change in ARAT score from baseline at three months post-stroke was 9.6 points (95%CI 1.2-17.9;  $p$  0.0244) in favor of active cTBS. Active cTBS was associated with better scores on the mRS at three months (OR 0.2; 95%CI 0.1-0.8;  $p$  0.0225) and with an 18 days shorter length of stay at the rehabilitation center than sham cTBS (95%CI 0.0-36.4;  $p$  0.0494). There were no serious adverse events.

### **Conclusions**

Ten daily sessions of cTBS of the contralesional M1 combined with upper limb training, started within three weeks after stroke onset, promote recovery of the upper limb, reduce disability and dependence and leads to earlier discharge from the rehabilitation center.

## INTRODUCTION

Upper limb motor impairment is one of the most frequent long-term neurological consequences of ischemic stroke or intracerebral haemorrhage.<sup>1,2</sup> Despite recent developments in acute stroke treatment and rehabilitative therapy, recovery of upper limb motor function is often incomplete, resulting in limitations in functioning and participation.<sup>3-6</sup> More effective rehabilitation strategies that improve stroke recovery and lead to better clinical outcomes are therefore required.<sup>7</sup>

Spontaneous recovery after stroke is believed to be driven by neurobiological processes that occur mainly during a period of heightened brain plasticity in the first three months after stroke.<sup>8,9</sup> Conventional rehabilitation strategies focus on regaining function within this period primarily through physical therapy. Previous studies have shown that patients who have recovered from stroke present a more symmetrical inhibitory drive between the primary motor cortices.<sup>10-14</sup> An increased and persistent inhibitory drive from the contralesional to the ipsilesional primary motor cortex (M1) has been associated with more severe post-stroke motor deficits.<sup>10-13</sup> It has been suggested that restoration of the interhemispheric balance can result in a brain state that is more prone to spontaneous recovery and rehabilitation therapy of the affected arm.<sup>13</sup> On the other hand, excitability of the contralesional M1 may be within normal levels after stroke<sup>15</sup> and others have suggested that an interhemispheric imbalance might be a consequence of underlying processes of motor recovery.<sup>15,16</sup>

An interhemispheric imbalance may be restored through excitation of the lesioned M1 or inhibition of the contralesional M1.<sup>17</sup> Repetitive transcranial magnetic stimulation (rTMS) is a non-invasive brain stimulation method to up-<sup>18</sup> or downregulate<sup>19</sup> cortical excitability. Inhibitory rTMS of the contralesional M1 combined with upper limb therapy was initially investigated as a treatment for the promotion of upper limb recovery in chronic stroke patients.<sup>20</sup> However, a recent guidelines paper and a meta-analysis of randomized controlled trials indicate that inhibition of the contralesional M1 using inhibitory low-frequency (LF) rTMS followed by upper limb therapy is more effective in promoting upper limb recovery when started within the first two to three months post-stroke.<sup>21,22</sup> This has been shown to be the sensitive period for improvement of motor recovery<sup>23</sup>, presumably associated with heightened plasticity, which could potentially also facilitate a therapeutic effect of rTMS. Yet, it remains to be determined whether additional recovery achieved with rTMS treatment reduces disability and dependency and whether the effects persist after the first three months post-stroke.

Conventional LF rTMS treatment consists of 15-minute sessions, while continuous theta-burst stimulation (cTBS), a novel inhibitory rTMS paradigm, has a much shorter treatment duration of 40 seconds per session. Therefore, the use of cTBS can improve patient comfort and increase cost-effectiveness of the intervention.<sup>24,25</sup> So far, the effect of cTBS on upper limb recovery has only been tested in a single randomized trial randomizing only 14 patients to receive active cTBS group and 13 patients to receive sham cTBS.<sup>26</sup> This did not reveal an effect of cTBS started within 10 weeks after stroke on the change on a multifaceted upper limb motor function score (obtained from four upper limb function tests) within 30 days after treatment with respect to the change in this score (over a period of 7 days) before treatment. We assessed whether two weeks of daily contralesional cTBS started within the first three weeks after stroke improves long-term upper limb motor recovery up to 12 months post-stroke.

## **METHODS**

### **Study design**

We performed a single-center, prospective, randomized, sham-controlled clinical trial with a single-blind intervention and a double-blind primary outcome evaluation at rehabilitation center De Hoogstraat (Utrecht, The Netherlands), according to CONSORT guidelines. Deidentified participant data are available from the corresponding author upon reasonable request. A summary of the trial protocol has been published<sup>27</sup> and the full protocol is available in the supplementary materials. The study was approved by the Medical Research Ethics Committee of the University Medical Center Utrecht.

### **Participants**

We included patients aged 18 years or older with first-ever ischemic stroke or intracerebral hemorrhage and a paresis of one arm, as defined by a Motricity Index (MI)<sup>28</sup> between 9 and 99, in whom treatment could be started within three weeks after stroke onset.<sup>29</sup> Patients were excluded from participation if they had another disabling medical condition, as determined by the treating physician; could use the hand of the paretic arm (almost) normally (MI pinch grip score of 33); had a severe deficit in communication, memory, or understanding that would impede proper study participation; or had a contraindication to rTMS according to TMS safety guidelines.<sup>30</sup> All patients gave written informed consent.

### **Randomization and masking**

Patients were randomly assigned to ten daily sessions of contralesional cTBS or to sham cTBS during two weeks, in addition to regular care upper limb therapy, using a secured online allocation system (Research Online V2.0, Julius Centre, the Netherlands) by the investigator performing the treatment. Randomization was stratified according to the ability to extend one or more fingers of the paretic arm.<sup>31</sup> Sham cTBS was performed at 10% of the resting motor threshold (RMT), which was defined as the minimum machine output (MO) at which stimulation evoked at least five out of ten MEPs with a peak-to-peak amplitude of over 50  $\mu\text{V}$ <sup>25</sup>, with the TMS coil rotated 45 degrees relative to the scalp, and patients were masked to treatment allocation using auditory masking of the TMS coil sound.

### **Procedures**

Treatment was delivered in ten daily sessions on consecutive working days. cTBS was delivered over the contralesional M1, which was defined as the position on the scalp at which motor-evoked potentials (MEPs) with the largest peak-to-peak amplitude could be evoked in the contralateral first dorsal interosseous (FDI) muscle by delivering TMS pulses and monitoring the electromyogram (EMG). A Neuro-MS/D advanced therapeutic magnetic stimulator and an angulated 100 mm figure-of-eight TMS coil (Neurosoft, Ivanovo, Russia) were used for stimulation. EMG was recorded, amplified, and digitized at a sampling frequency of 20 kHz using a four-channel Neuro-MEP amplifier (Neurosoft, Ivanovo, Russia). cTBS consisted of continuous delivery of three stimuli bursts at 50 Hz repeated at five bursts per second for a duration of forty seconds with a biphasic TMS-induced current at 45 degrees to the midline. Stimulation intensity was set at 70% of the RMT. TMS coil placement was recorded using a neuronavigation system (Brain Science Tools BV, De Bilt, The Netherlands) starting from the 16<sup>th</sup> patient. cTBS or sham cTBS was delivered 15 minutes before standard upper limb therapy, which consisted of a 60-minute group therapy session of individualized upper limb exercises, according to the Concise Arm and hand Rehabilitation Approach in



Stroke (CARAS).<sup>32</sup> CARAS consists of a daily training program during which patients perform specific exercises with the paretic arm under guidance of physical or occupational therapists, supplemented with exercises they can perform independently during the rest of the day.

## Outcomes

The primary outcome measure was the change in the action research arm test (ARAT) score from baseline at three months after stroke, as recommended by the Stroke Recovery and Rehabilitation Roundtable (SRRR).<sup>33</sup> The ARAT is a performance test that assesses the ability to perform gross movements and to grasp, move and release objects differing in size, weight, and shape, of which validity and reliability have been demonstrated previously.<sup>34,35</sup> The ARAT ranges from 0 to 57, with higher scores indicating better performance. The ARAT was measured at three months after stroke by an independent trained physician assistant, blinded to treatment allocation.

Predefined secondary outcomes included the change in ARAT score <12 hours, 1 week and 1 month post-treatment, and 6 and 12 months post-stroke. Other predefined secondary outcomes were tests that assess different domains of the international classification of functioning, disability, and health (ICF) framework.<sup>36</sup> These included the upper limb section of the Fugl-Meyer assessment (FMA) score<sup>37</sup> for motor impairment; the stroke upper limb capacity score (SULCS),<sup>38</sup> Jebsen Taylor test (JTT)<sup>39</sup> score, Barthel Index<sup>40</sup> and Nine Hole Peg Test (NHPT)<sup>41</sup> for activity; the modified Rankin Scale (mRS)<sup>42</sup> for disability; and the upper limb section of the stroke impact scale (SIS-UL)<sup>43</sup> and EuroQol(EQ)-5D<sup>44</sup> for quality of life. Secondary outcomes were assessed by an investigator who was aware of the treatment allocation. Table 2 shows an overview of the measures that were assessed for each visit. We also assessed the length of stay (LOS) in the rehabilitation center, the dose of upper limb therapy and self-practice during the two-week treatment period and the week thereafter, and the contralesional RMT before each cTBS session. We monitored and recorded (serious) adverse events (AEs) that occurred during the two-week treatment period or one week thereafter.

## Statistical analysis

The sample size calculation was based on an effect size of 0.55 on the ARAT score obtained from a meta-analysis.<sup>27</sup> To detect the hypothesized effect with 80% power, and a two-sided alpha of 0.05, a total sample size of 56 patients was required. We included sixty patients, with thirty patients per group, to account for loss to follow-up.

We followed the pre-specified statistical analysis plan, which is available in the supplementary materials and was completed prior to data-lock. The primary outcome was the change in ARAT score from baseline (pre-treatment) at three months post-stroke.<sup>27</sup> The primary analysis was performed using a linear mixed model for repeated measures (MMRM) with an unstructured variance-covariance matrix in the intention-to-treat (ITT) population, includes all randomized participants irrespective of follow-up. Missing data were assumed to be missing at random. The model included the baseline value of the investigated outcome; the stratification factor (ability vs. no ability to extend one or more fingers), visit (<12 hours, 1 week and 1 month post-treatment, and 3, 6 and 12 months post-stroke) and the interaction of treatment (sham cTBS; active cTBS) by visit. We performed a sensitivity analysis of the primary outcome in the per-protocol (PP) population (defined as those who had an ARAT score assessed at three months) and additional sensitivity analyses in which additional covariates, i.e. MEP status and dominant hand paresis, were included in the main analysis.

We performed similar analyses for the effect of treatment on the secondary outcomes at all visits except for the mRS and LOS. The mRS was analyzed using a cumulative link mixed

model of the total mRS scores due to the ordinal nature of the data. The effect of treatment on the LOS and the dose of upper limb therapy and self-practice that patients received were analyzed with independent samples t-tests. The effect of treatment on excitability of the contralesional M1 was analyzed using a linear mixed-effects model (LME). The outcome was the contralesional RMT determined before each cTBS session and the LME included the baseline RMT, number of cTBS session (1 to 10) and type of treatment (sham cTBS; active cTBS). Pearson's correlation was used to calculate the correlation between the change in contralesional RMT during the treatment period and the change in ARAT score between baseline and 3 months post-stroke.

Statistical analysis was performed with R 4.1 and SPSS 26.0 (IBM, Chicago, IL, USA). All hypotheses were tested with a two-sided alpha of 0.05.

## RESULTS

Between April 14, 2017 and February 12, 2021, 494 stroke patients with arm weakness were screened for eligibility, of whom 60 were enrolled (**Figure 1**). Twenty-nine patients were randomly assigned to receive active cTBS, of whom one withdrew consent before starting treatment, leaving 28 patients in the cTBS group, and 31 patients were assigned to receive sham cTBS. Therefore, the ITT population consisted of 59 patients. The ARAT could not be assessed at three months in three patients (one in the active cTBS group and two in the sham cTBS group) due to physical limitations (shoulder pain, tiredness) and one patient in the sham cTBS group had a recurrent stroke. These four patients were excluded from the PP population (**Figure 1**).

Patient characteristics are shown in **Table 1**. None of the patients had previously been treated with cTBS.

The <12 hours, 1 week and 1 month post-treatment visits were assessed 29 (SD 4), 36 (SD 5) and 59 (SD 7) days post-stroke, respectively, and the 3, 6 and 12 months post-stroke visits were assessed 90 (SD 4), 184 (SD 11) and 368 (SD 10) days post-stroke, respectively. The change in ARAT score from baseline at three months post-stroke was 27.6 points in the active cTBS group compared to 18.0 points in the sham cTBS group, with a mean difference of 9.6 points (95% CI 1.2 to 17.9; p 0.0244; **Figure 2A**). Sensitivity analysis showed a mean difference in ARAT change score of 9.9 points (95% CI 1.1 to 18.7; p 0.0276) in the PP population in favor of active cTBS. Sensitivity analyses including baseline MEP status or dominant hand paresis as additional covariate showed mean differences in ARAT change score of 8.4 points (95% CI 0.3 to 16.5; p 0.0414) and 9.2 points (95% CI 0.7 to 17.6; p 0.0341), respectively, both in favor of active cTBS.

In the secondary analyses, the mean difference at three months post-stroke between active and sham cTBS groups was 9.1 points on the FMA (95% CI 1.5 to 16.7; p 0.0196; **Figure 2B**), 1.3 points on the SULCS (95% CI 0.1 to 2.5; p 0.0496), -19.4 points on the JTT (95% CI -37.3 to -1.5; p 0.0342), -3.5 points on the NHPT (95% CI -7.5 to 0.6; p 0.0907; **Figure 2C**), 1.2 points on the BI (95% CI 0.5 to 2.0; p 0.0015), 4.3 points on the SIS-UL (95% CI 1.4 to 7.2; p 0.0041) and -0.5 on the EQ-5D (95% CI -1.9 to 0.9; p 0.4852), all indicating better outcomes except for the NHPT and EQ-5D. Score on the mRS were better with active than with sham cTBS (odds ratio 0.2; 95% CI 0.1 to 0.8; p 0.0225; **Figure 3**). Details are presented in **Table 2**.

The mean LOS was 63 days in the active cTBS group compared to 81 days in the sham cTBS group with a mean difference of 18 days (95% CI 0.0 to 36.4; p 0.0494). Mean duration of upper limb therapy in the first three weeks after TMS treatment onset was 17.0 hours in the active cTBS group compared to 17.4 hours in the sham cTBS group (95% CI -2.2 to 1.4; p 0.6628). Mean duration of independent self-practice was 8.1 hours in the active cTBS group compared

to 8.5 hours of in the sham cTBS group (95% CI -4.9 to 4.1; p 0.8572). Active cTBS resulted in a mean increase of 1.4% of the contralesional RMT (95% CI -0.0 to 2.7; p 0.0515). The change in contralesional RMT during the treatment was not associated with the change in ARAT score between baseline and 3 months post-stroke in the active cTBS group (r 0.02; p 0.9082).

No serious adverse events (SAEs) were reported. Headache was the most prevalent side effect, which occurred more frequently with active cTBS (in ten out of 279 sessions) than with sham cTBS (in three out of 307 sessions). Other side effects (i.e., muscle pain and nausea) were rare (Table 3).

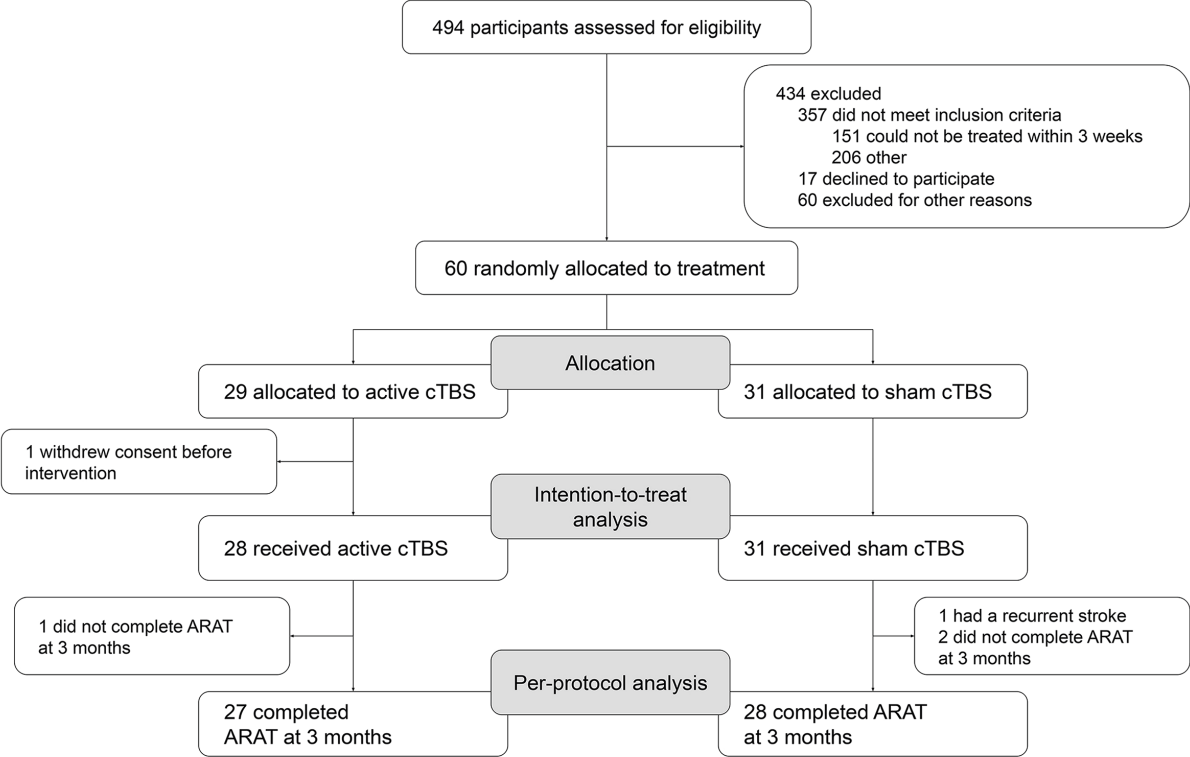
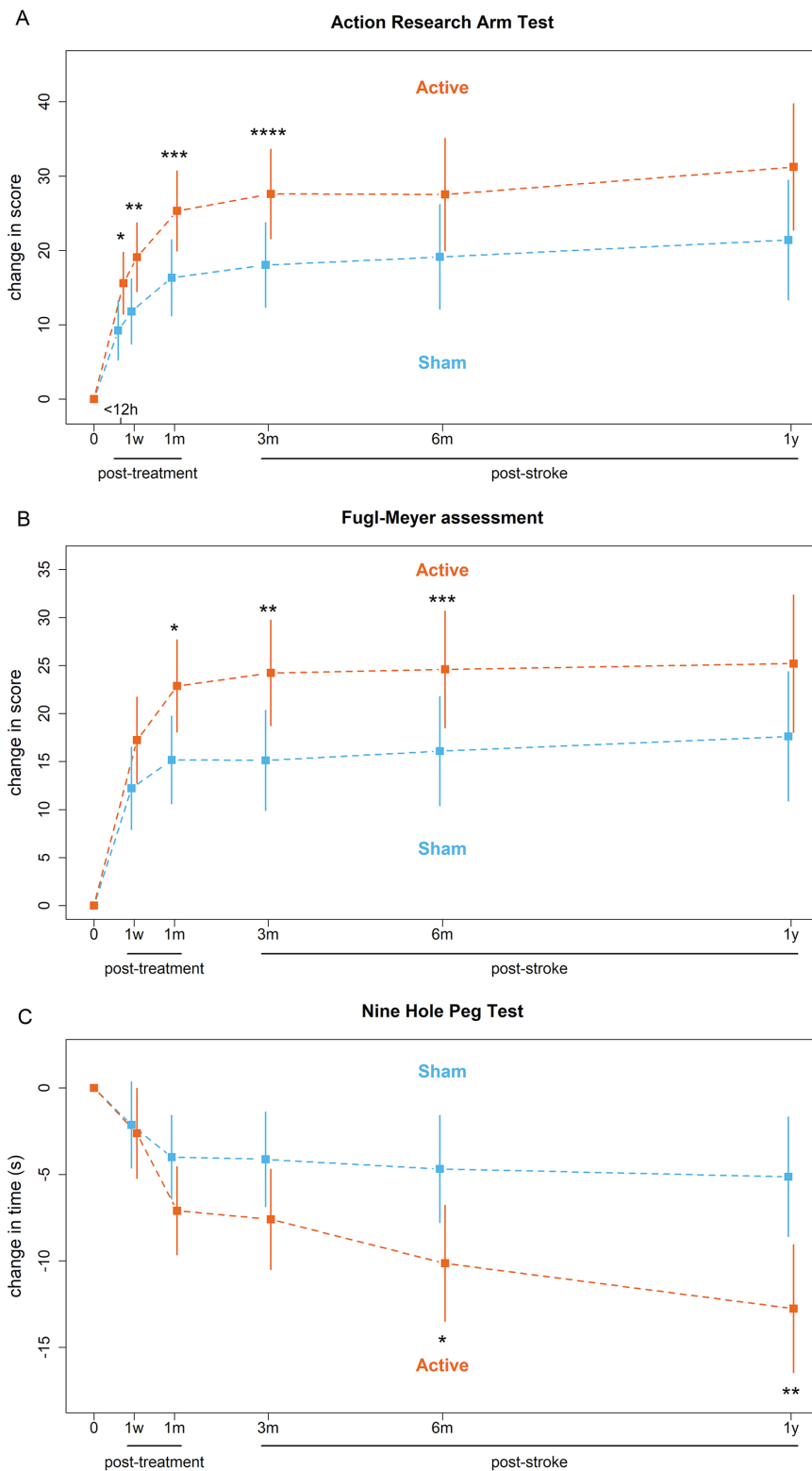


Figure 1. Participant flow diagram

**Table 1.** Baseline characteristics (full table available in supplemental materials)

Patient characteristics	Total (n = 59)	Active cTBS (n = 28)	Sham cTBS (n = 31)
Sex, n (%)			
Male	40 (68)	18 (64)	22 (71)
Female	19 (32)	10 (36)	9 (29)
Age, mean (SD), years	60.2 (12)	56.8 (12)	63.4 (12)
Intervention			
cTBS onset, mean (SD), days post-stroke	14 (4)	14 (5)	15 (4)
Stroke information			
Lesion type, n (%)			
Ischaemic stroke	50 (85)	24 (86)	26 (84)
Intracerebral haemorrhage	9 (15)	4 (14)	5 (16)
Impaired arm, n (%)			
Dominant arm <sup>1</sup>	24 (41)	15 (56)	9 (29)
Onset intervention			
Days post-stroke, mean (SD)	16 (4)	16 (4)	17 (4)
Baseline assessment			
Days post-stroke, mean (SD)	14 (4)	14 (5)	15 (4)
Electrophysiology			
MEP presence, n (%)			
Affected hemisphere	20 (34)	11 (39)	9 (29)
Unaffected hemisphere	59 (100)	28 (100)	31 (100)
Baseline function			
Motor impairment, mean (SD)			
Fugl-Meyer Assessment Arm score	25.6 (18.6)	24.1 (18.0)	27.0 (19.3)
Motor function, mean (SD)			
Action Research Arm Test	12.4 (16.6)	11.5 (16.6)	13.2 (16.8)
Motor activity, mean (SD)			
Stroke Upper Limb Capacity Score	3.1 (2.8)	2.9 (2.7)	3.3 (3.0)
Jebsen Taylor Test	100.7 (32.7)	104.3 (28.9)	97.6 (35.8)
Nine Hole Peg Test	1.7 (4.4)	1.3 (3.7)	2.1 (4.9)
Barthel Index	12.4 (4.2)	12.6 (3.9)	12.3 (4.5)
Disability, median (IQR)			
modified Rankin Scale	4 (1)	4 (1)	4 (1)
Quality of life, mean (SD)			
Stroke Impact Scale – upper limb	7.6 (4.3)	7.6 (4.1)	7.6 (4.6)
EuroQol-5D	7.1 (4.3)	6.0 (4.0)	8.2 (4.4)

<sup>1</sup>Bimanual ignored. cTBS: continuous Theta Burst Stimulation; SD: Standard deviation; MEP: Motor-evoked potential



**Figure 2.** Mean and 95% confidence intervals of the changes in (A) Action Research Arm Test (ARAT) scores, (B) Fugl-Meyer assessment (FMA) arm scores and (C) Nine Hole Peg Test (NHPT) times for the active and sham cTBS groups calculated using mixed-effects model for repeated measures. 0: baseline; h: hours; w: weeks; m: months; y: years (A) ARAT score ranges from 0 to 57 points and a higher score indicates better outcome. \* $p < 0.0310$ . \*\* $p < 0.0259$ . \*\*\* $p < 0.0183$ . \*\*\*\* $p < 0.0244$ . (B) FMA score ranges from 0 to 66 points and a higher score indicates better outcome. \* $p < 0.0241$ . \*\* $p < 0.0196$ . \*\*\* $p < 0.0461$ . (C). Maximum NHPT time is 50 seconds and a

lower time indicates better outcome. \* $p$  0.0204. \*\* $p$  0.0036.

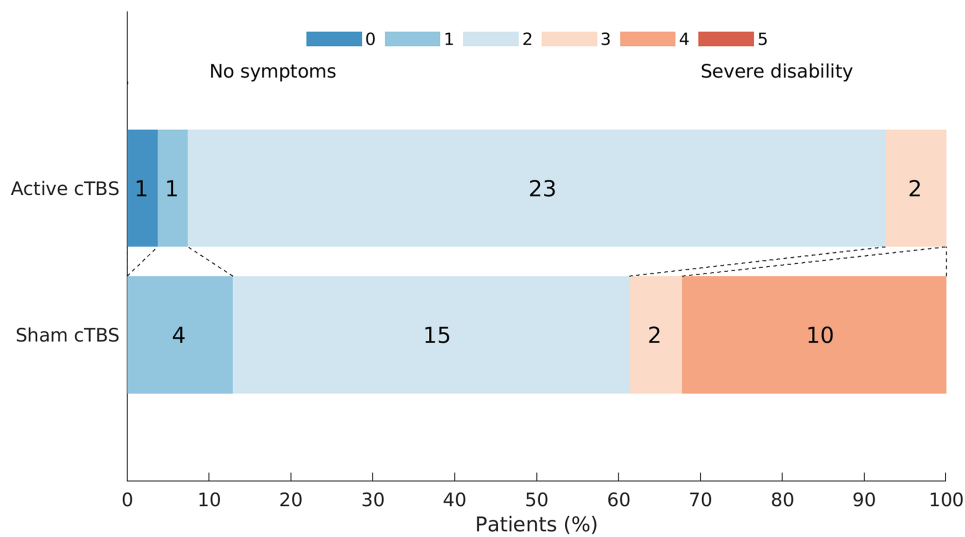


**Figure 3.** Modified Rankin Scale (mRS) scores at three months post-stroke for the active and sham cTBS groups. The mRS ranges from 0 to 5 and a lower score indicates better outcome.  $p$  0.0225.

**Table 2.** Primary and secondary outcomes (full table available in supplemental materials).

Outcome	Visit (n)	Mean difference in the change score between groups or odds ratio (95% CI)	P-value
Primary outcome			
Action Research Arm Test	3 months (56)	9.6 (1.2-17.9)	0.0244
Secondary outcomes			
Motor impairment			
Fugl-Meyer Assessment Arm	1 week(58)	5.0 (-1.2 to 11.3)	0.1149
	1 month(57)	7.7 (1.0 to 14.4)	0.0241
	3 months(55)	9.1 (1.5 to 16.7)	0.0196
	6 months(47)	8.5 (0.1 to 16.9)	0.0461
	12 months(50)	7.6 (-2.3 to 17.5)	0.1316
Motor function			
Action Research Arm Test	<12 hours(59)	6.4 (0.6 to 12.1)	0.0310
	1 week(58)	7.3 (0.9 to 13.7)	0.0259
	1 month(57)	9.0 (1.5 to 16.5)	0.0183
	3 months	See primary outcome	
	6 months(45)	8.4 (-2.0 to 18.8)	0.1121
	12 months(49)	9.8 (-1.9 to 21.6)	0.1011
Motor activity			
Stroke Upper Limb Capacity Scale	1 month(55)	1.1 (-0.1 to 2.3)	0.0812
	3 months(55)	1.3 (0.1 to 2.5)	0.0496
	6 months(46)	1.9 (0.5 to 3.2)	0.0082
	12 months		
Jebsen Taylor Hand Test	1 week(57)	-14.5 (-31.4 to 2.4)	0.0911
	1 month(56)	-15.4 (-32.1 to 1.4)	0.0714
	3 months(55)	-19.4 (-37.3 to -1.5)	0.0342
	6 months(45)	-21.9 (-42.5 to -1.3)	0.0372

Nine Hole Peg Test	<12 hours		
	1 week(58)	-0.5 (-4.1 to 3.1)	0.7908
	1 month(57)	-3.1 (-6.7 to 0.5)	0.0873
	3 months(57)	-3.5 (-7.5 to 0.6)	0.0907
	6 months(47)	-5.5 (-10.1 to -0.9)	0.0204
	12 months(49)	-7.6 (-12.7 to -2.5)	0.0036
Barthel Index	1 week(58)	1.7 (0.5 to 2.9)	0.0069
	1 month(57)	1.1 (0.1 to 2.0)	0.0310
	3 months(56)	1.2 (0.5 to 2.0)	0.0015
	6 months(57)	0.5 (-0.1 to 1.1)	0.1273
	12 months(53)	0.2 (-0.4 to 0.9)	0.4564
Disability (OR)			
modified Rankin Scale <sup>1</sup>	1 month(57)	0.23 (0.05 to 0.95)	0.0418
	3 months(58)	0.20 (0.05 to 0.79)	0.0225
	6 months(57)	0.39 (0.1 to 1.58)	0.1886
	12 months(53)	1.81 (0.44 to 7.44)	0.4109
Quality of life			
Stroke Impact Scale - upper limb	1 month(55)	2.7 (-0.1 to 5.4)	0.0552
	3 months(58)	4.3 (1.4 to 7.2)	0.0041
	6 months(50)	3.1 (-0.1 to 6.2)	0.0545
EuroQol-5D	3 months(56)	-0.5 (-1.9 to 0.9)	0.4852
	6 months(55)	0.1 (-1.3 to 1.5)	0.8421
	12 months(51)	0.6 (-0.8 to 1.9)	0.4029

<sup>1</sup>Odds ratios are reported because an ordinal statistical analysis was performed. Visits within 12 hours, at 1 week and at 1 month are post-treatment, while visits at 3, 6 and 12 months are post-stroke. n = number of observed data points per visit. OR: Odds ratio.

**Table 3.** Adverse events reported during the two-week treatment period and 1 week thereafter.

Adverse event, n (%)	Total (n=586 <sup>1</sup> )	Active cTBS (n=279)	Sham cTBS (n=307)	P-value
Nausea	1 (0.17)	0 (0)	1 (0.33)	0.524
Headache	13 (2.22)	10 (3.58)	3 (0.98)	0.030
Muscle pain	2 (0.34)	2 (0.72)	0 (0)	0.226
Sensory impairment	1 (0.17)	0 (0)	1 (0.33)	0.524
Slowed thinking	2 (0.34)	0 (0)	2 (0.65)	0.274

<sup>1</sup>Total amount of cTBS sessions performed.

## DISCUSSION

Patients who received active cTBS showed greater improvement in upper limb recovery as measured with the ARAT at three months post-stroke compared to patients who received sham cTBS. The mean additional improvement of 9.5 points (17% of the maximum ARAT score) on the ARAT is clinically meaningful and exceeds the previously established minimal clinically important difference (MCID) of 5.7 points (10% of the maximum ARAT score).<sup>45</sup> The treatment benefit was observed directly after the two-week treatment period and until follow-up at 3 months after stroke. The therapeutic effect could not be established at 6 and 12 months post-stroke, possibly due to a plateau effect on the ARAT. A similar treatment effect was observed for the FMA arm score, which was also clinically meaningful,<sup>37</sup> and the Barthel Index. However, other tests (NHPT, SULCS, JTT) in the activity domain did show a treatment benefit up to 12 months post-stroke. These tests are more sensitive to improvement in fine motor skills<sup>46</sup> and manual dexterity.<sup>47</sup> Patients in the sham cTBS group showed little improvement on these test

after three months, while patients in the active cTBS group showed continued improvement of fine motor skills and manual dexterity up to 12 months post-stroke. We hypothesize that additional upper limb recovery in the first months after stroke, which may plateau out on commonly used upper limb motor scales, leads to more frequent use of the affected limb in more complex daily life activities, resulting in increased performance of fine motor skills and manual dexterity that persists over longer times.

Patients who received active cTBS showed more improvement on metrics of disability and dependency (mRS) and quality of life (SIS-UL) at 1 month post-treatment and at 3 months post-stroke, compared to patients who were treated with sham stimulation. The EuroQol-5D was a quality of life metric that did not show a treatment effect, presumably due to involvement of factors that are not directly related to an improvement in upper limb recovery, like pain and anxiety. In addition to a treatment effect on these metrics, the length of stay in the rehabilitation center, an indicator of independency, was 18 days shorter in patients treated with active cTBS compared to patients who received sham cTBS. These findings suggest that patients who received active cTBS were able to independently perform activities of daily living and participate in society at an earlier stage compared to patients who received sham cTBS. Equally important to efficacy, the investigated cTBS treatment was safe and tolerable, as no serious adverse events were reported. Headache was more prevalent in the active cTBS group, but overall mild side-effects (headache/nausea) were uncommon (less than 4% of cases).

We did not detect a significant effect of active cTBS on contralesional M1 excitability, although a trend toward long-lasting (days) inhibition of the contralesional M1 could be observed. We speculate that active cTBS leads to a short-lasting reduction (< 2 hours) in contralesional M1 excitability, which has dissipated the next day, but which facilitates the effects of upper limb therapy directly following cTBS. Unfortunately, the acute effect of cTBS could not be measured as the cTBS treatments were directly followed by upper limb therapy. Our findings are in line with a recent meta-analysis that showed that contralesional inhibitory rTMS improves upper limb recovery on the FMA arm score with a similar mean difference of 9 points at 3 months post-stroke.<sup>22</sup> Our study provides additional evidence that contralesional cTBS started within 3 weeks post-stroke effectively promotes upper limb recovery after stroke with a continued benefit until at least 12 months. Furthermore, we also observed a positive effect on scores of activity, disability and quality of life, which were not identified in aforementioned meta-analysis.<sup>22</sup>

Earlier meta-analyses of effects of rTMS treatment within the first months post-stroke were based (almost) exclusively on inhibition with conventional LF rTMS.<sup>17,22</sup> A recently completed trial on contralesional LF rTMS in 77 patients did not find an effect on upper limb recovery.<sup>48</sup> Continuous TBS has a substantially shorter treatment duration than LF rTMS, which increases patient comfort, makes it more suitable for use in time-constrained rehabilitation programs and potentially increases cost-effectiveness. An earlier study that assessed the impact of contralesional cTBS in the subacute post-stroke stage did not observe a clinical effect on motor function.<sup>26</sup> This apparent discrepancy with our study may be explained by the smaller sample size (fourteen patients in the cTBS group), the later start of cTBS treatment with respect to stroke onset, the lower frequency of cTBS sessions (three sessions per week over three weeks), or the non-matching of upper limb physical therapy with cTBS sessions in that study.

A third of the screened patients did not meet the inclusion criteria because the treatment could not be started within 3 weeks after stroke onset. Extension of the treatment time window would have increased the number of eligible patients, but posed the risk of reducing the treatment efficacy, as a previous meta-analysis demonstrated efficacy for



treatment only when started within the first month post-stroke.<sup>22</sup>

### Limitations

Our study had some limitations. First, the researchers were not blinded to the treatment allocation due to practical reasons concerning the sham condition, what could have introduced bias during the treatment period. In addition, while we performed double-blinded assessment of the primary outcome at three months, most secondary outcomes were assessed in a single-blind fashion. However, the considerably shorter length of stay in the rehabilitation center strongly suggests that the benefits observed on the other secondary outcomes are real.

Second, the sham condition did not consist of electrical stimulation to mask sensory sensations on the scalp evoked by peripheral nerve stimulation during TMS, and successful blinding of patients was not verified by asking patients which treatment group they believed they were assigned to. However, all patients were naive to cTBS treatment, which potentially reduces the bias introduced by limitations in the sham condition.

Third, we only measured the duration of upper limb therapy that patients received during the two-week treatment period and the week thereafter. However, it is unlikely that patients in both groups received different durations of upper limb therapy after this period, as all patients were part of the same treatment schedule. While upper limb therapy content was balanced between groups at onset of treatment, this may have changed based on additional improvement in upper limb function due to active cTBS, in accordance with the CARAS protocol. However, because both patients and therapists were blinded to treatment allocation, we consider it unlikely that patients in the active cTBS group received different upper limb therapy content unless the change in therapy was the direct result of improved motor function caused by active cTBS.

Fourth, we only scored the upper limb component of the FMA. Assessment of the lower limb component could have provided insights into the specificity of the treatment.

Fifth, the investigated sample consisted predominantly of males, which could limit generalizability of the results to females.

Finally, our treatment paradigm was based on the theoretical interhemispheric imbalance model. However, we did not explicitly evaluate the interhemispheric balance before or after the intervention.

### Future research

The results in this single-center study are promising and provide a strong foundation for future multi-center trials to provide conclusive evidence on the efficacy of cTBS treatment in the promotion of upper limb recovery after stroke. These trials could tailor treatment to individual patients, as recent studies suggest that efficacy of contralesional cTBS may depend on stroke severity<sup>49</sup> or stroke type.<sup>50</sup>

### CONCLUSION

In the present study, treatment with cTBS of the contralesional M1 combined with upper limb training, started within three weeks after stroke onset, improved upper limb motor recovery and led to better functional outcomes. Some treatment benefits persisted up to at least twelve months after stroke.

## REFERENCES

1. Go AS, Mozaffarian D, Roger VL, et al. Executive summary: heart disease and stroke statistics—2014 update: a report from the American Heart Association. *Circulation*. American Heart Association. Published online 2014.
2. Langhorne P, Bernhardt J, Kwakkel G. Stroke rehabilitation. *The Lancet*. 2011;377(9778):1693-1702. doi:10.1016/S0140-6736(11)60325-5
3. Broeks JG, Lankhorst GJ, Rumping K, Prevo AJ. The long-term outcome of arm function after stroke: results of a follow-up study. *Disabil Rehabil*. 1999;21(8):357-364.
4. Mayo NE, Wood-Dauphinee S, Ahmed S, et al. Disablement following stroke. *Disabil Rehabil*. 1999;21(5-6):258-268. doi:10.1080/096382899297684
5. Nichols-Larsen DS, Clark PC, Zeringue A, Greenspan A, Blanton S. Factors influencing stroke survivors' quality of life during subacute recovery. *Stroke*. 2005;36(7):1480-1484. doi:10.1161/01.STR.0000170706.13595.4f
6. Lieshout ECC van, van de Port IG, Dijkhuizen RM, Visser-Meily JMA. Does upper limb strength play a prominent role in health-related quality of life in stroke patients discharged from inpatient rehabilitation? *Top Stroke Rehabil*. 2020;00(00):1-9. doi:10.1080/10749357.2020.1738662
7. Fisicaro F, Lanza G, Grasso A, et al. Repetitive transcranial magnetic stimulation in stroke rehabilitation: review of the current evidence and pitfalls. *Ther Adv Neurol Disord*. 2019;12:1-22. doi:10.1177/175628641987317
8. Krakauer JW, Carmichael ST, Corbett D, Wittenberg GF. Getting neurorehabilitation right: what can be learned from animal models? *Neurorehabil Neural Repair*. 2012;26(8):923-931. doi:10.1177/1545968312440745
9. Hordacre B, Austin D, Brown KE, et al. Evidence for a Window of Enhanced Plasticity in the Human Motor Cortex Following Ischemic Stroke. *Neurorehabil Neural Repair*. 2021;35(4):307-320. doi:10.1177/1545968321992330
10. Duque J, Hummel F, Celnik P, Murase N, Mazzocchio R, Cohen LG. Transcallosal inhibition in chronic subcortical stroke. *Neuroimage*. 2005;28(4):940-946. doi:10.1016/j.neuroimage.2005.06.033
11. Murase N, Duque J, Mazzocchio R, Cohen LG. Influence of Interhemispheric Interactions on Motor Function in Chronic Stroke. *Ann Neurol*. 2004;55(3):400-409. doi:10.1002/ana.10848
12. Nowak DA, Grefkes C, Ameli M, Fink GR. Interhemispheric competition after stroke: Brain stimulation to enhance recovery of function of the affected hand. *Neurorehabil Neural Repair*. 2009;23(7):641-656. doi:10.1177/1545968309336661
13. Boddington LJ, Reynolds JNJ. Targeting interhemispheric inhibition with neuromodulation to enhance stroke rehabilitation. *Brain Stimul*. 2017;10(2):214-222. doi:10.1016/j.brs.2017.01.006
14. Casula EP, Pellicciari MC, Bonni S, et al. Evidence for interhemispheric imbalance in stroke patients as revealed by combining transcranial magnetic stimulation and electroencephalography. *Hum Brain Mapp*. 2021;42(5):1343-1358. doi:10.1002/hbm.25297
15. McDonnell MN, Stinear CM. TMS measures of motor cortex function after stroke: A

meta-analysis. *Brain Stimul.* 2017;10(4):721-734. doi:10.1016/j.brs.2017.03.008

16. Xu J, Branscheidt M, Schambra H, et al. Rethinking interhemispheric imbalance as a target for stroke neurorehabilitation. *Ann Neurol.* 2019;85(4):502-513.
17. Lefaucheur JP, Aleman A, Baeken C, et al. Evidence-based guidelines on the therapeutic use of repetitive transcranial magnetic stimulation (rTMS): An update (2014–2018). *Clinical Neurophysiology.* 2020;131(2):474-528. doi:10.1016/j.clinph.2019.11.002
18. Arai N, Okabe S, Furubayashi T, et al. Differences in after-effect between monophasic and biphasic high-frequency rTMS of the human motor cortex. *Clinical Neurophysiology.* 2007;118(10):2227-2233.
19. Taylor JL, Loo CK. Stimulus waveform influences the efficacy of repetitive transcranial magnetic stimulation. *J Affect Disord.* 2007;97(1-3):271-276.
20. Harvey RL, Edwards D, Dunning K, et al. Randomized sham-controlled trial of navigated repetitive transcranial magnetic stimulation for motor recovery in stroke: the NICHE trial. *Stroke.* 2018;49(9):2138-2146.
21. Lefaucheur JP, Aleman A, Baeken C, et al. Evidence-based guidelines on the therapeutic use of repetitive transcranial magnetic stimulation (rTMS): An update (2014-2018). *Clin Neurophysiol.* 2020;131(2):474-528. doi:10.1016/j.clinph.2019.11.002
22. van Lieshout ECC, van der Worp HB, Visser-Meily JMA, Dijkhuizen RM. Timing of Repetitive Transcranial Magnetic Stimulation Onset for Upper Limb Function After Stroke: A Systematic Review and Meta-Analysis. *Front Neurol.* 2019;10(1269):1-16. doi:10.3389/fneur.2019.01269
23. Dromerick AW, Geed S, Barth J, et al. Critical Period After Stroke Study (CPASS): A phase II clinical trial testing an optimal time for motor recovery after stroke in humans. *Proceedings of the National Academy of Sciences.* 2021;118(39):e2026676118.
24. Iezzi E, Suppa A, Conte A, Li Voti P, Bologna M, Berardelli A. Short-term and long-term plasticity interaction in human primary motor cortex. *European Journal of Neuroscience.* 2011;33(10):1908-1915. doi:10.1111/j.1460-9568.2011.07674.x
25. Rossini PM, Burke D, Chen R, et al. Non-invasive electrical and magnetic stimulation of the brain, spinal cord, roots and peripheral nerves: Basic principles and procedures for routine clinical and research application: An updated report from an I.F.C.N. Committee. *Clinical Neurophysiology.* 2015;126(6):1071-1107. doi:10.1016/j.clinph.2015.02.001
26. Nicolo P, Magnin C, Pedrazzini E, et al. Comparison of Neuroplastic Responses to Cathodal Transcranial Direct Current Stimulation and Continuous Theta Burst Stimulation in Subacute Stroke. *Arch Phys Med Rehabil.* 2018;99(5):862-872.e1. doi:10.1016/j.apmr.2017.10.026
27. van Lieshout ECC, Visser-Meily JMA, Neggers SFW, van der Worp HB, Dijkhuizen RM. Brain stimulation for arm recovery after stroke (B-STARs): protocol for a randomised controlled trial in subacute stroke patients. *BMJ Open.* 2017;7(8):e016566. doi:10.1136/bmjopen-2017-016566
28. Collin C, Wade D. Assessing motor impairment after stroke: A pilot reliability study. *J Neurol Neurosurg Psychiatry.* 1990;53(7):576-579. doi:10.1136/jnnp.53.7.576
29. Demeurisse G, Demol O, Robaye E. Motor evaluation in vascular hemiplegia. *Eur Neurol.* 1980;19(6):382-389.

30. Rossi S, Hallett M, Rossini PM, et al. Safety, ethical considerations, and application guidelines for the use of transcranial magnetic stimulation in clinical practice and research. *Clinical Neurophysiology*. 2009;120(12):2008-2039. doi:10.1016/j.clinph.2009.08.016
31. Kwakkel G, Winters C, Van Wegen EEH, et al. Effects of Unilateral Upper Limb Training in Two Distinct Prognostic Groups Early after Stroke: The EXPLICIT-Stroke Randomized Clinical Trial. *Neurorehabil Neural Repair*. 2016;30(9):804-816. doi:10.1177/1545968315624784
32. Franck JA, Halfens J, Smeets R, Seelen H. Concise Arm and hand Rehabilitation Approach in Stroke (CARAS): A practical and evidence-based framework for clinical rehabilitation management. *Open J Occup Ther*. 2015;3(4):10.
33. Kwakkel G. Standardised measurement of sensorimotor recovery in stroke trials: consensus-based core recommendations from the Stroke Recovery and Rehabilitation Roundtable (SRRR). *International Journal of Stroke*. 2017;12(5):451-461. doi:10.1177/1747493017711813
34. van der Lee JH, Roorda LD, Beckerman H, Lankhorst GJ, Bouter LM. Improving the action research arm test: A unidimensional hierarchical scale. *Clin Rehabil*. 2002;16(6):646-653. doi:10.1191/0269215502cr534oa
35. Van der Lee JH, De Groot V, Beckerman H, Wagenaar RC, Lankhorst GJ, Bouter LM. The intra- and interrater reliability of the action research arm test: A practical test of upper extremity function in patients with stroke. *Arch Phys Med Rehabil*. 2001;82(1):14-19. doi:10.1053/apmr.2001.18668
36. World Health Organization (WHO). International classification of functioning, disability and health. World Health Organization.
37. Gladstone DJ, Danells CJ, Black SE. The fugl-meyer assessment of motor recovery after stroke: A critical review of its measurement properties. *Neurorehabil Neural Repair*. 2002;16(3):232-240. doi:10.1177/154596802401105171
38. Houwink A, Roorda LD, Smits W, Molenaar IW, Geurts AC. Measuring upper limb capacity in patients after stroke: Reliability and validity of the stroke upper limb capacity scale. *Arch Phys Med Rehabil*. 2011;92(9):1418-1422. doi:10.1016/j.apmr.2011.03.028
39. Bovend'Eerd T, Dawes H, Johansen-Berg H, Wade DT. Evaluation of the Modified Jebsen Test of Hand Function and the University of Maryland Arm Questionnaire for Stroke. *Clin Rehabil*. 2004;18:195-202. doi:10.1191/0269215504cr722oa
40. Collin C, Wade DT, Davies S, Horne V. The barthel ADL index: A reliability study. *Disabil Rehabil*. 1988;10(2):61-63. doi:10.3109/09638288809164103
41. Grice KO, Vogel KA, Le V, Mitchell A, Muniz S, Vollmer MA. Adult norms for a commercially available nine hole peg test for finger dexterity. *American Journal of Occupational Therapy*. 2003;57(5):570-573. doi:10.5014/ajot.57.5.570
42. Kasner SE. Clinical interpretation and use of stroke scales. *Lancet Neurology*. 2006;5(7):603-612. doi:10.1016/S1474-4422(06)70495-1
43. Duncan PW, Bode RK, Lai SM, Perera S. Rasch analysis of a new stroke-specific outcome scale: The stroke impact scale. *Arch Phys Med Rehabil*. 2003;84(7):950-963. doi:10.1016/S0003-9993(03)00035-2
44. Krabbe PFM, Stouthard MEA, Essink-Bot ML, Bonsel GJ. The effect of adding a cognitive dimension to the EuroQol multiattribute health-status classification system. *J Clin Epidemiol*.

1999;52(4):293-301. doi:10.1016/S0895-4356(98)00163-2

45. Lang CE, Edwards DF, Birkenmeier RL, Dromerick AW. Estimating Minimal Clinically Important Differences of Upper-Extremity Measures Early After Stroke. *Arch Phys Med Rehabil.* 2008;89(9):1693-1700. doi:10.1016/j.apmr.2008.02.022

46. Jepsen RH. An objective and standardized test of hand function. *Arch Phys Med Rehabil.* 1969;50(6):311-319.

47. Grice KO, Vogel KA, Le V, Mitchell A, Muniz S, Vollmer MA. Adult norms for a commercially available nine hole peg test for finger dexterity. *American Journal of Occupational Therapy.* 2003;57(5):570-573. doi:10.5014/ajot.57.5.570

48. Kim WS, Kwon BS, Seo HG, Park J, Paik NJ. Low-Frequency Repetitive Transcranial Magnetic Stimulation Over Contralesional Motor Cortex for Motor Recovery in Subacute Ischemic Stroke: A Randomized Sham-Controlled Trial. *Neurorehabil Neural Repair.* 2020;34(9):856-867. doi:10.1177/1545968320948610

49. Bertolucci F, Chisari C, Fregni F. The potential dual role of transcallosal inhibition in post-stroke motor recovery. *Restor Neurol Neurosci.* 2018;36(1):83-97. doi:10.3233/RNN-170778

50. Thickbroom GW, Cortes M, Rykman A, et al. Stroke subtype and motor impairment influence contralesional excitability. *Neurology.* 2015;85(6):517-520. doi:10.1212/WNL.0000000000001828



## Chapter 6

# **Treatment efficacy of contralesional rTMS for post-stroke upper limb recovery is associated with residual motor function and corticospinal tract integrity**

Jord JT Vink

Alex Bhogal

Eline CC van Lieshout

Willem M Otte

Sebastiaan FW Neggers

Johanna MA Visser-Meily

H Bart van der Worp

Rick M Dijkhuizen

*In preparation*

## **ABSTRACT**

### **Introduction**

Inhibitory repetitive transcranial magnetic stimulation (rTMS) of the contralesional primary motor cortex (M1) is a promising treatment to promote upper limb recovery after stroke. However, treatment efficacy may depend on various stroke characteristics. We assessed the relationship between treatment efficacy of contralesional continuous theta burst stimulation, an inhibitory rTMS paradigm, administered within three weeks after stroke, and the integrity of the intact corticospinal tract (CST), residual motor function and lesion location.

### **Methods**

Patients were part of a randomized controlled trial (B-STARS) on inhibitory contralesional rTMS to promote upper limb recovery after stroke. Forty-eight of sixty patients participated in one or more MRI sessions. Patients received ten daily sessions of active (n=22) or sham continuous theta burst stimulation (cTBS) of the contralesional M1 (n=26), combined with standard upper limb training, started within three weeks post-stroke and continued for two weeks. Upper limb outcome was determined with the Fugl-Meyer assessment (FMA) arm score and the nine hole peg test (NHPT), and ipsilesional cortical excitability was determined with the TMS-based resting motor threshold (RMT), measured at baseline and during six follow-up visits up to one year after stroke. MRI sessions, including T<sub>1</sub>-weighted MRI for lesion detection and diffusion-weighted MRI for calculation of fractional anisotropy (FA) in the posterior limb of the internal capsule (PLIC) took place at one week post-treatment and at three, six and twelve months post-stroke. Statistical analyses were performed using mixed models for repeated measures (MMRM) and Pearson's correlations.

### **Results**

Patients with a PLIC FA between 0.4 and 0.6 and patients with a baseline FMA arm score between 8 and 48 points had a better outcome on either the FMA arm score at three months post-stroke or the NHPT at one year post-stroke in the active cTBS group compared to sham ( $p < 0.05$ ). Ipsilesional M1 excitability within twelve hours after the last cTBS session was higher in the active cTBS group compared to sham for patients with a PLIC FA between 0.5 and 0.6 ( $p < 0.05$ ). The FMA arm score at three months post-stroke ( $r 0.51$ ; 95% CI 0.28 to 0.68;  $p < 0.0001$ ) and the NHPT at one year post-stroke ( $r 0.57$ ; 95% CI 0.35 to 0.74;  $p < 0.0001$ ) were associated with ipsilesional M1 excitability within twelve hours after treatment.

### **Conclusion**

The efficacy of ten sessions of cTBS treatment in promoting upper limb recovery is associated with residual motor function and intact CST integrity. The treatment effect is potentially mediated through modulation of ipsilesional M1 excitability. Individualization of rTMS treatment based on residual motor function or CST integrity may improve upper limb outcome.



## INTRODUCTION

Stroke is a leading cause of long-term adult disability, with most stroke patients suffering from upper limb impairment.<sup>1</sup> The impact of stroke is not restricted to damage in the ischemic or hemorrhagic area, but extends throughout the connected neural network, a phenomenon called diaschisis.<sup>2</sup> Post-stroke diaschisis differentially affects the motor network, but disruption of the balance between interhemispheric interactions has been shown to strongly impact motor impairment.<sup>3,4</sup> More specifically, the extent of motor impairment has been associated with an imbalance in interhemispheric signaling between the bilateral primary motor cortices (M1s), e.g. reflected by a reduction in ipsilesional M1 activity and excitability.<sup>5-7</sup> Normalization of ipsilesional M1 excitability has been associated with improved upper limb outcome.<sup>8</sup> Furthermore, functional magnetic resonance imaging (fMRI) of the activation response in the ipsi- and contralesional M1 during movement of the affected hand has revealed that restoration of ipsilesional M1 activity is associated with good outcome.<sup>4,9</sup> Interhemispheric imbalance is potentially mediated by an increased inhibitory drive from the contralesional M1, but the effect thereof on post-stroke motor recovery remains unclear.<sup>10,11</sup>

Repetitive transcranial magnetic stimulation (rTMS) is a promising neuromodulatory therapy that may be used to restore the interhemispheric balance after stroke.<sup>12</sup> It can be applied to up- or downregulate excitability in the stimulated area, using facilitatory or inhibitory rTMS paradigms, respectively.<sup>13,14</sup> Inhibitory rTMS paradigms over the contralesional M1 in the early subacute phase after stroke have demonstrated the most promising therapeutic effect when combined with physical therapy of the upper limb.<sup>15</sup> Contralesional inhibitory rTMS has been shown to increase cortical excitability of the ipsilesional M1 during treatment<sup>16</sup> and up to at least three months post-stroke.<sup>17</sup>

The extent of interhemispheric imbalance and its effect on upper limb outcome most probably depend on stroke characteristics, such as time after stroke, extent of cortical damage, structural integrity of the intact ipsilesional corticospinal tract (CST) and potentially other factors.<sup>18-20</sup> Paradigms to inhibit contralesional M1 excitability have been suggested to more effectively restore interhemispheric imbalance in patients with higher intact CST integrity,<sup>20,21</sup> or moderate to high residual motor function.<sup>19</sup> Individualizing treatment based on these stroke characteristics could increase treatment efficacy. Unfortunately, evidence to support this is limited and thresholds for these factors have not been clearly defined.

We aimed to determine the relationship between lesion location, CST integrity and residual motor function and modulation of ipsilesional M1 excitability and improvement of upper limb recovery induced by contralesional inhibitory rTMS treatment applied in the first weeks after stroke.

## METHODS

### Study Design

This is a substudy of the B-STARS trial, a randomized, sham-controlled, clinical trial on early continuous theta burst stimulation (cTBS) treatment over the contralesional M1 to promote upper limb recovery after stroke. The study was approved by the Medical Research Ethics Committee of the University Medical Center Utrecht and all patients gave written informed consent. The protocol of the B-STARS trial has been published previously<sup>22</sup> and the primary study results have been published elsewhere.<sup>23</sup> The data described here have been acquired in the subset of patients who participated in the B-STARS trial.

Upper limb outcome and cortical excitability were assessed at baseline (within three weeks after stroke) and during follow-up visits directly after treatment, one week and one

month after treatment, and at three, six and twelve months post-stroke. MRI was performed at baseline and during follow-up visits one week after treatment and at three, six and twelve months after stroke onset.

### **Population and Study Sample**

Patients were recruited from rehabilitation center De Hoogstraat (Utrecht, The Netherlands). Patients who met the following inclusion criteria were eligible for participation: (1) age  $\geq 18$  years; (2) first-ever ischemic stroke or intracerebral hemorrhage; (3) paresis of one arm, as determined by a Motricity Index (MI)<sup>24</sup> of the arm between 9 and 99; (4) baseline assessment within the first three weeks after stroke onset; (5) participation in at least one MRI session. Patients were excluded from participation based on the following criteria: (1) disabling medical history as determined by the treating physician; (2) normal to almost normal use of the hand; (2) severe deficits in communication, memory, or understanding that impede proper study participation; and (3) contraindications to TMS as based on TMS safety guidelines.<sup>25</sup>

### **TMS Intervention**

TMS treatment consisted of ten daily sessions of real or sham cTBS delivered over the contralesional M1.<sup>22</sup> Treatment was started within three weeks after stroke onset, continued for two weeks and was combined with regular care upper limb therapy.

### **Upper limb outcome**

Upper limb outcome was assessed with the upper limb section of the Fugl-Meyer assessment (FMA)<sup>26</sup> at three months post-stroke and the nine hole peg test (NHPT)<sup>27</sup> at one year post-stroke.<sup>26,27</sup> The FMA arm score at three months post-stroke was used to measure recovery of upper limb function in the subacute phase. The upper extremity section of the FMA consists of 33 tasks, executed with the affected upper limb. Task execution is rated from 0 to 2 with a higher score indicating better performance with a maximum of 66 points. The NHPT at one year post-stroke was used to measure continued recovery of fine motor skills and manual dexterity in the chronic phase. The NHPT requires patients to place nine pegs into slots and remove them, one at a time. The duration of the exercise is measured, with a maximum of 50 seconds. We investigated the relationship between residual motor function and the mean difference between active and sham cTBS in the FMA arm score at three months post-stroke and the NHPT at one year post-stroke.

### **TMS cortical excitability measurements**

TMS was executed with a Neuro-MS/D Advanced Therapeutic stimulator with an angulated 100-mm figure-of-eight TMS coil (Neurosoft, Ivanovo, Russia) and a Neural Navigator neuronavigation system (Brain Science Tools, De Bilt, The Netherlands). Electromyography (EMG) of the bilateral first dorsal interosseous (FDI) muscles was recorded using a four-channel Neuro-MEP amplifier (Neurosoft, Ivanovo, Russia). The motor hotspot was identified by delivering TMS pulses over M1 and identifying the stimulation location with the motor evoked potential (MEP) with the largest peak-to-peak amplitude. The resting motor threshold (RMT) was defined as the minimal intensity, expressed as percentage of maximum machine output (%MO), at which TMS over the motor hotspot evoked at least five out of ten MEPs with a peak-to-peak amplitude of  $>50\mu\text{V}$  in the FDI muscle contralateral to stimulation.<sup>28</sup>

### **MRI acquisition**

MRI scans were acquired with a Philips Achieva 3.0T scanner (Philips, Best, The

Netherlands). An anatomical 3D T1-weighted image was acquired with a repetition time (TR) of 8.25ms, echo time (TE) of 3.78ms, flip angle of 8°, matrix size of 512x512, voxel size of 0.47x0.47x1.00mm<sup>3</sup>, and a scan duration of 2.9 min.

A multi-shell diffusion-weighted imaging (DWI) scan was acquired with three shells at b values of 500, 1000 and 2000 s/mm<sup>2</sup> with 15, 32 and 64 diffusion directions, a TR of 3,517ms, TE of 98.7ms, flip angle of 90°, matrix size of 112x112, 66 slices, voxel size of 2.0x2.0x2.0 mm<sup>3</sup>, and a scan duration of 8.1 min.

### Data analysis

Data was analyzed using custom scripts and SPM12 in the MATLAB environment (MathWorks Inc., United States), and MRtrix3.

#### *Lesion segmentation*

Stroke lesions were manually segmented using MRtrix3.

#### *DWI preprocessing*

DWI data were coregistered with the T<sub>1</sub>-weighted anatomical scan, by coregistering the whole-brain FA map with the whole-brain white matter segmentation of the T<sub>1</sub>-weighted scan. Coregistered data were visually verified. Data were denoised and Gibbs ringing artifacts were removed. Next, data were realigned and eddy currents and bias field corrections were performed. Lastly, data were resampled to an isotropic voxel size of 1.3mm.

#### *DWI analysis*

The preprocessed DWI data were used to compute diffusion tensors using constrained spherical deconvolution. Next, the diffusion tensors were used to calculate a whole-brain fractional anisotropy (FA) map.<sup>29</sup> Mean FA in the posterior limb of the internal capsule (PLIC) across all available visits was used to measure intact CST integrity.<sup>21</sup> The PLIC mask was obtained from the international consortium for brain mapping (ICBM) atlas and inversely normalized to the individual T<sub>1</sub>-weighted anatomical scan.<sup>30</sup> The PLIC masks were visually inspected and voxels overlapping with the lesion area were masked out.

### Statistical analysis

Statistical analysis was performed using R 4.1. All tests were two-tailed with an alpha of 0.05.

The primary analysis of the B-STARS trial data, as described in the original protocol,<sup>22</sup> was adapted to include a three-way interaction with group assignment based on the aforementioned stroke characteristics. The outcome measures were the FMA arm score and NHPT score. Analysis was done using a mixed model for repeated measures (MMRM). The model included visit (baseline, directly after treatment, one week and one month after treatment, and three, six and twelve months post-stroke), the stroke characteristic, treatment (sham cTBS; active cTBS), stratification (low performance; high performance), and two-way interactions between treatment and visit and the stroke characteristic (PLIC FA; baseline FMA; stroke location) and visit, and a three-way interaction between visit, treatment and the stroke characteristic. For continuous stroke characteristics (i.e. residual motor function and CST integrity) a third-order restricted cubic spline (RCS) was used. Bootstrap analysis with 1000 iterations was performed on the MMRM to calculate the mean difference between the active and sham cTBS group for different values of each stroke characteristic. Mean differences, 95% confidence intervals (95% CI) and p-values were calculated from the distributions. FA of the

PLIC between treatment groups was also analyzed using a MMRM, which included visit, the interaction between treatment and visit and stratification. Correlations were calculated using Pearson's correlations.

## RESULTS

### Patients

Sixty patients were enrolled in the B-STARS trial, of whom 48 participated in the MRI study. Of these 48 patients, 22 were randomized to receive active cTBS, and 26 were assigned to receive sham cTBS. Patient characteristics of the patients who participated in the MRI study are shown in **Table 1** (patient characteristics of all patients have been reported previously).<sup>23</sup> Baseline MRI sessions could not be executed due to logistic reasons. Follow-up MRI was acquired in 28, 31, 20 and 27 patients at one week post-treatment and three, six and twelve months post-stroke, respectively.

We previously found that active cTBS promoted upper limb outcomes<sup>23</sup> and that active cTBS increased ipsilesional M1 excitability (**Chapter 7**).

**Table 1.** Baseline characteristics of patients who participated in the MRI study.

Patient characteristics	Total (n = 48)	Active cTBS (n = 22)	Sham cTBS (n = 26)
Sex, n (%)			
Male	32 (67)	13 (59)	19 (73)
Female	17 (33)	9 (41)	7 (27)
Age, mean (SD), years	59 (12)	55 (12)	63 (12)
Intervention			
treatment onset, mean (SD), days post-stroke	14 (4)	14 (5)	15 (4)
Stroke information			
Lesion type, n (%)			
Ischemic stroke	39 (81)	18 (82)	21 (81)
Intracerebral hemorrhage	9 (19)	4 (18)	5 (19)
Lesion location, n (%)			
Subcortical	23 (48)	11 (50)	12 (45)
Cortical	16 (33)	7 (32)	9 (35)
Brainstem	7 (15)	4 (18)	3 (12)
Unknown	2 (4)	0 (0)	2 (8)
Impaired side, n (%)			
Right arm	19 (40)	9 (41)	10 (38)
Left arm	29 (60)	13 (59)	16 (62)
Stroke severity upon hospital admission			
NIHSS, median (IQR)	9 (7)	9 (8)	9 (7)
Electrophysiology			
MEP presence, n (%)			
Affected hemisphere	17 (35)	10 (45)	7 (27)
Unaffected hemisphere	48 (100)	22 (100)	26 (100)
RMT, mean (SD), %MO			
Affected hemisphere <sup>1</sup>	83 (26)	80 (25)	84 (26)
Unaffected hemisphere	38 (8)	38 (8)	39 (9)
Baseline function			
Function scores, mean (SD)			
FMA arm score	25.4 (18.2)	25.2 (18.6)	25.6 (18.3)

<sup>1</sup>RMT was set at 100%MO if a MEP could not be measured. SD: Standard deviation; IQR: Interquartile Range; NIHSS: National Institutes of Health Stroke Scale; MEP: Motor-evoked potential; RMT: resting motor threshold; %MO: Percentage of maximum machine output; FMA: Fugl-Meyer Assessment.

### CST integrity

**Figure 1A** shows a whole brain FA map overlaid on a T<sub>1</sub>-weighted anatomical scan from a representative patient, and the FA map of the PLIC. FA in the ipsilesional PLIC increased between six and twelve months post-stroke irrespective of treatment (mean difference 0.07; 95% CI 0.05 to 0.11; p 0.0001; **Figure 1B**). FA in the contralesional PLIC increased between three and six months post-stroke (mean difference 0.05; 95% CI 0.03 to 0.08; p 0.0004) and between six and twelve months post-stroke (mean difference 0.07; 95% CI 0.05 to 0.10; p < 0.0001). There were no differences in FA in the contralesional or ipsilesional PLIC between the active and sham cTBS groups.

**Figures 2A and B** show the relationships between the FA of the PLIC in the intact ipsilesional CST, and outcome on the FMA arm score at three months and the NHPT at one year post-stroke. Across both groups and upper limb outcome measures, outcome was more favorable for patients with a high PLIC FA. The FMA arm score was higher in the active cTBS group compared to the sham cTBS group for patients with a PLIC FA between 0.45 and 0.55 (p < 0.05; **Figure 2A**), with a mean difference between groups between 11.4 (95% CI 1.9 to 20.8; p 0.0130) and 12.7 (95% CI 1.7 to 23.7; p 0.0130) points. Outcome on the NHPT was better in the active cTBS group compared to the sham cTBS group for patients with a PLIC FA between 0.4 and 0.6 (p < 0.05; **Figure 2B**), with a mean difference between groups between -7.4 (95% CI -14.4 to -0.4; p 0.0190) and -11.6 (95% CI -18.0 to -5.2; p 0.0010) points. 77% of patients had an ipsilesional PLIC FA between 0.4 and 0.6.

### Residual motor function

**Figures 2C and D** show the relationships between baseline FMA arm score and outcome on the FMA arm score at three months and the NHPT at one year post-stroke. Across both treatment groups and upper limb outcome measures, outcome was more favorable for patients with a high baseline FMA arm score. The FMA arm score at three months post-stroke was higher in the active cTBS group compared to the sham cTBS group for patients with a baseline FMA arm score between 8 and 26 points (p < 0.05; **Figure 2C**), with a mean difference between groups of 11.1 (95% CI 0.0 to 22.1; p 0.0200) and 13.4 (95% CI 1.9 to 24.8; 0.0190) points. The NHPT score at one year post-stroke was higher in the active cTBS group compared to the sham cTBS group for patients with a baseline FMA arm score between 12 and 48 points (p < 0.05; **Figure 2D**), with a mean difference between groups of -6.7 (95% CI -13.1 to -0.4; p 0.0170) and -12.3 (95% CI -2.5 to -22.2; p 0.0070) points. 64% of patients had a baseline FMA arm score between 8 and 48 points.

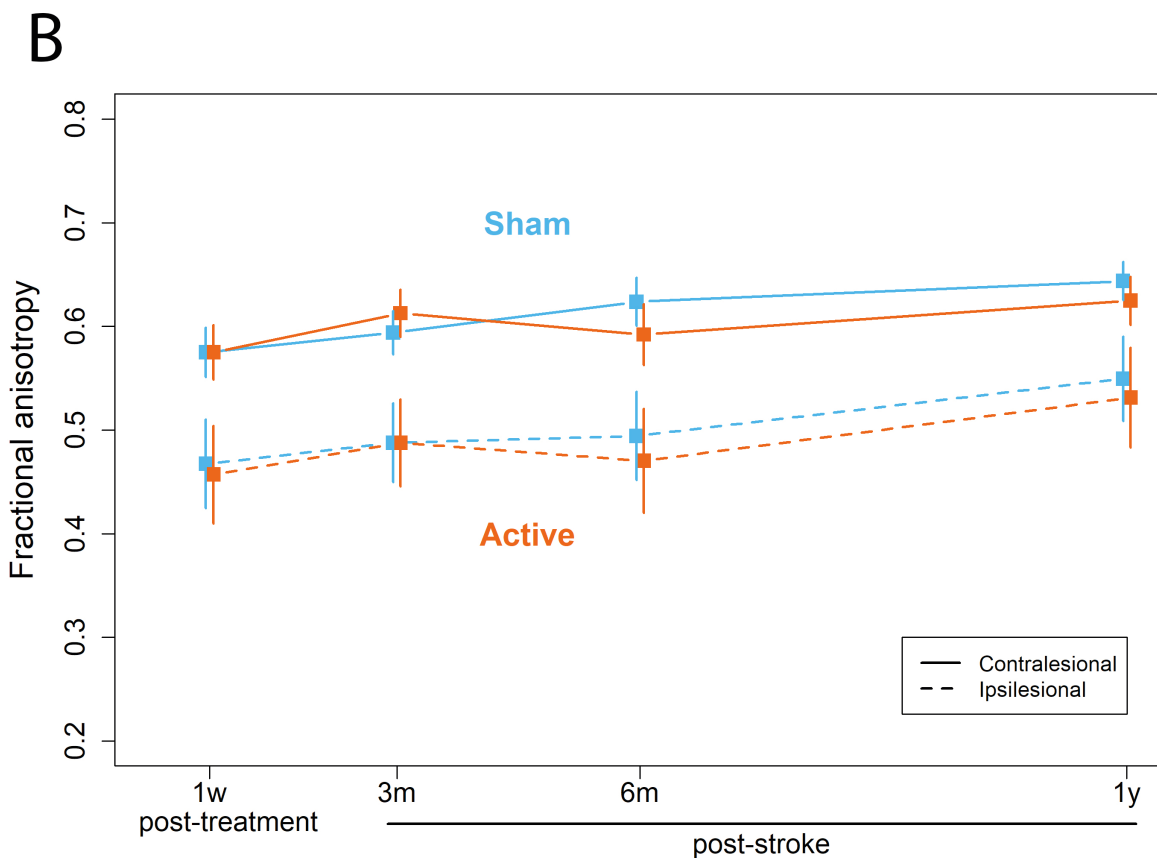
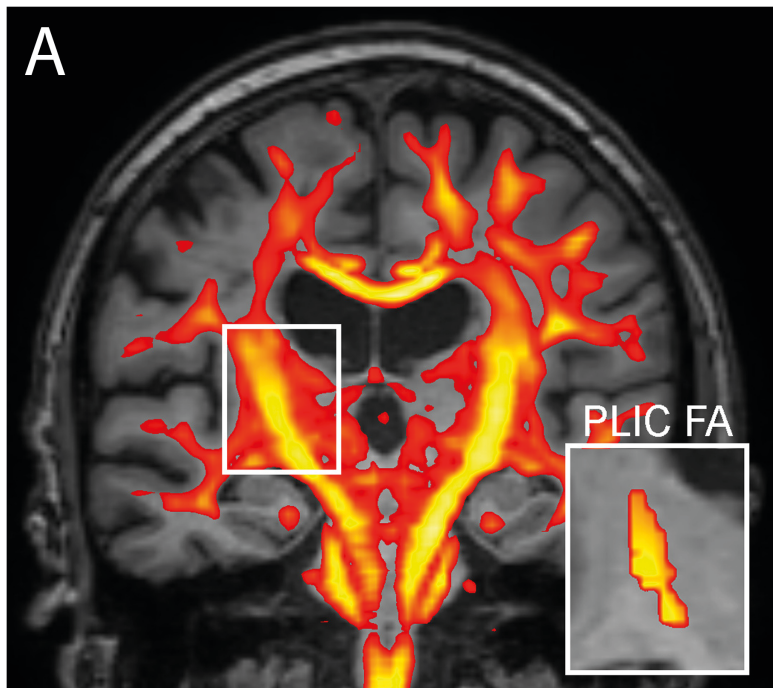


**Figure 1. (A)** White matter fractional anisotropy (FA) map overlaid on a  $T_1$ -weighted anatomical scan (coronal slice) of a patient's brain 6 months after stroke. The FA map of the region of interest, the posterior limb of the internal capsule (PLIC) (ipsilesional side) is shown in the bottom right. **(B)** Mean and 95% confidence interval of the FA of the contralesional (solid line) and ipsilesional (dashed line) PLIC for patients who received active (orange) or sham (blue) cTBS, as calculated with a mixed model for repeated measures.

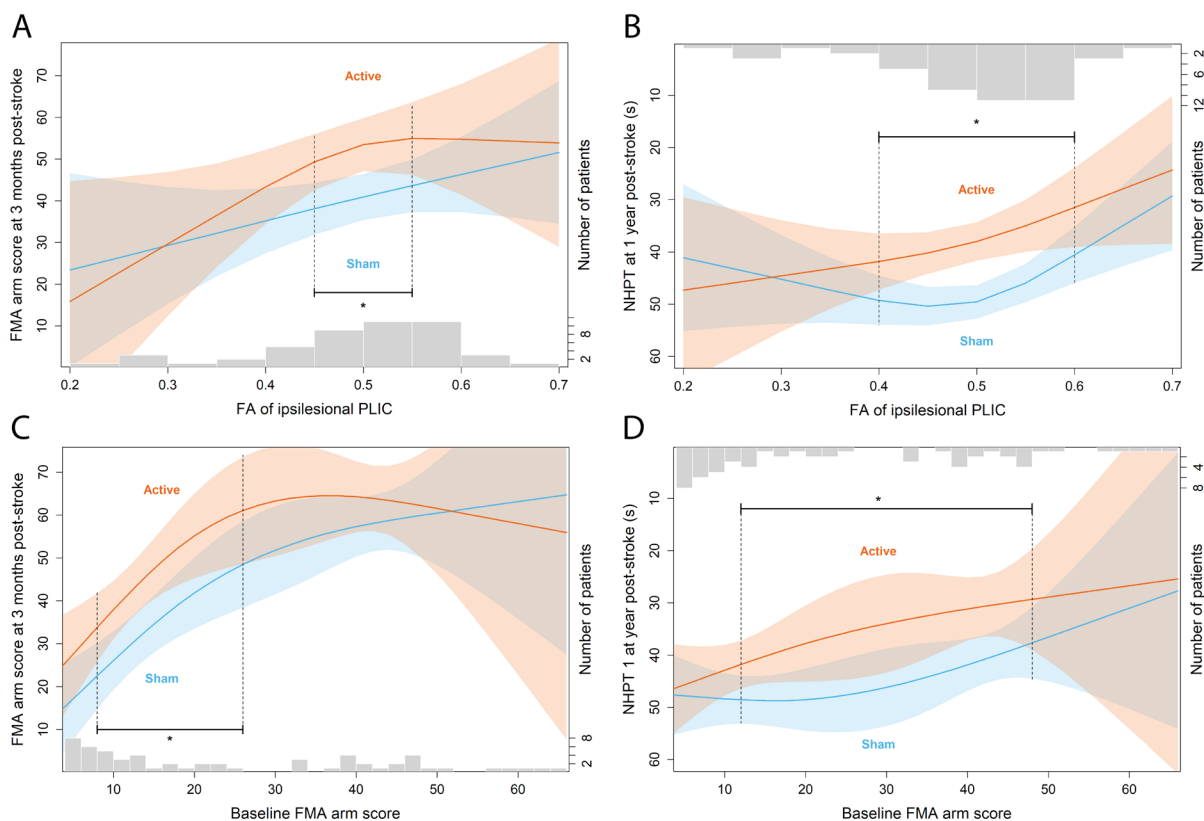


**Figure 2.** Mean and 95% confidence interval of the relationship between **(A,B)** fractional anisotropy (FA) of the ipsilesional posterior limb of the internal capsule (PLIC) and **(C,D)** baseline Fugl-Meyer Assessment (FMA) arm score (residual motor function) and outcome on **(A,C)** the FMA arm score at three months post-stroke and **(B,D)** the nine hole peg test (NHPT) at one year post-stroke for patients who received active (orange) or sham (blue) cTBS, as calculated with a mixed model for repeated measures. The number of patients for categories of **(A,B)** ipsilesional PLIC FA values and **(C,D)** baseline FMA arm scores is shown in grey bars. \* $p < 0.05$  for the mean difference between groups.

### Lesion location

Sixteen patients had a stroke lesion with cortical involvement and 43 patients had a stroke lesion without. Structural MRI scans of representative patients are shown in **Figures 3A and B**. Active cTBS resulted in better outcome on the FMA arm score compared to sham cTBS at three months post-stroke in patients without cortical involvement (mean difference 8.4; 95% CI -0.9 17.7;  $p$  0.0440; **Figure 3C**, S1), but not in patients with cortical involvement (mean difference 11.2; 95% CI -3.2 to 25.8;  $p$  0.0699). Active cTBS did not result in better outcome on the NHPT compared to sham cTBS at one year post-stroke in patients without cortical involvement (mean difference -4.0; 95% CI -9.6 to 1.6;  $p$  0.0889; **Figure 3D**), but did in patients with cortical involvement (mean difference -15.0; 95% CI -24.5 to -5.5;  $p$  0.0020).

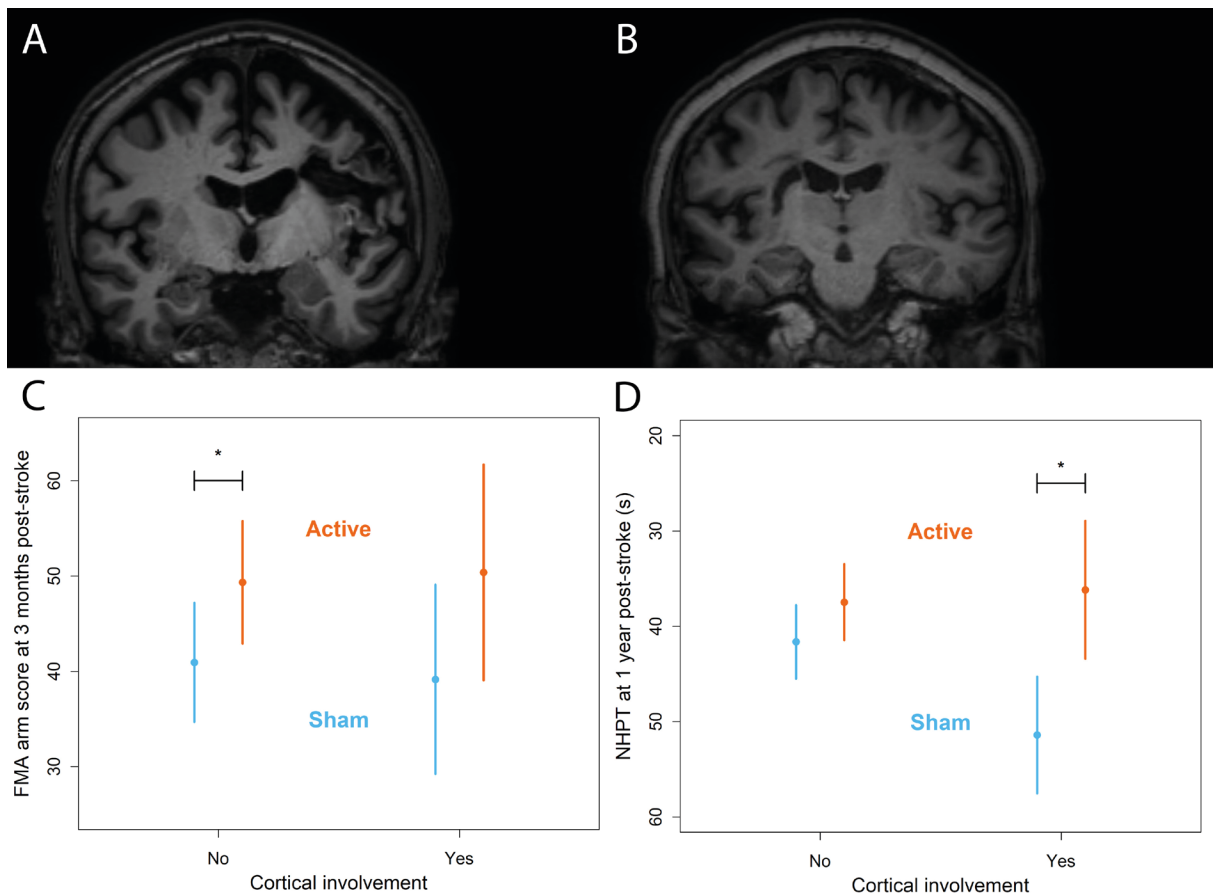


**Figure 3.** T1-weighted anatomical brain scan (coronal slice) of **(A)** a patient with a stroke lesion in the left hemisphere with cortical involvement and **(B)** a patient with a right-sided lesion without cortical involvement. Mean and 95% confidence interval of the outcome on **(C)** the Fugl-Meyer Assessment (FMA) arm score at three months post-stroke and **(D)** the nine hole peg test (NHPT) at one year post-stroke for patients with and without cortical involvement in the active (orange) and sham (blue) cTBS groups, as calculated with a mixed model for repeated measures (MMRM). **(C)**  $p = 0.0440$  and **(D)**  $p = 0.0020$  for the mean difference between groups.

### Cortical excitability

**Figure 4A** shows the relationship between the FA of the ipsilesional PLIC and the ipsilesional RMT within twelve hours after the last cTBS session. Across both treatment groups, lower RMT, i.e. increased ipsilesional M1 excitability, was associated with higher PLIC FA. Ipsilesional M1 excitability was higher in the active cTBS group compared to the sham cTBS group for patients with a PLIC FA between 0.5 and 0.6 ( $p < 0.05$ ), with a mean difference of the RMT between groups between -12% (95% CI -24 to 0) and -17% (95% CI -2 to -32). 47% of the patients had an ipsilesional PLIC FA within this range.

The FMA arm score at three months post-stroke ( $r = 0.51$ ; 95% CI 0.28 to 0.68;  $p < 0.0001$ ; **Figure 4B**) and the NHPT at one year post-stroke ( $r = 0.57$ ; 95% CI 0.35 to 0.74;  $p < 0.0001$ ; **Figure 4C**) were associated with the ipsilesional M1 excitability within twelve hours after treatment



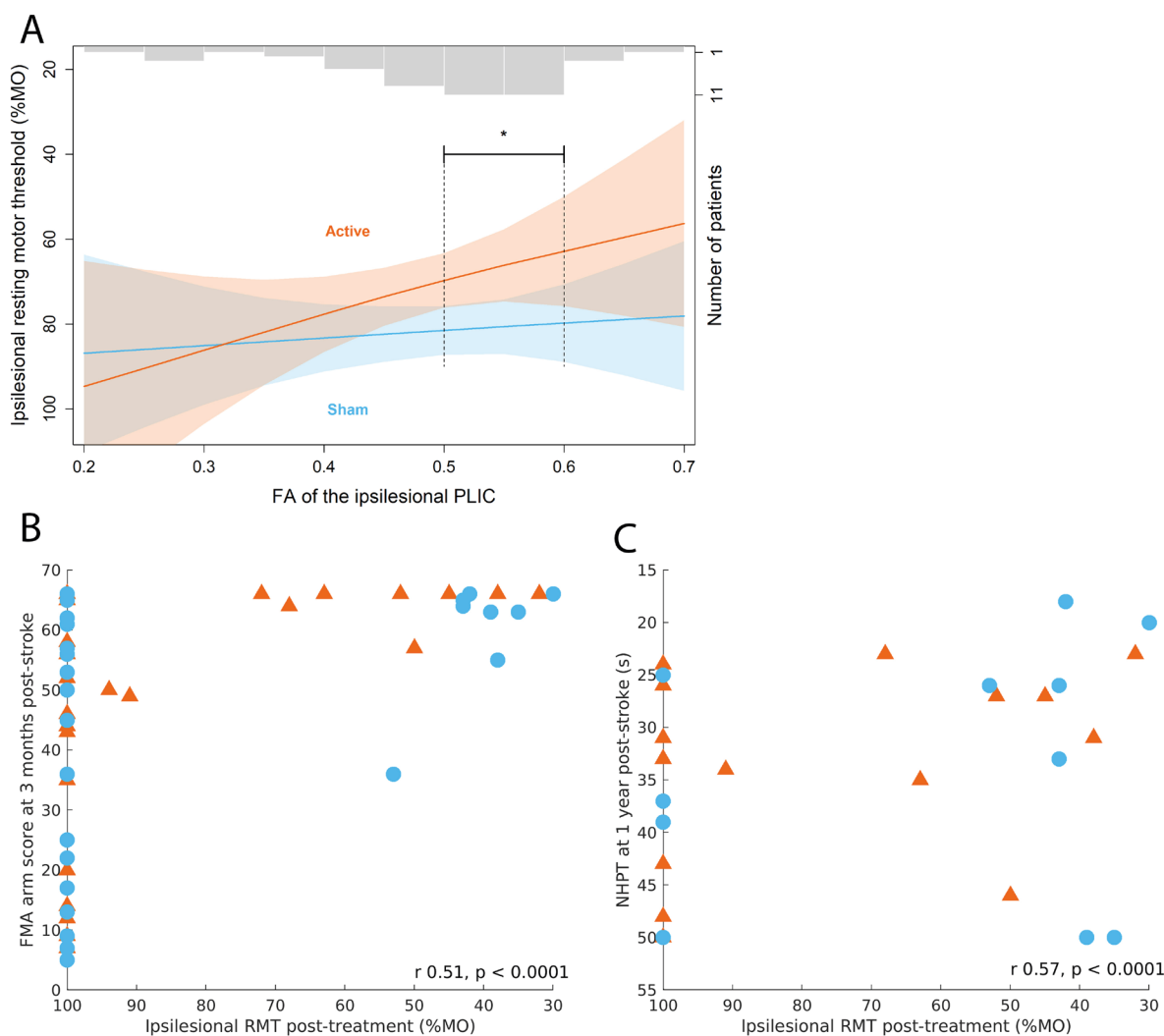


**Figure 4. (A)** Mean and 95% confidence interval of the relationship between the ipsilesional resting motor threshold (RMT) within twelve hours post-treatment and the FA of the ipsilesional PLIC for patients who received active (orange) or sham (blue) cTBS, as calculated with a mixed model for repeated measures. Relative distribution of ipsilesional PLIC FA values among patients is shown in grey bars.  $*p < 0.05$  for the mean difference between groups. Correlation between outcome on **(B)** the Fugl-Meyer Assessment (FMA) arm score at three months post-stroke **(C)** the Nine hole peg test (NHPT) at one year post-stroke and the ipsilesional RMT within twelve hours post-treatment. Individual data points are shown, with patients who received active cTBS in orange triangles and patients who received sham in blue circles.

## DISCUSSION

Previous studies have suggested that rTMS treatment efficacy depends on stroke characteristics, like structural integrity of the CST, residual motor function and cortical involvement. Our results demonstrate that characterization of residual motor function and CST integrity may aid in selecting patients who can benefit from contralesional cTBS treatment. Treatment outcome was, however, not unambiguously related to cortical involvement of the stroke lesion.

### Integrity of the ipsilesional intact CST and M1 excitability

We found that active cTBS promotes upper limb outcome for patients with a PLIC FA between 0.4 and 0.6. Outcome on the FMA arm score at three months post-stroke showed a plateau effect for patients with a high PLIC FA ( $> 0.55$ ), presumably because patients with

a high integrity of the intact CST reach a maximum FMA arm score at three months post-stroke, regardless of cTBS treatment. Outcome on the NHPT showed an effect of active cTBS for patients with a PLIC FA up to 0.6. Because the NHPT measures fine motor skills and manual dexterity, it is sensitive to continued upper limb recovery in patients with a maximum FMA arm score.<sup>27</sup>

Our results confirm previously reported evidence that patients with a low integrity of the ipsilesional CST (PLIC FA < 0.4) do not benefit from contralesional inhibitory rTMS treatment.<sup>21,31</sup> Additionally, we identified a threshold for high versus low CST integrity based on the outcome at three months post-stroke, which is lower than a previously identified threshold, i.e. a PLIC FA of 0.5, which was based on the direct effect of inhibitory rTMS of the contralesional M1.<sup>31</sup> Patients with a low PLIC FA (< 0.4) may potentially benefit from facilitatory 5Hz rTMS of the contralesional dorsal premotor cortex.<sup>31</sup>

The treatment effect of repetitive contralesional cTBS sessions may have been accomplished by restoring the post-stroke interhemispheric imbalance. We previously found that cTBS treatment increased ipsilesional M1 excitability in the first twelve hours after treatment (Chapter 7). Our current study shows that this particularly occurs in patients with higher structural integrity of the intact CST. We also found that upper limb outcome at three months post-stroke correlates with cortical excitability of the ipsilesional M1 within twelve hours post-treatment. This relationship is consistent with previous observations.<sup>3</sup> Thus, modulation of ipsilesional cortical excitability provides a potential mechanism for the therapeutic effect of contralesional cTBS treatment in patients with preserved structural integrity of the intact CST.

### **Residual motor function**

We found that contralesional cTBS treatment is efficacious for patients with a baseline FMA arm score between 8 and 48 points. The FMA arm score at three months post-stroke showed a plateau effect for patients with a baseline FMA arm score higher than 26 points, presumably because patients with high residual motor function have a maximum FMA arm score at three months post-stroke, irrespective of TMS treatment. Outcome on the NHPT showed an effect of active cTBS for patients with a baseline FMA arm score up to 48 points, potentially due to increased sensitivity in patients with a maximum FMA arm score, as discussed above.

It has previously been suggested that stroke patients with low residual motor function do not benefit from contralesional inhibitory rTMS treatment.<sup>19</sup> This was based on indirect evidence that increased transcallosal inhibition from the contralesional to ipsilesional hemisphere is associated with motor impairment in chronic stroke patients with high residual motor function.<sup>19</sup> In our study, we could not establish efficacy of contralesional cTBS in early subacute stroke patients with a baseline FMA arm score of 5 to 8 points (patients with a score of less than 5 were not included because of the selection criteria of this study).

It remains unclear whether (lack of) treatment response in patients with poor residual motor function depends on altered transcallosal inhibition, whether this is similar in patients with high residual motor function in the early subacute phase, and whether imbalanced transcallosal inhibition may be a cause or consequence of the underlying recovery process.<sup>32</sup> Further research is required to elucidate the underlying neurophysiological processes and determine if and how (alternative) rTMS treatment strategies may aid in rehabilitation of patients with poor residual motor function.

### **Lesion location**

Kim et al. previously reported that contralesional inhibitory rTMS is only effective in patients with stroke lesions without cortical involvement.<sup>18</sup> Correspondingly, we measured

a positive effect of contralesional cTBS treatment on upper limb outcome at three months post-stroke exclusively in patients without cortical involvement, however, the mean difference between the active and sham cTBS groups was similar between patients with and without cortical involvement in our study. There was a higher variability in outcome for patients with cortical involvement, which was also reported by Kim et al.<sup>18</sup>

At one year post-stroke, we found a positive effect of active cTBS on fine motor skills and manual dexterity, exclusively in patients with cortical involvement. Thus, patients with and without cortical involvement may still benefit from contralesional cTBS treatment and current data insufficiently support personalization of cTBS treatment based on lesion location.

### Limitations

The current dataset did not include baseline MRI data, for several logistic reasons: the short time window between admission to the rehabilitation center and the start of treatment, the limited availability of the MRI scanner and certified personnel, and transport complications to the MRI facilities. The latter two reasons also explained restricted participation in the follow-up MRI visits. Although the missing data in the follow-up MRI sessions reduced statistical power of the analyses, it did not affect the assessment of CST integrity, which was based on the mean FA value within the PLIC across all available visits. Since FA values were relatively stable over time, all patients undergoing at least one MRI session could be included in this analysis.

Intact CST integrity was assessed from PLIC FA, as this is a straightforward, commonly used and specific measure of CST integrity.<sup>21</sup> We did not analyze alternative DWI-based measures of white matter integrity or other regions of interest in the CST.

Subgroup analyses were performed on data from a single-center phase 2 trial (47 patients for the analysis of CST integrity and 60 patients for the analysis of residual motor function and cortical involvement). Our findings should be confirmed in a large multi-center clinical trial.

### CONCLUSION

Contralesional cTBS treatment combined with upper limb physical therapy promotes upper limb recovery in early subacute stroke patients with FMA arm scores between 8 and 48, and PLIC FA values between 0.4 and 0.6. Preserved structural integrity of the CST may secure functional effects of treatment-induced modulation of cortical excitability of the ipsilesional M1. Future studies should further investigate individualization of rTMS treatment based on these characteristics.

## REFERENCES

1. Mozaffarian, D. *et al.* Heart disease and stroke statistics—2015 update: a report from the American Heart Association. *Circulation* **131**, e29–e322 (2015).
2. Carrera, E. & Tononi, G. Diaschisis: past, present, future. *Brain* **137**, 2408–2422 (2014).
3. Veldema, J., Nowak, D. A. & Gharabaghi, A. Resting motor threshold in the course of hand motor recovery after stroke: a systematic review. *J Neuroeng Rehabil* **18**, 1–28 (2021).
4. Favre, I. *et al.* Upper limb recovery after stroke is associated with ipsilesional primary motor cortical activity: A meta-analysis. *Stroke* **45**, 1077–1083 (2014).
5. Duque, J. *et al.* Transcallosal inhibition in chronic subcortical stroke. *Neuroimage* **28**, 940–946 (2005).
6. Boddington, L. J. & Reynolds, J. N. J. Targeting interhemispheric inhibition with neuromodulation to enhance stroke rehabilitation. *Brain Stimul* **10**, 214–222 (2017).
7. McDonnell, M. N. & Stinear, C. M. TMS measures of motor cortex function after stroke: A meta-analysis. *Brain Stimul* **10**, 721–734 (2017).
8. Stinear, C. M., Petoe, M. A. & Byblow, W. D. Primary motor cortex excitability during recovery after stroke: Implications for neuromodulation. *Brain Stimul* **8**, 1183–1190 (2015).
9. Tang, Q. *et al.* Modulation of interhemispheric activation balance in motor-related areas of stroke patients with motor recovery: systematic review and meta-analysis of fMRI studies. *Neurosci Biobehav Rev* **57**, 392–400 (2015).
10. Carson, R. G. Inter-hemispheric inhibition sculpts the output of neural circuits by co-opting the two cerebral hemispheres. *J Physiol* **598**, 4781–4802 (2020).
11. Gerges, A. N. H. *et al.* Do Adults with Stroke have Altered Interhemispheric Inhibition ? A Systematic Review with Meta-Analysis . *Journal of Stroke and Cerebrovascular Diseases* **31**, 106494 (2022).
12. Lefaucheur, J. P. *et al.* Evidence-based guidelines on the therapeutic use of repetitive transcranial magnetic stimulation (rTMS): An update (2014–2018). *Clinical Neurophysiology* **131**, 474–528 (2020).
13. Rossi, S. *et al.* Safety and recommendations for TMS use in healthy subjects and patient populations, with updates on training, ethical and regulatory issues: Expert Guidelines. *Clinical Neurophysiology* **132**, 269–306 (2021).
14. Lefaucheur, J. P. *et al.* Evidence-based guidelines on the therapeutic use of repetitive transcranial magnetic stimulation (rTMS): An update (2014–2018). *Clinical Neurophysiology* **131**, 474–528 (2020).
15. van Lieshout, E. C. C., van der Worp, H. B., Visser-Meily, J. M. A. & Dijkhuizen, R. M. Timing of Repetitive Transcranial Magnetic Stimulation Onset for Upper Limb Function After Stroke: A Systematic Review and Meta-Analysis. *Front Neurol* **10**, 1–16 (2019).
16. Khedr, E. M., Etraby, A. E., Hemeda, M., Nasef, A. M. & Razek, A. A. E. Long-term effect of repetitive transcranial magnetic stimulation on motor function recovery after acute ischemic stroke. *Acta Neurol Scand* **121**, 30–37 (2010).
17. Du, J. *et al.* Effects of repetitive transcranial magnetic stimulation on motor recovery and motor cortex excitability in patients with stroke: a randomized controlled trial. *Eur J Neurol*

- 23**, 1666–1672 (2016).
18. Kim, W. S., Kwon, B. S., Seo, H. G., Park, J. & Paik, N. J. Low-Frequency Repetitive Transcranial Magnetic Stimulation Over Contralesional Motor Cortex for Motor Recovery in Subacute Ischemic Stroke: A Randomized Sham-Controlled Trial. *Neurorehabil Neural Repair* **34**, 856–867 (2020).
19. Bertolucci, F., Chisari, C. & Fregni, F. The potential dual role of transcallosal inhibition in post-stroke motor recovery. *Restor Neurol Neurosci* **36**, 83–97 (2018).
20. Di Pino, G. *et al.* Modulation of brain plasticity in stroke: A novel model for neurorehabilitation. *Nat Rev Neurol* **10**, 597–608 (2014).
21. Bradnam, L. V., Stinear, C. M., Barber, P. A. & Byblow, W. D. Contralesional hemisphere control of the proximal paretic upper limb following stroke. *Cerebral Cortex* **22**, 2662–2671 (2012).
22. van Lieshout, E. C. C., Visser-Meily, J. M. A., Neggers, S. F. W., van der Worp, H. B. & Dijkhuizen, R. M. Brain stimulation for arm recovery after stroke (B-STARS): protocol for a randomised controlled trial in subacute stroke patients. *BMJ Open* **7**, e016566 (2017).
23. Vink, J. *et al.* Continuous theta-burst stimulation of the contralesional M1 for promotion of upper limb recovery after stroke: a RCT. *medRxiv* 2022–2023 (2023).
24. Collin, C. & Wade, D. Assessing motor impairment after stroke: A pilot reliability study. *J Neurol Neurosurg Psychiatry* **53**, 576–579 (1990).
25. Rossi, S. *et al.* Safety, ethical considerations, and application guidelines for the use of transcranial magnetic stimulation in clinical practice and research. *Clinical Neurophysiology* **120**, 2008–2039 (2009).
26. Platz, T. *et al.* Reliability and validity of arm function assessment with standardized guidelines for the Fugl-Meyer Test, Action Research Arm Test and Box and Block Test: a multicentre study. *Clin Rehabil* **19**, 404–411 (2005).
27. Grice, K. O. *et al.* Adult norms for a commercially available Nine Hole Peg Test for finger dexterity. *The American journal of occupational therapy* **57**, 570–573 (2003).
28. Rossini, P. M. *et al.* Non-invasive electrical and magnetic stimulation of the brain, spinal cord, roots and peripheral nerves: Basic principles and procedures for routine clinical and research application: An updated report from an I.F.C.N. Committee. *Clinical Neurophysiology* **126**, 1071–1107 (2015).
29. Veraart, J., Sijbers, J., Sunaert, S., Leemans, A. & Jeurissen, B. Weighted linear least squares estimation of diffusion MRI parameters: strengths, limitations, and pitfalls. *Neuroimage* **81**, 335–346 (2013).
30. Mazziotta, J. C. *et al.* A probabilistic atlas of the human brain: theory and rationale for its development. *Neuroimage* **2**, 89–101 (1995).
31. Sankarasubramanian, V. *et al.* Inhibition versus facilitation of contralesional motor cortices in stroke: Deriving a model to tailor brain stimulation. *Clinical Neurophysiology* **128**, 892–902 (2017).
32. Xu, J. *et al.* Rethinking interhemispheric imbalance as a target for stroke neurorehabilitation. *Ann Neurol* **85**, 502–513 (2019).



## Chapter 7

# **Continuous theta-burst stimulation of the contralesional primary motor cortex leads to expansion of the ipsilesional motor-eloquent area in recovering stroke patients**

Jord JT Vink

Camille FM Biemans

Eline CC van Lieshout

Ruben PA van Eijk

Sebastiaan FW Neggers

JM Anne Visser-Meily

H Bart van der Worp

Rick M Dijkhuizen

*Under review for publication*

## **ABSTRACT**

### **Background**

Inhibitory repetitive transcranial magnetic stimulation (rTMS) of the contralesional primary motor cortex (M1) can promote upper limb recovery after stroke. However, its working mechanism remains unclear.

### **Hypothesis**

We hypothesized that contralesional inhibitory rTMS increases ipsilesional M1 excitability and promotes ipsilesional motor-eloquent area (MEA) reorganization.

### **Methods**

Sixty patients who participated in a trial on contralesional continuous theta burst stimulation (cTBS), an inhibitory form of rTMS, for the promotion of upper limb recovery after stroke, were included. M1 excitability and upper limb function were measured from TMS-based resting motor thresholds (RMTs) and the Fugl-Meyer assessment (FMA) arm score, respectively, before cTBS treatment and at six follow-up visits up to one year after stroke. Forty-four patients additionally underwent longitudinal navigated TMS-based motor mapping. Reorganization of the motor-eloquent area (MEA) was assessed from longitudinal changes in MEA overlap. Outcomes were analyzed using mixed models for repeated measures.

### **Results**

The ipsilesional RMT was 11% lower after active cTBS compared to sham cTBS (95% CI -18.7 to -2.6;  $p$  0.0099) within 12 hours after the series of treatments. Compared to the sham cTBS group, MEA overlap was 27% (95% CI -44 to -11;  $p$  0.0030), 25% (95% CI -45 to -5;  $p$  0.0224) and 29% (95% CI -48 to -11;  $p$  0.0038) less in the active cTBS group within 12 hours and at 1 week post-treatment, and 3 months post-stroke, respectively. Ipsilesional M1 excitability and FMA arm score were significantly correlated at 1 year post-stroke ( $r$  0.55;  $p$  < 0.0001)

### **Conclusion**

Upper limb recovery after cTBS treatment of the contralesional M1 after stroke may be caused by increased ipsilesional M1 excitability and MEA reorganization.



## INTRODUCTION

It has become increasingly apparent that recovery of motor function during rehabilitation after stroke is associated with plasticity of the motor cortex.<sup>1</sup> Physical therapy as applied during stroke rehabilitation may promote functional reorganization of the primary motor cortex (M1) and has been shown to lead to the expansion of the motor-eloquent cortex into neighboring cortex in animal models, potentially driven by the sprouting of new connections to surrounding tissue.<sup>2,3</sup> However, the underlying neurophysiological mechanisms of therapy-induced functional recovery in patients after stroke remain poorly understood.<sup>4-7</sup>

Transcranial magnetic stimulation (TMS) is a non-invasive method that enables assessment of the neurophysiological underpinnings of post-stroke upper limb recovery.<sup>8,9</sup> TMS of the motor cortex can evoke a muscular response, which can be measured as a motor-evoked potential (MEP) with electromyography (EMG).<sup>9</sup> Single-pulse TMS in combination with EMG and MRI-guided neuronavigation allows localization of the motor-eloquent area (MEA).<sup>10</sup> Applied longitudinally, this approach can be used to detect changes in the topological representation of the MEA to identify MEA remapping.<sup>11</sup> MEA reorganization can be further characterized by a change in size or a shift relative to structural anatomy. TMS-based motor mapping has previously revealed an increase in MEA size after stroke, which was associated with spontaneous or constraint-induced movement therapy (CIMT)-induced recovery of the upper limb.<sup>9,12</sup> A MEA shift, on the other hand, has been shown to be variable and a relationship with upper limb recovery has not been established.<sup>9</sup>

When applied repetitively, TMS may up- or downregulate activity in the targeted area, depending on the stimulation paradigm. Inhibitory repetitive TMS (rTMS) of the contralesional M1 combined with physical therapy, started within the first month after stroke onset, can improve upper limb recovery in patients.<sup>13-15</sup> Inhibitory rTMS can be performed with low-frequency (LF) rTMS or continuous theta burst stimulation (cTBS). The latter is an accelerated form of inhibitory rTMS with a treatment duration of less than a minute.<sup>16</sup> Upper limb recovery after stroke has been associated with an increase in ipsilesional M1 excitability, reducing or eliminating the interhemispheric imbalance in M1 excitability.<sup>17</sup> Therefore, a potential mode of action of LF rTMS or cTBS of the contralesional M1 is restoration of the balance of interhemispheric interactions, through downregulation of contralesional M1 excitability and potentially (consequent) upregulation of ipsilesional M1 excitability.<sup>18,19</sup> However, the relationship between (rTMS-induced) restoration of the interhemispheric balance, MEA reorganization and upper limb recovery remains unclear.

We hypothesized that ten sessions of cTBS of the contralesional M1, combined with physical therapy of the affected arm, delivered within the first three weeks after stroke, restores the interhemispheric balance through an increase in ipsilesional M1 excitability<sup>20</sup> and promotes reorganization of the ipsilesional MEA, in association with upper limb recovery. To that aim, we measured M1 excitability and MEA changes in both hemispheres before active or sham cTBS, and at six follow-up visits after treatment, until one year post-stroke.

## METHODS

### Study design

This study was part of a randomized, sham-controlled clinical trial on early cTBS treatment over the contralesional M1 for the promotion of upper limb recovery after stroke (B-STARS).<sup>21</sup> The study was approved by the Medical Research Ethics Committee of the University Medical Center Utrecht, and all patients gave written informed consent. The protocol of the B-STARS trial has been published previously.<sup>21</sup>

## Participants

Patients were recruited from rehabilitation center De Hoogstraat (Utrecht, the Netherlands). Patients who met the following inclusion criteria were eligible for participation: (1) age  $\geq 18$  years; (2) first-ever ischemic stroke or intracerebral hemorrhage; (3) paresis of one arm, as determined by a Motricity Index (MI) of the arm between 9 and 99; (4) baseline assessment within three weeks after stroke onset. Patients were excluded from participation based on the following criteria: (1) disabling medical history as determined by the treating physician; (2) normal to almost normal use of the hand; (2) severe deficits in communication, memory, or understanding that impede proper study participation; and (3) contraindications to TMS as based on TMS safety guidelines.<sup>22</sup> Acquisition of motor mapping data started after the 16<sup>th</sup> patient was included in the B-STARS trial.

## Procedures

### *TMS intervention*

TMS treatment consisted of ten daily sessions of real or sham cTBS treatment delivered over the contralesional M1.<sup>21</sup> Treatment was started within three weeks after stroke onset and combined with regular care upper limb therapy.

### *TMS motor mapping*

Navigated TMS (nTMS) motor mapping was performed at baseline (within three weeks after stroke), at the final (10<sup>th</sup>) day of the treatment period, at one week and one month after treatment, and at 3, 6 and 12 months after stroke onset.

Stimulation was performed using a biphasic Neuro-MS/D Advanced Therapeutic stimulator with an angulated 100mm figure-of-eight TMS coil (Neurosoft, Ivanovo, Russia). EMG Ag/AgCl surface electrodes were placed over the bilateral first dorsal interosseous (FDI) muscles. EMG was recorded, amplified and digitized at a sampling frequency of 20 kHz using a four-channel Neuro-MEP amplifier (Neurosoft, Ivanovo, Russia).

The 'motor hotspot' was identified by delivering TMS pulses over M1 and identifying the stimulation location at which the MEP with the largest peak-to-peak amplitude was evoked. Next, the resting motor threshold (RMT) was determined, which was defined as the minimal intensity at which TMS over the motor hotspot led to at least five out of ten MEPs with a peak-to-peak amplitude of  $>50\mu\text{V}$  in the FDI muscle contralateral to stimulation.<sup>23</sup>

Neuronavigation was performed on a generic MRI head model using the Neural Navigator neuronavigation system (Brain Science Tools, De Bilt, the Netherlands). Accurate registration of the MRI head model with the patient's head across sessions was ensured by adjusting the alignment markers in the MRI head model based on the position of the facial landmarks captured during the alignment procedure. This also allowed registration of the MRI head model with a post-hoc acquired individual MRI scan. This was performed by refitting the facial landmarks measured before treatment, with the same locations marked in the post-hoc acquired individual MRI scan. A predefined grid of points was placed over the scalp, spaced 8mm apart in both directions, covering the entire scalp. The neuronavigation system was used to guide the TMS coil to the predefined grid points.

A motor map was acquired by delivering five TMS pulses at 120%RMT to each point of a 4-by-4 grid around the motor hotspot, totaling 80 stimuli per motor map. The same 4-by-4 grid was applied at all visits (**Figure 1**).

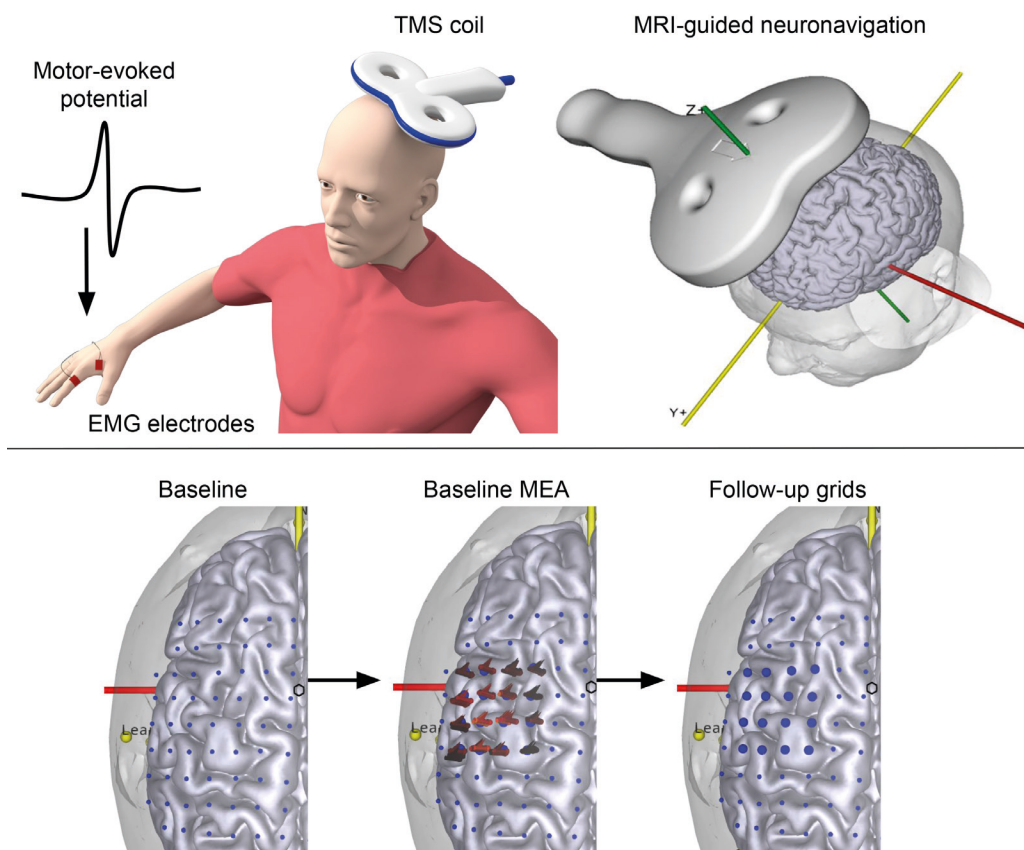


**Figure 1.** Schematic overview of the motor mapping procedure. Motor potentials evoked by TMS pulses delivered over M1 were recorded in the FDI muscle for both hemispheres. TMS coil placement was guided and recorded using an MRI-guided neuronavigation system. At baseline, the motor-eloquent area (MEA) was sampled in a 4-by-4 grid around the motor hotspot. The same grid points were stimulated at follow-up visits. The locations of the flags indicate the intersection of the TMS coil isocenter with the cortex, while the direction of the flag indicates the direction of the TMS-induced current. A brighter flag color indicates a higher MEP amplitude evoked in the FDI muscle.

### Upper limb function assessment

Upper limb function was assessed from the Fugl-Meyer Assessment (FMA) arm score at baseline (within three weeks after stroke), at one week and one month after treatment, and at 3, 6 and 12 months after stroke onset. The FMA arm score is a reliable and valid motor performance test consisting of 33 tasks that involve movements of the affected upper limb, with higher scores indicating better performance.<sup>17</sup> Upper limb recovery was measured from the change in FMA arm score between the baseline and follow-up visits.

### Data analysis

Data were analyzed using custom scripts in MATLAB environment (MathWorks Inc., United States).

Cortical excitability was defined by the RMT value. MEA reorganization was defined from the change in overlap between the first measured MEA (depending on the presence of MEPs) and subsequent measured MEAs. In healthy individuals the overlap in MEAs has been shown to have a higher test-retest reliability as compared to center of gravity (COG) shifts, making it more reliable for measurement of longitudinal changes in MEA representation.<sup>11</sup> Percent overlap was calculated using the following formula:<sup>24</sup>

$$overlap_{\%} = \frac{a_{12}}{a_1 + a_2 - a_{12}} \cdot 100\%$$

$\alpha_{12}$ : the number of common grid points at which an average MEP with amplitude of  $>50\mu\text{V}$  could be identified across two visits; and  $\alpha_1$  and  $\alpha_2$  the number of grid points at which an average MEP with amplitude of  $>50\mu\text{V}$  could be measured during the first and second visit, respectively. An overlap of 100% indicates MEAs with identical spatial representation.

MEA remapping was additionally analyzed from MEA size change and COG displacement over time. MEA size was calculated by multiplying the number of grid points at which an average MEP with an amplitude of more than  $50\mu\text{V}$  could be measured with the area covered by a single grid point ( $0.64\text{cm}^2$ ). MEA displacement was measured from the displacement of the COG of the spatial distribution of MEP amplitudes in the MEA, along the mediolateral (ML) and anteroposterior (AP) axes, between the first visit (depending on the presence of MEPs) and subsequent visits. COGs were calculated by the following formulas:<sup>25</sup>

$$COG_{ML} = \frac{\sum_i (A_i \cdot X_i)}{\sum_i A_i} \text{ and } COG_{AP} = \frac{\sum_i (A_i \cdot Y_i)}{\sum_i A_i}$$

$X_i$  and  $Y_i$ : the coordinates of stimulation target  $i$  along the ML axis and the AP axis, respectively;  $A_i$ : amplitude of the MEP evoked at stimulation target  $i$ . COG displacement was assessed along the individual axes and as the Euclidian displacement.

### Statistical analysis

Statistical analysis was performed using R 4.1. All hypotheses were tested two-tailed with an alpha of 0.05. Missing data were assumed to be missing at random. Analyses on M1 excitability were performed in all 60 randomized participants. The other analyses were performed on the 44 patients who underwent TMS-based motor mapping.

First, we investigated the effect of time on the outcomes: M1 excitability, MEA overlap, MEA size and COG displacement irrespective of treatment. We investigated the change in outcomes over time using a linear mixed model (LME). The model included hemisphere (ipsilesional; contralesional) and the interaction between hemisphere and time (<12 hours, 1 week and 1 month post-treatment and 3, 6 and 12 months post-stroke visits converted to weeks post-stroke).

Second, we investigated the effect of treatment on the outcomes in the ipsilesional hemisphere at different visits. We investigated this using a mixed model for repeated measures (MMRM) with an unstructured variance-covariance matrix with visit (<12 hours, 1 week and 1 month post-treatment and 3, 6 and 12 months post-stroke) and the interaction between visit and treatment (active and sham cTBS). The models with M1 excitability and MEA size as outcomes also included the baseline values of the investigated outcome.

Pearson's correlation coefficients, or Spearman's correlation coefficients in case of non-normally distributed data, were calculated to evaluate the relationship between the neurophysiological outcomes and upper limb recovery outcome.

## RESULTS

All sixty patients underwent cortical excitability and motor function measurements. The baseline characteristics and patient flow diagram of the full patient population have been reported previously.<sup>15</sup> Forty-four out of sixty patients enrolled in the B-STARS study underwent additional motor mapping measurements. Of these forty-four patients, twenty-one patients

were randomized to receive active cTBS, and twenty-three were assigned to receive sham cTBS. Patient characteristics are shown in **Table 1** and the participant flow diagram is shown in **Figure 2**. Not all patients could undergo motor mapping measurements at all visits due to temporary suspension of study activities as a result of the COVID-19 pandemic. A single patient showed signs of syncope during RMT determination and was excluded from the remaining motor mapping sessions. No serious adverse events (SAEs) were reported during the motor mapping sessions.

**Table 1.** Baseline characteristics for TMS-based motor mapping sessions.

Patient characteristics	Total (n = 44)	Active cTBS (n = 21)	Sham cTBS (n = 23)
Sex, n (%)			
Male	27 (61)	12 (57)	15 (65)
Female	17 (39)	9 (43)	8 (35)
Age, mean (SD), years	61 (12)	57 (11)	65 (12)
Intervention			
Treatment onset, mean (SD), days post-stroke	14 (4)	14 (4)	15 (4)
Stroke information			
Lesion type, n (%)			
Ischemic stroke	37 (84)	18 (86)	19 (83)
Intracerebral hemorrhage	7 (16)	3 (14)	4 (17)
Lesion location, n (%)			
Subcortical	20 (45)	11 (52)	9 (39)
Cortical	11 (25)	4 (19)	7 (31)
Brainstem	7 (16)	4 (19)	3 (13)
Unknown	6 (14)	2 (10)	4 (17)
Impaired side, n (%)			
Right arm	20 (45)	10 (48)	10 (43)
Left arm	24 (55)	11 (52)	13 (57)
Stroke severity upon hospital admission			
NIHSS, median (IQR)	7 (7)	7 (7)	8 (7)
Electrophysiology			
MEP presence, n (%)			
Affected hemisphere	15 (34)	8 (38)	7 (30)
Unaffected hemisphere	44 (100)	21 (100)	23 (100)
Resting Motor Threshold, mean (SD), %MO			
Affected hemisphere <sup>1</sup>	85 (24)	87 (20)	83 (27)
Unaffected hemisphere	40 (11)	41 (13)	39 (9)
Baseline function			
Function scores, mean (SD)			
Fugl-Meyer Assessment Arm score	25.7 (19.3)	25.4 (19.1)	25.9 (20.0)

<sup>1</sup>RMT was set at 100%MO if an MEP could not be measured. SD: Standard deviation; IQR: Inter Quartile Range; NIHSS: National Institutes of Health Stroke Scale; MEP: Motor-evoked potential; %MO: Percentage of maximum machine output.

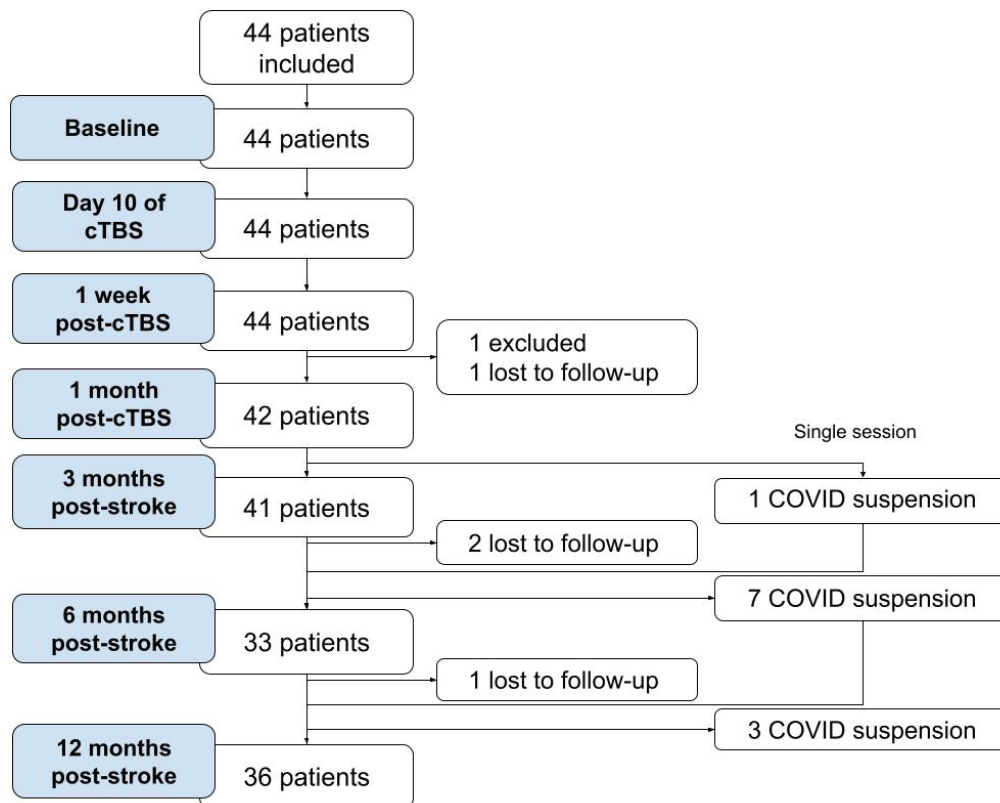


**Figure 2.** Participant flow diagram for TMS-based motor mapping sessions. Exclusions due to COVID suspension are single session exclusions.

The ipsilesional RMT decreased by 0.41% per week (95% CI -0.50 to -0.32;  $p < 0.0001$ ) whereas the contralesional RMT did not change over time (95% CI -0.08 to 0.10;  $p 0.7627$ ). The ipsilesional RMT was 10.6% lower in the active cTBS group compared to the sham cTBS group (95% CI -18.7 to -2.6;  $p 0.0099$ ) within 12 hours after the series of treatments (**Figure 3A**). This difference was -8.2% at 1 week after treatment (95% CI -16.5 to 0.1;  $p 0.0533$ ). After that, the ipsilesional RMT in both groups gradually converged over time.

MEA overlap reduced over time with 0.23% per week in the ipsilesional hemisphere (95% CI -0.41 to -0.05;  $p 0.0143$ ) but did not change in the contralesional hemisphere (95% CI -0.21 to 0.03;  $p 0.1354$ ). Compared to sham-stimulated patients, patients who received active cTBS had 27% (95% CI -44 to -11;  $p 0.0030$ ), 25% (95% CI -45 to -5;  $p 0.0224$ ) and 29% (95% CI -48 to -11;  $p 0.0038$ ) less overlap with the first MEA within 12 hours post-treatment, at 1 week post-treatment and at 3 months post-stroke, respectively (**Figure 3B**).

MEA overlap and change in RMT at the stage of their maximum changes, i.e. within 12 hours post-treatment were not correlated ( $r 0.17$ ;  $p 0.572$ ).

Ipsilesional MEA size decreased over time with  $0.02\text{cm}^2$  per week (95% CI -0.04 to 0.00;  $p 0.0352$ ) while contralesional MEA size did not change (95% CI -0.03 to 0.00;  $p 0.1134$ ). Ipsilesional MEA size was larger in the active cTBS treatment group compared to the sham stimulation group at 6 months post-stroke (mean difference 2.52; 95% CI 0.55 to 4.49;  $p 0.0134$ ; **Figure 4**).

There was no Euclidean COG displacement of the ipsilesional MEA over time and there were no differences between the active and sham cTBS groups (**Figure 5**).

Ipsilesional M1 excitability (i.e., RMT) and ipsilesional MEA size, measured at 1 year post-stroke, correlated with outcome on the FMA arm score at 1 year post-stroke (Spearman's rho 0.52;  $p 0.0001$  and Pearson's rho 0.5;  $p 0.022$ , respectively; **Figure 6**). Ipsilesional MEA

overlap (Pearson's rho 0.18; p 0.466) as well as COG displacement of the ipsilesional MEA in posterior (Pearson's rho 0.44; p 0.058) and lateral direction (Pearson's rho 0.02; p 0.950) did not correlate with the FMA arm score at 1 year post-stroke.

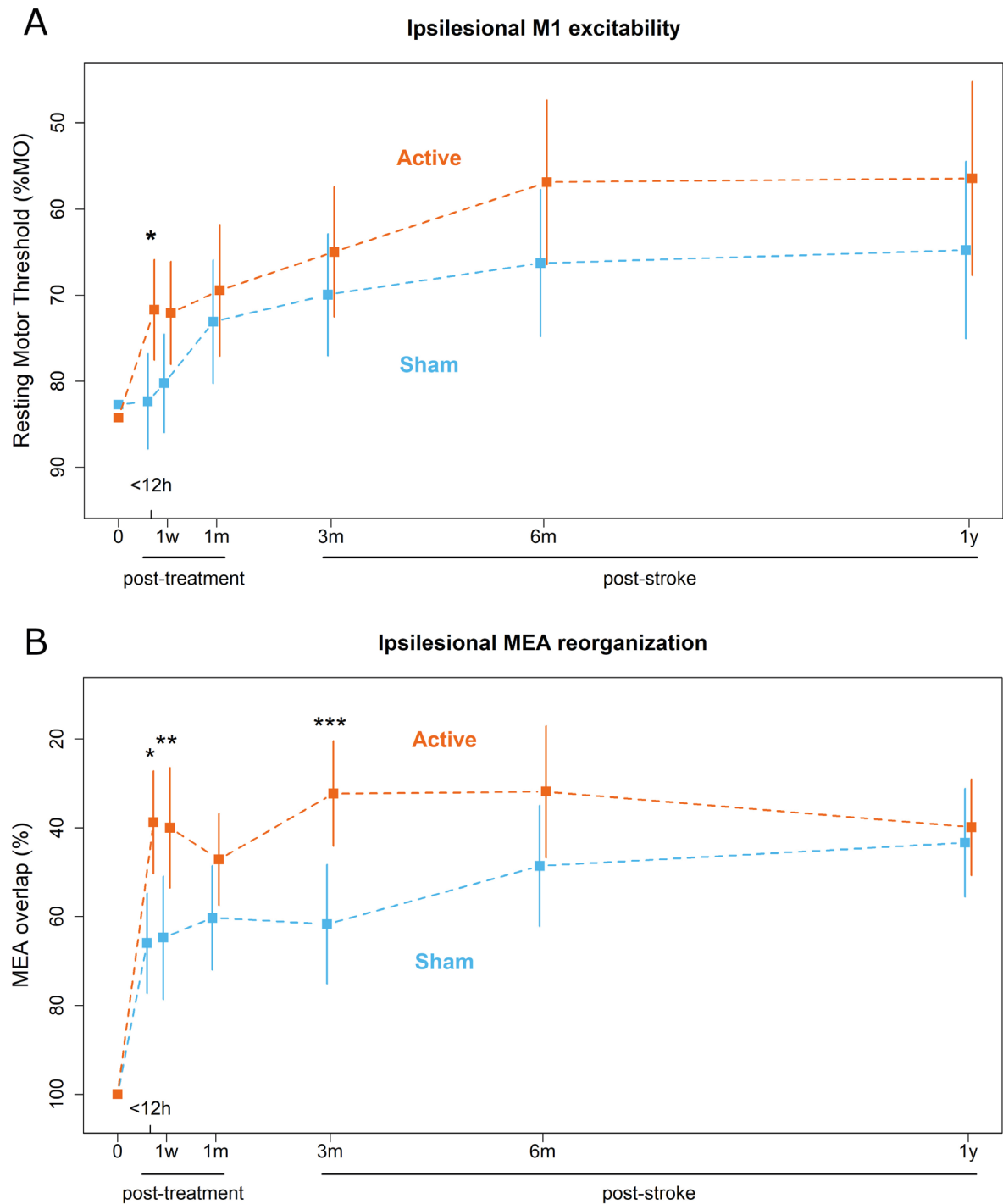


**Figure 3A.** Mean and 95% confidence intervals of the ipsilesional RMT in the active and sham cTBS groups were calculated using a mixed model for repeated measures. The vertical axis is inverted to reflect an increase in M1 excitability along the axis. \*p 0.0099. **Figure 3B.** Mean and 95% confidence intervals of MEA overlap with the first observed MEA in the active and sham cTBS groups calculated using mixed-effects model for repeated measures. The vertical axis is inverted to reflect an increase in MEA reorganization along the axis. 0: baseline; h: hours; w: weeks; m: months; y: years. \*p 0.0030. \*\*p 0.0224. \*\*\*p 0.0038

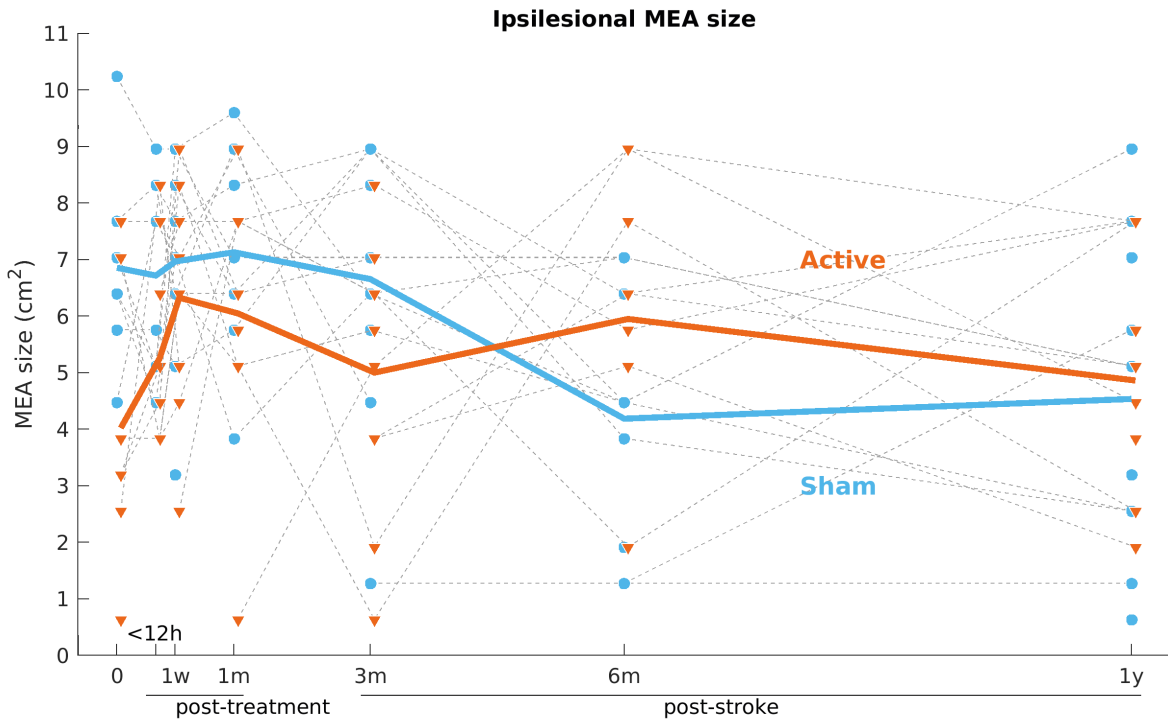


**Figure 4.** Ipsilesional motor-eloquent area (MEA) size at different visits. Individual data are connected by a dashed line, with patients who received active cTBS in orange and patients who received sham cTBS in blue. The group averages are shown as solid lines. 0: baseline; h: hours; w: weeks; m: months; y: years.



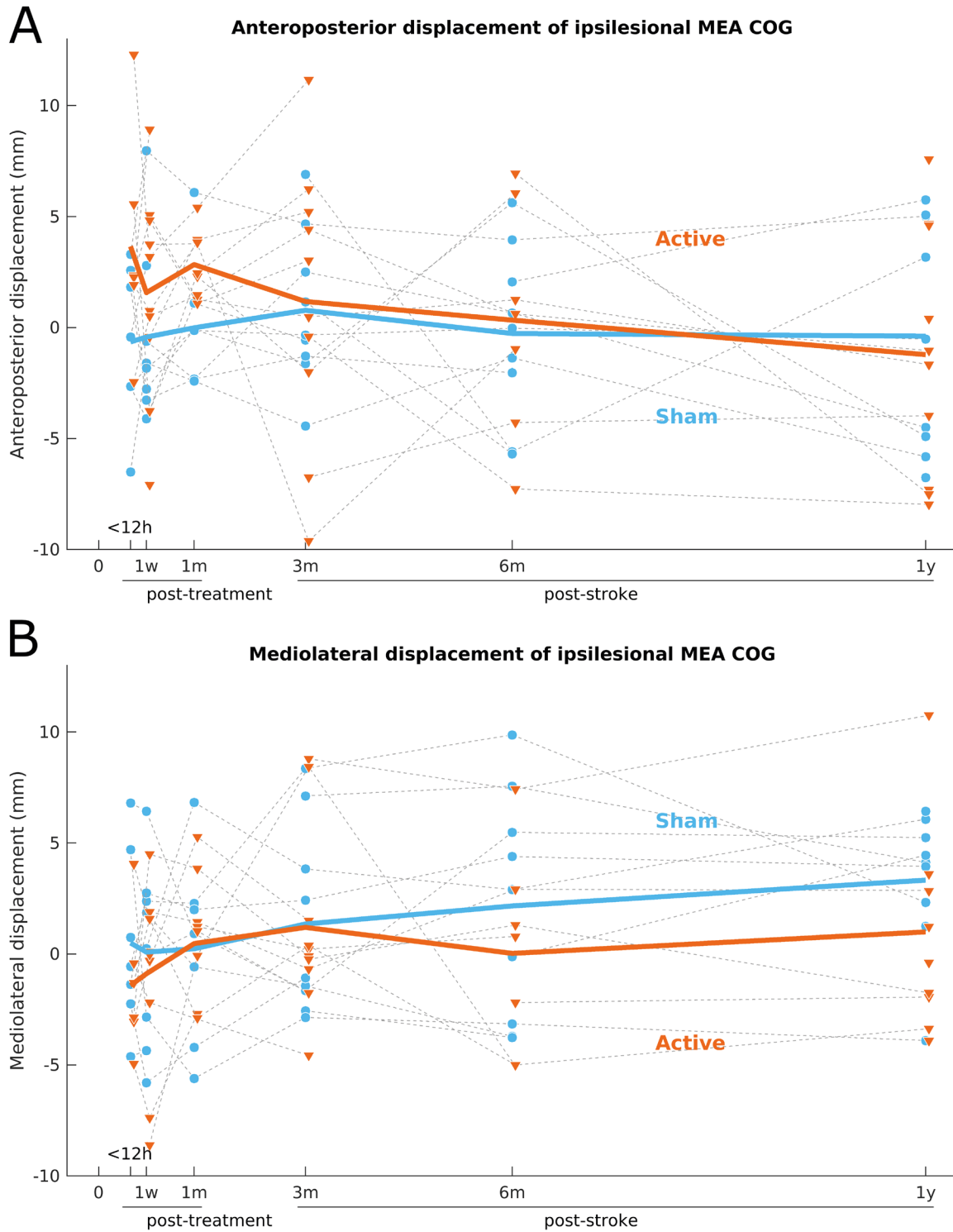


**Figure 5.** Anteroposterior (A) and mediolateral (B) displacement of the center of gravity (COG) of the ipsilesional motor-eloquent area (MEA) with respect to the first measured MEA at different visits. Individual data are connected by a dashed line, with patients who received active cTBS in orange and patients who received sham cTBS in blue. The group averages are shown as solid lines. 0: baseline; h: hours; w: weeks; m: months; y: years.

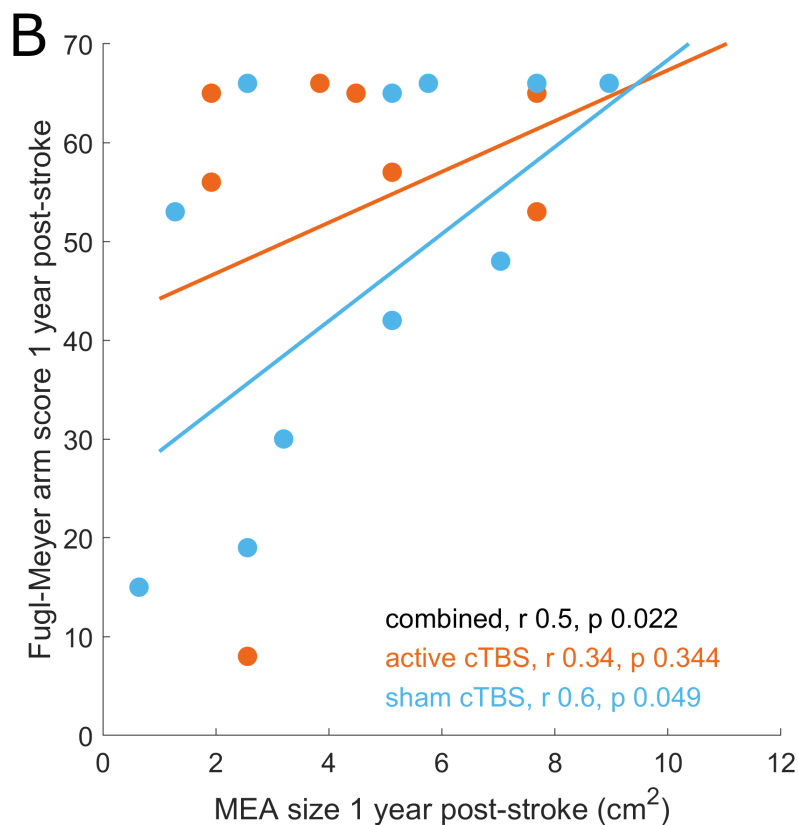
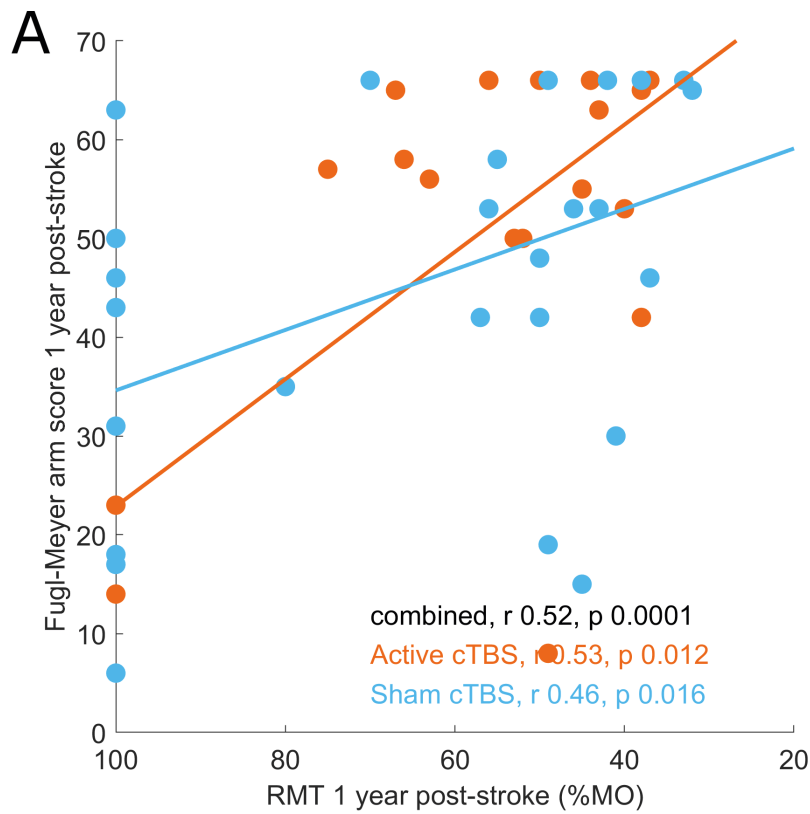


**Figure 6.** Ipsilesional resting motor threshold (**A**) and ipsilesional MEA size (**B**) at one year post-stroke versus Fugl-Meyer Assessment arm score at 1 year post-stroke. Spearman's correlation coefficients are shown and the horizontal axis is inverted to reflect an increase in M1 excitability along the axis (**A**). Pearson's correlation coefficients are shown (**B**). Patients in the active cTBS group are shown in orange and patients in the sham cTBS group are shown in blue.

## DISCUSSION

We previously showed that ten sessions of cTBS of the contralesional M1, combined with upper limb physical therapy, promote upper limb recovery, reduce disability and dependence, and improve quality of life in recovering stroke patients.<sup>15</sup> We hypothesized that the therapeutic mechanism of the investigated cTBS treatment involves the elimination or reduction of a post-stroke interhemispheric imbalance in M1 excitability and a consequent increase in ipsilesional M1 excitability, and facilitation of ipsilesional MEA reorganization. Our randomized controlled trial data point toward normalization of the interhemispheric balance, indicated by an increase in ipsilesional M1 excitability, and a greater extent of ipsilesional MEA reorganization, indicated by longitudinally less MEA overlap, in patients who received ten sessions of active cTBS compared to patients who received sham cTBS. These changes primarily took place within the first three months post-stroke, during the presumed window of enhanced plasticity in stroke patients.<sup>26,27</sup>

It has been shown that cTBS can inhibit M1 excitability and increase excitability of the contralateral (non-stimulated) M1.<sup>28</sup> In stroke patients, this effect, combined with subsequent physical therapy of the affected arm, could potentially facilitate an enduring increase in ipsilesional M1 excitability. We previously found a trend toward a reduction in contralesional M1 excitability during the treatment period, although this was not associated with upper limb function.<sup>15</sup> The current study shows that ipsilesional M1 excitability at one year post-stroke is associated with upper limb function at one year post-stroke, in line with earlier studies.<sup>29</sup> We speculate that heightened ipsilesional M1 excitability plays a causal role in upper limb recovery, which may be promoted by cTBS of the contralesional M1.

Rehabilitative training-induced motor recovery, but not spontaneous restoration of motor function, has previously been associated with ipsilesional MEA reorganization in non-human primates.<sup>2,30</sup> We show that reorganization can be observed in the ipsilesional MEA in patients (across both treatment arms) who received physical therapy of the upper limb. The observed reorganization is specific to the ipsilesional MEA, as the contralesional MEA did not significantly change over time. Additionally, we found that patients who received ten sessions of cTBS, combined with upper limb physical therapy, showed a greater extent of ipsilesional MEA reorganization compared to patients who received sham stimulation.

Ipsilesional MEA reorganization was characterized by a mean increase in size and a mean shift in posterior direction in the first weeks after treatment. These observations are in agreement with previous studies that reported enlargement and posterior relocation of the hand representation after stroke.<sup>27,31,32</sup> The observed MEA reorganization may have occurred through recruitment of normally inactive or latent motor representations or through recruitment of neural circuits that are normally not associated with motor function.<sup>33</sup> The posterior shift in response to the contralesional cTBS treatment may represent recruitment of direct projections from neurons in the postcentral gyrus to spinal or bulbar motor neurons.<sup>34</sup> Yet, (anteroposterior or mediolateral) displacement of the ipsilesional MEA after stroke may vary<sup>35</sup>, as we also observed in the current study. We speculate that the direction of the displacement depends on the location of latent motor representations towards which the MEA could shift, which may differ between stroke patients.

We found that upper limb function at one year post-stroke is associated with ipsilesional MEA size. Previous studies reported a similar relationship in the subacute<sup>36,37</sup> and the chronic post-stroke phases.<sup>38</sup> Furthermore, an increase in MEA size associated with improvement in upper limb function has been found after constraint-induced movement therapy.<sup>12,39</sup> We observed a slight decrease in ipsilesional MEA size over the first post-stroke year across both treatment arms. A reduction in MEA of distant upper limb muscle representations has

previously been reported in non-human primates that did not receive rehabilitative training.<sup>30</sup> A possible explanation for this finding in our study could be reduced upper limb use, despite upper limb physical therapy, due to persisting stroke-induced functional limitations in activities of daily living.

The measured increases in ipsilesional M1 excitability and MEA reorganization were most prominent within 12 hours after the treatment period. However, these neurophysiological changes were not correlated, suggesting that these are two possible treatment mechanisms that operate independently. However, future studies should elucidate whether enhanced M1 excitability and MEA reorganization are a direct cause or rather a consequence of upper limb recovery after stroke.

### **Limitations**

Our study had some limitations. First, TMS-based motor mapping depends on the ability to evoke MEPs upon stimulation of the motor cortex. Unfortunately, MEPs can typically not be evoked in severely impaired patients in the first weeks to months after stroke,<sup>40</sup> hampering the collection of data early after stroke in these patients. Therefore, longitudinal changes in MEA characteristics were calculated relative to the first available MEA, potentially reducing statistical power at the early post-stroke time points.

Second, we did not perform masking of sensory sensations on the scalp evoked by peripheral nerve stimulation during active or sham cTBS treatment. However, all patients were naive to rTMS treatment and the measured outcomes were derived from electrophysiological recordings, which likely limited bias introduced by the lack of sensory masking.

### **CONCLUSION**

Ten sessions of cTBS of the contralesional M1 combined with physical therapy lead to heightened ipsilesional M1 excitability and a larger extent of reorganization of the ipsilesional MEA, shortly after the treatment course. MEA reorganization was characterized by a mean shift in posterior direction. Increased ipsilesional M1 excitability and MEA expansion were associated with recovery of the upper limb, potentially reflecting a therapeutic mode of action of contralesional cTBS treatment after stroke.

## REFERENCES

1. Grefkes C, Ward NS. Cortical reorganization after stroke: how much and how functional? *Neuroscientist*. 2014;20(1):56-70. doi:10.1177/1073858413491147
2. Nudo RJ, Wise BM, SiFuentes F, Milliken GW. Neural substrates for the effects of rehabilitative training on motor recovery after ischemic infarct. *Science (1979)*. 1996;272(5269):1791-1794.
3. Carmichael ST, Wei L, Rovainen CM, Woolsey TA. New patterns of intracortical projections after focal cortical stroke. *Neurobiol Dis*. 2001;8(5):910-922. doi:10.1006/nbdi.2001.0425
4. Darling WG, Wolf SL, Butler AJ. Variability of motor potentials evoked by transcranial magnetic stimulation depends on muscle activation. *Exp Brain Res*. 2006;174(2):376-385. doi:10.1007/s00221-006-0468-9
5. Kiers L, Cros D, Chiappa KH, Fang J. Variability of motor potentials evoked by transcranial magnetic stimulation. *Electroencephalogr Clin Neurophysiol*. 1993;89(6):415-423. doi:10.1016/0168-5597(93)90115-6
6. Maeda F, Gangitano M, Thall M, Pascual-Leone A. Inter- and intra-individual variability of paired-pulse curves with transcranial magnetic stimulation (TMS). *Clin Neurophysiol*. 2002;113(3):376-382. doi:10.1016/s1388-2457(02)00008-1
7. Wassermann EM. Variation in the response to transcranial magnetic brain stimulation in the general population. *Clin Neurophysiol*. 2002;113(7):1165-1171. doi:10.1016/s1388-2457(02)00144-x
8. McDonnell MN, Stinear CM. TMS measures of motor cortex function after stroke: A meta-analysis. *Brain Stimul*. 2017;10(4):721-734. doi:10.1016/j.brs.2017.03.008
9. Lüdemann-Podubecá J, Nowak DA. Mapping cortical hand motor representation using TMS: A method to assess brain plasticity and a surrogate marker for recovery of function after stroke? *Neurosci Biobehav Rev*. 2016;69:239-251. doi:10.1016/j.neubiorev.2016.07.006
10. Klomjai W, Katz R, Lackmy-Vallée A. Basic principles of transcranial magnetic stimulation (TMS) and repetitive TMS (rTMS). *Ann Phys Rehabil Med*. 2015;58(4):208-213. doi:10.1016/j.rehab.2015.05.005
11. Nazarova M, Novikov P, Ivanina E, Kozlova K, Dobrynina L, Nikulin V V. Mapping of multiple muscles with transcranial magnetic stimulation: absolute and relative test-retest reliability. *Hum Brain Mapp*. 2021;42(8):2508-2528. doi:10.1002/hbm.25383
12. Liepert J, Bauder H, Miltner WHR, Taub E, Weiller C. Treatment-induced cortical reorganization after stroke in humans. *Stroke*. 2000;31(6):1210-1216. doi:10.1161/01.STR.31.6.1210
13. Lefaucheur JP, Aleman A, Baeken C, et al. Evidence-based guidelines on the therapeutic use of repetitive transcranial magnetic stimulation (rTMS): An update (2014-2018). *Clin Neurophysiol*. 2020;131(2):474-528. doi:10.1016/j.clinph.2019.11.002
14. van Lieshout ECC, van der Worp HB, Visser-Meily JMA, Dijkhuizen RM. Timing of Repetitive Transcranial Magnetic Stimulation Onset for Upper Limb Function After Stroke: A Systematic Review and Meta-Analysis. *Front Neurol*. 2019;10(1269):1-16. doi:10.3389/fneur.2019.01269
15. Vink J, van Lieshout ECC, Otte WM, et al. Continuous theta-burst stimulation of the

contralesional M1 for promotion of upper limb recovery after stroke: a RCT. *medRxiv*. Published online 2023:2022-2023.

16. Lefaucheur JP, Aleman A, Baeken C, et al. Evidence-based guidelines on the therapeutic use of repetitive transcranial magnetic stimulation (rTMS): An update (2014–2018). *Clinical Neurophysiology*. 2020;131(2):474-528. doi:10.1016/j.clinph.2019.11.002
17. Stinear CM, Petoe MA, Byblow WD. Primary motor cortex excitability during recovery after stroke: Implications for neuromodulation. *Brain Stimul*. 2015;8(6):1183-1190. doi:10.1016/j.brs.2015.06.015
18. Khedr EM, Etraby AE, Hemeda M, Nasef AM, Razeq AAE. Long-term effect of repetitive transcranial magnetic stimulation on motor function recovery after acute ischemic stroke. *Acta Neurol Scand*. 2010;121(1):30-37.
19. Du J, Tian L, Liu W, et al. Effects of repetitive transcranial magnetic stimulation on motor recovery and motor cortex excitability in patients with stroke: a randomized controlled trial. *Eur J Neurol*. 2016;23(11):1666-1672.
20. Boddington LJ, Reynolds JNJ. Targeting interhemispheric inhibition with neuromodulation to enhance stroke rehabilitation. *Brain Stimul*. 2017;10(2):214-222. doi:10.1016/j.brs.2017.01.006
21. van Lieshout ECC, Visser-Meily JMA, Neggers SFW, van der Worp HB, Dijkhuizen RM. Brain stimulation for arm recovery after stroke (B-STARS): protocol for a randomised controlled trial in subacute stroke patients. *BMJ Open*. 2017;7(8):e016566. doi:10.1136/bmjopen-2017-016566
22. Rossi S, Hallett M, Rossini PM, et al. Safety, ethical considerations, and application guidelines for the use of transcranial magnetic stimulation in clinical practice and research. *Clinical Neurophysiology*. 2009;120(12):2008-2039. doi:10.1016/j.clinph.2009.08.016
23. Rossini PM, Burke D, Chen R, et al. Non-invasive electrical and magnetic stimulation of the brain, spinal cord, roots and peripheral nerves: Basic principles and procedures for routine clinical and research application: An updated report from an I.F.C.N. Committee. *Clinical Neurophysiology*. 2015;126(6):1071-1107. doi:10.1016/j.clinph.2015.02.001
24. Nazarova M, Novikov P, Ivanina E, Kozlova K, Dobrynina L, Nikulin V V. Mapping of multiple muscles with transcranial magnetic stimulation: absolute and relative test–retest reliability. *Hum Brain Mapp*. 2021;42(8):2508-2528. doi:10.1002/hbm.25383
25. Novikov PA, Nazarova MA, Nikulin V V. TMSmap – Software for Quantitative Analysis of TMSMappingResults. *Front Hum Neurosci*. 2018;12(July):1-12. doi:10.3389/fnhum.2018.00239
26. Dromerick AW, Geed S, Barth J, et al. Critical Period After Stroke Study (CPASS): A phase II clinical trial testing an optimal time for motor recovery after stroke in humans. *Proceedings of the National Academy of Sciences*. 2021;118(39):e2026676118.
27. Cramer SC. Repairing the human brain after stroke: I. Mechanisms of spontaneous recovery. *Ann Neurol*. 2008;63(3):272-287. doi:10.1002/ana.21393
28. Suppa A, Ortu E, Zafar N, et al. Theta burst stimulation induces after-effects on contralateral primary motor cortex excitability in humans. 2008;18:4489-4500. doi:10.1113/jphysiol.2008.156596
29. Veldema J, Nowak DA, Gharabaghi A. Resting motor threshold in the course of hand

- motor recovery after stroke: a systematic review. *J Neuroeng Rehabil.* 2021;18(1):1-28. doi:10.1186/s12984-021-00947-8
30. Nudo RJ, Milliken GW. Reorganization of movement representations in primary motor cortex following focal ischemic infarcts in adult squirrel monkeys. *J Neurophysiol.* 1996;75(5):2144-2149. doi:10.1152/jn.1996.75.5.2144
31. Buma FE, Raemaekers M, Kwakkel G, Ramsey NF. Brain function and upper limb outcome in stroke: A cross-sectional fMRI study. *PLoS One.* 2015;10(10):1-18. doi:10.1371/journal.pone.0139746
32. Calautti C, Baron JC. Functional neuroimaging studies of motor recovery after stroke in adults: a review. *Stroke.* 2003;34(6):1553-1566. doi:10.1161/01.STR.0000071761.36075.A6
33. Chen R, Cohen LG, Hallett M. Nervous system reorganization following injury. *Neuroscience.* 2002;111(4):761-773. doi:10.1016/S0306-4522(02)00025-8
34. Pineiro R, Pendlebury S, Johansen-Berg H, Matthews PM. Functional MRI Detects Posterior Shifts in Primary Sensorimotor Cortex Activation After Stroke. *Stroke.* 2001;32(5):1134-1139. doi:10.1161/01.STR.32.5.1134
35. Lüdemann-Podubecká J, Nowak DA. Mapping cortical hand motor representation using TMS: A method to assess brain plasticity and a surrogate marker for recovery of function after stroke? *Neurosci Biobehav Rev.* 2016;69:239-251. doi:10.1016/j.neubiorev.2016.07.006
36. Freundlieb N, Philipp S, Drabik A, Gerloff C, Forkert ND, Hummel FC. Ipsilesional motor area size correlates with functional recovery after stroke: A 6-month follow-up longitudinal TMS motor mapping study. *Restor Neurol Neurosci.* 2015;33(2):221-231. doi:10.3233/RNN-140454
37. Boake C, Noser EA, Ro T, et al. Constraint-induced movement therapy during early stroke rehabilitation. *Neurorehabil Neural Repair.* 2007;21(1):14-24. doi:10.1177/1545968306291858
38. Bastings EP, Greenberg JP, Good DC. Hand motor recovery after stroke: a transcranial magnetic stimulation mapping study of motor output areas and their relation to functional status. *Neurorehabil Neural Repair.* 2002;16(3):275-282.
39. Sawaki L, Butler AJ, Leng X, et al. Constraint-induced movement therapy results in increased motor map area in subjects 3 to 9 months after stroke. *Neurorehabil Neural Repair.* 2008;22(5):505-513. doi:10.1177/1545968308317531
40. Stinear CM, Byblow WD, Ackerley SJ, Smith MCC, Borges VM, Barber PA. PREP2: A biomarker-based algorithm for predicting upper limb function after stroke. *Ann Clin Transl Neurol.* 2017;4(11):811-820. doi:10.1002/acn3.488





Chapter 8

## **General discussion**

The first part of this thesis (chapters 2 to 4) focused on increasing our understanding of healthy brain networks and how non-invasive brain stimulation methods, like TMS, can be used to investigate healthy brain function through interaction with these brain networks. The second part of this thesis (chapters 5 to 7) focused on therapeutic rTMS as a novel treatment for the promotion of upper limb recovery after stroke and on its working mechanism. In this discussion, the findings reported in the first part of this thesis will be put in a broader context first. Second, we will discuss rTMS treatment for the promotion of upper limb recovery after stroke, the clinical implications and its working mechanism. Future perspectives for personalization of rTMS treatment will be discussed next. Finally, we conclude with a summary of the main findings.

### **Assessing brain networks using TMS**

To effectively probe brain networks using TMS for therapeutic or diagnostic purposes, we have to understand how it affects these brain networks. In **chapter 2**, we measured network activity in response to activity evoked with TMS at different stimulation sites with concurrent TMS-fMRI in healthy individuals. We found that network activity evoked at M1 was predominantly observed in brain regions associated with the sensorimotor network. Furthermore, TMS-evoked activity was similar to sensorimotor network activation in response to voluntary hand movements. These findings were relatively consistent between individuals and in line with previous observations.<sup>1,2</sup> However, network activity evoked at the dorsolateral prefrontal cortex (DLPFC) was substantially more variable between individuals, which is consistent with previous concurrent TMS-fMRI studies that showed that prefrontal stimulation evokes more variable network activity.<sup>3</sup> Networks involved in working memory, inhibition, attention, and language have been shown to exhibit substantially more variability in resting-state functional connectivity compared to the somatomotor network,<sup>4</sup> which indicates that the DLPFC is part of a network with an intrinsically more variable organization compared to the somatomotor network.<sup>3</sup> The variability in network connectivity is likely to reflect in the propagation of TMS-evoked network activity as well.

These findings provide the basis for **chapter 3**, in which we investigated whether TMS-evoked activity preferentially propagates through functionally connected brain regions. Functional connectivity, i.e. the synchrony between resting-state hemodynamic or electrical brain signals, is frequently used to characterize brain networks.<sup>5-7</sup> The spread of TMS-evoked network activity is associated with synchronicity between resting-state blood oxygenation level-dependent (BOLD) fMRI signals, although substantial variability has been observed between individuals.<sup>3</sup> It remains unclear whether this is also true for synchronicity between electrical brain signals, i.e. resting-state functional connectivity of EEG signals. We found that TMS-evoked network activity was related to resting-state functional connectivity, but the variance explained by functional connectivity was very limited. A more recent study found that the spread of TMS-evoked network activity within the default mode network (DMN) and dorsal attention network (DAN) was defined by structural connectivity rather than resting-state functional connectivity (measured with EEG or fMRI).<sup>8,9</sup> Furthermore, propagation of TMS-evoked activity was defined by the overall structural integrity of macro-scale networks, rather than whole-brain structural connectivity with the stimulated area.<sup>8</sup> Altogether, this suggests that propagation of TMS-evoked activity is predominantly defined by macro-scale structural network connectivity rather than individual functional or structural connectivity. This would mean that the spread of TMS-evoked activity is characterized by the macro-scale network that was stimulated, rather than individual whole-brain functional or structural connectivity with the stimulated seed. This is potentially caused by the aforementioned variability of individual

whole-brain functional or structural connectivity of the investigated networks. Therefore, future studies should consider structural connectivity of the stimulated target for adequate investigation or modulation of the network of interest.

In **chapter 4**, we laid the groundwork for the nTMS-EMG motor mapping study described in **chapter 7**, by investigating how TMS-induced electrical fields interact with cortical neurons in the identification of motor-eloquent areas. We found that the spatial organization of the recorded motor-eloquent area depends on the orientation of the TMS-induced electrical fields. These results highlight the complexity of the interaction between TMS-induced electrical fields and neuronal activation, suggesting caution in the interpretation of nTMS-based motor mapping results for the identification of motor-eloquent cortex. However, the complex interaction between an induced electrical field and neuronal activation also applies to the gold standard for the identification of motor-eloquent areas, direct cortical stimulation (DCS). The distance between the cortical representation of different muscle groups identified using nTMS and DCS varies between 2 and 16 mm, depending on the study.<sup>10</sup> The variability between studies suggests that the nTMS-based motor maps likely depend on variability in methodology, rather than intrinsic variability in local cortical excitability. This stresses the importance of accurately controlling the TMS coil orientation during nTMS-EMG measurements with an MRI-guided neuronavigation system to obtain reliable nTMS-based motor mapping results. A recent study showed that TMS-based motor mapping with accurately controlled TMS coil placement has a high test-retest reliability when overlap between motor-eloquent areas is considered rather than the conventionally used center of gravity (COG).<sup>11</sup> Therefore, nTMS-based motor mapping can be considered a reliable tool for the investigation of functional reorganization after stroke if TMS coil placement is carefully considered, which we did in **chapter 7**.

### **TMS treatment for the promotion of post-stroke motor recovery**

In **chapter 5**, we investigated whether inhibiting the contralesional M1 within 3 weeks post-stroke with repetitive TMS promotes long-term recovery of the upper limb. We showed that contralesional continuous theta burst stimulation (cTBS), a time-efficient inhibitory rTMS paradigm, delivered to the contralesional M1 promotes upper limb recovery at 3 months post-stroke when combined with regular care physical therapy. Patients who were treated with active cTBS continued to improve fine motor skills and manual dexterity until 1 year post-stroke compared to patients who were treated with sham cTBS. This was accompanied by an improvement in quality of life measures and an earlier discharge from the rehabilitation center.

These findings add to the existing evidence from recent meta-analyses that inhibitory rTMS treatment of the contralesional M1 applied within 1 month post-stroke promotes upper limb recovery after stroke.<sup>12,13</sup> In addition, our findings show that a similar outcome can be achieved with a more time-efficient theta burst stimulation paradigm, which takes less than a minute compared to around 15 minutes for conventional low-frequency stimulation. Additionally, we showed that the therapeutic effect lasts at least up to a year after stroke while existing evidence was limited to a maximum of 6 months post-stroke. Lastly, the shorter length of stay at a clinical rehabilitation center after active cTBS treatment provides a first indication of a possible reduction in healthcare costs associated with rTMS treatment in post-stroke rehabilitation.

Despite these promising findings, the amount of evidence remains insufficient for the widespread application of inhibitory rTMS treatment in clinical rehabilitation centers. The next required step would be a large phase 3 multi-center study. In addition to measures of upper limb recovery and quality of life, this study should include cost-effectiveness measures,

including the length of stay at the rehabilitation center.

In addition to a phase 3 multi-center study, future research should focus on an implementation strategy for inhibitory rTMS treatment in rehabilitation centers. We interviewed healthcare professionals (HCPs) in rehabilitative stroke care, including occupational and physical therapists and rehabilitation physicians, to identify barriers and facilitators in the application of TMS techniques. Most HCPs were not familiar with TMS, complicating further analysis regarding user-friendliness, cost-effectiveness, and time efficiency of TMS treatment. HCPs did express concerns related to tolerance of severely affected stroke patients to the TMS treatment procedures. HCPs were also concerned about how the implementation of TMS treatment would affect current rehabilitation programs. Education, detailed work protocols, and training were identified as important facilitators for implementation.

Although the majority of HCPs in rehabilitative care is currently not familiar with rTMS treatment, its proven safety and the simplicity of the treatment procedures should ease introduction in rehabilitative care. Repetitive TMS treatment procedures can be performed by physiotherapists after a two-day training program and safety recommendations and screening questionnaires are readily available.<sup>14</sup> The proposed rTMS treatment is primarily neurophysiological. As such, implementation in a rehabilitative care setting will require further integration of the domains of neurology/neurophysiology and rehabilitation, and improved cooperation and knowledge transfer between HCPs who operate in these domains.

### **Mechanism of rTMS treatment**

In **chapter 5**, we showed that inhibitory rTMS treatment of the contralesional M1 within the first weeks after stroke promotes recovery of the upper limb. This treatment strategy was rooted in the interhemispheric imbalance model, which is based on a landmark paper that demonstrated that a net inhibitory drive from the contralesional to ipsilesional M1 was present when chronic stroke patients moved the affected hand.<sup>15,16</sup> The extent of the inhibitory drive was related to the level of impairment<sup>15,16</sup> and restoration of the interhemispheric balance was associated with upper limb recovery.<sup>17</sup> Therefore, inhibitory rTMS of the contralesional hemisphere has been suggested as a treatment option to reduce the inhibitory drive to promote recovery of the upper limb.

In **chapter 6**, we found that the treatment efficacy of contralesional cTBS was higher in patients with high structural reserve. This is consistent with the bimodal balance-recovery model, an extension of the interhemispheric imbalance model, proposed based on evidence that suggested that patients with low structural reserve would not benefit from inhibition of the contralesional M1.<sup>18</sup> We also showed that patients with high structural reserve show an increase in ipsilesional cortical excitability after contralesional cTBS treatment, while patients with low structural reserve do not. This suggests that modulation of ipsilesional excitability depends on the level of structural reserve, which is consistent with previously described observations that the spread of TMS-evoked activity depends on structural network connectivity.<sup>8,9</sup> Normalization of ipsilesional motor cortex excitability has been associated with improved function of the affected upper limb.<sup>19,20</sup> Therefore, contralesional inhibitory rTMS treatment may induce its therapeutic effect in patients with high structural reserve through restoration of ipsilesional cortical excitability. However, a causal relationship has not been established and it remains unclear how inhibition of the contralesional M1 increases ipsilesional excitability. A recent study showed that the persistence of a net inhibitory drive upon the ipsilesional M1 was absent in subacute stroke patients and only developed in patients who recovered poorly.<sup>21</sup> Therefore, the conditions under which inhibitory rTMS affects the contralesional to ipsilesional inhibitory drive in promoting upper limb recovery remain to be

further elucidated.

Nevertheless, in **chapter 5** we showed that inhibitory rTMS slightly reduced contralesional M1 excitability during the course of the treatment. Therefore, inhibitory rTMS before physical therapy of the affected arm might reduce contralesional M1 excitability, and potentially decrease the inhibitory drive upon the ipsilesional M1 during physical therapy. In **chapter 2**, we found that the effects of TMS are not restricted to the stimulated area but spread throughout the somatomotor network. Combined, this could explain an increase in ipsilesional cortical excitability shortly after the course of treatment, as shown in **chapter 7**. Future studies should include cortical excitability measurements directly after physical therapy to further elucidate the working mechanism of inhibitory rTMS treatment.

In **chapter 7**, we also investigated whether rTMS treatment combined with physical therapy may promote upper limb recovery through facilitation of functional reorganization of the peri-infarct area. We found that contralesional inhibitory rTMS treatment led to reorganization of the motor-eloquent area, characterized by an expansion of the motor-eloquent area in posterior direction. The reorganization of the motor-eloquent area may be associated with the recruitment of latent motor representations in peri-infarct areas.<sup>22</sup> Reorganization of M1 was not associated with an increase in ipsilesional M1 excitability, suggesting that these recovery processes operate independently.

### **Personalization of rTMS treatment**

We found that inhibitory rTMS treatment improves upper limb recovery in a heterogeneous group of stroke patients with varying stroke types and stroke locations. However, heterogeneity in stroke characteristics translates directly to a heterogeneous pathophysiology of post-stroke motor impairment, resulting in substantial variability in outcome.<sup>23</sup> Stroke heterogeneity alone can explain negative findings in neuroprotective trials, which is likely to apply to neurorehabilitation trials as well.<sup>24</sup> This stresses the importance of personalization of neurorehabilitation treatment to improve clinical efficacy.<sup>25</sup> This also applies to inhibitory rTMS treatment, as previous studies have shown that treatment efficacy may depend on certain stroke characteristics.<sup>18,26,27</sup>

In **chapter 6**, we investigated whether selecting patients for inhibitory rTMS treatment based on certain stroke characteristics affected treatment efficacy. As mentioned above, we showed that treatment efficacy was higher in patients with high structural reserve, while treatment efficacy could not be established in patients with low structural reserve. The identification of stroke characteristics that can be used to select patients for inhibitory rTMS treatment is the first step toward true personalization of rTMS treatment.

The next step in treatment personalization would be the identification of a therapeutic option for patients with poor structural reserve and little residual motor function. Patients with severe motor impairment can have a stronger facilitatory influence from the contralesional dorsal premotor cortex (dPMC) to the ipsilesional M1 during task performance with the affected hand, suggesting dPMC activity supports affected hand movement.<sup>28</sup> This was corroborated by a study that showed that facilitation of the contralesional dPMC with facilitatory rTMS treatment was effective in promoting upper limb recovery in severely affected stroke patients.<sup>29</sup> Although this is a promising rTMS treatment variant, evidence supporting facilitation of dPMC activity in severely affected stroke patients remains limited.

The strategy for personalization of treatment proposed in the previous sections relies on correlation rather than causation. A final step in treatment personalization is the identification of individualized treatment targets that directly influence affected hand performance. Concurrent TMS-fMRI, as proposed in **chapter 2**, provides a way to identify

such individualized treatment targets. Concurrent TMS-fMRI can be used to evoke activity in personalized stimulation targets to detect the direct inhibitory or facilitatory effect of this region on ipsilesional M1 activity during task performance with the affected hand. Such measurements were used to corroborate the facilitatory effect of the contralesional dPMC on affected hand performance in severely affected stroke patients.<sup>28</sup> These measurements can be used to identify personalized treatment targets that provide the strongest facilitatory or inhibitory effect on the ipsilesional M1 and to stratify these patients to receive facilitatory or inhibitory rTMS treatment of their treatment target, respectively. Unfortunately, concurrent TMS-fMRI equipment is currently not available in rehabilitation centers, complicating clinical feasibility.

A more clinically feasible alternative is TMS interference, which can be applied using a standard therapeutic magnetic stimulator. TMS interference uses a train of TMS pulses to temporarily interfere with voluntary physiological activity in the stimulated brain area during movement of the affected hand. When TMS interference of the target area negatively affects performance, the target area is assumed to have a facilitatory effect on the ipsilesional M1 and when TMS interference positively affects performance, the stimulated area is assumed to inhibit ipsilesional M1 activity. This strategy has been used to identify the effect of the contralesional M1 on affected hand performance during different post-stroke phases.<sup>30</sup> It was found that interference with the contralesional M1 improved affected hand performance in the early subacute phase (within 2 weeks post-stroke), in line with our findings (chapter 5), but it did not affect performance in the late subacute to chronic phase (after 3 months post-stroke).<sup>30</sup> Another study found that interference with dPMC activity negatively influenced performance of the affected hand in stroke patients with severe impairment, supporting previously discussed evidence.<sup>31</sup> A disadvantage of TMS interference is the reliance on the ability of stroke patients to perform voluntary activity with the affected arm or hand, which is often not possible in severely affected stroke patients.

Currently, to the best of our knowledge, there are no randomized sham-controlled clinical trials that have investigated rTMS treatment based on personalized targets obtained using concurrent TMS-fMRI or TMS interference. The use of concurrent TMS-fMRI requires an MRI scanner and highly specialized MRI-compatible TMS equipment, making it less suitable for clinical use at this time. TMS interference, on the other hand, can be performed using the same magnetic stimulator that is used for rTMS treatment, without additional equipment. However, it is possible that the novelty and added complexity of this technique potentially limits application in a clinical rehabilitation setting.

### **Conclusion and future perspectives**

We showed that contralesional inhibitory rTMS treatment promotes upper limb recovery after stroke, leading to a reduction in disability and dependence and a shorter length of stay at the rehabilitation center. Although these findings are very promising, a phase 3 trial is required to substantiate its clinical efficacy, before it can be implemented in clinical rehabilitation programs. When its clinical efficacy has been established, rTMS treatment can be introduced in rehabilitation centers with relative ease, as the treatment procedures are safe and simple. However, successful application of rTMS treatment, which is primarily neurophysiological, in a rehabilitative care setting will depend on further integration of neurology/neurophysiology and rehabilitation disciplines.

We identified two potential underlying mechanisms of inhibitory rTMS treatment that seem to operate independently. First, inhibitory rTMS treatment may (partially) restore the interhemispheric imbalance through downregulation of contralesional M1 excitability

during the treatment course which could lead to an increase in ipsilesional M1 excitability. Second, inhibitory rTMS may facilitate reorganization of the ipsilesional M1, associated with a posterior expansion of the functional motor area. Further research should focus on the causal relationships between inhibition of the contralesional M1, (long-term) changes in M1 excitability and reorganization, and physical therapy-induced functional effects. A deeper understanding of the treatment mechanisms can help identify patients eligible for treatment, identify an optimal treatment window, paradigm, dose, and regimen, and personalize treatment to further improve treatment efficacy.

Finally, we showed that treatment efficacy depends on patient characteristics like residual motor function and structural integrity of the intact ipsilesional CST, i.e. structural reserve. To further increase treatment efficacy, we provided a framework for the personalization of rTMS treatment for the promotion of upper limb recovery using TMS interference or concurrent TMS-MRI. However, future studies should validate the clinical value and efficacy of these personalization methods.

## REFERENCES

1. Bestmann S, Baudewig J, Siebner HR, Rothwell JC, Frahm J. Functional MRI of the immediate impact of transcranial magnetic stimulation on cortical and subcortical motor circuits. *European Journal of Neuroscience*. 2004;19(7):1950-1962. doi:10.1111/j.1460-9568.2004.03277.x
2. de Weijer AD, Sommer IEC, Bakker EJ, et al. A setup for administering TMS to medial and lateral cortical areas during whole-brain fMRI recording. *Journal of clinical neurophysiology*. 2014;31(5):474-487. doi:10.1097/WNP.0000000000000075
3. Hawco C, Voineskos AN, Steeves JKE, et al. Spread of activity following TMS is related to intrinsic resting connectivity to the salience network: A concurrent TMS-fMRI study. *Cortex*. 2018;108:160-172. doi:10.1016/j.cortex.2018.07.010
4. Chen B, Xu T, Zhou C, et al. Individual variability and test-retest reliability revealed by ten repeated resting-state brain scans over one month. *PLoS One*. 2015;10(12):1-21. doi:10.1371/journal.pone.0144963
5. Bastos AM, Schoffelen JM. A tutorial review of functional connectivity analysis methods and their interpretational pitfalls. *Front Syst Neurosci*. 2016;9:175.
6. van den Heuvel MP, Hulshoff Pol HE. Exploring the brain network: A review on resting-state fMRI functional connectivity. *European Neuropsychopharmacology*. 2010;20(8):519-534. doi:10.1016/j.euroneuro.2010.03.008
7. Sakkalis V. Review of advanced techniques for the estimation of brain connectivity measured with EEG/MEG. *Comput Biol Med*. 2011;41(12):1110-1117. doi:10.1016/j.combiomed.2011.06.020
8. Momi D, Ozdemir RA, Tadayon E, et al. Network-level macroscale structural connectivity predicts propagation of transcranial magnetic stimulation. *Neuroimage*. 2021;229:117698.
9. Momi D, Ozdemir RA, Tadayon E, et al. Perturbation of resting-state network nodes preferentially propagates to structurally rather than functionally connected regions. *Sci Rep*. 2021;11(1):1-11. doi:10.1038/s41598-021-90663-z
10. Jeltema HR, Ohlerth AK, de Wit A, et al. Comparing navigated transcranial magnetic stimulation mapping and “gold standard” direct cortical stimulation mapping in neurosurgery: a systematic review. *Neurosurg Rev*. 2021;44(4):1903-1920. doi:10.1007/s10143-020-01397-x
11. Nazarova M, Novikov P, Ivanina E, Kozlova K, Dobrynina L, Nikulin V V. Mapping of multiple muscles with transcranial magnetic stimulation: absolute and relative test-retest reliability. *Hum Brain Mapp*. 2021;42(8):2508-2528. doi:10.1002/hbm.25383
12. van Lieshout ECC, van der Worp HB, Visser-Meily JMA, Dijkhuizen RM. Timing of Repetitive Transcranial Magnetic Stimulation Onset for Upper Limb Function After Stroke: A Systematic Review and Meta-Analysis. *Front Neurol*. 2019;10(1269):1-16. doi:10.3389/fneur.2019.01269
13. Lefaucheur JP, Aleman A, Baeken C, et al. Evidence-based guidelines on the therapeutic use of repetitive transcranial magnetic stimulation (rTMS): An update (2014–2018). *Clinical Neurophysiology*. 2020;131(2):474-528. doi:10.1016/j.clinph.2019.11.002
14. Rossi S, Antal A, Bestmann S, et al. Safety and recommendations for TMS use in healthy subjects and patient populations, with updates on training, ethical and regulatory issues: Expert Guidelines. *Clinical Neurophysiology*. 2021;132(1):269-306. doi:10.1016/j.clinph.2020.10.003



15. Duque J, Hummel F, Celnik P, Murase N, Mazzocchio R, Cohen LG. Transcallosal inhibition in chronic subcortical stroke. *Neuroimage*. 2005;28(4):940-946. doi:10.1016/j.neuroimage.2005.06.033
16. Murase N, Duque J, Mazzocchio R, Cohen LG. Influence of Interhemispheric Interactions on Motor Function in Chronic Stroke. *Ann Neurol*. 2004;55(3):400-409. doi:10.1002/ana.10848
17. Boddington LJ, Reynolds JNJ. Targeting interhemispheric inhibition with neuromodulation to enhance stroke rehabilitation. *Brain Stimul*. 2017;10(2):214-222. doi:10.1016/j.brs.2017.01.006
18. Di Pino G, Pellegrino G, Assenza G, et al. Modulation of brain plasticity in stroke: A novel model for neurorehabilitation. *Nat Rev Neurol*. 2014;10(10):597-608. doi:10.1038/nrneurol.2014.162
19. McDonnell MN, Stinear CM. TMS measures of motor cortex function after stroke: A meta-analysis. *Brain Stimul*. 2017;10(4):721-734. doi:10.1016/j.brs.2017.03.008
20. Stinear CM, Petoe MA, Byblow WD. Primary motor cortex excitability during recovery after stroke: Implications for neuromodulation. *Brain Stimul*. 2015;8(6):1183-1190. doi:10.1016/j.brs.2015.06.015
21. Xu J, Branscheidt M, Schambra H, et al. Rethinking interhemispheric imbalance as a target for stroke neurorehabilitation. *Ann Neurol*. 2019;85(4):502-513. doi:10.1002/ana.25452
22. Chen R, Cohen LG, Hallett M. Nervous system reorganization following injury. *Neuroscience*. 2002;111(4):761-773. doi:10.1016/S0306-4522(02)00025-8
23. van der Vliet R, Selles RW, Andrinopoulou ER, et al. Predicting Upper Limb Motor Impairment Recovery after Stroke: A Mixture Model. *Ann Neurol*. 2020;87(3):383-393. doi:10.1002/ana.25679
24. Muir KW. Heterogeneity of stroke pathophysiology and neuroprotective clinical trial design. *Stroke*. 2002;33(6):1545-1550.
25. Bradnam L V, Stinear CM, Barber PA, Byblow WD. Contralesional hemisphere control of the proximal paretic upper limb following stroke. *Cerebral Cortex*. 2012;22(11):2662-2671.
26. Bertolucci F, Chisari C, Fregni F. The potential dual role of transcallosal inhibition in post-stroke motor recovery. *Restor Neurol Neurosci*. 2018;36(1):83-97. doi:10.3233/RNN-170778
27. Kim WS, Kwon BS, Seo HG, Park J, Paik NJ. Low-Frequency Repetitive Transcranial Magnetic Stimulation Over Contralesional Motor Cortex for Motor Recovery in Subacute Ischemic Stroke: A Randomized Sham-Controlled Trial. *Neurorehabil Neural Repair*. 2020;34(9):856-867. doi:10.1177/1545968320948610
28. Bestmann S, Swayne O, Blankenburg F, et al. The role of contralesional dorsal premotor cortex after stroke as studied with concurrent TMS-fMRI. *Journal of Neuroscience*. 2010;30(36):11926-11937. doi:10.1523/JNEUROSCI.5642-09.2010
29. Sankarasubramanian V, Machado AG, Conforto AB, et al. Inhibition versus facilitation of contralesional motor cortices in stroke: Deriving a model to tailor brain stimulation. *Clinical Neurophysiology*. 2017;128(6):892-902. doi:10.1016/j.clinph.2017.03.030
30. Volz LJ, Vollmer M, Michely J, Fink GR, Rothwell JC, Grefkes C. Time-dependent functional role of the contralesional motor cortex after stroke. *Neuroimage Clin*. 2017;16(July):165-174.

doi:10.1016/j.nicl.2017.07.024

31. Johansen-Berg H, Rushworth MFS, Bogdanovic MD, Kischka U, Wimalaratna S, Matthews PM. The role of ipsilateral premotor cortex in hand movement after stroke. *Proc Natl Acad Sci U S A*. 2002;99(22):14518-14523. doi:10.1073/pnas.222536799





Chapter 9

## **Addendum**



# Supplemental materials

Supplemental materials can be downloaded through:

[https://drive.google.com/file/d/1Iz9-UB8FgASKirxIAJw6\\_9ONL4IUTg5\\_](https://drive.google.com/file/d/1Iz9-UB8FgASKirxIAJw6_9ONL4IUTg5_)





# Nederlandse samenvatting

Beroerte is de meest voorkomende cardiovasculaire ziekte na coronaire hartziekten en de meest voorkomende oorzaak van invaliditeit bij volwassenen.<sup>1</sup> Ondanks ontwikkelingen in de acute behandeling van en revalidatie na een beroerte hebben veel patiënten een blijvende beperking van de hand- en armfunctie.<sup>2</sup> Repetitieve transcraniële magnetische stimulatie (rTMS) van de gezonde motorische cortex wordt onderzocht als mogelijke nieuwe therapie voor het verbeteren van het herstel van de hand- en armfunctie na een beroerte.<sup>3</sup> Met rTMS kan op een niet-invasieve manier (zonder dat er een operatie nodig is) hersenactiviteit in het gestimuleerde gebied gefaciliteerd of geremd worden door middel van elektromagnetische inductie.<sup>4</sup> Voordat rTMS-behandeling gebruikt kan worden in de klinische revalidatie moeten de effectiviteit, factoren die invloed hebben op de effectiviteit en het werkingsmechanisme beter onderzocht worden.

Het eerste deel van dit proefschrift (hoofdstukken 2 tot en met 4) beschrijft hoe bij gezonde participanten TMS (in niet-repetitieve vorm) gebruikt kan worden om hersenfunctie in kaart te brengen, en hoe magnetische stimuli invloed hebben op signalen tussen verschillende hersengebieden.

Om TMS effectief in te zetten voor therapeutische of diagnostische doeleinden moeten we begrijpen hoe TMS hersennetwerken beïnvloedt. In **hoofdstuk 2** hebben we in kaart gebracht hoe het brein reageert op stimulatie van verschillende hersengebieden door de opgewekte activiteit in de verschillende hersennetwerken te meten met functionele MRI. Netwerkactiviteit die werd opgewekt door stimulatie van de primaire motorische cortex werd voornamelijk waargenomen in hersengebieden die onderdeel zijn van het motorische netwerk en in beperkte mate ook buiten dit netwerk. De activiteit die opgewekt werd met TMS was bovendien vergelijkbaar met activiteit door vrijwillige handbewegingen. Deze bevindingen laten zien dat hersenactiviteit opgewekt met TMS zich primair verspreidt binnen de functionele organisatie van het gestimuleerde hersennetwerk.

Hoe de door TMS opgewekte hersenactiviteit zich verspreidt door het brein hebben we verder onderzocht in **hoofdstuk 3**. We onderzochten of deze hersenactiviteit zich bij voorkeur verspreidt via functioneel verbonden hersengebieden door de mate van synchronisatie van elektrische hersensignalen in rusttoestand te meten met behulp van elektro-encefalografie (EEG). Hier ontdekten we dat door TMS opgewekte netwerkactiviteit zich maar in beperkte mate verspreidt richting de functioneel verbonden gebieden. Op basis van een andere studie is het waarschijnlijker dat door TMS opgewekte hersenactiviteit zich verspreidt binnen hersennetwerken die gedefinieerd zijn op basis van globale structurele verbindingen.<sup>5</sup> Dit betekent dat verschillen in hersenactiviteit minder relevant zijn voor de verspreiding van met TMS opgewekte activiteit dan de overeenkomsten in de globale structuur van het hersennetwerk.

Voor **hoofdstuk 4** onderzochten we de relatie tussen verschillende met TMS geïnduceerde elektrische velden en de daarmee opgewekte hersenactiviteit. We richtten ons specifiek op het identificeren van motorische gebieden met behulp van TMS. We ontdekten dat de spatiële organisatie van het motorische gebied, geïdentificeerd met TMS, afhangt van de oriëntatie van de geïnduceerde elektrische velden. Deze resultaten benadrukken de complexiteit van de interactie tussen het met TMS geïnduceerde elektrische veld en de

opgewekte hersenactiviteit, en het belang van de oriëntatie van de TMS-spoel. Een ander recent onderzoek toont aan dat identificatie van motorische gebieden met behulp van TMS een hoge betrouwbaarheid heeft zolang de oriëntatie van het elektrisch veld goed wordt gecontroleerd.<sup>6</sup> Dit bevestigt de potentie van TMS voor onderzoek naar de reorganisatie van motorische gebieden na een beroerte, zoals beschreven in **hoofdstuk 7**.

Het onderzoek in het tweede deel van dit proefschrift (hoofdstukken 5 tot en met 7) richtte zich op het effect van rTMS-behandeling op het herstel van de hand- en armfunctie na een beroerte, en op het werkingsmechanisme van deze behandeling.

In **hoofdstuk 5** wordt beschreven hoe we onderzocht hebben of remming van het motorische gebied in de gezonde hersenhelft door rTMS-behandeling het herstel van de bovenste extremiteit bevordert. De gedachtegang hierbij was dat activiteit in het motorische gebied van de gezonde hersenhelft mogelijk het herstel in de weg staat doordat deze de activiteit in het motorisch gebied van de aangedane hersenhelft remt. We laten zien dat een specifieke rTMS behandeling, in combinatie met reguliere fysiotherapie, het herstel van hand- en armfunctie bevordert. Bij patiënten die behandeld werden met rTMS verbeterden bovendien de fijne motoriek en handvaardigheid meer dan bij patiënten die deze behandeling niet kregen. De verbetering in hand- armfunctie ging gepaard met een verbetering in kwaliteit van leven en versneld ontslag uit het revalidatiecentrum.

In **hoofdstuk 6** laten we zien dat de rTMS behandeling beschreven in hoofdstuk 5 minder effectief is bij patiënten met ernstige uitval van hand- en armfunctie en relatief veel schade aan de corticospinale banen (deze vormen de verbinding tussen de motorische gebieden in het brein en het ruggenmerg). Deze resultaten suggereren dat deze patiënten geen baat zouden hebben bij remming van het motorische gebied in de gezonde hersenhelft.

De rTMS behandeling uit **hoofdstuk 5** gaat uit van de aanwezigheid van een disbalans tussen de activiteit in de motorische gebieden van beide hersenhelften. De aanwezigheid van deze disbalans is gebaseerd op een belangrijke studie die liet zien dat het motorische gebied in de gezonde hersenhelft een remmend effect heeft op het motorisch gebied in de aangedane hersenhelft wanneer patiënten met een beroerte de aangedane hand bewegen.<sup>7,8</sup> De mate van remmende werking was gerelateerd aan de ernst van de verminderde hand- en armfunctie, en herstel van de balans was gerelateerd aan functieherstel van de hand en arm.<sup>7,8</sup> Deze disbalans wordt met name gekarakteriseerd door een afname in de exciteerbaarheid van het motorisch gebied in de aangedane hersenhelft (d.w.z. de gevoeligheid voor een externe stimulus).<sup>9</sup> De afname in exciteerbaarheid is bovendien gerelateerd aan de ernst van de hand- en arm dysfunctie.<sup>9,10</sup>

In **hoofdstuk 7** wordt beschreven hoe we twee potentiële werkingsmechanismen van de rTMS-behandeling hebben geïdentificeerd. Ten eerste vonden we dat de exciteerbaarheid van het motorische gebied in de aangedane hersenhelft verhoogd is na tien rTMS behandelingen. De exciteerbaarheid van dit motorische gebied bleek bovendien gerelateerd te zijn aan de hand- en armfunctie een jaar na de beroerte. Ten tweede vonden we dat rTMS-behandeling leidt tot reorganisatie van de intacte motorische gebieden rondom het infarct. Dierstudies hebben laten zien dat veranderingen in de organisatie van de intacte motorische gebieden rondom het infarct ten grondslag kunnen liggen aan het herstel van motorische functie.<sup>11</sup> Deze reorganisatie wordt mogelijk ondersteund door rekrutering van latente motorische representaties in de gebieden rondom het infarct.<sup>12</sup>

Dit proefschrift biedt nieuwe inzichten in het gebruik van rTMS-behandeling voor het bevorderen van het herstel van de hand- en armfunctie na een beroerte. Allereerst beschrijft dit proefschrift nieuwe bevindingen met betrekking tot het effect van TMS op hersenactiviteit en hersennetwerken. Daarnaast werd de effectiviteit van rTMS behandeling bepaald in een fase-2 klinische studie en zijn beroerte-specifieke factoren die invloed hebben op de effectiviteit van de behandeling en twee potentiële werkingsmechanismen van deze behandeling geïdentificeerd. Het werk in dit proefschrift biedt een sterke basis voor vervolgonderzoek in de vorm van een fase-3 studie waaruit moet blijken of deze behandeling geïmplementeerd kan worden in de reguliere revalidatiezorg.

## REFERENTIES

1. Virani SS, Alonso A, Aparicio HJ, et al. Heart Disease and Stroke Statistics-2021 Update: A Report From the American Heart Association. *Circulation*. 2021;143(8):e254-e743. doi:10.1161/CIR.0000000000000950
2. van der Vliet R, Selles RW, Andrinopoulou ER, et al. Predicting Upper Limb Motor Impairment Recovery after Stroke: A Mixture Model. *Ann Neurol*. 2020;87(3):383-393. doi:10.1002/ana.25679
3. van Lieshout ECC, van der Worp HB, Visser-Meily JMA, Dijkhuizen RM. Timing of Repetitive Transcranial Magnetic Stimulation Onset for Upper Limb Function After Stroke: A Systematic Review and Meta-Analysis. *Front Neurol*. 2019;10(1269):1-16. doi:10.3389/fneur.2019.01269
4. Lefaucheur JP, Aleman A, Baeken C, et al. Evidence-based guidelines on the therapeutic use of repetitive transcranial magnetic stimulation (rTMS): An update (2014–2018). *Clinical Neurophysiology*. 2020;131(2):474-528. doi:10.1016/j.clinph.2019.11.002
5. Momi D, Ozdemir RA, Tadayon E, et al. Network-level macroscale structural connectivity predicts propagation of transcranial magnetic stimulation. *Neuroimage*. 2021;229:117698.
6. Nazarova M, Novikov P, Ivanina E, Kozlova K, Dobrynina L, Nikulin V V. Mapping of multiple muscles with transcranial magnetic stimulation: absolute and relative test–retest reliability. *Hum Brain Mapp*. 2021;42(8):2508-2528. doi:10.1002/hbm.25383
7. Murase N, Duque J, Mazzocchio R, Cohen LG. Influence of Interhemispheric Interactions on Motor Function in Chronic Stroke. *Ann Neurol*. 2004;55(3):400-409. doi:10.1002/ana.10848
8. Duque J, Hummel F, Celnik P, Murase N, Mazzocchio R, Cohen LG. Transcallosal inhibition in chronic subcortical stroke. *Neuroimage*. 2005;28(4):940-946. doi:10.1016/j.neuroimage.2005.06.033
9. McDonnell MN, Stinear CM. TMS measures of motor cortex function after stroke: A meta-analysis. *Brain Stimul*. 2017;10(4):721-734. doi:10.1016/j.brs.2017.03.008
10. Stinear CM, Petoe MA, Byblow WD. Primary motor cortex excitability during recovery after stroke: Implications for neuromodulation. *Brain Stimul*. 2015;8(6):1183-1190. doi:10.1016/j.brs.2015.06.015
11. Nudo RJ, Wise BM, SiFuentes F, Milliken GW. Neural substrates for the effects of rehabilitative training on motor recovery after ischemic infarct. *Science (1979)*. 1996;272(5269):1791-1794.
12. Chen R, Cohen LG, Hallett M. Nervous system reorganization following injury. *Neuroscience*. 2002;111(4):761-773. doi:10.1016/S0306-4522(02)00025-8





# Acknowledgements

De wetenschap beschreven in dit proefschrift was niet mogelijk geweest zonder de ondersteuning door mijn promotieteam, collega's, vrienden en familie. Ik wil hen hiervoor graag bedanken middels de woorden hieronder.

## Promotieteam

**Rick**, ik wil jou enorm bedanken voor de bijzonder prettige samenwerking. Jouw visie en deskundigheid in combinatie met jouw ongeremde enthousiasme is een belangrijke bron van inspiratie geweest tijdens mijn promotietraject. Daarnaast boden onze gesprekken over reizen, sport en politiek op de juiste momenten ook de broodnodige afleiding. Maar in het bijzonder wil ik je bedanken dat je een rol als mentor hebt aangenomen, en mij het vertrouwen hebt gegeven dat ik een eigen pad uit kan stippelen binnen de wetenschap. Ik kijk erg uit naar onze voortgezette samenwerking!

**Bas**, allereerst wil ik jou bedanken dat je het balletje hebt opgegooid om aan dit promotietraject te beginnen. Je zag toen al in dat een promotietraject binnen de cardiologie niets voor mij was;-). Gelukkig heb ik alsnog Marijn leren kennen! In het bijzonder wil ik je bedanken voor alle wandelingen door landgoed Oostbroek waarin we wetenschappelijke ambities, persoonlijke avonturen en bedrijfsstrategiën bespraken. Onze samenwerking binnen de MedTech wereld heeft me bijzonder veel waardevolle kennis, ervaringen en contacten opgeleverd.

**Anne**, ook jou wil ik bedanken voor de fijne samenwerking. Ik waardeer in het bijzonder hoe onze band is gegroeid over de jaren. Jouw visie, waarin je mensen verbindt en de patiënt centraal staat, zal een belangrijke plek krijgen in mijn verdere wetenschappelijke carrière.

**Bart**, jij stond altijd klaar met een oplossing voor welk probleem dan ook en combineerde dat altijd met een vleugje humor (ook al was ik hier niet altijd op voorbereid in onze meetings;-)). Jouw deskundigheid, oog voor detail en gevoel voor humor waren cruciaal voor het succes van een langdurige klinische studie zoals het B-STARS project.

## Beoordelingscommissie

**Jaap Kappelle, Gerard Ribbers, Birgitta Velthuis, Nick Ramsey, Frans Leijten**, bedankt voor jullie tijd en het kritisch beoordelen van mijn proefschrift.

## Paranimfen

**Geo**, mijn promotietraject vormde eigenlijk maar een klein onderdeel van de grote reis die wij de afgelopen jaren samen hebben gemaakt. Er is namelijk zoveel gebeurd wat onze vriendschap heeft gevormd. Dit dankwoord geeft mij de gelegenheid om bij alle aspecten van deze reis stil te staan. Want deze reis heeft me bijzonder veel geleerd, over mijzelf, onze vriendschap en mijn plek op deze aardbol, als wetenschapper en als mens. Mijn dank hiervoor is groot!

**Sjouke**, het komt denk ik zelden voor dat iemand je net zo goed kent als je gezin. Maar aangezien jij zowel mijn eerste als 31<sup>ste</sup> verjaardag hebt meegemaakt, durf ik wel te zeggen dat je me inmiddels door en door kent. Alle avonturen die we samen hebben meegemaakt vormen nu de basis voor een rotsvaste vriendschap waarbij twee verschillende persoonlijkheden precies weten wat ze aan elkaar hebben, en dat is onbetaalbaar!

## Vrienden

**Edward**, het liefst had ik drie paranimfen uitgenodigd, want jij hoort daar thuis, zonder twijfel. Onze 'end of the world' trips vormen een goede metafoor voor onze vriendschap: twee vrienden die nieuwsgierig zijn naar wat er zich achter de volgende bergtop bevindt, zowel letterlijk als figuurlijk. Deze nieuwsgierigheid vormt de basis voor interessante en soms ook kwetsbare gesprekken waar onze twee verschillende visies op het leven samenkomen. Ik ben erg dankbaar voor onze avonturen en gesprekken!

**Frank**, het is goed om te zien dat deze granola boy met zijn vlotte babbel weer terug is op Nederlandse bodem. Ik heb je gemist! **Nick**, bedankt voor onze goede lunchgesprekken en inzichtelijke avonden bij 'Behind bars'. **Dennis**, een 'end of the world' trip is niet hetzelfde zonder jou. Volgende keer weer? **Billy**, onze diepgaande discussies over religie en de zin van het leven tijdens de puberteit hebben zeker een zaadje geplant voor mijn wetenschappelijke nieuwsgierigheid. Bedankt!

**Mark**, lotgenoot, bedankt voor het gedeelde leed, en de gedeelde glorie tijdens onze promotietrajecten. **Rik** en **Amy**, bedankt voor de vele mooie en hilarische avonturen met het Kwartet. Jullie boden hoognodige afleiding op het juiste moment, in de vorm van concerten en festivals en goede gesprekken tot in de late uurtjes. **Jack**, bedankt voor onze goede gesprekken waarin twee compleet verschillende belevingswerelden samenkomen!

**Sjors**, bedankt voor je hulp tijdens de B-STARS studie en onze samenwerking bij BST. Wat begon als gedeelde worstelingen op de werkvloer en gesprekken over muziek vormde zich tot een mooie vriendschap.

**Sander, Koen**, bedankt voor alle klim- en boulder sessies, deze hebben het brein weer scherp gekregen!

## Collega's

**Eline**, onze samenwerking was als een dieseltje, het duurde even voordat ie goed op gang kwam, maar daarna was hij niet meer te stoppen. Bedankt daarvoor!

Collega's bij het lab, **Eline, Vera, Bart, Annette, Geralda, Gerard, Esther, Anu, Lois en Jamila**, bedankt voor de inspirerende labmeetings en de gezellige activiteiten en uitjes!

Collega's bij de Hoogstraat revalidatie, **Mirjam**, bedankt voor je betrokkenheid bij de B-STARS studie. Ook zonder hulp van de andere **revalidatieartsen, de verpleegkundigen, ergo- en fysiotherapeuten** en de **planning** was de B-STARS studie niet mogelijk geweest. **Raquel**, bedankt voor de filosofische zoektochten en koffiegesprekken!

Collega's bij het UMC Utrecht, **Wim**, bedankt voor de goede gesprekken bij het koffiezetapparaat, jouw inspirerende visie en de geniale presentaties op de dinsdagochtend. **Petar** and **Stefano**, thank you for our late-night MRI sessions and good talks at the Basket. **Alex**, thanks for our B-STARS MRI sessions and the good talks about our science struggles! **Ruben** en **Ben**, bedankt voor jullie bijdrage aan de B-STARS studie!

Collega's bij Brain Science Tools, **Bas, Petar, Jorinde, Marelyn, Robin, Manuela, Yvonne, Joris, Yumas** en **Dasha** bedankt voor de gezellige lunches, bedrijfsuitjes en conferenties! **Robin**,



viend, studiegenoot, stagiair en collega, volgens mij hebben we alles nu wel gehad?

Colleagues from Boston, **Brandon** and **Mo**, thanks a lot for the inspiring collaboration! **Mo**, a special thank you for your guidance during my first steps into the scientific world.

Andere collega's en samenwerkingspartners, **Maaike, Debby, Helene en Fenne**, bedankt!

Stagiairs, **Safiyah, Stefan, Mira, Camille, Marius, Hosna, Marit, Ida, Sjors, Frederieke, Robin, Roosmarijn, Beatriz, Liliane, Lisette, Marielle, Marissa, Adam, Marloes en Rosa**, bedankt voor jullie bijdrage aan het onderzoek. Zonder jullie hulp was dit zeker niet gelukt!

### **Familie**

Lieve schoonfamilie, **Ronald, Rian, Anniek, Daan en Bram**, bedankt dat jullie me hebben opgenomen in het Peters universum! De peters-humor vergt alleen nog wat oefening.

Lieve **oma**, bedankt voor het stimuleren van een ruimdenkende geest. Dit heeft mij geleid naar het pad dat ik nu bewandel.

Lieve **zus**, Jij hoeft niet veel woorden te gebruiken om mij het gevoel te geven dat je achter me staat. Jouw steun en liefde voelen onvoorwaardelijk. Bedankt daarvoor! **Robbin**, de ideale schoonbroer. What more can I say?

**Pap en mam**, jullie hebben mij geleerd om nieuwsgierig te zijn en de wijde wereld te ontdekken en tegelijkertijd bieden jullie een warm nest om naar terug te keren. Voor deze gouden combinatie ben ik jullie eeuwig dankbaar!

Liefste **Marijn**, het kon geen toeval zijn. De rationele neurowetenschapper die niet altijd begrijpt wat zijn hart hem vertelt ontmoet een expert op het gebied van het hart. Het brein en hart, de ratio en emotie, de yin en yang zijn verenigd. Deze synergie symboliseert mijn liefde voor jou. Jij bent mijn inspiratiebron, mijn sensei, mijn pitbull en mijn kalmte. Ik hoop dat we samen nog vele avonturen zullen beleven!



# List of publications

## Published

**Vink, J. J.**, van Lieshout, E. C. C., Otte, W. M., van Eijk, R. P. A., Kouwenhoven, M., Neggers, S. F. W., van der Worp, H. B., Visser-Meily, J. M. A., & Dijkhuizen, R. M. (2023). Continuous Theta-Burst Stimulation of the Contralesional Primary Motor Cortex for Promotion of Upper Limb Recovery After Stroke: A Randomized Controlled Trial. *Stroke*, 10.1161/STROKEAHA.123.042924.

**Vink, J. J.**, Mandija, S., Petrov, P. I., van den Berg, C. A., Sommer, I. E., & Neggers, S. F. (2018). A novel concurrent TMS-fMRI method to reveal propagation patterns of prefrontal magnetic brain stimulation. *Human brain mapping*, 39(11), 4580-4592.

**Vink, J. J.**, Klooster, D. C., Ozdemir, R. A., Westover, M. B., Pascual-Leone, A., & Shafi, M. M. (2020). EEG functional connectivity is a weak predictor of causal brain interactions. *Brain topography*, 33, 221-237.

van Lieshout, E. C., Boonzaier, J., Pel, A. J., van Heijningen, C. L., **Vink, J. J.**, Visser-Meily, J. M., ... & Dijkhuizen, R. M. (2021). Translational value of skilled reaching assessment in clinical and preclinical studies on motor recovery after stroke. *Neurorehabilitation and Neural Repair*, 35(5), 457-467.

Mandija, S., Petrov, P. I., **Vink, J. J.**, Neggers, S. F., & van den Berg, C. A. (2021). Brain tissue conductivity measurements with MR-electrical properties tomography: an in vivo study. *Brain topography*, 34, 56-63.

## Preprint

**Vink, J. J.**, Petrov, P. I., Mandija, S., Dijkhuizen, R. M., & Neggers, S. F. (2018). Outcome of TMS-based motor mapping depends on TMS current direction. *bioRxiv*, 371997.

## Submitted

**Vink, J. J.**, Biemans, C. F., van Lieshout, E. C., van Eijk, R. P., Neggers, S. F., Visser-Meily, J. M., van der Worp, H. B., Dijkhuizen, R. M. (2023). Contralesional cTBS treatment leads to changes in the ipsilesional motor area in recovering stroke patients.

## Curriculum Vitae

Jord Vink was born on January 19<sup>th</sup> 1992 in Valkenswaard, The Netherlands. After finishing high school at Were Di in Valkenswaard, he completed his bachelor and master in Technical Medicine at the University of Twente. During the Master program, he spent 4 months at Massachusetts General Hospital and Beth Israel Deaconess Medical Center in Boston, MA, USA, to collaborate on a project investigating the relationship between functional connectivity and propagation of evoked potentials using transcranial magnetic stimulation (TMS) and electroencephalography. He wrote his Master thesis on the real-time measurement of blood-oxygen level dependent imaging of TMS-evoked activity with a specific focus on the clinical application of TMS in major depressive disorder. During this period, he joined



Brain Science Tools as product specialist, contributing to product development and customer support. He continued his research with a PhD at the group of Rick Dijkhuizen at the Center for Image Sciences of the UMC Utrecht. During this period, he coordinated the BSTARS study, a single-center randomized sham-controlled trial on inhibitory repetitive TMS treatment for the promotion of upper limb recovery after stroke.